

INVESTIGATIONS INTO THE IMMUNOMODULATORY PROPERTIES OF SLAMF7 AND ERAP1

By

Patrick O'Connell

A DISSERTATION

Submitted to
Michigan State University
in partial fulfillment of the requirements
for the degree of

Cell and Molecular Biology—Doctor of Philosophy

2021

ABSTRACT

INVESTIGATIONS INTO THE IMMUNOMODULATORY PROPERTIES OF SLAMF7 AND ERAP1

By

Patrick O'Connell

Autoimmune diseases represent one of the most complex pathological conditions recognized by modern medicine; however, through investigations of these conditions we not only gain a deeper understanding of these diseases, but also of the immune system as a whole. In this regard, we have used autoimmunity, and Multiple Sclerosis (MS) in particular, as a lens through which to better understand how the proteins SLAMF7 and ERAP1 regulate the immune system. Both of these genes have been linked to increased MS susceptibility, yet the underlying mechanisms remain a mystery. Our efforts have shown that these highly disparate proteins, with vastly differing functions, both modulate CNS autoimmunity via alteration of B cell responses. We also expand our investigations of how SLAMF7 modulates the immune system to other diseases and cell types, greatly broadening the known biological roles of this fascinating immune cell receptor.

In summary, our efforts here both expand our knowledge by identifying underlying mechanisms as to why certain genes are linked to increased MS susceptibility, and also broaden the known biological roles of these immunoregulatory proteins. Armed with this new knowledge, the puzzle that is MS becomes just a little bit clearer, and new potential therapeutic targets for MS and a number of other diseases, start to emerge.

This work is dedicated to all those whose immune systems have turned against them; may we one day have the ability to give every man, woman, and child mastery over our body's microscopic sentinels.

ACKNOWLEDGMENTS

While this thesis bares one name on the cover, it was a team effort in every sense of the word. None of this would have been possible if not for the efforts and support from many individuals. First among them are Dr. Justin McCormick and Bethany Heinlen, who took a chance on me and gave me the opportunity to train as a physician scientist here at MSU. Without them I would have spent my years as a medical student merely memorizing the discoveries of others, instead of making my own.

Learning to be a scientist is easier said than done, and without the expert guidance of Dr. Andrea Amalfitano and Dr. Yasser Aldhamen I never would have done it. Having Andy as a mentor has been one of the most fortuitous opportunities in my career. I have yet to hear of another graduate student mentor who allows their trainee the freedom Andy has provided me. He has always supported my curiosity, providing me the freedom to take projects any which way I please, and has nurtured my innate sense of curiosity, all the while guiding me with a subtle hand. Similarly, Yasser has taught me not only immunology, but science. He has guided me every step of the way, away from my really crazy ideas, and towards the pragmatic ones. He has taken so much of his time and effort to teach me the basics of how to answer a scientific question, what questions to ask, and how to interpret the results. Together we have delved down obscure immunological signaling pathways, often discussed at length during our walks through MSU's campus. These I will miss.

I would be remiss if I did not acknowledge all of the assistance I received from my fellow graduate student lab mates including Dr. David Rastall, Dr. Yuliya Pepelyayeva, and Maja Blake. David and Yuliya were excellent mentors and fantastic sources of interesting (and sometimes obscure) conversation during our marathon experiments late into the night; but I suppose that is to be expected from future neurologists. Maja has always been willing to work with me on whatever crazy experiments I concoct and has always put up with my crazy lab antics.

It is safe to say I could not have made it through this PhD without the help of Sarah Godbehere. She has been a constant source of reason, support, and girl scout cookies; all of which I would be lost without. Her ability to tame my, at times, overexuberant scientific excitement is nothing short of miraculous and I could not envision a better lab manager and person to have worked with over the past six years.

This work, and my research training in general, have been greatly supported and nurtured by my excellent graduate committee: Dr. Margaret Petroff, Dr. Kefei Yu, Dr. Nara Parameswaran, Dr. Cheryl Rockwell, and Dr. Andrea Amalfitano. Together, they have pushed me to think deeper and broader about my research, and science in general. Always willing to support me with reagents, mice, or just an ear to talk too, this thesis and my PhD have benefited greatly from their expert guidance.

I would also like to thank the current leadership of the DO/PhD program at MSU: Dr. John Goudreau, Dr. Brian Schutte, and Michelle Volker for their omniscient support and apt handling

of all the unexpected issues us DO/PhD students cause.

I have been fortunate enough to receive financial support both for myself and my research endeavors from: the MSU College of Natural Sciences, the MSU CMB program, the John A. Penner Endowed Research Fellowship, the American Osteopathic Association, and Illumina Inc. For all this support I am sincerely grateful.

I must also thank the excellent MSU core facilities which have supported all of our research endeavors over the years including the MSU genomics core, MSU histology core, and MSU flow cytometry core. In particular I would like to thank Dr. Louis King for teaching me how to operate and troubleshoot a flow cytometer, and for his patience and stimulating conversation during marathon flow sorting experiments. A special thanks to Dr. Matthew Bernard and Dr. Daniel Vocelle for continuing to teach me more about flow and spectral cytometry than I ever knew there was to learn.

Finally, I would like to thank my family and DO/PhD comrades for their constant support through this arduous journey; this would not have been possible without you. In particular, Krishna Yelleswarapu who has been a great friend and constant source of support through our journey together along the long and winding road to becoming physician scientists.

TABLE OF CONTENTS

LIST OF TABLES	xi
LIST OF FIGURES	xii
KEY TO ABBREVIATIONS	xv
CHAPTER: 1 Introduction	1
Overview of Multiple Sclerosis	2
SLAMF7 is a member of the SLAM Family of Receptors	4
Immune Responses to Viral Infections	6
SLAMF1 (SLAM, CD150)	10
SLAMF2 (CD48)	12
SLAMF3 (Ly-9, CD229)	16
SLAMF4 (2B4, CD244)	17
SLAMF5 (CD84)	21
SLAMF6 (NTB-A, Ly-108, CD352)	23
SLAMF7 (CRACC, CS1, CD319)	25
SLAMF8 (BLAME, CD353)	28
SLAMF9 (SF2001, CD84H1)	30
Potential for Targeting SLAM Family of Receptors in HIV and other Viral Infections.....	31
SLAM receptors: Summary	33
SLAMF7 and its association with Multiple Sclerosis	34
ERAP1 and its link MS and other autoimmune diseases	35
Mouse model of MS	37
CHAPTER: 2 SLAMF7 Is a Critical Negative Regulator of IFN- α -Mediated CXCL10 Production in Chronic HIV Infection	40
Abstract	41
Introduction	42
Materials and Methods	44
Results	48
HIV+ individuals have increased expression of SLAMF7 on their peripheral blood mononuclear cells (PBMCs).	48
SLAMF7 is upregulated in response to IFN α in total PBMCs and monocytes from HIV+ individuals.	50
SLAMF7 activation on monocytes of HCs inhibits IFN α -mediated CXCL10 production.	51
A subset of HIV+ patients are nonresponsive to SLAMF7 inhibitory signaling.	52
SLAMF7 responsive and SF7S patients have distinct peripheral immune activation signatures.	53

Monocytes from SF7S and SLAMF7 responsive patients do not differ in expression levels of the SLAMF7 receptor or EAT-2 adaptor.	56
SLAMF7 signaling in monocytes selectively inhibits IFN α -mediated production of alpha chemokines over other interferon-stimulated genes (ISGs) and host restriction factors.	57
SLAMF7-mediated inhibition of CXCL10 production in monocytes may be independent of SHP1, SHP2, SHIP1, or CD45.....	58
SLAMF7 inhibits monocyte infection with HIV-1 in vitro.....	59
Neutrophils constitutively express CXCL10 and do not express SLAMF7.	60
Neutrophils are unable to upregulate SLAMF7 in response to IFN α and SLAMF7 activation does not inhibit proinflammatory cytokine and chemokine release from neutrophils.....	61
Discussion	62
 CHAPTER: 3 In vitro infection of primary human monocytes with HIV-1.....	68
Abstract	69
Background.....	69
Materials and Reagents	70
Equipment	72
Software	72
Procedure	72
Data analysis.....	77
Notes	78
Recipes.....	79
 CHAPTER: 4 SLAMF7 Signaling Reprograms T Cells toward Exhaustion in the Tumor Microenvironment	81
Abstract	82
Introduction.....	83
Materials and Methods	85
Results	92
SLAMF7 is co-expressed with multiple exhaustion markers on activated T cells. 92	
Activation of SLAMF7 alone on T cells induces inhibitory receptors and exhaustion-associated transcription factors.	93
In vitro SLAMF7-activated T cells are distinct from terminally exhausted T cells and are capable of producing cytokines upon re-stimulation.	96
SLAMF7 signaling in CD8+ T cells induces STAT1 and STAT3 phosphorylation.....	99
SLAMF7 expression is correlated with inhibitory receptor expression in clear cell renal cell carcinoma patients and is linked to poor survival.....	100
SLAMF7 expression patterns in human ccRCC tumors, associations with exhausted T cells, and links to patient survival.	102
SLAMF7 expression in the TME propels CD8+ T cells towards terminal exhaustion and impacts tumor growth.	106
Expression of SLAMF7 on TAMs drives T cells to express inhibitory receptors. .	108

Discussion	109
CHAPTER: 5 Adenoviral delivery of an immunomodulatory protein to the tumor microenvironment controls tumor growth	
Abstract	115
Introduction.....	116
Results	119
Ad-SF7-Fc induces high expression of SF7-Fc and activates the innate immune system.....	119
Ad-SF7-Fc augments Th1 cytokine and interferon responses.	121
Ad-SF7-Fc controls CT26 tumor growth in the absence of increased adaptive immune responses.	124
Ad-SF7-Fc controls B16-F10 tumor growth without modulating T cell exhaustion or remodeling the TME.....	125
SLAMF7 expression across the TME and tumor-infiltrating myeloid cell phenotypes in Ad-SF7-Fc treated mice.....	127
EAT-2 expression in tumor-infiltrating innate immune cells identifies mice able to control B16 tumors.....	129
Cell type specific, single-cell predictions of the function of Ad-SF7-Fc in vivo. .	133
Alterations in the immune TME in SLAMF7 ^{-/-} mice.....	133
Immunological Elastic Net identifies features underlying tumor response to Ad- SF7-Fc.....	135
Discussion	136
Methods	139
CHAPTER: 6 The immune cell receptor SLAMF7 is linked to susceptibility to CNS autoimmunity via modulation of B cell responses	
Abstract	149
Introduction.....	150
Results	151
SLAMF7 is protective against CNS autoimmunity and displays unique cell type expression patterns.	153
SLAMF7-mediated changes in the CNS immune landscape during EAE.	155
SLAMF7 does not alter the CNS-resident IL-10 immune niche during EAE.	158
SLAMF7 induced changes in B cell maturation.....	160
Deep phenotyping of B cells at steady state and during EAE reveals plasma cell alterations in SLAMF7 ^{-/-} mice.....	162
Discussion	165
Materials and Methods	168
CHAPTER: 7 Absence of ERAP1 in B cells increases susceptibility to CNS autoimmunity, alters B cell biology, and mechanistically explains genetic associations between ERAP1 and Multiple Sclerosis.....	
Abstract	173
Abstract	174

Introduction.....	175
Results	177
ERAP1 ^{-/-} mice have increased neuroinflammation and an altered CNS immune landscape following EAE induction.....	177
Exhaustive profiling of the resident CNS IL-10 immune compartment.	179
Comparison of CNS immune cell states and IL-10 production between WT and ERAP1 ^{-/-} mice.	181
ERAP1 ^{-/-} susceptibility to EAE is B cell-dependent.....	184
Deep phenotyping of B cells during EAE reveal increased activation and specific decreases in B1 B cells in ERAP1 ^{-/-} mice.....	186
Lack of ERAP1 in B cells leads to reduced proliferation in vivo and lack of B cell engraftment during EAE.	188
Human B cell subset dysregulation in individuals carrying the ERAP1 K528R SNP.	190
Discussion	192
Materials and Methods	199
CHAPTER: 8 Summary/Discussion	207
CHAPTER: 9 Future work	212
REFERENCES	217

LIST OF TABLES

Table 1: Signaling lymphocytic activation molecule [SLAM] family members and their known roles during viral infection.....	9
Table 2: Cluster characteristics.....	54

LIST OF FIGURES

FIGURE 1: Role of SLAMF2 in orchestrating DC–T cell interactions.....	13
FIGURE 2: Viral manipulation of SLAMF2 to evade host immunity	15
FIGURE 3: SLAMF7 silent and responsive monocytes.	27
FIGURE 4: HIV+ individuals have increased expression of SLAMF7 on their PBMCs and SLAMF7 is upregulated by IFN α	49
FIGURE 5: Activation of the SLAMF7 receptor on monocytes inhibits their IFN α -mediated production of CXCL10.....	51
FIGURE 6: SLAMF7 silent patients have elevated plasma levels of proinflammatory factors and cluster distinctly from SLAMF7 responsive patients.	53
FIGURE 7: Monocytes from SF7S and SLAMF7 responsive patients do not differ in expression levels of SLAMF7 or EAT-2.....	55
FIGURE 8: SLAMF7 activation on monocytes is selective for alpha chemokines and may not be mediated by any of the inhibitory phosphatases known to interact with SLAMF7.	57
FIGURE 9: SLAMF7 activation inhibits monocyte infection with HIV-1 in vitro and down-regulates CD16.	59
FIGURE 10: Neutrophils are SLAMF7- and CXCL10+ and do not respond to SLAMF7 activation.	62
FIGURE 11: Graphical diagram for selected steps in part 1 of procedure (PBMC) isolation.	75
FIGURE 12: FACS plots showing subtypes of monocytes between 2 healthy blood donors.	77
FIGURE 13: Example FACS analysis.....	78
FIGURE 14: SLAMF7 is co-expressed with multiple exhaustion markers on CD3/CD28 stimulated human T cells.....	92
FIGURE 15: SLAMF7 activation induces expression of inhibitory receptors and exhaustion promoting transcription factors in CD8+ and CD4+ T cells.....	95
FIGURE 16: SLAMF7-activated T cells are distinct from terminally exhausted T cells and are capable of producing cytokines upon re-stimulation.....	97

FIGURE 17: Alterations in T cell signaling pathways following SLAMF7 activation	99
FIGURE 18: SLAMF7 correlates with exhaustion markers and is linked to poor survival in ccRCC.	101
FIGURE 19: SLAMF7 expression in the ccRCC immune niche and associations with T cell phenotypes and patient survival.	103
FIGURE 20: SLAMF7 expression in the TME propels CD8+ T cells towards terminal exhaustion and impacts tumor growth.....	106
FIGURE 21: SLAMF7 expression on TAMs drives T cell exhaustion.	108
FIGURE 22: Ad-SF7-Fc expresses SF7-Fc and activates NK cells and DCs.	120
FIGURE 23: Ad-SF7-Fc induces a Th1 cytokine and interferon response.....	122
FIGURE 24: Control of CT26 tumor growth by Ad-SF7-Fc in the absence of an increased adaptive immune response.....	123
FIGURE 25: Ad-SF7-Fc controls B16 tumor growth without affecting T cell exhaustion or remodeling the TME.	126
FIGURE 26: SLAMF7 expression across the TME and tumor inflating myeloid cell phenotypes following Ad-SF7-Fc treatment.....	128
FIGURE 27: EAT-2 expression in immune cells from adenovirus treated B16 tumors as an indicator of response to treatment.	130
FIGURE 28: Mechanistic predictions of the function of SF7-Fc in B16 tumors.....	132
FIGURE 29: iEN machine learning identifies factors underlying tumor response to Ad-SF7-Fc.	134
FIGURE 30: SLAMF7 displays unique expression patterns in the CNS and protects from EAE...	154
FIGURE 31: SLAMF7-induced changes in the CNS immune cell landscape and elsewhere during EAE.....	156
FIGURE 32: The resident CNS IL-10 immune niche in WT and SLAMF7 ^{-/-} mice during EAE.....	159
FIGURE 33: SLAMF7 modulation of B cells and CNS B cell differences between WT and SLAMF7 ^{-/-} /- mice.	161
FIGURE 34: Deep phenotyping of splenic and CNS B cell subsets in WT and SLAMF7 ^{-/-} mice. .	163

FIGURE 35: ERAP1 ^{-/-} mice are more susceptible to EAE and exhibit alterations in the CNS immune landscape.	178
FIGURE 36: Single-cell profiling of the CNS resident IL-10 ⁺ immune compartment.	180
FIGURE 37: In depth comparison of resident CNS immune cell states and IL-10 production between WT and ERAP1 ^{-/-} mice.	182
FIGURE 38: Loss of ERAP1 in B cells renders mice more susceptible to EAE.	183
FIGURE 39: Reconstruction of the splenic and CNS B cell compartments during EAE reveal specific decreases in B1 cells and increased activation of ERAP1 ^{-/-} B cells.	187
FIGURE 40: ERAP1 ^{-/-} B cells display impaired proliferation in vivo during EAE.	189
FIGURE 41: Integrated scRNA-seq analysis of human B cells reveal subset-conserved dysregulation in B cells carrying the K528R ERAP1 SNP.	191

KEY TO ABBREVIATIONS

SLAMF7	SLAM family member 7
SF7	SLAMF7
SLAM	Signaling lymphocytic activation molecule
TME	Tumor microenvironment
ccRCC	clear cell renal cell carcinoma
TCGA	The Cancer Genome Atlas
TAM	tumor-associated macrophage
CytoF	Cytometry by time of flight
CL	Cross-linking
tSNE	t-distributed stochastic neighbor embedding
EAT-2	Ewing's sarcoma associated transcript 2
ITSM	Immunoreceptor tyrosine-based switch motif
SAP	SLAM-associated protein
XLP	X-linked lymphoproliferative disorder
PRR	Pattern recognition receptor
TLR	Toll-like receptor
IFN	Interferon
CMI	Cell-mediated immunity
HAND	HIV-associated neurocognitive disorder
CMV	Cytomegalovirus

HCV	Hepatitis C virus
ILC	Innate lymphoid cell
GPI	Glycosylphosphatidylinositol
HTLV-1	Human T cell leukemia virus 1
CTL	Cytotoxic lymphocyte
TIL	Tumor-infiltrating lymphocyte
EBV	Epstein-Barr virus
HSC	Hematopoietic stem cell
RSV	Respiratory syncytial virus
cART	Combined anti-retroviral therapy
SLE	Systemic lupus erythematosus
SF7S	SLAMF7 silent
TNF	Tumor necrosis factor
CNS	Central nervous system
MTB	Mycobacterium Tuberculosis
EAE	Experimental autoimmune encephalomyelitis
UMAP	Uniform manifold approximation and projection
FACS	Fluorescence-assisted cell sorting
PMBCs	Peripheral blood mononuclear cells
HC	healthy control
ISG	Interferon stimulated gene
LTNP	Long term non-progressor

RCC	Renal cell carcinoma
RNA-seq	RNA sequencing
TF	Transcription factor
TIDE	Tumor immune dysfunction and exclusion
Treg	Regulatory T cell
WT	Wild type
MS	Multiple Sclerosis
BAMs	Border-associated macrophages
MdCs	Myeloid-derived cells
BCR	B cell receptor
TCR	T cell receptor
iEN	Immunological elastic net
I.T.	Intra-tumoral
I.P.	Intra-peritoneal
I.V.	Intra-venous
ADCC	Antibody-dependent cellular cytotoxicity
Ad	Adenovirus
AUROC	Area under the receiver operating curve
GLMM	Generalized linear mixed model
ERAP1	Endoplasmic reticulum aminopeptidase 1
SNP	Single nucleotide polymorphism
MDS	Multidimensional scaling

AS	Ankylosing spondylitis
Breg	regulatory B cell
FO	Follicular
MZ	Marginal zone
APC	Antigen presenting cell
ER	Endoplasmic reticulum
DEG	Differentially expressed gene
CFA	Complete Freund's Adjuvant

CHAPTER: 1 Introduction

Portions of this chapter are reproduced from: O'Connell, P., et al. "SLAM Family Receptor Signaling in Viral Infections HIV and Beyond". Vaccines 2019.

Overview of Multiple Sclerosis

MS is a chronic, degenerative, inflammatory autoimmune disease affecting the CNS and is most common in women of child-bearing age with a 3:1 female:male affected ratio [1]. Along with various symptoms presenting across time and space, MS is first and foremost characterized by the presence of plaques of demyelination across the CNS, characteristically diagnosed by the finding of gadolinium-enhancing lesions on MRI [1]. The array of MS symptoms is vast, but some common ones include: limb weakness, movement issues, vision issues, tremors, altered skin sensation, numbness, vertigo, neuropathic pain, and dysphagia [2]. There are five subtypes of MS: clinically isolated syndrome, RRMS, SPMS, PPMS, and radiologically isolated syndrome [2]. Clinically isolated syndrome is diagnosed when an individual has a single episode yet improves without treatment; this however can progress to full MS in some cases [2]. RRMS, or relapsing remitting MS, is the most common form of MS and involves acute episodes of symptoms separated by periods of remission [2]. PPMS, or primary progressive MS, is the most severe form of the disease and is characterized by a constant decline in patient function without periods of remission [2]. SPMS, or secondary progressive MS, occurs when RRMS develops into PPMS [2]. Finally, a newly defined subtype exists, radiologically isolated syndrome, which is defined as a positive MRI diagnosis of MS in the absence of any symptoms [3].

The precise mechanism(s) underlying MS pathogenesis remains a mystery, but decades of research have confirmed that both genetic and environmental elements contribute to MS susceptibility [1]. On the environmental side, individuals living farther from the equator and/or who receive low levels of Vitamin D/sunlight have an increased risk for MS [1]. On the genetics

side, numerous large GWAS studies have identified over 500 genomic regions linked to MS [4], yet most of these associations have not been investigated in depth. Many of the strongest genetic associations to MS are with genes involved in immune regulation including: various MHC isoforms (including *HLA-DR15* which represents the strongest association), *IL4*, *IL6*, *IL2RA*, *IL17R*, and more [2]. Sibling studies have determined that both monozygotic and dizygotic twins have an increased risk of co-occurrence of MS; more so in monozygotic twins, as would be expected for a disease with a strong genetic component [1]. Together, these findings paint MS as a highly complex autoimmune disease, with no currently identifiable central mechanism. The evidence does point to some defect(s) in the immune system as being the most likely culprit though [1, 4]. What precisely causes the immune system to enter a state rendering individuals susceptible to CNS autoimmunity, and what sets this off, are currently the most pressing questions in the field.

Early research into the immunological mechanism(s) of MS pointed to a purely T cell-based model of autoimmunity [1]. More recent work has shown that many different immune cell types contribute to MS pathogenesis, in different ways, at differing stages of the disease course [1]. It is also appreciated that the CNS resident myeloid cell type, microglia, play an important role in MS [1]. Other CNS infiltrating myeloid cells tend to have proinflammatory roles in MS and can contribute to disease progression [1]. But perhaps the most intriguing immune cell type implicated in MS pathogenesis now is the B cell [5]. This came after the surprising discovery that MS patients treated with a B cell-depleting antibody, rituximab, in an effort to ablate production of CNS antibodies, often went into sustained remission [6]. Subsequent studies

however found that the remission was not dependent upon loss of antibody production, as rituximab does not deplete terminally differentiated plasma cells [7]. This finding spurred the development of more effective B cell depleting antibodies (ie. ocrelizumab), which are now a mainstay MS therapy showing some of the best efficacy of all MS disease modifying agents [1]. However, why depleting B cells leads to remission in MS is a highly investigated topic of great importance to the field, as this may lead to more targeted therapies lacking the side effects that ensue with the current strategies that results in non-discriminate, pan-B cell depletion [1]. Such targeted B cell therapies may also spare beneficial B cell subsets thus offering better disease control. This could be especially important for PPMS and SPMS since these do not respond well to current, pan-B cell depleting therapies [8].

SLAMF7 is a member of the SLAM Family of Receptors

The signaling lymphocytic activation molecule [SLAM] family of receptors are a set of nine conserved cell-surface glycoproteins present on the cell surface of immune cells (Table 1). SLAM family receptors are special in that most of them (SLAMF1, 3, 5, 6, and 7) are self ligands [9]. SLAMF2 and SLAMF4 serve as ligands for each other, and the ligands of SLAMF8 and SLAMF9 are unknown. SLAM family receptors are generally understood to function as both adhesion molecules and immuno-modulators [9]. Most SLAM family members (except SLAMF2, 8, and 9) contain immunoreceptor tyrosine-based switch motifs (ITSMs) in their cytoplasmic domain, which become phosphorylated upon receptor ligation, and serve as docking stations to recruit various SH2-domain-containing proteins. Tyrosine-phosphorylated SLAM family ITSMs recruit a number of well-characterized inhibitory phosphatases (SHP-1, SHP-2, SHIP-1), in addition to the

two SLAM family unique adaptor proteins, SLAM-associated protein (SAP, also known as SH2D1A) and EAT-2 (also known as SH2D1B) [10].

Decades ago, it was discovered that inactivating mutations in the SAP protein, rendering it inactive, caused the rare genetic disease X-linked lymphoproliferative disorder (XLP) [11]. XLP is characterized by alterations of cellular and humoral immune responses, thus predisposing young males to Epstein–Barr virus [12]-associated morbidity and mortality. The discovery of this genetic association spurred research into the function of SAP, its ligands—the SLAM family of receptors—and what role these molecules play in immune regulation and response to infection.

As SLAM receptors are present on most immune cells, but in varying amounts and combinations, they comprise a complex immuno-regulatory network that plays an important role in maintaining balanced immune responses. Efforts to distill the basic elements of this system have revealed that SLAM family receptors can have both activating or inhibitory functions on immune cells. Whether or not they function to promote immune cell activation typically depends on the presence of their adaptors, SAP and/or EAT-2. In the presence of these adaptors, ligation of SLAM family receptors often results in cellular activation, and in their absence, vice-versa [10]. This simple regulatory mechanism is most conserved and apparent in SLAMF7 and SLAMF7 regulated networks.

For more detailed information on the specifics of SLAM family receptor signaling and the various adaptors capable of binding SLAM family members, please refer to any of these reviews [9, 10, 13, 14].

Immune Responses to Viral Infections

Host responses to viral infections comprise a complex interplay between the innate and adaptive arms of the immune system [15]. Initial responses by the innate immune system serve to quickly combat the offending pathogen and begin to prime and train the adaptive immune system to commence generation of long-lasting immunity [16]. Infection with HIV follows this paradigm, but notably, the innate immune system is not able to prevent long term infection due to some unique characteristics of HIV [17]. Here we will provide a brief summary of host anti-viral responses, using HIV as an example, and highlighting distinct ways in which HIV causes disruption of these processes, and identifying points in this process where SLAM family receptors play a role.

Initial infection with HIV typically occurs in the vaginal or rectal mucosa, where virions infect local CD4⁺ memory T cells and macrophages. HIV infected cells eventually migrate out of the mucosa and reach draining lymph nodes where the virus is further spread to other memory CD4⁺ T cells, macrophages, and dendritic cells [18, 19]. Peak viremia occurs around the third to fourth week following infection [20]. During this time the innate immune system mounts an acute anti-viral response to HIV and HIV-infected cells through the use of pattern recognition receptors (PRRs). PRRs, specifically toll-like receptors (TLRs), on macrophages, monocytes, dendritic cells (DCs), and

other immune cells recognize virion glycoproteins, viral dsRNA, and viral ssRNA [21, 22]. This in turn triggers signaling through NF κ B, IRF3/7, and MAPK pathways among others. Signaling through these well-studied pathways produces a host of pro-inflammatory cytokines, chemokines, and viral restriction factors to help combat early infection [23]. Importantly, myeloid cell responses to PRR activation can be tuned based on signaling from SLAMF1, SLAMF5, SLAMF7, SLAMF8, and SLAMF9 [24-30]. Therefore, the specific microenvironment, including other immune cells interacting with PRR-responding myeloid cells, is essential for tuning myeloid cell responses by SLAMF family-dependent mechanisms. This suggests that modulating SLAM family signaling might impact host anti-viral immune responses. Indeed, we have shown previously that altering SLAM family signaling by overexpressing EAT-2 enhanced both innate and adaptive immune responses to antigens such as HIV-Gag [31]. HIV infection is notable in that it also causes breakdown of the gastrointestinal mucosal barrier allowing for translocation of bacteria and their products into the circulation [32]. Elevated levels of bacteria in the circulation trigger different TLRs contributing to broad activation of the innate immune system. Additionally, SLAM receptors [such as SLAMF1 [33], SLAMF6 [34], and SLAMF8 [29]] have also been shown to modulate innate immune responses following infection with both gram-negative and positive bacteria. Therefore, SLAM receptors may indirectly modulate HIV-induced bacterial translocation.

One of the most important anti-viral cytokines produced is IFN α which is primarily produced by activated plasmacytoid dendritic cells (pDCs) [17, 35, 36]. pDC stimulation through TLR7/8/9 triggers production of high levels of IFN α which orchestrates global anti-viral responses across nearly all cell types [37]. It has been shown recently that SLAMF9 signaling contributes to proper

migration and function of pDCs [38], indicating a potential role for SLAMF9 in pDC-mediated antiviral responses. Following the acute phase of HIV infection, plasma viremia drops significantly, and circulating CD4⁺ T cell levels return to normal levels. During this time activated DCs are also able to present peptides derived from HIV-specific antigens and interact with T cells to begin to develop long-term (adaptive) immunity [16]. DC–CD8⁺ T cell interactions result in clonal expansion of virus specific memory CD8⁺ T cells, which recognize and destroy HIV infected cells presenting HIV-specific antigens [39]. SLAMF2–SLAMF4 interactions between DCs and CD8⁺ T cells, respectively, are necessary to ensure survival of DCs effectively presenting HIV-1 antigens [40]. In tandem, CD4⁺ T cells in lymph nodes activate B cells to generate HIV-specific antibody responses, a process also regulated by SLAMF5 interactions between these cell types [41, 42]. For the vast majority of viral infections, this complex process is successful in fighting off the current infection and generating humoral and cell-mediated immunity (CMI) for prevention of future infections by the same pathogen. However, HIV has a number of ways to circumvent this [43, 44].

Because the body is not able to fully clear HIV, the virus is able to create a state of chronic immune activation believed to underlie many of the secondary pathologies associated with HIV (HIV-associated neurocognitive disorder (HAND), atherosclerosis, insulin resistance, renal failure, osteoporosis, and hepatitis), and be a major cause of disease progression to AIDS [21, 43]. Sustained IFN α production by pDCs is implicated in this progression, a state potentially exacerbated by the presence of HIV-specific antibodies [45]. Chronic translocation of bacteria and bacterial products into the circulation from the gut, termed the “leaky gut hypothesis”, has

SLAM Family Member	Known Direct Interactions with A Virus	Known Immuno-Modulatory Roles during Viral Infection	Expression Pattern
SLAMF1 (SLAM, CD150)	Measles [46]	Th2 polarization [26, 47]	T cells, B cells, macrophages, DCs, platelets, HSCs
SLAMF2 (CD48)	Down-regulated via CMV viral protein m154 [48]	Regulates DC survival and antigen-presentation during T cell interactions [40]	Nearly all hematopoietic cells
SLAMF3 (Ly-9, CD229)	HCV E2 protein [49]		CD4+ T cells, CD8+ T cells, B cells, plasma cells, NK cells, NKT cells, ILCs, DCs, monocytes, macrophages, and HSCs
SLAMF4 (2B4, CD244)	Can be blocked via interactions with CMV SLAMF2 decoy receptor [50] Influenza viral HA protein [51]	T cell exhaustion [52-57]	NK cells, CD8+ T cells, NKT cells, $\gamma\delta$ T cells, monocytes, basophils, eosinophils, DCs, mast cells
SLAMF5 (CD84)		DC pro-inflammatory signaling [28] Germinal center formation [42]	B cells, T cells, monocytes, macrophages, DCs, platelets, thymocytes, NK cells, NKT cells, basophils, eosinophils.
SLAMF6 (NTB-A, Ly-108, CD352)	Degradation via interactions with HIV-1 vpu viral protein [58-60]	Cytotoxic interactions between virally infected cells and NK cells [51]	NK cells, NKT cells, T cells, B cells, macrophages, pDCs, DCs, thymocytes, eosinophils, neutrophils.
SLAMF7 (CRACC, CD319, CS1)		Regulates monocyte responses to type I interferons [27] Regulates monocyte susceptibility to HIV-1 infection [27]	NK cells, CD4+ T cells, CD8+ T cells, NKT cells, classical monocytes, inflammatory monocytes, macrophages, DCs, B cells, plasma cells
SLAMF8 (BLAME, CD353)		Regulation of macrophage pro- and anti-inflammatory functions [29]	B cells, T cells, monocytes, macrophages, DCs, platelets, thymocytes, NK cells, NKT cells, basophils, eosinophils.
SLAMF9 (SF2001, CD84H1)		Regulation of macrophage and pDC responses [30, 38]	Monocytes, pDCs, DCs, T cells, B cells, macrophages.

Table 1: Signaling lymphocytic activation molecule [SLAM] family members and their known roles during viral infection. Cytomegalovirus, CMV; dendritic cells, DCs; hepatitis C virus, HCV; innate lymphoid cells, ILCs; hematopoietic stem cells, HLCs; NK cells, Natural Killer cells.

also been suggested to contribute to these sustained responses [32]. HIV is also able to interfere with proper development of the adaptive immune response by interfering with B cell antibody production. It has been observed that gp120 can induce chronic activation of B cells through CD40-independent pathways, thus preventing the generation of powerful, broadly-neutralizing antibodies [61]. These are just a few of the many ways HIV has been shown to dysregulate the immune system; for a more detailed summary please refer to the following references [17, 21].

SLAMF1 (SLAM, CD150)

The first identified member of the SLAM family, SLAMF1 was initially discovered as the binding partner of SAP [62]. It is expressed on T cells, B cells, macrophages, DCs, platelets, and hematopoietic stem cells (HSCs), and is characterized by its flexible structure and high degree of glycosylation [14]. It functions on immune cells to modulate their activation states, milieu of secreted cytokines, and phagocytic ability. With regard to phagocytosis, it has been shown that SLAMF1 is able to bind to *escherichia coli* via OmpC and OmpF, and upon ligation, recruits Beclin-1 to its intracellular domain allowing for enhancement of bacterial phagocytosis [5].

Of all the SLAM family members, SLAMF1 has arguably been the most well-known association with viral infections, as it was discovered to be one of the receptors used by the measles virus to gain entry into cells [46]. In fact, it was later found that the measles virus binds to SLAMF1 via interactions with hemagglutinin MH-V, and that SLAMF1 is a universal receptor for all morbilliviruses (of which measles is a member). This genus-level receptor tropism likely stems from a few highly conserved domains on the extracellular region of SLAMF1 [63].

In addition to serving as a direct viral receptor on immune cells, SLAMF1 has various immunomodulatory roles in the immune cells it is expressed on. On cells of myeloid lineage, including macrophages and DCs, SLAMF1 is typically expressed at a low level, but becomes up-regulated in response to pro-inflammatory stimuli such as LPS, IL-1 β , TNF α , and IL-6 [24, 34]. The precise function of SLAMF1 on activated DCs has been debated in the literature. Bleharski et al. initially described SLAMF1 activation on CD40L-stimulated DCs as being pro-inflammatory, noting increased levels of IL-8 and IL-12 [25]. However, a later paper by Rethi et al. demonstrated that SLAMF1 signaling on CD40L-stimulated DCs was in fact inhibitory, with decreased IL-12 secretion and impaired ability to induce naïve T cells into Th1 cells [24]. The difference in results was attributed to the mode of SLAMF1 activation, with the initial report using soluble anti-SLAMF1 antibodies, and the latter paper using L929 cells stably expressing SLAMF1 as the mode of receptor ligation [24]. The discrepancy in the results obtained using these different methods suggests that the first report, using a soluble anti-SLAMF1 antibody, may be blocking the SLAMF1 receptor, as most soluble antibodies perform blocking functions unless they have been specifically designed as agonistic antibodies.

Complicating matters further is a study demonstrating that SLAMF1 knockout macrophages have impaired production of IL-12p70, IL-12p40, TNF α , and nitric oxide [26], suggesting SLAMF1 may be an activating receptor. It is hard to compare this study to the two previously mentioned studies, as those were performed using primary human cells and this study used a murine model. Differences in immune responses to signaling from various members of the SLAM family has been noted between human and murine immune cells [27, 51].

SLAMF1 has also been described to have a specific role in T cells. SLAMF1 was noted to be necessary for optimal production of IL-4 and IL-13, classical Th2 polarizing cytokines [26, 51]. This suggests that SLAMF1 plays a role in regulating the production of antibodies during infections. Altogether, the role of SLAMF1 in infection is interesting in that it both acts directly as a viral cell surface receptor, and modulates signaling on immune cells key to combating viral and bacterial infections.

SLAMF2 (CD48)

SLAMF2 is unique among SLAM family members in that it is expressed on most lymphocytes, contains a Glycosylphosphatidylinositol (GPI) anchor, and is not a homotypic receptor. SLAMF2 is the ligand for SLAMF4 (2B4), and vice-versa. Additionally, in rodents, SLAMF2 is also able to bind CD2, but this binding is not conserved in humans which can make translating discoveries in murine models regarding SLAMF2 function difficult [64]. On immune cells it has been observed to generally function as an adhesion molecule and co-stimulator of NK and T cells.

SLAMF2 was initially believed to play an indirect role in regulating CMI during viral infections, as SLAMF4 is a well described modulator of NK and CD8⁺ T responses during viral infections [40, 65-67]. In support of this indirect role it was shown that SLAMF2 ligation on free DNA-activated DCs (mimics viral infection) prolonged their survival [40]. The mechanism underlying this effect was shown to be due to decreased apoptosis via impaired production of DC-generated IFN β [40]. Furthermore, SLAMF2 ligation on activated DCs induced the production of granzyme B inhibitor protease inhibitor-9 (SERPINB9), which prevented T cell-mediated lysis of DCs (Figure 1A) [40].

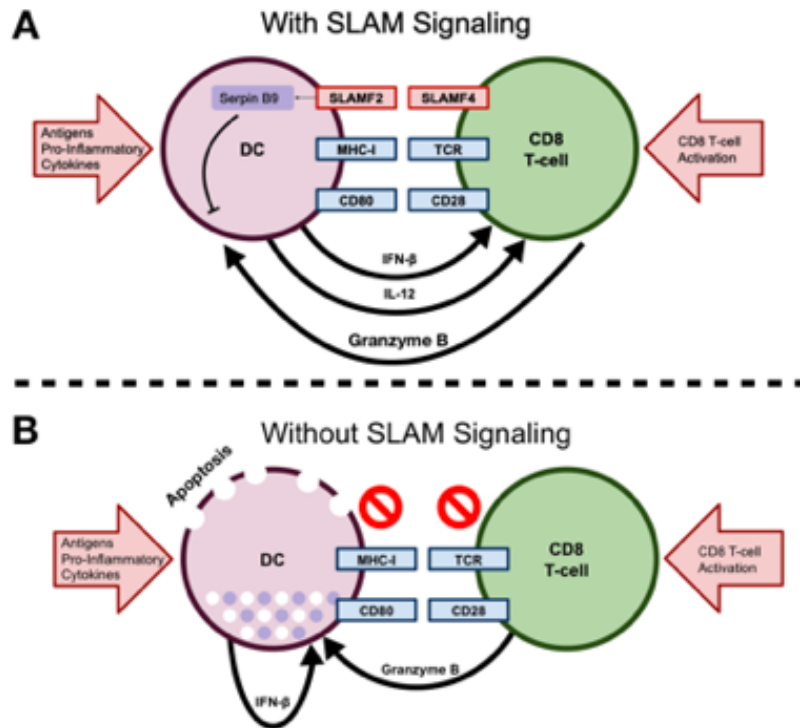


FIGURE 1: Role of SLAMF2 in orchestrating DC-T cell interactions

(A) Ligation of SLAMF2 on DCs (or other antigen presenting cells) via interactions with SLAMF4 on an interacting CD8 T cell results in increased expression of SERPINB9. SERPINB9 protects DCs from lysis granzyme B-dependent T cell lysis. (B) Interactions between DCs and CD8 T cells when SLAMF2–SLAMF4 interactions are absent on DCs, which renders DCs susceptible to apoptosis, both from autocrine IFN β production and by granzyme B produced by CD8 T cells.

This led to the proposition of an intriguing model where proper SLAMF2–SLAMF4 interaction between DCs and activated T cells (express high levels of SLAMF4) allows for enhanced DC survival and antigen presentation to assist in clearing infections. In scenarios where there was an absence of CD8⁺ T cell–DC interactions (i.e., no SLAMF2–SLAMF4 interaction), the DC undergoes apoptosis via production of its own pro-inflammatory cytokine, IFN β (Figure 1B). This regulatory mechanism helps to ensure that only DCs presenting useful antigens to CD8⁺ T cells persist, and other DCs that are inducing non-specific, background inflammation do not persist [40]. This complex model describing SLAM family receptor interactions between various immune cells in

the context of viral infection shows how SLAM family receptors are important maestros orchestrating immune responses.

Furthermore, SLAMF2 has been identified as being a direct modulator of CD4⁺ T cell and macrophage inflammatory responses [68, 69]. Studies utilizing SLAMF2 deficient mice revealed that SLAMF2 is necessary for proper CD4⁺ T cell activation and proliferation [68, 69]. Additionally, it was determined that SLAMF2 expression on macrophages was necessary for optimal TNF α and IL-12 production in response to innate stimuli [69].

Due to SLAMF2's importance in regulating CMI, it was theorized that some viruses may attempt to modulate SLAMF2 to circumvent its role in combating viral infections. Indeed, it was found that cytomegalovirus (CMV), HIV, and potentially, human T cell leukemia virus type 1 (HTLV-1), have evolved to do just this [48, 50, 66, 67]. CMV is able to evade SLAMF2-mediated immune responses via two independent mechanisms: down-regulation of SLAMF2 on infected cells via the viral protein m154 [48] and by producing a soluble SLAMF2 decoy receptor [50]. The CMV viral protein m154 was shown to directly down-regulate SLAMF2 in infected macrophages via proteolytic degradation (Figure 2A) [48]. This led to impaired NK cell cytotoxicity against CMV infected cells and, critically, infection with a m154 deficient CMV virus displayed an attenuated phenotype in vivo [48]. Certain strains of CMV, notably Owl Monkey CMV, encode a decoy SLAMF2 protein in their genome [50]. Infection of cells with these viruses was observed to secrete high levels of a soluble SLAMF2 decoy protein [50]. These SLAMF2 decoy proteins were able to bind with high affinity to SLAMF4 on host immune cells and could prevent NK cell adhesion and

cytotoxicity against infected cells (Figure 2B) [50]. A similar, but less well understood, method of SLAMF2 modulation occurs during HIV infection [66]. In vitro cell culture experiments using primary human T cells and HIV-1 showed that HIV-1 infected T cells down-regulated a number of important NK cell ligands including SLAMF2 [66]. This prevented optimal NK cell-mediated lysis of HIV-1 infected T cells [66]. Additionally, there is preliminary evidence that the tax protein from HTLV-1 is able to down-regulate SLAMF2 in infected cells and prevent CD8⁺ T cell-mediated cytotoxicity [67].

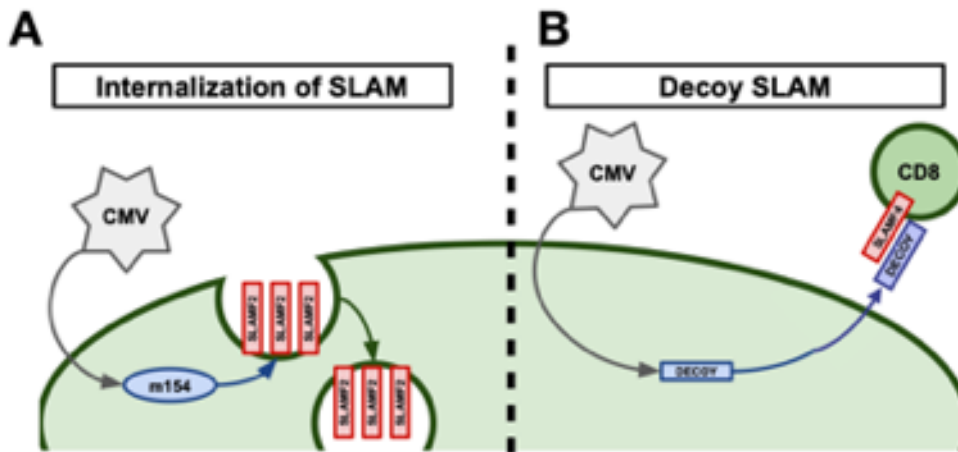


FIGURE 2: Viral manipulation of SLAMF2 to evade host immunity

(A) Following infection, the CMV viral protein m154 proteolytically degrades SLAMF2 in order to decrease receptor expression on the cell surface. (B) Owl Monkey CMV produces a decoy SLAMF2 receptor following infection of a cell. The SLAMF2 decoy protein is secreted and, once soluble, prevents proper SLAMF2–SLAMF4 interactions from occurring between CMV infected cells and cytotoxic lymphocytes, respectively.

However, not all viruses display the ability to interfere with host immunity through SLAMF2-specific mechanisms. Epstein–Barr virus [12] infection of B cells is known to induce up-regulation of SLAMF2, which has been suggested to assist in CMI towards infected cells [65]. Such a mechanism would in theory allow for better adhesion and cytotoxicity (via SLAMF4 signaling on CD8⁺ T cells and NK cells). It is clear that SLAMF2 plays an important role in controlling cell-

mediated immunity in the setting of viral infections, and we are only just beginning to understand the breadth of evasion strategies used by viruses to undermine it

SLAMF3 (Ly-9, CD229)

The third member of the SLAM family of receptors, SLAMF3, is widely expressed on lymphocytes, notably on CD4⁺ T cells, CD8⁺ T cells, B cells, plasma cells, NK cells, NKT cells, innate lymphoid cells (ILCs), DCs, monocytes, macrophages, and hematopoietic stem cells (HSCs). Interestingly, it is also known to be expressed on hepatocytes [49]. SLAMF3 is a relatively understudied member of the SLAM family, and to date, studies have only revealed roles for SLAMF3 in control of T cell inflammatory responses and NKT cell development [14].

SLAMF3 may play a role in adenovirus (Ad) infections, as a large-scale interactome study using the E3 protein from Ad revealed binding to SLAMF3, in addition to a number of other SLAM family members [70]. The importance and consequences of this interaction are not yet known and this represents an interesting area of future study.

Compared to other SLAM family members, many of which modulate DC and macrophage function in some manner, loss of SLAMF3 on macrophages was not observed to affect immune responses [71]. While loss of SLAMF3 on T cells was shown to impair Th2 responses [71], mice with global loss of SLAMF3 did not display enhanced susceptibility to LCMV infection in the same manner as SAP knockout mice do [71]. This suggest that while SLAMF3 does play some role in

modulating immune cell function, the effects are not as important as that of other SLAM family members and may be redundant.

SLAMF3's expression on hepatocytes is its only known direct link to viral infections. A single report has shown that HCV is able to bind directly to the first N-terminal domain of SLAMF3 and use this as a cellular entry mechanism [49]. More specifically, they noted that the HCV envelope protein, E2, was responsible for this interaction. In further support of this important interaction for HCV pathogenesis, it was observed that SLAMF3 expression on hepatocytes correlated with their susceptibility to HCV infection [49].

SLAMF4 (2B4, CD244)

SLAMF4 is arguably the most well studied member of the SLAM family of receptors, with extensively-characterized functions on multiple lymphoid cell types [72]. SLAMF4 is expressed on NK cells, CD8⁺ T cells, NKT cells, $\gamma\delta$ T cells, monocytes, basophils, eosinophils, DCs, and mast cells [9, 14]. Deciphering the underlying signaling mechanisms of SLAMF4 have been complicated by the fact that it can bind both SAP and EAT-2 adaptors, in addition to numerous inhibitory phosphatases. Furthermore, studies have shown that the antigen density of SLAMF4 on CD8⁺ T cells differentially determines its function, with ligation of SLAMF4 when it is present at low levels inducing activating signals, and ligation of SLAMF4 when it is present at high levels producing inhibitory signals [52, 73, 74]. A further difference between SLAMF4 and other SLAM family members is that it is not a homotypic receptor and functions via ligation to SLAMF2.

To date, SLAMF4 is best known for its function on CD8⁺ T cells as an exhaustion marker and inhibitory receptor. This fact, combined with our current knowledge that chronic viral infections induce large numbers of exhausted CD8⁺ T cells, has contributed to a significant body of knowledge regarding SLAMF4 in the setting of chronic viral infections. Studies of SLAMF4 on CD8⁺ T cells of patients with chronic hepatitis B virus (HBV) infection have shown that chronic HBV infection increases the number of SLAMF4⁺ CD8⁺ T cells both in the peripheral circulation and in the liver, often with co-expression of PD-1 [53]. Clearance of viral infection decreased the numbers of SLAMF4⁺ CD8⁺ T cells, and blocking of SLAMF4 ex vivo allowed for improved T cell proliferation, cytokine production, and cytotoxicity [53]. Very similar effects were noted in patients with chronic hepatitis C virus (HCV) infection [54]. In the setting of chronic HCV infection, SLAMF4 was observed to be up-regulated on virus-specific CD8⁺ T cells, functioned as an inhibitory receptor on these cells, and prevented virus-specific CD8⁺ T cell proliferation [54]. A separate report, studying the role of SLAMF4 in HIV infection, noted that respiratory syncytial virus (RSV)-specific CD8⁺ T cells in HIV⁺ patients responded differentially to SLAMF4 ligation. The subset of RSV-specific CD8⁺ T cells that had the capability to down-regulate SLAMF4 were able to respond best to stimulation and those that retained high levels of SLAMF4 showed impaired IFN γ production [55].

The role of SLAMF4 directly on HIV-specific CD8⁺ T cells has also been studied [75]. During HIV infection, patients with elevated SLAMF4⁺ CD8⁺ T cells showed marked disease progression in comparison to those with low levels of SLAMF4⁺ CD8⁺ T cells [75]. This suggested that SLAMF4 may be a marker of dysfunctional CD8⁺ T cells or activated CD8⁺ T cells that preferentially destroy

host CD4⁺ T cells; both of which could lead to disease progression in HIV. Support for the former hypothesis came from a study looking at SLAMF4 signaling more in-depth [56]. Here it was observed that HIV-1-specific CD8⁺ T cells from patients exhibited an immature phenotype, displaying high levels of SLAMF4 and PD-1. Co-expression of these two markers correlated with other markers of disease progression including viral load. Blocking of SLAMF4 and PD-1 in ex vivo T cell cultures from HIV patients allowed for increased HIV-1-specific CD8⁺ T cell proliferation [56]. This suggested that SLAMF4 expression on CD8⁺ T cells in the setting of chronic HIV-1 infection is a true inhibitory receptor. Confirming this, is work showing that SLAMF4⁺ CD8⁺ T cells from HIV-1 negative persons, stimulated with HIV-antigen-pulsed DCs, have less cytolytic activity compared to SLAMF4⁻ CD8⁺ T cells [57].

In contrast to the number of reports studying the inhibitory function of SLAMF4 on CD8⁺ T cells, there are a few reports describing activating effects for SLAMF4 on CD8⁺ T cells during viral infections [51, 76]. For example, it has been shown that HIV elite controllers harbor a population of HIV-specific SLAMF4⁺ CD8⁺ T cells with high cytolytic capacity, and this unique subset is not commonly present in chronic progressors [77], suggesting that signaling downstream of SLAMF4 might be important for the control of HIV infection. In the setting of HTLV-1 infection, which can present with a CD8⁺ T cell-mediated encephalitis, elevated levels of SLAMF4 were observed on CD8⁺ T cells compared to uninfected controls [76]. Additionally, infected individuals presenting with neurological disease had elevated levels of SAP in their CD8⁺ T cells compared to those without neurological disease. Blockade of SLAMF4 signaling in ex vivo cultures inhibited production of cytotoxic factors, suggesting that, in this setting, SLAMF4 is functioning as an

activating receptor. It is possible that the high levels of SAP, which are known to control SLAMF4 signaling, are responsible for SLAMF4 functioning as an activating receptor here. Similarly, there is evidence that SLAMF4 plays an activating role during influenza infection [51]. Here, SLAMF4 was discovered to be able to directly bind the influenza viral HA protein, stimulate CD8⁺ T cell activation, and induce lysis of influenza-infected cells. This activating effect could potentially be attributed to the binding of SLAMF4 to a different ligand than it normally does. Interestingly, the authors found that murine SLAMF4 lacked the conserved residues in human SLAMF4 that were required for binding to influenza HA, and as expected, could not bind to influenza [51]. This further highlights the complexities of studying SLAM family members using murine models.

While SLAMF4 has been best studied on CD8⁺ T cells, there are a number of reports assessing the role of SLAMF4 on NK and NKT cells in the setting of HIV infection [78, 79]. In NK cells it was found that SLAMF4 expression increased on NK cells over a course of two years on HIV⁺ individuals, even in the presence of combined anti-retroviral therapy (cART) [78]. Additionally, reductions in the number of SLAMF4⁺ NK cells negatively correlated with levels of cells containing pro-virus [78]. Together, this suggests that SLAMF4 signaling on NK cells in the setting of chronic HIV infection is important for viral control via CMI. Invariant NKT cells (iNKT) are an understudied subset of NKT cells which play a role in innate immunity. A recent study looking into the role of SLAMF4 on iNKT cells during chronic HIV infection found potentially important associations [79]. It was observed that iNKT cells from HIV⁺ individuals have high levels of SLAMF4 on their CD4⁺ iNKT cells and show impaired IFN γ production. Furthermore, the percent of SLAMF4⁺ iNKT cells inversely correlated with CD4⁺ T cell count and CD4⁺/CD8⁺ ratio, and positively correlated with

viral load [79]. This indicates that dysregulation of SLAMF4 on iNKT cells may be a marker of disease progression, and potentially, excessive CMI, causing destruction of host lymphocytes. While the precise roles of SLAMF4 signaling both in a variety of immune cell types and a variety of viral infections remains to be determined, it is clear that HIV and other viral infections up-regulate SLAMF4 and that this is a potential mechanism underlying immune dysfunction.

SLAMF5 (CD84)

SLAMF5 is broadly expressed on many immune cell types including B cells, T cells, monocytes, macrophages, DCs, platelets, thymocytes, NK cells, NKT cells, basophils, and eosinophils. SLAMF5 can bind to both SAP and EAT-2, and is best known for its role in regulating adhesion between T cells and B cells, allowing for proper humoral responses, it also plays a role in regulating immune signaling in numerous other immune cells.

In contrast to some of the other SLAM family receptors, the only known association between SLAMF5 and viral infections is from a large-scale interactome screen [70]. Similarly to SLAMF3, SLAMF5 was observed to bind to E3 from adenovirus with high affinity. Follow-up studies discovered that binding of E3 proteins to SLAMF5 stimulated activation of the receptor as evidenced by phosphorylation of its ITSM. This receptor activation had functional importance as it inhibited T cell receptor signaling in Jurkat cells as determined by ERK1/2 phosphorylation [70]. While these in vitro studies of SLAMF5 signaling in the context of T cell activation in adenovirus infection are interesting, simple studies using SLAMF5 deficient mice in the context of adenovirus

infection or Ad-mediated vaccination strategies [31, 80, 81] would be important to confirm physiologic significance.

Dendritic cell responses to viral infections are important for generating both innate and adaptive anti-viral responses. SLAMF5 signaling in DCs is necessary for proper pro-inflammatory immune responses involving IL-1 β , IL-23, and IL-12, and this is dependent on IRF8 [28]. Specifically, IRF8 is induced in DCs when they become activated and is an important transcription factor that orchestrates many of their responses [82]. Agod et al. have shown that SLAMF5 signaling in DCs is important for stabilizing IRF8, preventing its degradation by TRIM21, and allowing for proper inflammatory responses [28].

While T cell–DC interactions are important in viral immune responses, T cell–B cell interactions are critical for developing long-term humoral immunity; SLAMF5 has been described as being vital for this interaction [83]. Adhesion via SLAMF5-SLAMF5 homotypic interactions between B cells and T cells allows for appropriate germinal center formation in vivo [83]. This interaction requires the SLAM family adaptor SAP, and also interactions involving SLAMF6. Further supporting this is a study showing that SLAMF5 is up-regulated on memory B cells, is able to recruit both SAP and EAT-2, and functionally signals in memory B cells [84]. Furthermore, in a murine model of Systemic Lupus Erythematosus (SLE), SLAMF5 was shown to be important in preventing spontaneous germinal center formation and auto-antibody production, characteristic pathologies found in humans with SLE [42]. Proper regulation of humoral immunity is important in a number of viral infections, notably HIV-1, where it has been shown that the body has the

potential to develop potent broadly neutralizing antibodies against HIV-1 [85]. Importantly, the development of these broadly neutralizing antibodies can be a double-edged sword, as anti-HIV-1 antibodies can also chronically activate pDCs and allow for sustained IFN α production even in the presence of viral suppression [45]. Studies of SLAMF5 signaling in this pathogenic immune response would be highly relevant to understanding the body's natural response to HIV-1.

An additional manifestation in chronic HIV-1 infection is the phenomenon of T cell exhaustion, and similar to SLAMF4, SLAMF5 has been implicated as playing a role in this process [86]. In a chronic lymphocytic leukemia (CLL) model of T cell exhaustion, Lewinsky et al. observed that SLAMF5 interactions between T cells and stromal cells in their microenvironment are able to induce PD-L1 up-regulation throughout the microenvironment [86]. This in turn contributes to increased PD-1 expression on CD8⁺ T cells and results in T cell exhaustion. Studies assessing this same mechanism in the setting of chronic viral infection, such as HIV-1, are a promising area of future research.

SLAMF6 (NTB-A, Ly-108, CD352)

SLAMF6 is a particularly interesting SLAM family member to study in the context of viral infection, as it has both potent immuno-modulatory functions on cells important for CMI, and has a well-described interaction with the HIV-1 virus. SLAMF6 is expressed on NK cells, NKT cells, T cells, B cells, macrophages, pDCs, DCs, thymocytes, eosinophils, and neutrophils. SLAMF6 facilitates immune cell adhesion and also regulates immune cell signaling in a manner similar to other SLAM family members.

SLAMF6 is the only known SLAM family member to have direct interaction with HIV-1, which occurs through the viral protein vpu [58-60]. Initial studies found that SLAMF6–SLAMF6 interactions between infected T cells and NK cells were important for NK cell-mediated lysis of infected cells [58]. The vpu protein from the HIV-1 genome was observed to specifically down-regulate SLAMF6 on infected cells and this prevented efficient NK cell-mediated lysis [58]. Biochemical studies revealed that vpu bound to SLAMF6 through its transmembrane domain and induced proteolytic degradation. Follow-up studies by a separate group determined that an additional mechanism through which vpu is able to down-modulate SLAMF6 is via alterations in SLAMF6 glycosylation which affected its anterograde transport [60]. The alterations in SLAMF6 glycosylation resulted in the formation of a more immature form of SLAMF6, which was preferentially sequestered in the Golgi apparatus. Of note, there is a single study contradicting the ability of vpu to down-regulate SLAMF6 on infected cells [59], but it should be noted that results obtained from this study might require further investigation, as they used an early murine model of in vivo HIV-1 infection which is now known to have limitations [87, 88]. Additionally, there are important differences between murine and human SLAM family receptors that could be playing a role here. An interesting point to consider is that all of these studies looked at NK cell-CD4⁺ T cell SLAMF6 interactions, but never myeloid-CD4⁺ T cell interactions. As SLAMF6 is also present on myeloid cells [14], it is interesting to consider how SLAMF6 on myeloid cells affects HIV infected monocytes.

SLAMF6 has also been identified as a modulator, or potential modulator, of CD8⁺ T cell and NK cell function. A recent study identified SLAMF6 as a marker of progenitor exhausted CD8⁺ T cells

[89]. This is particularly noteworthy, as the progenitor subset of exhausted cells, in contrast to terminally exhausted cells, are capable of reversing their exhaustion in response to PD-1 blockade [89]. While this study merely used SLAMF6 as a marker of progenitor exhausted CD8⁺ T cells, it remains to be seen what, if any role, SLAMF6 has functionally in this important immune cell type. Furthermore, this study used a tumor model of T cell exhaustion and it is not known whether or not SLAMF6 expression will mark progenitor exhausted CD8⁺ T cells in a viral model of T cell exhaustion. Finally, SLAMF6 also has a described role for regulating NK cell-mediated lysis of influenza infected cells, similar to that described above for SLAMF4 [75].

SLAMF7 (CRACC, CS1, CD319)

The seventh member of the SLAM family, SLAMF7, is increasingly being recognized as both a marker and modulator of inflammation in a number of diseases. SLAMF7 is expressed on NK cells, CD4⁺ T cells (low levels), CD8⁺ T cells, NKT cells, classical monocytes (low levels), inflammatory monocytes (high levels), macrophages, DCs, B cells, and plasma cells. It is notably absent on granulocytes [9, 27]. SLAMF7 signaling is less complex than other SLAM family members in that its ITSM can only bind to EAT-2, and not SAP. In the presence of EAT-2 it performs functions that can generally be described as activating, and in the absence of EAT-2 it recruits a number of inhibitory phosphates (SHP-1, SHP-2, SHIP-1, CD45, and csk) to inhibit cellular functions [90-92]. However, there may be yet other, unidentified mediators of SLAMF7's inhibitory signaling, as we and others have found [27, 93]. Likewise, the positive, EAT-2-mediated signaling mechanism from SLAMF7 is not entirely elucidated, but it is known that EAT-2 can signal via PLC γ 1, PLC γ 2, ERK1/2, and PI3K to induce Ca²⁺ flux in NK cells [91].

While no studies have yet described a direct interaction between any particular virus and SLAMF7, there are numerous reports describing immuno-modulatory roles for SLAMF7 in the setting of viral infections. Our group has recently identified SLAMF7 as playing an important role in the modulation of peripheral immune activation in chronic HIV-1 infection [27]. We showed, using a cohort of middle-aged cART-treated HIV patients, that there are elevated numbers of SLAMF7⁺ cells in HIV patients compared to controls, and that patients who do not respond to therapy have severely elevated levels of SLAMF7. More in-depth analyses revealed that CD16⁺ monocytes were responsible for this increase in SLAMF7⁺ cells which fits with previous studies showing CD16⁺ monocytes are increased in chronic HIV-1 infection [36, 94, 95]. In vitro studies using samples from HIV-1 patients identified SLAMF7 as being a potent inhibitor of specific type I interferon-induced chemokines (CXCL9, CXCL10, CXCL11, and CXCL12) produced by monocytes (Figure 3A) [27]. Interestingly, this inhibitory mechanism was not retained in a subset of HIV-1 individuals termed SLAMF7-silent (SF7S), and these individuals all had high levels of multiple

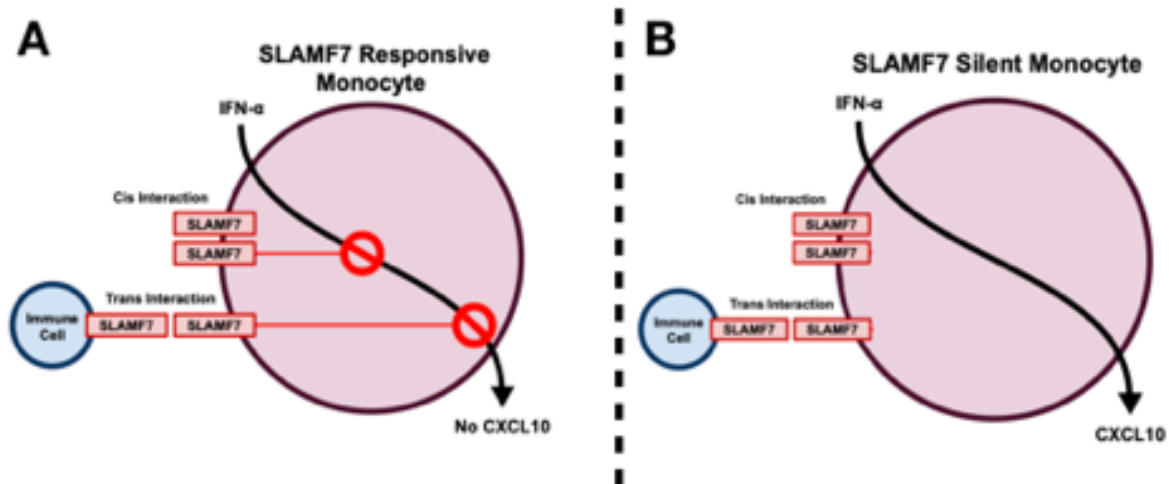


FIGURE 3: SLAMF7 silent and responsive monocytes

SLAMF7, which is present at low levels on monocytes and upregulated in response to IFN α , typically restrains production of alpha chemokines such as CXCL10 (A). This can occur either through cis interactions (ligation of SLAMF7 receptors found on the same cell) or trans interactions (ligation of SLAMF7 receptors found on separate cells (A). In a subset of HIV+ individuals SLAMF7 signaling on monocytes is unable to inhibit production of CXCL10, resulting in elevated levels of peripheral immune activation (B).

inflammatory cytokines and chemokines in their plasma (Figure 3B). Finally, in vitro HIV-1 infection studies revealed that SLAMF7 activation on monocytes could robustly prevent their infection with HIV-1 through a CCR5/CCL3L1 mechanism [27]. Together, this work highlights the important role that SLAMF7 plays in modulating immune responses in the setting of chronic HIV infection.

SLAMF7 has also been described to have an important role in a poly I:C/D-galactosamine model of hepatitis [96]. Poly I:C is a mimic of dsRNA and simulates viral infection; its use in combination with D-galactosamine has been shown to mimic fulminant hepatitis [97]. Here it was discovered that poly I:C induced SLAMF7 expression on hepatic NK cells, as well as kupffer cells [96]. Blocking the SLAMF7–SLAMF7 interactions between hepatic NK cells and kupffer cells decreased the severity of liver injury and decreased IFN γ and TNF α levels in the liver [96]. This study suggests that excessive SLAMF7 signaling between NK cells and SLAMF7 expressing cells in their

microenvironment can cause pathological inflammation, highlighting the importance of SLAMF7–SLAMF7 interactions between various immune cells during viral infection. As chronic HIV-1 infection is known to up-regulate SLAMF7 on monocytes and T cells [27], it is interesting to hypothesize how this affects other SLAMF7 expressing immune cells which regularly interact with monocytes, and what effect this would have on chronic inflammation in HIV infection.

SLAMF8 (BLAME, CD353)

SLAMF8, and its close relative, SLAMF9 are the most understudied members of the SLAM family. This is in part due to their relatively recent discovery, as well as the fact that they do not have ITSMs in their cytoplasmic domain [98, 99]. Because of this, it was theorized that these receptors may not signal; however, they do contain a short cytoplasmic domain with a very high number of positively charge amino acids, suggesting a potential for protein–protein interactions and downstream signaling [98, 99]. SLAMF8 is expressed on B cells, CNS macrophages, hepatic macrophages, monocytes, CD8⁺ T cells, DCs, and neutrophils. Murine microglia, a macrophage-like cell located in the brain parenchyma, have been noted to express SLAMF8 at the mRNA level, but have not yet been confirmed to express SLAMF8 at the protein level on the cell surface [100]. Our current knowledge of SLAMF8 suggests it is sensitive to innate immune stimuli and has an immuno-regulatory role in macrophages; factors that suggest it may also be involved in immune regulation during viral infection. Notably, SLAMF8 was observed to be up-regulated at the mRNA level in brain samples from patients co-infected with HIV-1 and mycobacterium tuberculosis (MTB) [101]. Since myeloid cells in the CNS (macrophages, monocytes, and microglia) are most

likely to express SLAMF8, it is likely that these cells have upregulated the expression of this receptor in response to chronic CNS inflammation associated with HIV-1 and/or MTB infections.

Insight into what role SLAMF8 could potentially be playing in myeloid cells of the CNS during viral infection comes from a report utilizing SLAMF8 knockout mice [29]. Here, the authors observed that SLAMF8 served as a negative regulator of Nox2 activity in macrophages in response to innate or bacterial challenge. This suggests that SLAMF8 up-regulation in the setting of CNS infection may be a natural anti-inflammatory response. It also suggests that SLAMF8 is able to signal in some manner, even though it lacks an ITSM. However, more recently, another report has been published with conflicting results [102]. In this SLAMF8 knockout mouse model, the authors do not note any differential response to inflammatory stimuli. Two explanations for this discrepancy are that 1) the mice used in each study are on different backgrounds (Balb/C in [29] and C57BL/6 in [102]) and 2) the readouts assessed in each report are different. Interestingly, in the C57BL/6 SLAMF8 knockout model, when both SLAMF8 and SLAMF9 were knocked out the authors observed decreased macrophage activation, suggesting they may have redundant functions as activating receptors in macrophages [102]. Interestingly, it was found that SLAMF8 and SLAMF9 were required to maintain normal levels of TLR4 expression [102]. This may have important implications in chronic HIV infection, where it is known that many patients suffer from a “leaky gut”, allowing egress of bacteria into circulation, which can activate the immune system. These data suggest that SLAMF8 and SLAMF9 may play a role in this pathological process.

An additional role for SLAMF8 in the regulation of phagocyte motility has also been described [103]. SLAMF8 was observed to inhibit macrophage migration in a manner opposite to that of SLAMF1 [103]. This is noteworthy, as phagocyte migration to lymph nodes, the CNS, and other locations during acute HIV and other viral infections is critically important to beginning to mount an immune response against the pathogen. This migration can actually have detrimental effects in HIV where monocytes and other phagocytes, become infected early in the disease course and migrate to the CNS where they set up a viral reservoir [104-106]. Future studies to understand the role of SLAMF8 signaling in early HIV-1 infection are certainly warranted.

SLAMF9 (SF2001, CD84H1)

Similar to SLAMF8, SLAMF9 is a newly discovered member of the SLAM family of receptors. SLAMF9 is the most recently identified SLAM family member and was found shortly following the completion of the Human Genome Project [99, 107, 108]. SLAMF9 has no ITSM similar to SLAMF8, but contains a large number of positively charged amino acids in its cytoplasmic domain [107]. SLAMF9 appears to be expressed on monocytes, pDCs, DCs, T cells, B cells, macrophages, and the monocytic cell line, THP-1 [107]. Of importance also, is that the ligand for SLAMF9 has yet to be identified. Studies of SLAMF9's expression and function have been hampered by lack of good monoclonal antibodies against SLAMF9, particularly ones that are amenable to flow cytometry.

While no direct role for SLAMF9 in anti-viral immunity has been discovered, roles for SLAMF9 on macrophages and pDCs have been described. A recent report identified SLAMF9 to be up-regulated on tumor-associated macrophages (TAMs) in melanoma [30]. Here, SLAMF9 was

observed to enhance TNF α production from macrophages following LPS stimulation and was itself up-regulated following IFN γ stimulation [30]. The alteration in LPS-stimulated macrophage responses by SLAMF9 suggests that it may be important for anti-microbial immunity. Indeed, a published abstract has stated that SLAMF9 knockout mice display impaired clearance of *Salmonella Typhimurium* [109]. Additionally, it has been shown that SLAMF9 is highly expressed on pDCs, where it is able to regulate their function and mouse susceptibility to Experimental Autoimmune Encephalomyelitis (EAE) [38]. The ability of SLAMF9 to control pDCs function suggests that this receptor may play a role indirectly in controlling viral infections, as pDCs are known to be critical in this respect [110].

Potential for Targeting SLAM Family of Receptors in HIV and other Viral Infections

Previously published reports by our group and others identified a critical role for SLAM family signaling in immune regulation suggesting the possibility of SLAM family modulation for therapeutic benefit during acute or chronic viral infections. While measles infections are rare in the United States due to the MMR vaccine, declining vaccination rates are making this infection more common, with potentially serious consequences for infected children. Monoclonal antibodies against SLAMF1, blocking the ability for measles to use this receptor as a cell entry mechanism, may prove to be a novel strategy to treat acute infection. A similar approach could be used against SLAMF3 to prevent its interactions with HCV. While blockade of SLAMF1 and SLAMF3 to directly prevent virus interactions are one approach, modulation of SLAMF9 signaling may allow for an indirect approach to treat acute or chronic viral infections. Monoclonal antibodies activating SLAMF9, specifically on pDCs, would, in theory, augment pDC IFN α

production and anti-viral responses [38]. While the approach may be beneficial during acute viral infections, an opposite approach may be useful in chronic HIV infection, where constitutive pDC activation is evident and pathogenic [45].

Targeted modulation of SLAMF7 signaling is additionally an exciting therapeutic approach in the setting of chronic HIV infection as we have shown that SLAMF7 signaling in human monocytes of healthy and HIV-infected patients counteracted type I interferon receptor-mediated signaling [27]. We also found that SLAMF7 signaling in human monocytes inhibits the production of various alpha chemokines, but not host restriction factors that are critical for combatting HIV-1 infection at the cellular level. These results have major implications, not only in HIV-associated pathogenesis, but also for other type I interferonopathies [111]. These discoveries suggest that SLAMF7 activation on monocytes of HIV infected individuals has the potential to prevent HIV infection of monocytes as well as pathogenic type I interferon signaling, all while sparing critical HIV host-restriction factors.

Moreover, modulation of the SLAMF7-EAT-2 signaling pathway has the potential to be co-opted for enhanced vaccination responses. We have previously shown that blockade of SLAMF7 using a SLAMF7-Fc fusion protein augmented the development of HIV Gag-specific T cell immune responses following adenovirus-mediated vaccination [112]. Additionally, our previous work indicated that prolonged SLAM family signaling via EAT-2 over-expression augments vaccine-induced innate and adaptive immune responses [31, 80, 81, 113, 114].

Finally, some of the SLAM family members have recently been identified as T cell exhaustion markers [89, 115], and signaling by these receptors impacts the development of proper T cell immune responses against cancer and viral antigens. Due to the huge success of CTLA-4 and PD-1 checkpoint blockade, it is tempting to speculate about the potential efficacy of SLAMF4 checkpoint blockade, as this receptor is a bona fide inhibitory receptor on CD8⁺ T cells. However, blocking SLAMF4 signaling on cytotoxic intra-tumoral T cells may be complicated by the fact that SLAMF4 actually seems to function as an activating receptor at low antigen densities [73].

SLAM receptors: Summary

Fueled by advances in multi-parametric flow cytometry and genomics, we now have the capability to rapidly discover and characterize new functions for the multitude of immune cell receptors. Of these immune receptors, the SLAM family represents a critical component in both the innate and adaptive arms of the immune system that requires further characterization. Their unique feature, self-ligation, makes them interesting targets, as their signaling is always triggered upon homotypic interactions between cells, or on the same cell (cis-interaction). Understanding their function in specific immune cells will facilitate the development of novel anti-viral and anti-cancer therapies. The conserved nature and ubiquitous functions of the SLAM family of receptors make them ideal targets for viruses looking to evade host immune responses. This has already been appreciated for a number of SLAM family receptors across a small number of viruses, but the true extent of SLAM receptor involvement remains to be seen. Studies of SLAM receptor signaling can be complicated by their homotypic interactions, differing roles across immune cell types, and occasional non-conserved functions between humans and mice. Additionally, co-

expression studies and studies looking at combinatorial effects of SLAM family receptors have scarcely been performed. With the more wide-spread use of single-cell technologies we anticipate more detailed studies to reveal important complexities in SLAM signaling networks never before appreciated.

SLAMF7 and its association with Multiple Sclerosis

Genome wide association studies (GWAS) are large population studies which seek to identify specific genomic regions (SNPs) associated with a particular disease or condition. Geneticists use advanced statistical approaches to determine when particular genetic polymorphisms are enriched in a large cohort of patients (often on the order of thousands to tens of thousands) compared to an equally large control cohort composed of individuals without the disease. These regions enriched in individuals with a particular condition are considered to be linked to that disease, and further efforts to characterize these associations are left to the larger scientific community. GWAS have been applied to MS at considerable scale, identifying over 500 genomic regions linked to MS from tens of thousands of patients [4]; most of these genetic associations have not been investigated in depth. In general, GWAS studies of MS have pointed to dysregulation of the immune system as a central culprit in MS disease progression and initiation, yet the specifics of such processes remain elusive. This work will help to shed light on why two such MS-linked genes, SLAMF7 and ERAP1, were identified in GWAS as being associated with susceptibility to MS.

SNPs in SLAMF7 (and other SLAM family genes) have been linked to MS in large GWAS studies [4, 116]. This is not surprising, since the current body of literature suggests that both peripheral and CNS immune cell response are the primary determinants of MS susceptibility [4]. A more recent study has looked into some of these genetic associations more closely in CD4+ and CD8+ T cells (both important players in MS pathogenesis) and found the presence of one of the SLAMF7 MS risk loci, rs35967351, to be increased specifically in both CD4+ and CD8+ T cells in MS patients [117]. Similarly, a study performing scRNA-seq on CSF immune cells from monozygotic twins with and without MS found SLAMF7 expression to be increased on CSF CD8+ T cells in MS patients [118]. The expression of some SLAM family members, including SLAMF7, has been profiled in the CSF of MS patients. Here, the authors found SLAMF7 expressed on similar immune cell subsets as in the periphery and also noted increased SLAMF7 expression on APCs following activation [119]. All of these studies highlight a potentially important role for SLAMF7 in the pathogenesis of MS, yet there have been no true confirmatory or mechanistic investigations into this link to date. This could be from a number of reasons, including: the limited number of labs studying SLAM family receptors, availability of genetically modified mice needed to perform these studies, and the fact that other more commonly studied genes often show more significant associations with MS.

ERAP1 and its link MS and other autoimmune diseases

Another gene associated with MS susceptibility is ERAP1. ERAP1 is an endoplasmic reticulum-localized amino peptidase that N-terminally trims peptides to the proper length so they can be presented on MHC-I [120]. This results in ERAP1 serving as a modulator controlling the global

immunopeptidome which, as one would expect, has implications in autoimmunity. Studies of the nature and function of ERAP1 were initiated once the strong genetic associations between SNPs in ERAP1 and various autoimmune diseases (Ankylosing Spondylitis, Multiple Sclerosis, Behcet's disease, Psoriatic Arthritis, and others) were uncovered [121, 122]. Our group and others have previously investigated the impact that ERAP1 proteins containing SNPs associated with autoimmune diseases have on its enzymatic mechanics, substrate specificity, and peptide products of ERAP1's peptide trimming ability [123-128]. In addition to peptide trimming and its effects on MHC-I pathways during adaptive immune responses, our lab has also uncovered novel roles for ERAP1 in modulating the innate immune system [123, 129, 130]. We have also previously determined that loss of ERAP1, or expression of human disease-associated forms of ERAP1, cause exaggerated, Th1-skewed immune responses [123, 129, 130].

What is puzzling about ERAP1's association to multiple autoimmune diseases, is that there has not yet been shown to be a common mechanistic explanation to these linkages, especially since many of these autoimmune diseases are not caused by a conserved set of antigenic epitopes. Over the years, this has led us and others to abandon the search for ERAP1's Occam's Razor and begin to apply the principle of Hickam's Dictum, that is: the simplest, single explanation for a phenomenon is not necessarily true, and there may be multiple contributing factors which explain said phenomenon. In beginning to consider that multiple ERAP1 functions maybe be responsible for this protein's association to different autoimmune diseases, our efforts have led us to uncover novel functions for ERAP1, some of which have been published [131] and some of which are included here. These new functions including controlling the frequency of IL-10-

producing FoxP3- CD4+ Tr1 cells [131], modulating myeloid cell inflammasome responses [130] (Blake, M.K., et al., *Manuscript in preparation*), and controlling B cell functions, offer a number of new lenses through which we can now investigate ERAP1's link to various autoimmune diseases.

Mouse model of MS

To study how specific genes like SLAMF7 and ERAP1 modulate susceptibility to MS, and to investigate new MS therapies, we have an excellent mouse model of MS termed the experimental autoimmune encephalomyelitis (EAE) model [132].

The EAE model has many variations [reviewed here [133]], but the most widely used version involved induction of neuroinflammation by immunizing mice with an emulsion of complete Freund's adjuvant and a 20-mer peptide derived from the human MOG protein (MOG₃₅₋₅₅). MOG is a protein found in myelin and since MS involves the destruction of myelin, it was originally theorized that this would result in a similar disease in mice. The mice are also injected on days 0 and 2 with *Bordetella pertussis* toxin which serves to further activate the immune system and to temporally disrupt the blood brain barrier which is thought to allow peripheral immune cells better access to the CNS, and thereby fostering CNS autoimmunity [134]. For example, we know that peripherally located APCs (primarily cDC1 cells) migrate to the site of immunization, uptake the MOG antigen, migrate back to draining lymph nodes where they present the MOG₃₅₋₅₅ antigen on MHC-II to CD4+ T cells [135]. These CD4+ T cells then migrate to the CNS and initiate inflammation, whereupon a host of other immune cells including

inflammatory myeloid cells are recruited to the CNS and propagate the inflammatory state. This results in demyelination primarily in the mouse spinal cord, along with weight loss, and an ascending paralysis. The paralysis can be scored and is used as the gold-standard in the field to quantitate EAE severity.

Though useful, we now recognize a number of key differences between EAE and MS which are critical to understand when using this model [132]. One of these is that the classical EAE model is a purely T cell-dependent disease, whereas actual MS is not [1]. This was not apparent early on, and led the MS research community down a years-long focus in T cell-specific investigations of EAE and MS. While these efforts did help us learn a great deal about T cell autoimmunity and T cell responses, it did not help us to understand the root cause of human MS. Importantly, the most widely used EAE model is B cell-independent and CD4+ T cell-dependent, which is at odds with what is currently known about MS. Additionally, this model is chronic and mice never fully recover or enter remission like most MS patients [although there are EAE models of RRMS [133]]. Also, this model is based on autoimmunity to a single antigen, which we know is not the case with human MS [1]. In fact, in humans CNS autoimmunity to MOG protein is a separate, but related disease to MS, termed MOG encephalomyelitis [136]. None the less, this model is a better model of autoimmunity than is available for almost any other autoimmune disease [137], and it is relatively cheap, reliable, reproducible, easy to perform, and well-studied [132, 133]. This has made it a useful tool for investigating the utility of new MS therapies, where it has been instrumental in proving the safety and efficacy of a number FDA-approved drugs including: rituximab, ocrelizumab, natalizumab, fingolimod, and others [138].

More recently, alternative models of EAE are being investigated, one of which is B cell-dependent. This model is the same as the classical (rhMOG₃₅₋₅₅) model described above, but uses full-length MOG protein (from human or mouse) instead of the human MOG₃₅₋₅₅ peptide [139]. Models like this are still not perfect as they use a single antigen, but now allow for the investigation into potential mechanisms involving B cells, paralleling clinical strategies that also focus on B cell targeting strategies to treat MS patients. This is critical, since we still do not know how exactly B cells contribute to MS pathogenesis, as multiple roles have been attributed to them in MS/EAE including: regulatory functions from Bregs, production of cytokines such as IL-6, antigen presentation to T cells, and direct co-stimulation of T cells [1, 140]. Notably, B cell production of auto-antibodies has been ruled out as a potential mechanism [1].

In the following chapters I will describe several studies given this background. In Chapter 2 I discuss our studies of the role of SLAMF7 in chronic HIV-1 infection. In Chapter 3 I provide a detailed method for the in vitro infection of human monocytes with HIV-1 and measurement of this by flow cytometry. In Chapter 4 I describe the role of SLAMF7 in driving T cell exhaustion in the setting of cancer. In Chapter 5 I describe the treatment of multiple murine cancers using an adenovirus expressing a SLAMF7-Fc fusion protein. In Chapter 6 I describe our group's investigation into the role of SLAMF7 in neuroinflammation and its association to MS. In Chapter 7 I present work providing the first mechanistic studies examining the genetic association of ERAP1 with MS. Finally, in Chapters 8 and 9 I summarize the entirety of this body of work and present opportunities for additional investigations into all of the aforementioned chapters.

CHAPTER: 2 SLAMF7 Is a Critical Negative Regulator of IFN- α -Mediated CXCL10 Production in
Chronic HIV Infection

This chapter is adapted from an article published in the Journal of Immunology, Volume 201, Issue 1, Pp. 228-238 January, 2019.

Authors: Patrick O'Connell, Yuliya Pepelyayeva, Maja K. Blake, Sean Hyslop, Robert B. Crawford, Michael D. Rizzo, Cristiane Pereira-Hicks, Sarah Godbehere, Linda Dale, Peter Gulick, Norbert E. Kaminski, Andrea Amalfitano and Yasser A. Aldhamen

Abstract

Current advances in combined anti-retroviral therapy (cART) have rendered HIV infection a chronic, manageable disease; however, the problem of persistent immune activation still remains despite treatment. The immune cell receptor SLAMF7 has been shown to be upregulated in diseases characterized by chronic immune activation. Here, we studied the function of the SLAMF7 receptor in immune cells of HIV patients and the impacts of SLAMF7 signaling on peripheral immune activation. We observed increased frequencies of SLAMF7⁺ PBMCs in HIV⁺ individuals in a clinical phenotype-dependent manner, with discordant and long-term nonprogressor patients showing elevated SLAMF7 levels, and elite controllers showing levels comparable to healthy controls. We also noted that SLAMF7 was sensitive to IFN α stimulation; a factor elevated during HIV infection. Further studies revealed SLAMF7 to be a potent inhibitor of the monocyte-derived proinflammatory chemokine CXCL10 (IP-10) and other CXCR3 ligands, except in a subset of HIV⁺ patients termed SLAMF7 silent (SF7S). Studies utilizing small molecule inhibitors revealed that the mechanism of CXCL10 inhibition is independent of known SLAMF7 binding partners. Furthermore, we determined that SLAMF7 activation on monocytes is able to decrease their susceptibility to HIV-1 infection *in vitro* via down-regulation of CCR5 and up-regulation of the CCL3L1 chemokine. Finally, we discovered that neutrophils do not express SLAMF7, are CXCL10⁺ at baseline, are able to secrete CXCL10 in response to IFN α and LPS, and are non-responsive to SLAMF7 signaling. These findings implicate the SLAMF7 receptor as an important regulator of IFN α -driven innate immune responses during HIV infection.

Introduction

HIV infection is now widely regarded as a manageable disease; however, cART, which controls viremia, fails to effectively control many secondary HIV-associated pathologies [141, 142]. The universal mechanism believed to underlie the development of these diseases is chronic, global immune activation [95, 143]. Known causes of which include increased gut permeability resulting in microbial translocation into systemic circulation [144] and constitutively elevated levels of proinflammatory cytokines and chemokines, including interferon alpha (IFN α) [36, 145-147].

Sustained levels of detectable IFN α in the plasma of cART-treated HIV patients results from persistent activation of plasmacytoid dendritic cells (pDCs) by HIV-antibody complexes [45] and causes a global type I interferon signature in circulating monocytes [94, 148]. This induces monocyte transition from the classical subtype (CD14⁺CD16⁻) into the proinflammatory (CD14⁺CD16⁺) and non-classical (CD14^{low}CD16⁺⁺) subtypes, as evidenced by upregulation of CD16 [149, 150]. While beneficial in acute infections, these type I interferon-mediated effects on monocytes prove to be deleterious in chronic infections [151].

Some HIV+ individuals are known to have persistently elevated levels of CXCL10 (IP-10) and other proinflammatory cytokines and chemokines [147, 152]. CXCL10 is produced primarily by monocytes and is of particular interest due to its ability to suppress T cell functions [153], induce neuronal apoptosis [154-156], and as a marker of systemic inflammation [157]. During HIV infection some CD16⁺ monocytes become activated by IFN α , upregulate CCR5 [105],

infected with HIV, and subsequently migrate across the blood-brain barrier where they set up a viral reservoir and are capable of inducing neuroinflammation and neuronal apoptosis via secretion of high levels of CXCL10, TNF α , IL-6, and IL-1 β [105, 158]. Here we investigated the role of an immune-modulatory receptor, signaling lymphocytic activation molecule family member 7 (SLAMF7) (a.k.a. CRACC, CS-1, CD319), in the context of HIV infection and immune activation.

SLAMF7 is a member of the signaling lymphocytic activation molecules [SLAM] family of receptors and is expressed on numerous immune cell types [9, 112]. SLAMF7, and other SLAM family receptors (except 2B4), function as homotypic receptors that, upon activation, recruit SLAM-associated protein (SAP) family of adaptors or other SH2 domain-containing proteins to their cytoplasmic immunoreceptor tyrosine-based switch motifs (ITSMs) [9]. SLAMF7 is unique among SLAM receptors in that it is only able to recruit a single SAP adaptor, EAT-2, to its tyrosine-phosphorylated ITSM [91]. SLAMF7 receptor ligation in cells expressing EAT-2 results in activation of cellular immune responses [159], while SLAMF7 activation in the absence of EAT-2 results in cellular inhibition via recruitment of a number of inhibitory phosphatases (SHP1, SHP2, SHIP1, and csk) [91].

SLAMF7 is well known for being over-expressed on multiple myeloma (MM) cells [160], as an important regulator of NK cell function [90, 91, 112], and recently, as a critical factor in macrophage-mediated phagocytosis of tumor cells [93]. Using a medium-sized cohort of middle-aged, HIV+ individuals, we sought to assess whether the SLAMF7 receptor was playing a

role in the context of HIV infection in cART-treated patients. Our results implicate the SLAMF7 receptor as an important immunomodulatory receptor in human monocytes, and in the context of HIV-associated peripheral immune activation.

Materials and Methods

Reagents used. The following antibodies were used: CD14-FITC (61D3), CD16-BV510 (3G8), SLAMF7-PE (162), CD3-PE-Cy7 (OKT3), CD19-PE-Cy7 (SJ25C1), CD57-PE-Cy7 (TB01), CD66b-APC (G10F5), CXCL10-PerCp-eFluor710 (4NY8UN), EAT-2-APC (LS-C240730), YY1-Alexa647 (H-10), Blimp-1-DyLight650 (3H2-E8), CCR5-PerCp-eFluor710 (NP-6G4) and SLAMF7 (162.1) (used for cross-linking). The SLAMF7-Fc recombinant protein was designed and produced similar to mCRACC-Fc as previously described [112], with the following modifications: a human SLAMF7 extracellular domain was swapped for the murine SLAMF7 extracellular domain, the murine IgG Fc portion was switched to a human IgG4 domain to reduce Fc receptor binding and ADCC, and S228P and L235E mutations were made in the IgG4 domain to further reduce interactions with Fc receptors [161]. Recombinant universal IFN α (PBL Assay Bioscience) and Recombinant human IFN γ were used at 100 IU/mL unless otherwise noted. SHP1/2 inhibitor (NSC87877) (Millipore Sigma) was used at 10 μ M. SHIP1 inhibitor (3AC) (Millipore Sigma) was used at 5 μ M. CD45 inhibitor (CAS 345630-40-2) (Millipore Sigma) was used at 1 μ M. Bortezomib (EMD Millipore) was used at 100nM. All HDACi's (Selleck chemicals) were used at concentrations indicated in relevant figure legends.

HC and HIV blood sample collection. HC PBMCs were obtained from either buffy coats purchased from Gulf Coast Regional Blood Center, Texas, or from whole blood samples

purchased from Stanford Blood Center, California. HIV+ blood samples were collected from donors enrolled in the Mid-Michigan HIV Consortium. Plasma was stored at -80°C until use. PBMCs were isolated with Ficoll-Plaque Plus (GE Healthcare) as previously described [162].

In vitro cell culture and stimuli. Cells were plated at 3×10^5 cells/well for PBMC and isolated monocyte experiments, and 1×10^5 cell/well for isolated neutrophil experiments, in 96-well plates. Cells were cultured in complete RPMI (RPMI 1640, 10% FBS, 1X PSF). For cross-linking experiments 10µg/mL anti-SLAMF7 mAb or SLAMF7-Fc was added to a sterile, high-binding 96-well cell culture plate O/N at 4°C. For all *in vitro* flow cytometry experiments cells were cultured in the presence of stimuli for 17-18h. In the monocyte maturation assay (Fig. 6E) the cells were stimulated with only 25 IU/mL IFN α and for exactly 24h. Small molecule inhibitors were added 45-60min before IFN α for all relevant experiments. For experiments involving intracellular staining, BD GolgiPlug was added for the final 5h. NK92 cells were purchased from ATCC and cultured as indicated by manufacturer.

BioPlex assay. For analysis of cell culture supernatant and plasma samples 80µL of media or plasma was used, undiluted, and the assay was run per manufacturer's instructions (Bio-Rad, Hercules, CA) via Luminex 100 technology. A 27-plex assay was run and analysis was performed on only those factors with detectable levels or contributing to the separation of Cluster 1 and Cluster 2.

Flow cytometry. Cells were prepared and stained as previously described [112]. Intracellular staining was performed using the BD fixation/permeabilization kit (BD Biosciences) per manufacturer's instructions. Transcription factor staining was performed with the Transcription Factor Buffer Set (BD Pharmingen) per manufacturer's instructions. Samples were analyzed on either a BD LSR II or BD FACSCanto. LIVE/DEAD staining with Aqua fixable stain (ThermoFisher) was included during initial experiments and cell viability was verified to be >90%. Monocyte and neutrophil gating strategy is shown in (Supplemental Fig. 1).

Monocyte and Neutrophil isolations. CD14⁺ monocytes were isolated from PBMCs via positive selection using CD14 Microbeads (Miltenyi Biotec) per manufacturer's instructions. Purity was consistently >90% as assessed by flow cytometry. Neutrophils were isolated from whole blood using the MACSxpress Neutrophil isolation kit (Miltenyi Biotec) per manufacturer's instructions. Purity was consistently >98% as assessed by flow cytometry.

qRT-PCR experiments. Isolated monocytes were plated in 96-well plates at 3×10^5 cells/well and stimulated as indicated for 4h. Cells were harvested and placed into Trizol (ThermoFisher) and RNA was isolated per manufacturer's instructions. RNA was reverse transcribed with SuperStrand First Strand Synthesis Kit III (Invitrogen) per manufacturer's instructions and analyzed on a QuantStudio7 system (ThermoFisher). GAPDH was used as a housekeeping gene and the $\Delta\Delta C_t$ method was used for analysis.

In vitro HIV-1 infection of monocytes. Isolated primary human monocytes from two HC's were plated at 2×10^5 cells/well in a 96-well high-binding cell culture plate. SLAMF7 activation was induced by antibody cross-linking the same as in IFN α stimulation experiments. Monocytes were isolated by positive selection with CD14 Microbeads (Miltenyi Biotec) per manufacturer's instructions. Purity of monocyte samples used in (Fig. 9D) was 95.5% and 92.6% for donors A and B, respectively. Cells were cultured for 24h before addition of HIV-1_{Ba-L}-GFP (a kind gift from Dr. Young-Hui Zheng, Michigan State University) at a final concentration of 190 pg/mL. HIV-1_{Ba-L}-GFP virus stock concentration was determined by p24 ELISA (HIV-1 p24 Quantikine ELISA, R&D Systems) per manufacturer's instructions. HIV-1_{Ba-L}-GFP was generated by replacing the gene coding for *nef* with GFP (Young-Hui Zheng, unpublished, personal communication). Cells were washed 4h following infection and collected at indicated time points post-infection for assessment of infectivity via FACS analysis. Cells were stained for CD14, CD16, and viability (LIVE/DEAD Violet) and GFP+, living, CD14+ cells were analyzed with FlowJo. The CCR5 blocking mAb (2D7) (BD Biosciences) was added at a concentration of 10 μ g/mL at the start of cell culture (24 hrs before HIV-1_{Ba-L}-GFP infection) and was replenished at each media change.

Clustering and statistical analysis. k-means and hierarchical clustering were performed using SPSS. Statistical analysis was performed in GraphPad Prism 7.0 as indicated. The heatmap from (Fig. 6B) was generated using the z-score normalized values of plasma biomarkers calculated in SPSS. The violin plots in (Fig. 4) were generated using the ggplot2 package in R. The gene expression heatmap from (Fig. 8B) was generated using the gplot package in R. MFI refers to "median fluorescence intensity" in all instances.

Study approval. Informed consent from all HIV patients was obtained prior to their enrollment in the study and approved by the MSU IRB (IRB#: 11-202). Patient data was de-identified and complies with all HIPAA regulations.

Results

HIV+ individuals have increased expression of SLAMF7 on their peripheral blood mononuclear cells (PBMCs).

The SLAMF7 receptor functions as a self-ligand, therefore, global receptor levels across the complete spectrum of PBMCs will impact the function of all SLAMF7⁺ cells. To investigate if HIV infection alters SLAMF7 expression we screened 81 HIV patients and 58 healthy controls (HCs) for global expression of SLAMF7 across all peripheral immune cells (Fig. 4A). Subjects were grouped according to their clinical phenotype: cART concordant (CD4 count >250 with no decrease in CD4 count over 6 months), cART discordant (CD4 count <250 with undetectable viral load and no improvement in CD4 count over 6 months), long-term nonprogressor (LTNP), or elite controller (EC). We observed that SLAMF7 levels were minimally increased in concordant patients while discordant and LTNP patients had significantly higher SLAMF7 levels (Fig. 4A). Interestingly, elite controllers had global SLAMF7 levels comparable to HCs (Fig. 4A). Assessment of SLAMF7 expression on CD4 and CD8 T cells revealed SLAMF7 to be significantly up-regulated on CD8 T cells from concordant and discordant patients (Fig. 4B and C). Expression of SLAMF7 on 4 subsets of NK cells (CD56^{bright}CD16⁻, CD56^{dim}CD16⁺, CD56⁻CD16⁺, and NKT cells) showed comparable expression between HCs and HIV patients (Fig. 4D). Interestingly, HIV

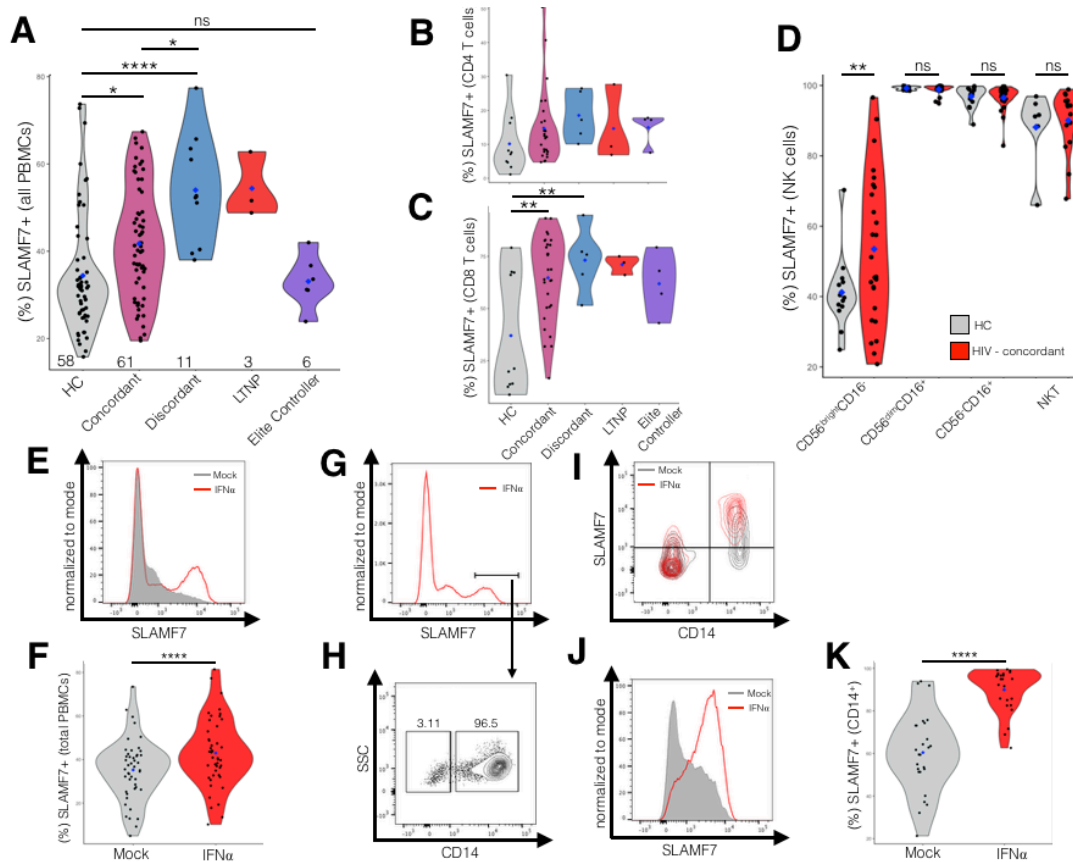


FIGURE 4: HIV+ individuals have increased expression of SLAMF7 on their PBMCs and SLAMF7 is upregulated by IFN α .

HIV+ patients and healthy controls (HC) were screened for total SLAMF7 expression across all peripheral immune cell types (A). SLAMF7 expression was assessed on CD4 T cells (B), CD8 T cells (C), and NKT cells (D). The n is indicated along the x-axis (A) and the blue diamonds indicate the mean. The n for (B and C) is: HC: 10, Concordant: 28, Discordant: 5, LTNP: 3, EC: 4. The n for (D) is: HC: 14, HIV: 26. The effect of IFN α (100 IU/mL) on SLAMF7 expression on total peripheral blood mononuclear cells (PBMCs) (E and F), and monocytes (J and K) was assessed *in vitro*. (F and K) n=46 and 26, respectively and data is pooled from 5 independent experiments. (G and H) CD14 expression on SLAMF7^{high} cells from IFN α stimulated total PBMCs. (I) Comparison of SLAMF7 expression on CD14⁺ and CD14⁻ cells following IFN α stimulation showing only CD14⁺ monocytes up-regulate SLAMF7. Groups compared using 1-way ANOVA with Tukey's multiple comparison test (A) and paired two-tailed T test (C and E). *P<0.05, ****P<0.0001. LTNP: long-term nonprogressor, ns: not significant.

patients had significantly more SLAMF7⁺ cells in the CD56^{bright}CD16⁻ regulatory NK cell subset, as compared to other NK cell subsets (Fig. 4D).

SLAMF7 is upregulated in response to IFN α in total PBMCs and monocytes from HIV+ individuals.

To examine whether SLAMF7 upregulation may be the result of chronic immune activation we stimulated PBMCs from HIV+ patients with IFN α ; known to be chronically elevated in HIV+ patients [36]. We observed a minor, but significant increase in the percent of SLAMF7⁺ PBMCs following IFN α stimulation (Fig. 4E and F). To identify if a specific cell type was responsible for this increase in SLAMF7⁺ cells we gated on the SLAMF7^{high} peak present in IFN α samples and not in mock treated and looked at various cell markers. We observed that >95% of the cells in this SLAMF7^{high} peak were CD14⁺ monocytes (Fig. 4G-I). Looking at just CD14⁺ monocytes we found they showed the most robust SLAMF7 response to IFN α (Fig. 4J and K). Since monocytes play a critical role in type I interferon responses and are implicated in the pathogenesis of a number of secondary HIV-associated pathologies [105], we next assessed what role SLAMF7 may be playing in monocytes.

SLAMF7 activation on monocytes of HCs inhibits IFN α -mediated CXCL10 production.

Monocytes are the primary source of CXCL10, especially in response to type I and II interferons [163]. Therefore, we examined the effect of SLAMF7 signaling on IFN α and IFN γ -stimulated PBMCs from HCs. Activation of SLAMF7 during IFN α (Fig. 5A and B) and IFN γ -stimulation

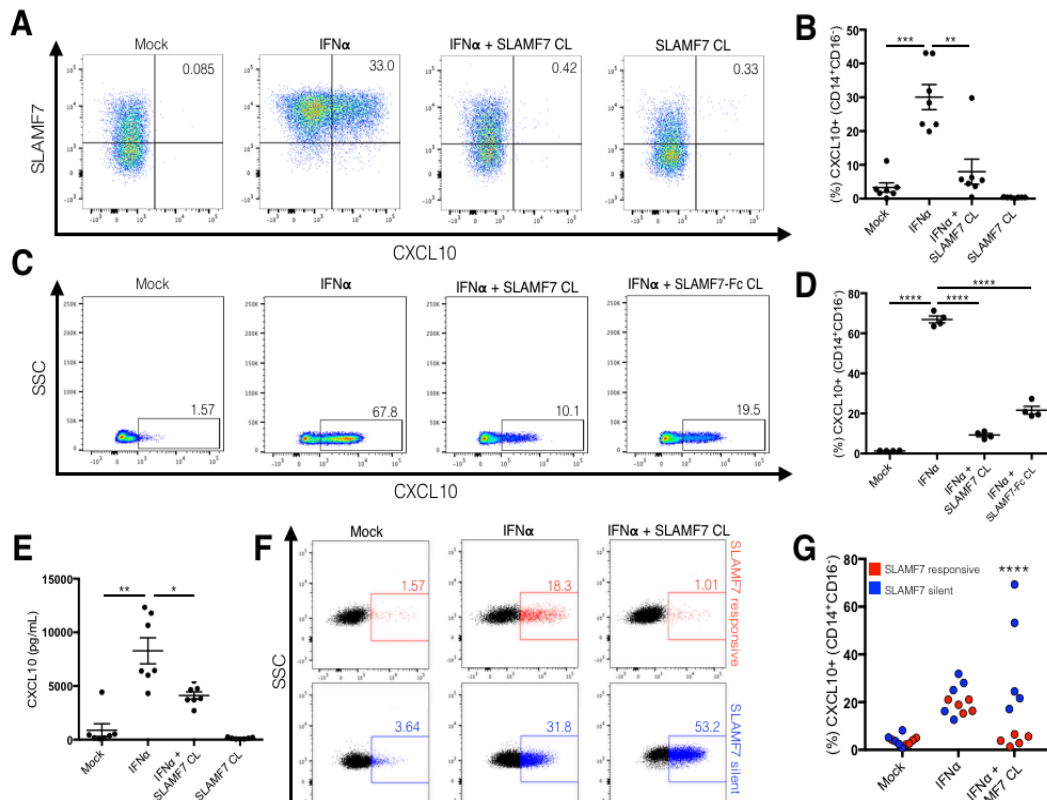


FIGURE 5: Activation of the SLAMF7 receptor on monocytes inhibits their IFN α -mediated production of CXCL10.

(A and B) PBMCs from healthy controls were stimulated *in vitro* with IFN α and the SLAMF7 receptor was activated by cross-linking where indicated. Expression of CXCL10 was measured by intracellular staining on flow cytometry. (C and D) The same experiment in (A) was carried out with isolated CD14⁺ monocytes. Cross-linking with a recombinant protein comprised of the extracellular domain of SLAMF7 fused to a modified IgG4 Fc fragment (SLAMF7-Fc) was performed to confirm that inhibition is SLAMF7 specific (C and D, last condition). (E) The levels of secreted CXCL10 in the supernatant from (A) was assessed by BioPlex assay. (F and G) PBMCs from HIV+ donors were isolated and the same experiment as in (A) was carried out. HIV patients failing to respond to SLAMF7 activation were classified as SLAMF7 silent (SF7S). (B and E n=7). (D) n=4 technical replicates from a single donor, representative of 3 independent experiments. (B and E) Data is presented as pooled results of 2 independent experiments, representative of 7 total experiments. (F and G) Data presented is pooled from 2 independent experiments. 3-4 HCs were run alongside HIV samples in all experiments to verify that assay worked. SF7S and SLAMF7 responsive groups are compared using 2-way ANOVA with Sidak's multiple comparison test. Data in (B, D, and E) presented as mean \pm SEM. Groups compared using 1-way ANOVA with Tukey's multiple comparison test. *P<0.05, **P<0.01, ***P<0.001, ****P<0.0001.

(Supplemental Fig. 2A) resulted in robust inhibition of CXCL10 production from monocytes. To confirm this effect was specific to monocytes we isolated primary CD14⁺ monocytes and repeated the previous experiment noting the same effect (Fig. 5C and D). To verify that CXCL10 inhibition was SLAMF7-specific we activated SLAMF7 via cross-linking with a recombinant version of the SLAMF7 extracellular domain, SLAMF7-Fc (Fig. 5C and D, final condition). Monocytes were also treated with soluble SLAMF7-Fc *in vitro* confirming that binding of cell surface SLAMF7 to an immobilized SLAMF7 extracellular domain was necessary for inhibition (Supplemental Fig. 2D and E). Furthermore, we confirmed that activation of SLAMF7 resulted in reduced secretion of CXCL10 from IFN α -stimulated PBMCs into the culture supernatant via BioPlex assay (Fig. 5E). However, it is important to note that SLAMF7 activation did not robustly reduce supernatant levels of CXCL10 to the degree we observed with flow cytometry, suggesting the putative involvement of another cell type(s).

A subset of HIV+ patients are nonresponsive to SLAMF7 inhibitory signaling.

We next examined if this effect was conserved in HIV+ individuals. The same experiment performed in (Fig. 5A and B) was repeated with freshly isolated PBMCs from HIV+ patients. We noted a dichotomous response in HIV+ patients with some responding the same as HCs (referred to hereafter as “SLAMF7 responsive”) and some showing a failure to inhibit CXCL10, which we termed “SLAMF7 silent” (SF7S) (Fig. 5F and G). As an internal control to verify that these differences were not due to experimental variability we included HCs alongside HIV+ samples in each experiment and noted in each case that all HCs did respond to SLAMF7 activation. Defining SLAMF7 as an inhibitory receptor in monocytes, and identifying a subset of

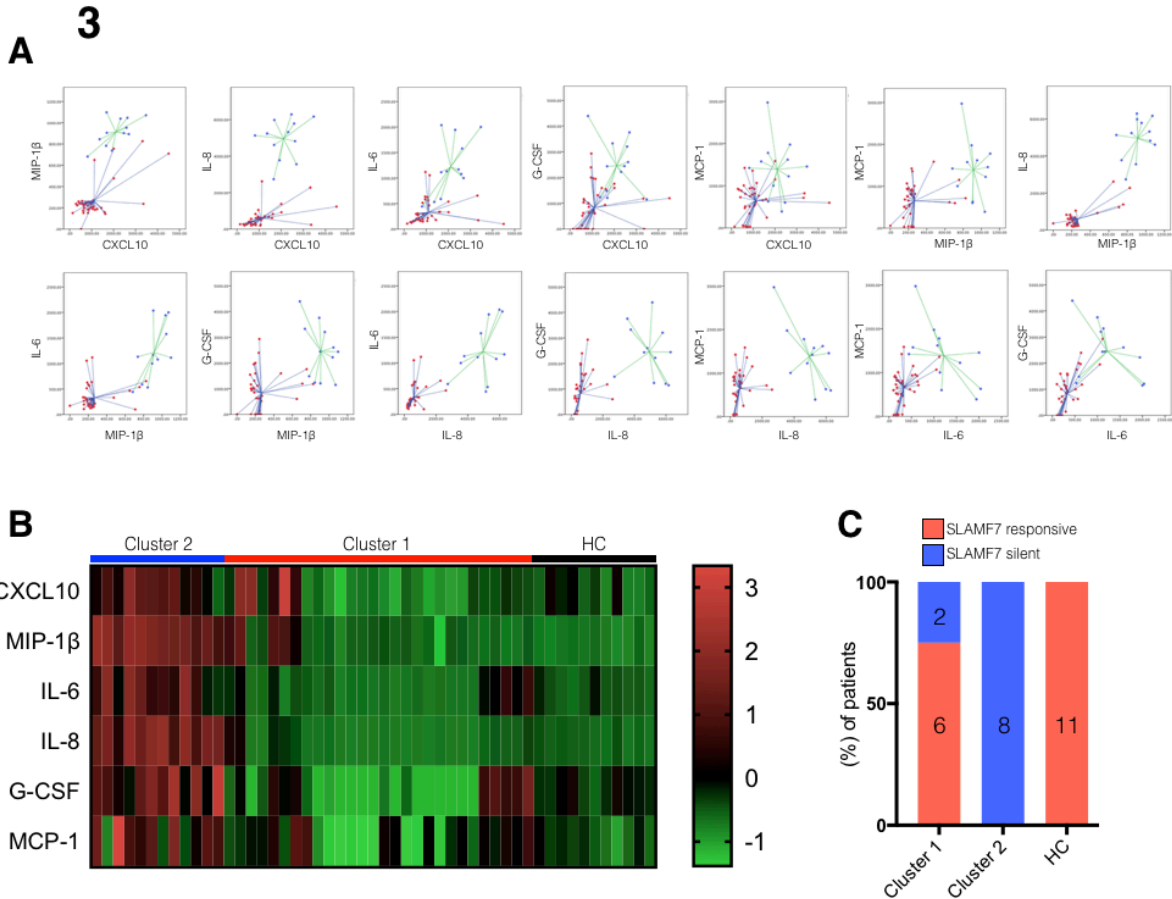


FIGURE 6: SLAMF7 silent patients have elevated plasma levels of proinflammatory factors and cluster distinctly from SLAMF7 responsive patients.

Plasma from HIV patients and HCs was assessed by BioPlex assay for 6 proinflammatory cytokines and chemokines known to be involved in HIV-associated immune dysfunction (CXCL10, MIP-1 β , IL-6, IL-8, G-CSF and MCP-1). **(A)** k-means clustering was performed with all 6 factors and plots depicting all relationships are shown. Previous hierarchal clustering identified two distinct clusters (data not shown). Red dots indicate cluster 1 (n=28) and blue dots indicate cluster 2 (n=12). **(B)** Heatmap of z-score normalized plasma cytokine and chemokine values. **(C)** Breakdown of percentages of SF7S and SLAMF7 responsive patients per cluster. Number of patients per group, per cluster indicated inside bars.

HIV+ patients with a defect in SLAMF7 signaling led us to examine if there was any correlation to clinical biomarkers associated with chronic immune activation.

SLAMF7 responsive and SF7S patients have distinct peripheral immune activation signatures.

The plasma levels of six proinflammatory cytokines and chemokines implicated in chronic immune activation [95] during HIV infection were evaluated. Hierarchal and k-means clustering

	Cluster 1	Cluster 2
n	28	12
Median age, (IQR)	51 (17.25)	54 (6.25)
Median BMI, (IQR)	28.5 (5.78)	28.75 (12.9)
Race- n, (%)		
Caucasian	17 (60.7)	7 (58.3)
African	8 (28.6)	3 (25)
Hispanic	3 (10.7)	1 (8.3)
Unknown	0	1 (8.3)
Sex- n, (%)		
Male	21 (75)	10 (83.3)
Female	7 (25)	2 (16.7)
Median CD4 count (cells/μL), (IQR)	591.5 (500)	688 (402)
Median CD4/CD8 ratio, (IQR)	0.61 (0.96)	0.45 (0.82)
CD4 nadir (cells/μL)-n, (%)		
<50	7 (25)	4 (33.3)
50-100	5 (17.9)	0
100-200	5 (17.9)	4 (33.3)
200-350	3 (10.7)	1 (8.3)
350-500	1 (3.6)	2 (16.7)
>500	7 (25)	0
Unknown	0	1 (8.3)
Clinical phenotype-n, (%)		
Concordant	20 (71.3)	8 (66.7)
Discordant	3 (10.7)	3 (25)
Elite Controller	4 (14.3)	0
LTNP	1 (3.6)	1 (8.3)
Viral load (copies/mL)-n, (%)		
ND	20 (71.3)	8 (66.7)
20-1000	5 (17.9)	3 (25)
1000-25000	2 (7.1)	1 (8.3)
Unknown	1 (3.6)	0
Median length of infection (years), (IQR)	16.5 (17.25)	14 (22.75)
Current MJ use- n, (%)		
Yes	9 (32.1)	6 (50)
No	18 (64.3)	6 (50)
Unknown	1 (3.6)	0

Table 2: Cluster characteristics.

was used to identify patients with similar peripheral immune activation profiles. Hierarchical clustering identified two distinct clusters and (Fig. 6A) shows the results of k-means clustering. Cluster one was characterized by low levels of all six proinflammatory factors, while Cluster two showed patients with elevated levels of all six proinflammatory factors. A heatmap of plasma cytokines and chemokines shows Cluster one patients exhibiting a similar profile to that of HCs, while Cluster two patients have a markedly different cytokine profile (Fig. 6B). Comparison of demographics and clinical characteristics showed the two clusters to be otherwise well balanced (Table 2). Interestingly, we found that Cluster 2 patients are all SF7S while Cluster 1

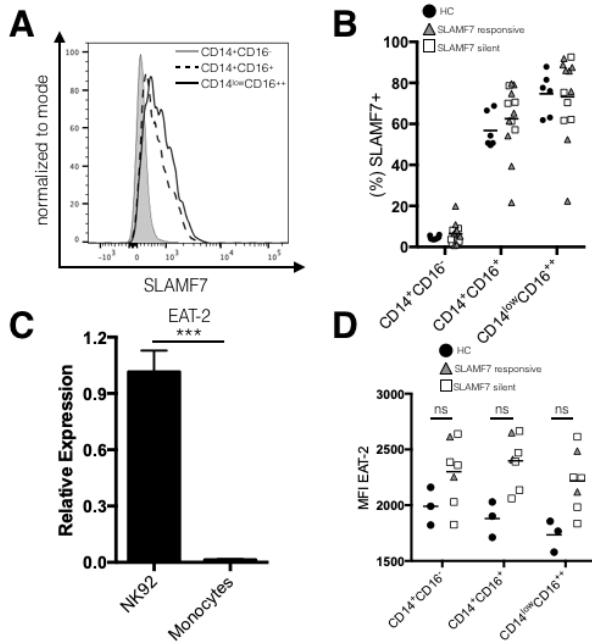


FIGURE 7: monocytes from SF7S and SLAMF7 responsive patients do not differ in expression levels of SLAMF7 or EAT-2.

(A) Expression of SLAMF7 on monocyte subsets. (B) Comparison of SLAMF7 expression between SF7S, SLAMF7 responsive, and HCs on all monocyte subsets. (C) We assessed the levels of EAT-2, a known SLAM family receptor adaptor, in a human cell line known to express EAT-2 (NK92) and isolated primary monocytes by qRT-PCR. (D) Analysis of EAT-2 protein levels in monocytes between SF7S and SLAMF7 responsive individuals by intracellular staining on flow cytometry. (C) Results are technical replicates from a single donor compared with unpaired 2-tailed T test. Groups in (B and D) compared using 1-way ANOVA with Tukey's multiple comparison test as well as a 2-way ANOVA with Sidak's multiple comparison. (B) n=6 for HCs, 8 for SLAMF7 responsive, and 5 for SF7S. (D) n=3 for HCs, 2 for SLAMF7 responsive, and 5 for SF7S. Data presented as mean ± SEM. ***P<0.001.

patients are predominantly SLAMF7 responsive (Fig. 6C). These results suggest that dysfunction of the SLAMF7 receptor may result in *in vivo* manifestations.

Monocytes from SF7S and SLAMF7 responsive patients do not differ in expression levels of the SLAMF7 receptor or EAT-2 adaptor.

To determine the mechanism behind this defective SLAMF7 function in SF7S patients we assessed levels of SLAMF7 expression across all monocyte subsets in HCs, SF7S, and SLAMF7 responsive patients. We noted that a small percentage of classical monocytes (~5%) express SLAMF7 at baseline, while a significantly higher percentage of both intermediate (~60%) and non-classical monocytes (~70%) express SLAMF7 (Fig. 7A and B). Critically, we did not notice a difference in SLAMF7 expression between SF7S and SLAMF7 responsive patients (Fig. 7B). Since it has been well established that the presence or absence of the SLAM family adaptor EAT-2 can dramatically alter SLAMF7 signaling and govern the activating function of SLAMF7 [91], we next looked to the levels of EAT-2 across all three monocyte subsets in HCs, SF7S, and SLAMF7 responsive individuals (Fig. 7D). However, we first examined whether monocytes from HCs express any EAT-2 at all. Comparison of EAT-2 mRNA levels between monocytes and a human NK cell line known to express EAT-2 (NK92), showed that monocytes have little to no EAT-2 (Fig. 7C). This result confirms previous findings [164] and partially explains why SLAMF7 acts in a purely inhibitory manner in monocytes. Comparison of EAT-2 at the protein level via flow cytometry showed that all HIV+ individuals have slightly increased EAT-2 expression over HCs (Fig. 7D). We did not, however, observe any differences in EAT-2 expression between SF7S and SLAMF7 responsive patients. Together, these results suggest that the mechanism underlying the loss of SLAMF7 inhibitory activity in monocytes may be independent of SLAMF7 and EAT-2 expression levels.

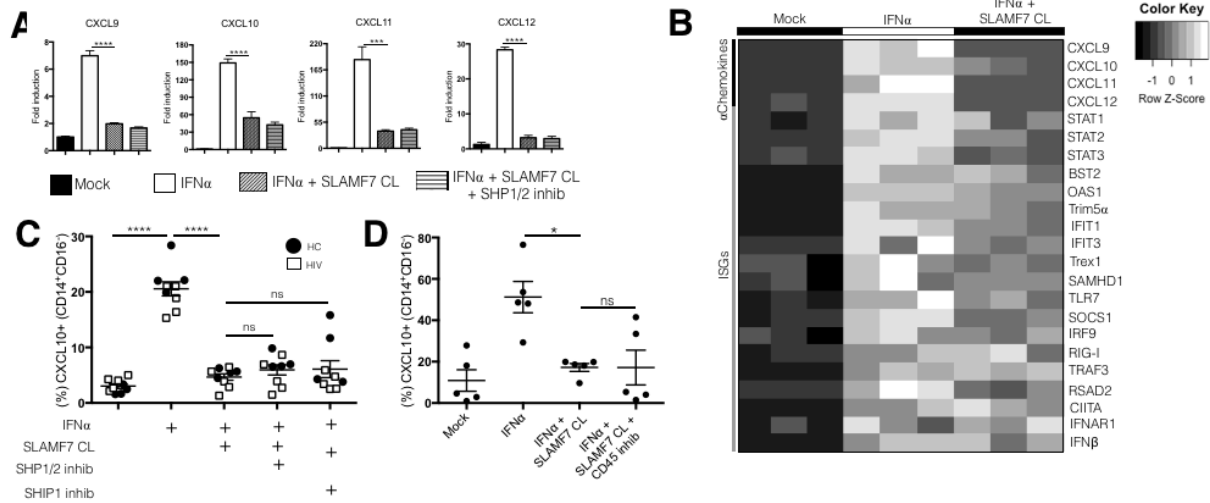


FIGURE 8: SLAMF7 activation on monocytes is selective for alpha chemokines and may not be mediated by any of the inhibitory phosphatases known to interact with SLAMF7.

(A and B) We assessed the effects of SLAMF7-mediated inhibition of other alpha chemokines (A) and ISGs (B) in isolated monocytes from HCs at the mRNA level by qRT-PCR. (C) The effects of SHP1/2 and SHIP1 on SLAMF7-mediated inhibition of CXCL10 was assessed via small molecule inhibitors (SHP1/2: NSC87877, 10 μ M) (SHIP1: 3AC, 5 μ M). SHP1/2 effects on alpha chemokines were also assessed at the mRNA level (A). (D) The role of CD45 in SLAMF7-mediated inhibition of CXCL10 was assessed via a small molecule inhibitor (CAS 345630-40-2, 1 μ M). (A and B) representative of 4 independent experiments. Groups in (A, B, C, and D) were compared using 1-way ANOVA with Tukey's multiple comparison test. Data presented as mean \pm SEM. *P<0.05, **P<0.01, ***P<0.001, ****P<0.0001.

SLAMF7 signaling in monocytes selectively inhibits IFN α -mediated production of alpha chemokines over other interferon-stimulated genes (ISGs) and host restriction factors.

We then investigated if the robust inhibition of CXCL10 was conserved across other alpha chemokines and ISGs. We noted that the inhibition of CXCL10 was conserved at the mRNA level and that this effect was consistent across CXCL9, CXCL11, and CXCL12 (Fig. 8A). Surprisingly, a number of other interferon stimulated genes and HIV-associated, interferon-modulated, host restriction factors including: BST2, OAS1, Trex1, and STAT1 showed only minor, or no inhibition following SLAMF7 activation (Fig. 8B).

SLAMF7-mediated inhibition of CXCL10 production in monocytes may be independent of SHP1, SHP2, SHIP1, or CD45.

To better understand the mechanism behind SLAMF7's inhibitory functions in monocytes, we evaluated a number of inhibitory phosphatases previously shown to interact with SLAMF7 and mediate its inhibitory functions [91, 92]. In an effort to continue using primary human monocytes, we tested a number of small molecule inhibitors targeting SHP1, SHP2, and SHIP1. Pre-treatment with either a small molecule inhibitor of SHP1/2 (NSC87877) (Fig. 8A and C) or SHIP1 (3AC) (Fig. 8C) did not result in recovery of CXCL10 expression in monocytes stimulated with IFN α and SLAMF7 cross-linking. We then hypothesized that SLAMF7's inhibitory function might be mediated by CD45, as CD45 has been previously implicated in SLAMF7's ability to propagate inhibitory signals in NK and multiple myeloma cells [92]. Pre-treatment with a small molecule inhibitor specific for CD45 (CAS 345630-40-2) in the presence of IFN α and SLAMF7 cross-linking also failed to rescue CXCL10 production (Fig. 8D). Finally, we speculated that SLAMF7 might prevent CXCL10 production by a mechanism that involves CXCL10 proteasomal degradation. Addition of the proteasome inhibitor Bortezomib did not result in recovery of CXCL10 expression in SLAMF7-stimulated cells, and actually further decreased CXCL10 production (Supplemental Fig. 2B). Interestingly, we also noted that Bortezomib acted synergistically with IFN α to upregulate SLAMF7 expression on monocytes (Supplemental Fig. 2C).

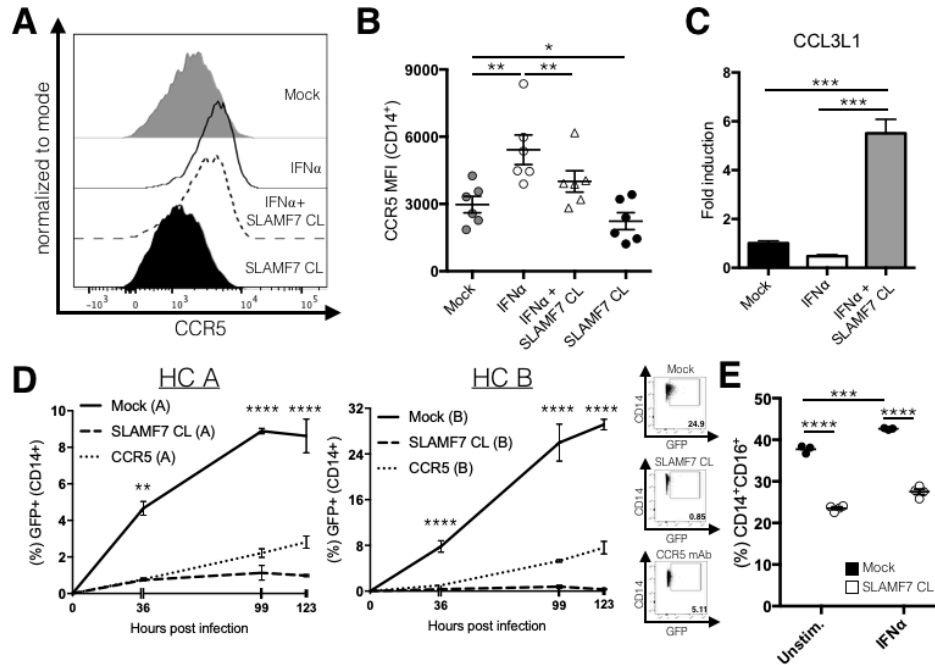


FIGURE 9: SLAMF7 activation inhibits monocyte infection with HIV-1 in vitro and down-regulates CD16.

(A and B) PBMCs from HIV+ individuals (n=6) were stimulated *in vitro* with IFN α and the SLAMF7 receptor was activated by cross-linking where indicated. Surface expression of CCR5 was measured by flow cytometry. (C) mRNA expression of CCL3L1 was assessed by qRT-PCR from the same samples in (Fig. 5A and B). (D) Isolated monocytes from 2 HCs (labeled “A” and “B”) were infected with HIV-1_{Ba-L}-GFP and infectivity was assessed at the indicated time points by FACS. Two technical replicates for each HC were analyzed. A CCR5 blocking mAb (10 μ g/mL) was included as a positive control. (E) PBMCs from a single HC were stimulated *in vitro* as indicated for 24 hours before analysis by flow cytometry. This experiment used 25 IU/mL IFN α . Percent indicated on y-axis is from all cells in FSC-A/SSC-A “monocyte” gate. (B and C) Groups compared using a 1-way ANOVA with Tukey’s multiple comparison test. (D and E) Groups compared using a 2-way ANOVA with Tukey’s multiple comparison test. Data presented as mean \pm SEM and are representative of 1 experiment (B and C) or 2 independent experiments showing similar results (D and E). *P<0.05, **P<0.01, ***P<0.001, ****P<0.0001.

SLAMF7 inhibits monocyte infection with HIV-1 in vitro.

HIV+ patients are known to have increased levels of circulating inflammatory monocytes (CD14⁺CD16⁺ and CD14^{low}CD16⁺⁺) which promote peripheral immune activation [165, 166], can become infected with HIV virus [105], and induce HIV-associated neurocognitive disorder (HAND). We next looked to see if SLAMF7 activation could affect the ability of monocytes to transition into pro-inflammatory subtypes (CD16⁺), as well as monocyte susceptibility to HIV

virus infection. Monocyte infection with HIV occurs via CCR5 [167, 168], which is known to be upregulated following IFN α stimulation [169]. We discovered that activation of SLAMF7 on monocytes from HIV+ individuals could down-regulate CCR5 both in the presence and absence of IFN α (Fig. 9A and B). Further supporting SLAMF7's utility as a means to prevent monocyte infection by HIV-1, we noted that activation of SLAMF7 in the presence of IFN α significantly upregulated the CCL3L1 chemokine (Fig. 9C), a chemokine that binds to CCR5 and directly prevents HIV infection of monocytes [170, 171]. Based on these findings we hypothesized that SLAMF7 activation in human monocytes might prevent HIV infection. Therefore, we performed an *in vitro* infection of isolated primary human monocytes from 2 HCs to determine if SLAMF7 activation could prevent HIV-1 infection. As a control, we also included a CCR5 blocking antibody. As expected, pre-treatment of human monocytes with anti-CCR5 mAb prevented HIV infection (Fig. 9D). Critically, infection of monocytes with HIV-1_{Ba-L}-GFP in the presence of SLAMF7 cross-linking resulted in dramatically reduced percentages of HIV-1 infected cells (Fig. 9D). To determine if SLAMF7 signaling affected CD16 expression on monocytes we utilized a previously described, IFN α -driven monocyte maturation assay [149]. We observed a significant down-regulation of CD16 on monocytes with SLAMF7 activation both in the presence and absence of IFN α stimulation (Fig. 9E) suggesting that SLAMF7 signaling can prevent induction of inflammatory monocyte subsets.

Neutrophils constitutively express CXCL10 and do not express SLAMF7.

Upon further review of our *in vitro* data we noticed a peculiar discrepancy between our flow cytometry and BioPlex results. Comparing (Fig. 5B and E) we noted that while we observed near

complete inhibition of CXCL10 from IFN α -stimulated monocytes following SLAMF7 activation on FACS analysis, we saw just an ~50% reduction in CXCL10 concentration in the culture supernatant. While this could have been from residual buildup of CXCL10 in the supernatant that occurs before SLAMF7 inhibition takes effect, we had determined that SLAMF7 begins to exert its inhibitory effects within a very short time frame (<4h), based on isolated monocyte experiments (Fig. 5D). This suggested that another cell type may also be responsible for CXCL10 production and may not be responding to SLAMF7 activation. We identified neutrophils (CD66b⁺ CD3⁻ CD19⁻ CD57⁻ CD16⁺⁺ CD14^{low/-}) as being SLAMF7⁻ and CXCL10⁺ at baseline in cART treated HIV individuals (Fig. 10A and B).

Neutrophils are unable to upregulate SLAMF7 in response to IFN α and SLAMF7 activation does not inhibit proinflammatory cytokine and chemokine release from neutrophils.

SLAMF7 expression on neutrophils in the presence and absence of IFN α stimulation was assessed by flow cytometry. We observed that neutrophils are unable to upregulate SLAMF7 in response to IFN α (Fig. 10C). This, combined with the knowledge that they are CXCL10⁺ at baseline, suggested that following appropriate stimulation, they should constitutively release CXCL10 regardless of the presence of SLAMF7 activating mAbs. We tested this via BioPlex analysis utilizing freshly isolated neutrophils from both HCs and HIV+ patients. We discovered that IFN α by itself can induce CXCL10 release from neutrophils, that this effect is enhanced by addition of LPS, and that addition of SLAMF7 cross-linking mAbs very minimally decreases CXCL10 release (Fig. 10D). Consistent with this result, we noted a similar pattern in regards to

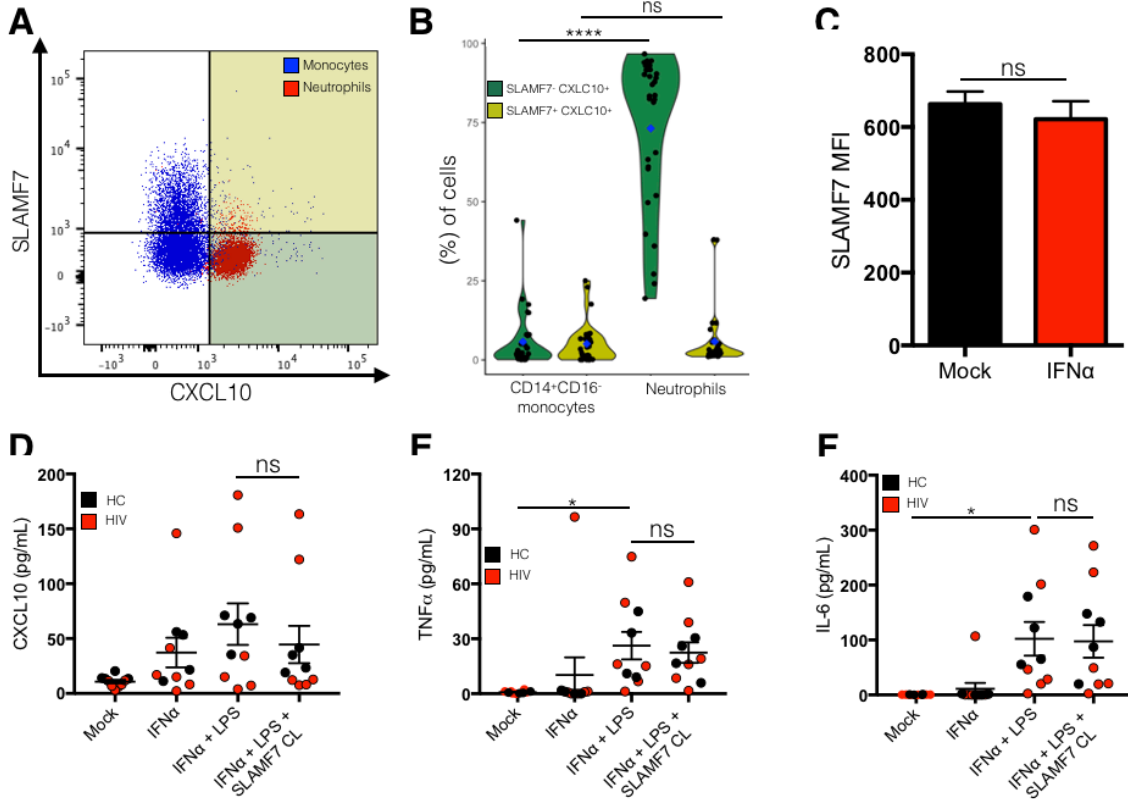


FIGURE 10: Neutrophils are SLAMF7⁻ and CXCL10⁺ and do not respond to SLAMF7 activation.

Baseline SLAMF7 and CXCL10 expression was examined on CD14⁺CD16⁻ monocytes and neutrophils by flow cytometry (A). (B) Quantification of results from (A) focusing on CXCL10⁺ cells. Color-coded quadrants in (A) correspond to dot colors in (B). (C) Neutrophils do not increase SLAMF7 expression in response to IFN α stimulation. (D-F) Isolated neutrophils from HCs and HIV patients were stimulated *in vitro* with IFN α , LPS, and SLAMF7 as indicated and supernatants were assessed by BioPlex assay for indicated cytokines/chemokines. (B) n=30. (C) n=3 independent donors from a single experiment. (D-F) Data presented is pooled from 2 independent experiments with n=10 donors. (B) Groups are compared using 2-way ANOVA with Sidak's multiple comparison test. Groups in (C) compared using 2-tailed T test. Groups in (D-F) compared using 1-way ANOVA with Tukey's multiple comparison test. Data presented as mean \pm SEM. *P<0.05, ****P<0.0001.

TNF α and IL-6 release from IFN α and LPS co-stimulated neutrophils (Fig. 10E and F, respectively).

Discussion

The discovery that global levels of SLAMF7⁺ PBMCs are increased in HIV infected patients in a clinical phenotype-dependent manner suggests that SLAMF7 receptor functions may play a role in modulating peripheral immune activation. Supporting the idea that SLAMF7 is a marker of

elevated type I interferons are reports showing SLAMF7 to be upregulated in systemic lupus erythematosus [172], rheumatoid arthritis [173], and multiple sclerosis [174]. While we focused on the effects of IFN α on SLAMF7 expression, it is well known that LPS can also up-regulate SLAMF7 through a NF- κ B-dependent mechanism [164]. HIV+ patients are known to have elevated levels of LPS in their blood as a result of a “leaky gut” [144]; we cannot exclude this as an additional possible reason for elevated SLAMF7 levels. The findings that discordant patients have extremely elevated SLAMF7 levels and that elite controllers have levels of SLAMF7 comparable to healthy controls supports the idea that assessing SLAMF7 expression levels on peripheral immune cells could be an effective gauge of a patients’ immune-activation status.

The finding that SLAMF7 activation can specifically inhibit CXCL10 and other alpha chemokines in monocytes is consistent with a previous study showing SLAMF7 has inhibitory effects in LPS-stimulated monocytes [164]. Interestingly, SLAMF7 activation minimally reduced HIV restriction factors, thus pharmacological modulation of SLAMF7 in the context of HIV infection could be beneficial in reducing peripheral immune activation, and preventing monocyte infection without affecting important viral restriction factors. However, this approach may only be effective in some HIV patients, since we identified a subset of HIV+ individuals, SF7S, who show a lack of response (or inverse response) to SLAMF7 activation. It is possible that the underlying mechanism to this paradoxical lack of SLAMF7 response is due to either genetic differences between patients, differential alterations in circulating cytokines or chemokines, or from specific interactions with HIV viral proteins.

Our small molecule studies suggest that there are yet other, unidentified inhibitory factor(s) which can interact with SLAMF7, or SLAMF7 may propagate its signals through ITSM-independent mechanisms [93]. Supporting this is the fact that most of the studies regarding the interaction of SLAMF7 with inhibitory phosphatases were performed in mice or human cell lines [91, 92, 159], thus it is possible that some of those findings are not entirely translatable to primary human cells. Regardless, SLAMF7 activation in monocytes may prove to be a useful method of preventing pathological activation of the CXCR3 receptor since it inhibits all CXCR3 ligands.

Both clinical and pre-clinical attempts at CXCL10 neutralization and/or CXCR3 receptor blockade have largely failed thus far [175-179]. Reasons for this include: failure of CXCL10-specific mAbs to inhibit all CXCR3 ligands, inability of anti-CXCL10 mAbs to compete with the high synthesis and turnover rate of CXCL10, and inability of some anti-CXCL10 mAbs to bind the glycosaminoglycan (GAG) bound form of CXCL10 (the active form of CXCL10). Importantly, SLAMF7-mediated inhibition of alpha chemokines has the ability to overcome all of these limitations and may find itself to be a useful therapeutic modality in diseases where over-expression of CXCL10 has been linked to pathogenesis including: rheumatoid arthritis [180], type I diabetes mellitus [181], systemic lupus erythematosus [182], multiple sclerosis [183], ulcerative colitis [184], and primary biliary cirrhosis [185].

It is well established that patients with HIV or a number of other diseases [186-188] have elevated levels of CD16⁺ monocytes and that these pro-inflammatory cells have been implicated in the pathogenesis of these conditions. To our knowledge there are currently no methods to reduce the number of circulating CD16⁺ monocytes in these individuals, except for a single *in vitro* report studying one of the components of cannabis, THC [149]. It would be interesting to see if SLAMF7-mediated down-regulation of CD16 is consistent *in vivo* and, if so, if there is any resultant effect on pathology in pre-clinical animal models.

Similar to its effect on CD16, the down-regulation of CCR5 on monocytes by SLAMF7 signaling could have potential benefits in the setting of HIV infection [189]. While there have been numerous attempts at either blocking/down-regulating CCR5 (notably, Maraviroc) or increasing the levels of chemokines, such as CCL3L1, (or engineered chemokines) specific for CCR5 for the treatment of HIV infection [190], there have not been any attempts to simultaneously apply both approaches. Activation of SLAMF7 on monocytes is unique in that it can accomplish this and potentially inhibit HIV-1 infection of monocytes and other CCR5-expressing immune cells.

We found that neutrophils are SLAMF7⁻ and CXCL10⁺ at baseline and are able to respond to stimulation by type I interferons, but not to SLAMF7 activation. The role of neutrophils in the context of HIV infection is complex and understudied [191]. Specifically, whether or not neutrophils contribute to peripheral immune activation in cART-treated individuals is unclear [191]. Our results suggest that neutrophils likely do contribute to peripheral immune activation.

Additionally, neutrophils are also known to play an important role in neuroinflammation [192] and have recently been discovered to be present in high levels in the brain at steady state [193]. While the role of neutrophils in the CNS of HIV+ individuals and in HAND is unknown, our results suggest that if they do play a role, it is likely one that cannot be modulated through the SLAMF7 receptor. The discovery that neutrophils were able to secrete CXCL10 following IFN α and LPS stimulation highlights the need to consider the effects neutrophils are playing in diseases characterized by chronic type I interferon activation.

In summary, we determined that SLAMF7 is up-regulated globally in HIV patients who have high levels of peripheral immune activation and that SLAMF7 functions to both prevent HIV viral infection of monocytes, and inhibit CXCL10 from monocytes stimulated with type I and II interferons, except in a subset of HIV patients. We also discovered that neutrophils fail to express SLAMF7, constitutively express CXCL10, and are non-responsive to SLAMF7 activation, implicating them as potential propagators of chronic, peripheral immune activation in type I interferon-mediated diseases.

Acknowledgments: We thank the MSU flow cytometry core and Dr. Louis King for assistance with flow cytometry, the MSU genomics core for assistance with qRT-PCR, the MSU Center for Statistical Training and Consulting (CSTAT) and Hope Akaeze for advice on clustering, MSU Clinical and Translational Sciences Institute (MSU-CTSI) for support with patient recruitment and sample collection, Candace Savonen for assistance with R, and to all of the patients for

graciously volunteering to assist with this study. Thanks to Joseph Henriquez for assistance with sample preparation and advice on assay design. Special thanks to Dr. Young-Hui Zheng for providing HIV-1-Ba-L-GFP virus.

Author contributions: PO and YAA designed the experiments. PO, YP, RBC, MDR, MKB, SH, and SG carried out the experiments and collected data. PO and YAA analyzed the data. CPH managed the cell line. NEK, PG, and AA established the mid-Michigan HIV Consortium Registry. LD and PG recruited patients, provided clinical data and collected patient samples. YAA supervised the project. PO and YAA drafted the manuscript and all authors assisted in editing the manuscript.

Conflicts of interest: YAA and AA hold a patent on the SLAMF7-Fc fusion protein. YAA and PO have a patent pending regarding the modulation of SLAMF7 signaling to prevent inflammation and HIV viral infection. The authors declare no additional conflicts of interest.

CHAPTER: 3 In vitro infection of primary human monocytes with HIV-1

This chapter is adapted from an article published in Bio-protocol, Volume 9, Issue 13, July, 2019.

Authors: Patrick O'Connell, Yong-Hui Zheng, Andrea Amalfitano and Yasser A. Aldhamen

Abstract

Monocyte infection by HIV-1 is an important component of chronic HIV pathogenesis. Following infection by HIV-1, monocytes are able to cross the blood brain barrier and set up a viral reservoir in the central nervous system. Additionally, in the setting of chronic HIV-1 infection, monocytes can become activated either directly through HIV-1 infection or indirectly via HIV-1-mediated systemic immune activation. Currently, there are few studies looking at HIV-1 infection of primary human monocytes in vitro. Furthermore, detection of successful HIV-1 infection of monocytes can be laborious requiring an ELISA for p24 or assessing levels of HIV-1 mRNA or DNA. This protocol utilizes an HIV-1 strain expressing GFP to allow for easy quantification of HIV-1 infection by fluorescence-assisted cell sorting (FACS). By determining HIV-1 infection by FACS one can take advantage of its multiparametric nature allowing for the use of less cells and the ability to assess the expression of other markers on HIV-1⁺ and HIV-1⁻ cells in the same experiment. Additionally, this protocol could be modified to study HIV-1 infection of other cells including CD4⁺ T cells.

Background

This protocol will be of use to those looking to perform studies assessing the role that myeloid cells play in HIV-1 infection. Myeloid cells, in particular, monocytes, have been recognized as crucial mediators of chronic and acute inflammation in HIV-1 infection [104, 194, 195]. Gaining a deeper understanding of the interactions between the HIV-1 virus and monocytes will be fundamental in advancing our knowledge on how HIV-1 infection produces a chronic state of immune activation, even in the presence of combined anti-retroviral therapy [194]. With persons infected by HIV-1 now exhibiting lower death rates, we are just now seeing the long-term effects

of HIV-1-induced chronic immune activation which can present as: HIV-associated neurocognitive disorder (HAND), hepatic steatosis, renal failure, hepatitis, atherosclerosis, insulin resistance, osteoporosis, and more [141, 142].

The method presented here will be useful to both study how HIV-1 infection of monocytes alters cellular function, and to facilitate the development of novel methods to modulate or prevent HIV-1 infection of monocytes. In particular, this protocol is advantageous in that it allows for quick and easy analysis of monocyte HIV-1 infection using FACS without the need to intracellular stain for p24.

Materials and Reagents

1. LS columns (Miltenyi Biotec, catalog number: 130-042-401)
2. Glass Pasteur pipettes, autoclaved (VWR, catalog number: 14672-200)
3. Aspirating bulb for use with Pasteur pipet (CELLTREAT Scientific Products, catalog number: 229279)
4. 50 ml conical tubes (Corning, catalog number: 430290)
5. Serological pipettes (Costar)
6. 1 ml micropipette
7. 96-well high-binding plates (Corning, catalog number: 3361)
8. Pipette tips
9. pNL-BaL-GFP recombinant HIV-1 virus

Construction of pNL-BaL-GFP HIV-1 vector. The pNL4-3env(-)GFP, which encodes full-

length NL4-3 HIV-1 proviral DNA with a frameshift in *env* and expresses GFP in place of *nef*, was described previously (He *et al.*, 1997). The CCR5-tropic HIV-1 proviral clone, R9BaL, was generated from R9 by replacing an EcoRI-XhoI fragment from the CCR5-tropic HIV-1 strain, BaL, which contains the entire *env* coding region (Gallay *et al.*, 1995). pNL-BaL-GFP was constructed by replacing a Sall-BamHI fragment in pNL4-3env(-)GFP with that from R9BaL.

10. Antibodies:

- a. CD14, PE-Cy7 (clone: 61D3) (Thermo Fisher, catalog number: 25-0149-42)
- b. CD16, BV510 (Clone: 3G8) (BD BioSciences, catalog number: 563830)
- c. SLAMF7, PE (Clone: 162) (BioLegend, catalog number: 331806)
- d. CCR5, unconjugated (Clone: 2D7) (BD BioSciences, catalog number: 555990)

11. Viability dye: Live/Dead Violet (Thermo Fisher, catalog number: L34964)

12. CD14 microbeads, human (Miltenyi Biotec, catalog number: 130-050-201)

13. Fresh human buffy coat (Gulf Coast Regional Blood Center, Texas, USA)

14. Lympholyte-H (Cedarlane Labs, catalog number: CL5020)

15. DPBS without calcium or magnesium (Gibco, catalog number: 14190250)

16. RPMI 1640 (Gibco, catalog number: 11875093)

17. ACK Lysis buffer (Gibco, catalog number: A1049201)

18. Fetal Bovine Serum (FBS) (Atlanta Biologicals, catalog number: S11550)

19. Antibiotic/Antimycotic (Penicillin, Streptomycin, Fungizone) (PSF) (Gibco, catalog number: 15240062)

20. Ethylenediaminetetraacetic acid (EDTA) (Millipore Sigma, catalog number: E6758)

21. BSA (Millipore Sigma, catalog number: A9056)
22. Sodium azide (Millipore Sigma, catalog number: S2002)
23. Fixation buffer from BD Fix/Perm kit (BD Biosciences, catalog number: 554714)
24. Cross-linking antibody of choice (for stimulation of monocytes during HIV-1 infection)
25. FACS solution (see Recipes)
26. MACS solution (see Recipes)
27. Complete RPMI solution (see Recipes)

Equipment

1. Biosafety cabinet
2. Gun pipette
3. QuadroMACS magnetic cell separator (Miltenyi Biotec, catalog number: 130-090-976)
4. LSRII flow cytometer (BD Biosciences)
5. Tabletop centrifuge with swinging bucket rotor
6. Automated cell counter (Countess) (Invitrogen)

Software

1. FlowJo version 10.5 (<https://www.flowjo.com>)
2. GraphPad Prism V7 (<https://www.graphpad.com/scientific-software/prism/>)

Procedure

1. Isolate PBMCs from a fresh human buffy coat using Lympholyte-H under sterile conditions.

Note: Perform all the following steps in a sterile biosafety cabinet.

- a. Allow Lympholyte-H to equilibrate to room temperature. This is important to ensure efficient isolation of peripheral blood mononuclear cells (PBMCs).
- b. Split approximately 50 ml buffy coat evenly into four 50 ml conical tubes (12.5 ml per tube).
- c. Add 22.5 ml DPBS to each tube containing pure buffy coat to bring the volume up to 35 ml. (The ratio of DPBS to buffy coat should be greater than 1:1.)
- d. Shake vigorously (or vortex) the 50 ml conical tubes for 10 s. This is important to prevent clumping of cells which will affect isolation and can cause RBC contamination.
- e. Shake lympholyte-H vigorously just before use.
- f. Work in a biosafety cabinet with lights off.

Note: Lympholyte-H is light sensitive.

- g. Place a sterile glass Pasteur pipette into the bottom of a 50 ml conical tube containing the blood/DPBS mixture. Add Lympholyte-H to the glass Pasteur pipette using a gun pipette. This is best accomplished using a 10 ml stripette with the power setting on the gun pipette set to "gravity". A total of 10 ml of Lympholyte-H should be added per 50 ml conical tube.
- h. Lympholyte-H should immediately begin to form a layer on the bottom of the conical tube, clearly separated from the buffy coat (Figure 11.h).
- i. Add a total of 10 ml lympholyte-H to each 50 ml conical tube.
- j. Repeat for each 50 ml conical tube. The final volume in each tube will now be 45 ml.
- k. Spin 50 ml conical tubes at 1,800 x g, 24 °C, no break, maximum acceleration, and

- minimum deceleration, for 30 min in any swinging bucket benchtop centrifuge.
- l. Attach a rubber suction bulb to a fresh Pasteur pipette. Carefully remove the middle lymphocyte band (approximately 5 ml) from each 50 ml conical tube. This band will be cloudy, may contain some RBCs, and will be located above the pelleted RBCs (at the bottom of the tube) (Figure 11.I).
 - m. Transfer these cells to a fresh 50 ml conical tube.
 - n. Repeat this for each of the four 50 ml conical tubes.
 - o. Add DPBS to a final volume of 50 ml into each new 50 ml conical tube containing pure lymphocytes.
 - p. Spin the tube at $1,500 \times g$, $24\text{ }^{\circ}\text{C}$, full break for 5 min.
 - q. Discard the supernatant.
 - r. Resuspend each pellet in 2 ml ACK Lysis buffer using a 1 ml micropipette. Ensure pellet is fully resuspended.
 - s. Incubate cells in ACK lysis buffer for exactly 6 min at room temperature.
 - t. Top with DPBS, spin the tube at $900 \times g$, $24\text{ }^{\circ}\text{C}$, full break for 5 min.
 - u. Discard the supernatant.
 - v. Resuspend in complete RPMI pre-warmed to $37\text{ }^{\circ}\text{C}$ using a 1 ml micropipette. Ensure cells are in a single cell suspension. Add a total of 10 ml of media per buffy coat. At this stage, you can combine cells from the 4 separate fractions (Figure 11.v).
 - w. Prepare 1:100 dilution of cells into complete RPMI and count on a Countess (or your preferred method) per manufacturer's instructions.

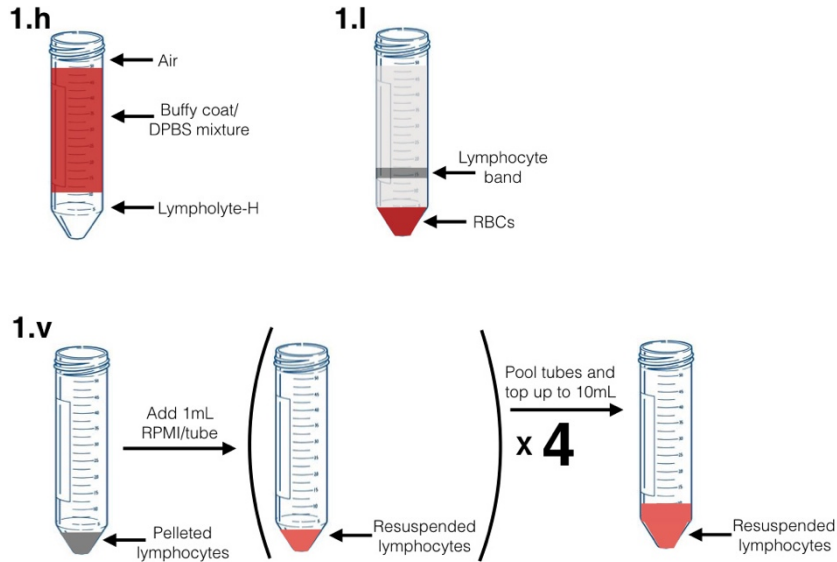


FIGURE 11: Graphical diagram for selected steps in part 1 of procedure (PBMC) isolation.

Figure labels correspond to indicated steps in PBMC isolation procedure.

2. Isolate CD14⁺ monocytes by positive selection (CD14 microbeads, Miltenyi Biotec) per manufacturer recommendation using MACS buffer.

Note: Incubate cells with anti-CD14 microbeads for 25 min to increase the purity of isolated monocytes.

3. Check the purity of monocytes before proceeding. Stain cells (pre and post-isolation) with CD14 PE-Cy7 mAb and Live/Dead Violet viability dye per manufacturer's instructions and as previously described (O'Connell *et al.*, 2018). Run cells on LSRII flow cytometer (or other flow cytometers) and determine % of cells CD14⁺ that are viable (Figure 12). If isolated monocyte samples are less than 90% CD14⁺ it is recommended not to proceed. Should monocyte purity be < 90% you may return the monocytes to MACS buffer (if you have already resuspended them in complete RPMI) and pass them through a fresh MACS LS

column exactly as performed in Step 2.

4. Resuspend monocytes in complete RPMI and plate in 96-well high-binding cell culture plates at 2×10^5 cells/well.
5. If activation of a monocyte cell surface receptor is desired [*e.g.*, SLAMF7, [27]], coat high-binding plate with an antibody against the desired receptor for 24 h at 4 °C beforehand. Dilute cross-linking antibody in DPBS before adding it to wells for cross-linking. Wash wells 3 times with DPBS before addition of cells and make sure wells do not dry out at any point.
6. As a positive control, if using an R5-tropic HIV-1 virus, add 10 µg/ml of the CCR5-blocking mAb (2D7) per appropriate well. Wells containing this soluble mAb should retain appropriate concentrations of this mAb at all media changes.
7. After 24 h of cell culture at 37 °C and 4% CO₂, remove media and add fresh media containing 190 pg/ml pNL-BaL-GFP.
8. After 4 h, wash pNL-BaL-GFP infected cells 2 times with complete RPMI.
9. Resuspend cells in 200 µl complete RPMI/well and culture at 37 °C and 4% CO₂.
10. Every 24-36 h remove an aliquot of cells (*i.e.*, one well) per condition and wash them with FACS.
11. Stain cells with CD14, CD16, Live/Dead Violet viability dye, and any other antibodies (*i.e.*, SLAMF7) desired as previously described [27].
12. Fix cells for 20 min at room temperature, protected from light, by adding 200 µl of BD Fixation buffer per well and thoroughly resuspending cells.
13. Wash cells twice with FACS.
14. Analyze stained cells on an LSRII (or similar flow cytometer) to determine (%) CD14⁺

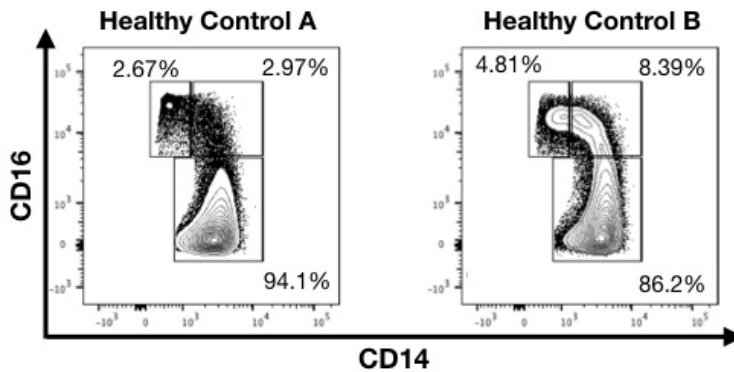


FIGURE 12: FACS plots showing subtypes of monocytes between 2 healthy blood donors.

Healthy control B has considerably more CD16⁺ monocytes. Cells shown are gated on singlets, myeloid cell population (based on FSC and SSC), living, and expressing CD14.

Live/Dead Violet⁻ GFP⁺ cells.

Note: Cells should be analyzed within 24 h of picking them up to ensure GFP signal is not lost. Fixation will not affect GFP signal over short term (less than 24 h), but prolonged fixation will degrade GFP.

15. GFP⁺ cells are considered to be HIV-1⁺ as all infected cells using this virus will express GFP. The addition of CD14 and viability markers ensure that cells analyzed are monocytes (*i.e.*, CD14⁺) and living (*i.e.*, Live/Dead Violet⁻).

Data analysis

1. Analyze all data using FlowJo v10.5 or greater (or other FACS analysis software per your preference).
2. Analyses should be conducted by assessing the (%) CD14⁺ Live/Dead Violet⁻ GFP⁺ cells per condition. Inclusion of other markers can be included to allow for additional analyses.
3. Example analyses are presented in Figure 13.

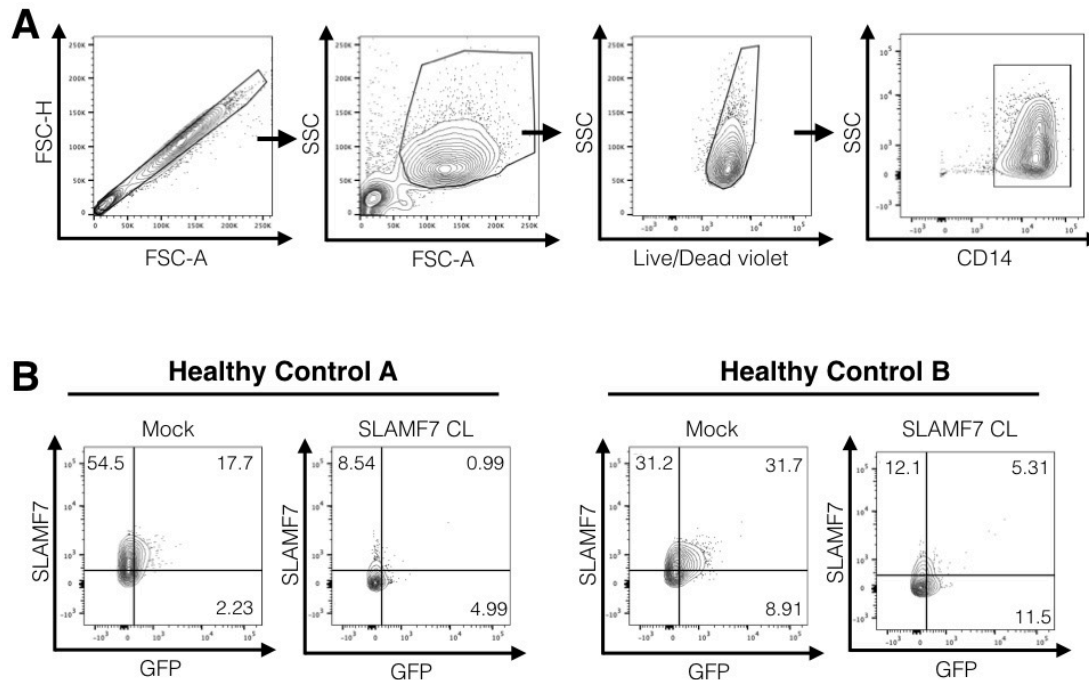


FIGURE 13: Example FACS analysis.

A. Representative gating scheme used for analysis of monocyte infectivity. B. Representative FACS plots showing examples of positive and negative GFP monocytes from the CD14⁺ gate above. Mock conditions are monocytes infected with pNL-BaL-GFP and no immune cell receptor cross-linking. Note how HIV-1⁺ monocytes tend to be positive for the SLAMF7 receptor and activation of the SLAMF7 receptor via cross-linking prevents monocyte infection. Co-expression analyses like this can be performed with any other marker of interest. CL; cross-linking.

4. When comparing infectivity between groups, use a student's *t*-test or one-way ANOVA as appropriate.
5. Data can be displayed as an X-Y graph with connecting lines (O'Connell *et al.*, 2018, Figure 6d) and also as a FACS dot plot to provide additional support for your results (O'Connell *et al.*, 2018, Figure 6d).

Notes

1. This protocol has been reproducible in our hands, and we have only noticed variability in the degree of infectivity between individual blood donors.
2. Refresh media on cultured monocytes every 48 h.

3. Culture cells for a maximum of 7 days. Primary human monocytes will not typically survive more than 7 days post-isolation.
4. Monocytes should show a time-dependent increase in the number of HIV-1⁺ cells until approximately 6-7 days, at which point the infectivity should level out as monocytes reach their terminal ex-vivo lifespan.
5. The efficiency of HIV-1 infection of monocytes will vary between subjects and is dependent on the percent of CD16⁺ monocytes. Individuals with higher levels of CD16⁺ monocytes will show a greater percent of HIV-1⁺ monocytes (Figures 12 and 13) [167, 168].

Recipes

1. FACS solution

500 ml DPBS (1 bottle)

1% (W/V) BSA

0.1% (W/V) sodium azide

2. MACS solution

500 ml DPBS (1 bottle)

0.5% BSA

2 mM EDTA (used for CD14 isolation)

3. Complete RPMI solution

500 ml RPMI 1640

10% FBS

1% PSF

Acknowledgments

This work was supported by the NIH in the form of an R21 grant to YAA (1R21AI122808-01).

We also thank Sarah Godbehere for her critical review of this manuscript. This method is adapted from Wang *et al.*, 2018.

Competing interests

PO and YAA have a patent pending regarding modulation of SLAMF7 signaling for the treatment of inflammation. The authors declare no additional conflicts.

CHAPTER: 4 SLAMF7 Signaling Reprograms T Cells toward Exhaustion in the Tumor
Microenvironment

This chapter is adapted from an article published in the *Journal of Immunology*, Volume 206, Issue 1, Pp. 193-205 January, 2021.

Authors: Patrick O'Connell, Sean Hyslop, Maja K. Blake, Sarah Godbehere, Andrea Amalfitano and Yasser A. Aldhamen

Abstract

T cell exhaustion represents one of the most pervasive strategies tumors employ to circumvent the immune system. While repetitive, cognate T cell receptor signaling is recognized as the primary driving force behind this phenomenon, it remains unknown what other forces drive T cell exhaustion in the tumor microenvironment (TME). Here, we show that activation of the self-ligand SLAMF7 immune receptor on T cells induced STAT1 and STAT3 phosphorylation, expression of multiple inhibitory receptors, and transcription factors associated with T cell exhaustion. Analysis of The Cancer Genome Atlas revealed that SLAMF7 transcript levels were strongly correlated with various inhibitory receptors, and that high SLAMF7 expression was indicative of poor survival in clear cell renal cell carcinoma (ccRCC). Targeted reanalysis of a CyTOF dataset which profiled the TME in 73 ccRCC patients, revealed cell-type specific SLAMF7 expression patterns, strong correlations between exhausted T cells and SLAMF7⁺ tumor-associated macrophages (TAMs), and a unique subset of SLAMF7^{high}CD38^{high} TAMs. These SLAMF7^{high}CD38^{high} TAMs showed the strongest correlations with exhausted T cells and were an independent prognostic factor in ccRCC. Confirmatory *ex vivo* co-culture studies validated that SLAMF7-SLAMF7 interactions between murine TAMs and CD8⁺ T cells induces expression of multiple inhibitory receptors. Finally, mice lacking SLAMF7 show restricted growth of B16-F10 tumors and CD8⁺ T cells from these mice express less PD-1 and TOX, and exhibited an impaired ability to progress through the exhaustion developmental trajectory to terminal exhaustion. These findings suggest that SLAMF7 might play an important role in modulating T cell function in the TME.

Introduction

The biological process of T cell exhaustion (or dysfunction), resulting from chronic T cell stimulation and activation has emerged as one of the most important topics in immunology and cancer biology [115, 196-198]. T cells undergoing persistent T cell receptor (TCR) stimulation, as occurs in the tumor microenvironment (TME), begin a process whereby they assume a cellular state less amenable to proliferation, cytokine production, and cytotoxicity [115, 197, 198].

Conversion of infiltrating T cells to an exhaustion phenotype is a well-known hallmark tumors use to evade the host immune response and continue unchecked growth [199-201].

These exhausted or dysfunctional T cells are characterized at the cellular level by epigenetic remodeling [197, 202, 203] and expression of a number of inhibitory receptors, also known as checkpoint receptors, including: PD-1, CTLA-4, LAG3, Tim3, TIGIT, VISTA, CD38, 2B4 [56], and others [115, 196]. Through both known and unknown mechanisms, these inhibitory receptors directly inhibit regulatory and effector T cell functions and are responsible for the characteristic loss of effector function observed in exhausted T cells [197]. Antibodies targeting these inhibitory receptors are showing great promise in generating responses in cancer patients, however responses vary by tumor type and the majority of patients do not respond effectively to checkpoint blockade of PD-1, PD-L1, or CTLA-4 [204], and a combination of PD-1 and CTLA-4 blockade results in substantial risk of serious adverse events [205, 206]. Consequently, there is a need to understand why some patients do not respond to checkpoint blockade, what additional signals besides repetitive TCR signaling induce inhibitory receptors on T cells in the TME, and if T cell exhaustion can be prevented from occurring in the first place [197].

Renal cell carcinoma [207] is the most common cancer of the genitourinary system, with over 400,000 new cases and over 175,000 deaths each year, and continues to increase in prevalence [208]. The clear cell renal cell carcinoma (ccRCC) subtype is the most common form of RCC, and while a heterogeneous disease, it has a unique TME making it an attractive target for immunotherapy [208, 209]. In contrast to most tumors where the TME is dominated by M-2 macrophages, the ccRCC TME is composed primarily of T cells, with a large portion consisting of CD8⁺ T cells [209, 210]. However, the infiltrate of cytotoxic T lymphocytes does not portend a favorable prognosis due to extensive levels of T cell exhaustion [211-213]. ccRCC is notable in that, of all the cancers in The Cancer Genome Atlas (TCGA), immune evasion occurs in ccRCC almost entirely via T cell exhaustion [213]. This has paved the way for trials of various checkpoint inhibitors in ccRCC, with the most recent findings of the CheckMate 214 trial establishing combination ipilimumab (anti-CTLA-4) and nivolumab (anti-PD-1) as first-line treatment for intermediate or poor-risk ccRCC patients [208, 214]. However, this regimen lacks effectiveness in all ccRCC patients [204] and can cause significant adverse effects [205, 206, 214], signifying the need to better understand T cell exhaustion mechanisms in ccRCC.

The SLAMF7 (CRACC, CD319, CS-1) receptor is a member of the signaling lymphocytic activation molecules [SLAM] family of receptors [9], with expression restricted to hematopoietic cells, and is present at differing frequencies on various types of immune cells [9, 215, 216]. SLAMF7, and other SLAM family members (except 2B4), are unique in that they function as homotypic receptors, which once activated, recruit various SH2 domain-containing proteins to their cytoplasmic immunoreceptor tyrosine-based switch motifs (ITSMs) [9, 91]. In doing so, SLAMF7

is able to modulate a host of immune cell-specific functions across various immune cell types [9, 91, 92, 216]. SLAM family receptors are increasingly being linked to T cell exhaustion, with expression of SLAMF6 recently discovered as a marker to identify progenitor exhausted CD8⁺ T cells [89], and both SLAMF6 and SLAMF4 (2B4) being shown to function as inhibitory receptors on CD8⁺ T cells [56, 217]. Notably, SLAMF7 has also recently been linked to a CD8⁺ T cell subset enriched in melanoma patients who fail to respond to checkpoint blockade [218], and expressed on certain memory-precursor and effector CD8⁺ T cells which respond indirectly to checkpoint blockade [219]. Here, we set out to define the role of SLAMF7 on T cell regulation in the context of T cell exhaustion. We uncovered a novel role for SLAMF7 in regulating the expression of various T cell inhibitory receptors, exhaustion-promoting transcription factors, and STAT1/3 phosphorylation in a TCR-independent manner. Also, we find that SLAMF7 self-ligation between TAMs and T cells is sufficient to induce the upregulation of these inhibitory receptors. Our data identify SLAMF7 as a novel regulator of T cell inhibitory programs, with potential clinical implications and therapeutic opportunities.

Materials and Methods

Reagents used. The following human antibodies were used: CD3-FITC (HIT3a), CD4-V450 (RPA-T4), CD8-Alexa700 (HIT8a), SLAMF7-PerCp-eFluor710 (162), LAG-3-APC-eFluor780 (T47-530), TIM-3-PE-Cy7 (F38-2E2), EZH2-PE (11/EZH2), PD-1-Alexa488 (EH12.2H7), FoxP3-BV421 (206D), YY1-Alexa594 (H-10), Blimp-1-DyLight650 (3H2-E8), CTLA4-FITC (14D3), IL-2-APC (MQ1-17H12), TNF α -Alexa488 (Mab11), IFN γ -PE (4S.B3), STAT1 (pY701)-Alexa647, STAT2 (p690)-PE, STAT3 (p704)-Alexa647, STAT5 (p694)-Alexa647, STAT6 (p641)-Alexa647, P38 MAPK (pT180/pY182)-

Alexa647, ERK1/2 (pT202/pY204)-Alexa647, ZAP70 (p319/p352)-PE, and SLAMF7 (162.1) (used for cross-linking). Mouse antibodies used include: CD3-APC (145-2C11), CD38-BV510 (90/CD38), CD8a-Alexa700 (53-6.7), LAG3-PE (C9B7W), Tim3-APC-Fire750 (B8.2C12), PD-1-PerCp-eFluor710 (J43), 2B4-FITC (eBio244F4), SLAMF7-BV421 (4G2), CD11b-BV570 (M1/70), CD19-PerCp-Cy5.5 (1D3), Ly6G-BV711 (1A8), Ly6C-BV421 (HK1.4), MHC-II-BV785 (M5/114.15.2), CD206-Alexa647 (C06862), CD45-Alexa532 (30-F11), NK1.1-PE-Cy7 (PK136), SLAMF7-APC (4G2), CD11c-PE-CF594 (HL3), CCR2-BV750 (475301), LAG3-BV785 (C9B7W), CD3-BUV737 (17A2), TOX-eFluor660 (TXRX10), SLAMF6-BUV395 (13G3), CD69-PE-Cy7 (H1.2F3), and CD4-eFluor450 (RM4-5). All antibodies were purchased from BioLegend, BD Biosciences, or ThermoFisher. Recombinant human IL-2 (PeproTech) was used at 300 IU/mL. Recombinant murine IL-2 (R&D Systems) was used at 300 IU/mL. CD3/28 Dynabeads (ThermoFisher) were added at a 1:1 cell:bead ratio.

Blood sample collection and human T cell isolation. Fresh PBMCs were obtained from buffy coats and processed as previously described [220]. CD3⁺ T cells were isolated from PBMCs via negative selection using Dynabeads Untouched Human T Cells Kit (ThermoFisher) per manufacturer's instructions.

In vitro human T cell culture and stimulation. Isolated, fresh, primary human CD3⁺ T cells were plated at 2×10^5 cells/well in 96-well plates. Cells were cultured in complete RPMI (RPMI 1640, 10% FBS, 1X penicillin, streptomycin, and fungizone). For cross-linking experiments, 8 μ g/ml anti-SLAMF7 (162.1) mAb was added to a sterile, high-binding 96-well cell culture plate overnight at 4°C. Wells were washed with PBS three times before addition of cells. Cells were

cultured for indicated times at 37°C and 5% CO₂. For 6 day time points, cells were cultured in the presence of stimuli for 3 days before being moved into a fresh SLAMF7 mAb cross-linked plate with fresh media and rhIL-2. For re-stimulation experiment, cells were washed and all stimuli removed after 6 days of culture. Cells were re-plated in fresh complete media with 300 IU/mL IL-2 and CD3/28 Dynabeads at a 0.2:1 bead:cell ratio, and cultured for an additional 3 days. GolgiPlug was added for the last 4 hrs of culture and intracellular staining of cytokines was performed with BD CytoFix/Perm kit per manufacturer's instructions.

Phosphoflow experiments. Isolated, primary human CD3⁺ T cells were rested for 24hrs in 40 IU/mL rhIL-2 in complete RPMI. Cells (300,000 per well) were stimulated in 96-well plates as indicated for various time points at 37°C and 5% CO₂ before being fixed in BD CytoFix/Perm buffer at 37°C and 5% CO₂. Permeabilization was performed with BD Phosflow Perm Buffer IV (0.5X) per manufacturer's instructions. Cells were stained with anti-CD4, anti-CD8, and a mAb against a single phosphorylated protein at the same time. Samples were run on a Cytex Aurora spectral cytometer.

Animal procedures and generation of SLAMF7^{-/-} mice. All mice used in experiments were bred in house. SLAMF7^{-/-} genotype was verified by PCR. 8-12 week old WT (C57BL/6J) or SLAMF7^{-/-} (C57BL/6J background) were used for all experiments. SLAMF7^{-/-} mice were generated at MSU Transgenic and Genome Editing Facility (MSU-TGEF) using CRISPR-Cas9 with gRNAs targeting introns between exon 2/3 and exon 5/6 of SLAMF7. Genomic deletion of this region of SLAMF7 completely abrogates SLAMF7 expression on all cells. A single founder mouse with homozygous

deletions in both introns was bred to a WT mouse, and the F1 progeny were bred together to establish a stable line of SLAMF7^{-/-} mice.

B16 tumor experiments and murine immune cell isolations. Investigators were blinded to mouse genotypes when measuring tumors. Either 7x10⁵ B16 tumor cells (for experiments involving isolation of TAMs) or 4x10⁵ B16 tumor cells (for tumor growth experiments) were injected into the hind flank of WT and SLAMF7^{-/-} mice. For TAM isolation experiments tumors were harvested 25 days later and manually dissociated into a single-cell suspension. For tumor growth and TIL phenotyping experiments tumors were harvested at completion of tumor measurements. Cell suspension was pelleted and resuspended in RPMI with 0.5 mg/mL Collagenase IV (Milipore-Sigma) and 1,000 IU/mL DNaseI (Millipore-Sigma) under constant, gentle agitation at 37°C for 1 hr. Digestion was stopped with EDTA and cell suspension was filtered through a 40µm cell strainer. Cells were then subject to a Ficoll-Paque gradient centrifugation step to enrich for immune cells. Cells were washed three times with complete RPMI before immune cell isolation procedures. TAMs were isolated from dissociated B16 tumors using a mouse CD11b positive selection kit (StemCell) per manufacturer's instructions. CD8⁺ T cells were isolated from excised B16 tumors and splenocytes using a CD8a positive selection kit (Miltenyi Biotec) per manufacturer's instructions. Murine immune cells were either stained directly for spectral cytometry analysis or plated for co-culture experiments. For TAM-CD8 T cell co-culture experiments, 5x10⁴ TAMs and 1.5x10⁵ CD8⁺ T cells (1:3 ratio) were plated in a 96-well cell culture plate in complete RPMI supplemented with an additional 1% PSF and 50 IU/mL rmlL-2. Cells were cultured for 6 days at 37°C and 5% CO₂ with a media change at 3 days.

For murine *in vitro* CD3/28 stimulation experiment, mouse total splenocytes were cultured for 6 days in complete RPMI and 50 IU/mL rIL-2 with or without murine CD3/28 Dynabeads at a 1:1 cell:bead ratio. BMDMs were generated as previously described [113].

Spectral cytometry. Cells were prepared and stained as previously described [216].

Transcription factor and cytokine staining was performed with the Transcription Factor Buffer Set (BD Biosciences) per manufacturer's instructions. For IL-2 intracellular staining, GolgiPlug (BD Biosciences) was added for the final 4.5 hrs of cell culture. Viability staining was performed with either Zombie NIR Fixable Viability Kit (BioLegend) or LIVE/DEAD Aqua fixable viability dye (ThermoFisher), and was included in all experiments. Fc receptors were blocked in all samples during staining with human Fc block (BD biosciences) or mouse Fc block (BD biosciences).

Samples were acquired on a 5-laser Cytex Aurora Spectral Cytometer. Spectra were unmixed using SpectroFlo software and data was analyzed using FlowJo version 10.6.1 (Tree Star). SPICE plots were generated using Pestle version 2.0 and SPICE version 6.0 (35). For (Fig. 15e), tSNE dimensionality reduction was performed in FlowJo on a concatenated FCS file containing Mock and SLAMF7 CL samples, in duplicate, from two healthy donors with the following tSNE parameters: iterations=7000, perplexity=70. FlowSOM clustering was performed in FlowJo with the number of meta-clusters set to 10. Clusters with very few cells and high similarity to existing clusters were manually merged with those clusters to obtain a final consensus of 4 CD8 T cell clusters and 2 CD4 T cell clusters. Merged FlowSOM clusters were color-coded and overlaid onto the tSNE map of all T cells. The same approach was repeated for (Fig. 16e).

IL-2 ELISA. Primary human CD3⁺ T cells were plated at 2x10⁵ cells/well in a 96-well plate with indicated stimuli. Exogenous rhIL-2 was not added. Supernatant was collected at indicated time points and IL-2 concentration was assessed by sandwich ELISA (BioLegend).

TCGA data analysis. FPKM RNA-seq expression values for genes of interest and survival data were obtained from The Cancer Genome Atlas TCGA-TARGET-GTex dataset using Xena (xena.ucsc.edu). Gene expression values were normalized to account for differences in total immune cells by dividing by *PTPRC* (CD45) and plotted using matplotlib in Python 3.7. Kaplan-Meier curves were generated using the lifelines package. Survival metrics used in each Kaplan-Meier plot were chosen based on previously published work [221]. TIDE analysis was performed on the TIDE webpage (<http://tide.dfci.harvard.edu/query/>) by querying the *SLAMF7* gene. Figures were taken directly from the resulting TIDE analysis.

ccRCC CyTOF data re-analysis. The entire ccRCC CyTOF dataset from Chevrier et al., 2017 [209] was downloaded from the Bodenmiller Lab webpage (<https://cytobank.org/bodenmillerlab/index.html>). All immune cell subsets were identified based on predetermined Phenograph-assigned cluster IDs present in the raw FCS files and were colored in figures in the same manner as in Chevrier et al., 2017 [209]. *SLAMF7* expression on various immune cell types was manually gated based on *a priori* knowledge of expected *SLAMF7* expression patterns and it was determined that a gate set at “1” was most appropriate and accurate for all immune cell subsets. This threshold was used consistently for *SLAMF7* gating on all immune cell types. While this threshold is lower than what some investigators use

for CyTOF analysis, to our knowledge, SLAMF7 has never been assessed or manually gated on CyTOF. Furthermore, while SLAMF7 is expressed at a very high antigen density on certain immune cells (ie. DCs and plasma cells), it is also present on many other immune cell types, albeit at a lower antigen density. For this reason we utilized manual gating to allow us to accurately assess marker expression, whereas some other techniques can make appreciating cells with a low density of SLAMF7 receptor difficult. Samples from healthy controls and rcc #17 (too few cells) were excluded.

Statistics. Violin plots were generated using the ggplot2 package in R. Heatmap correlation matrix was generated using the corrplot package in R. FlowJo v10.6.1 software was used for all spectral cytometry analysis and high-dimensional analyses. Pie charts were made in Prism v7 (GraphPad). All t-tests were paired and performed in GraphPad Prism v7. Log-rank test was used to analyze all Kaplan-Meier plots. 2-way ANOVA was used to compare tumor growth curves. Details on statistical analyses used for TIDE analysis can be found in the original publication [213]. SPICE plots were compared using the Permutation test included in the software. Groups in (Fig. 15a and Fig. 16b, d) compared by fitting to a mixed model before performing multiple comparison test. This was accomplished in Prism v8 and performed due to the presence of missing values due to random chance. No mice or human samples were censored from any analysis for any reason (except the CyTOF samples listed above).

Study approval. All animal procedures were approved by the Michigan State University Institutional Animal Care and Use Committee.

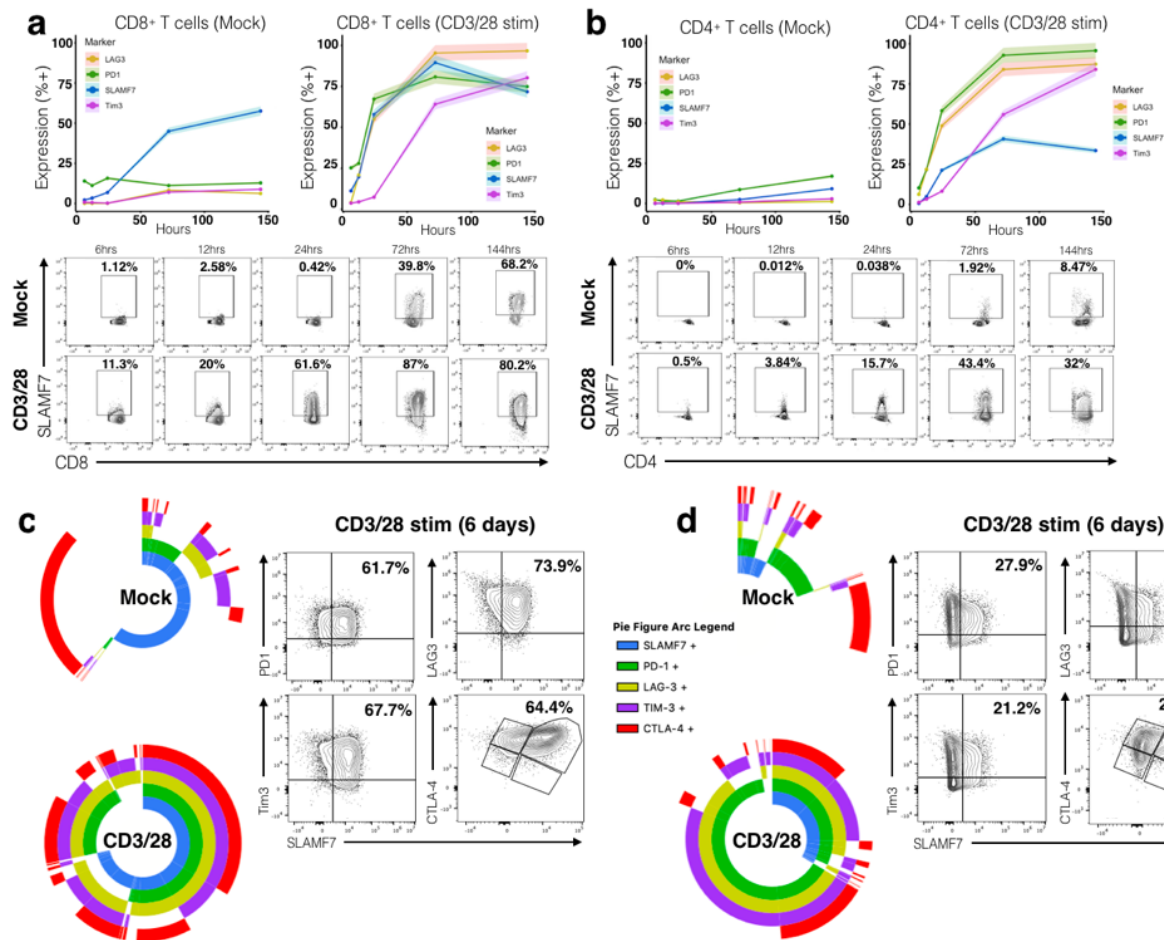


FIGURE 14: SLAMF7 is co-expressed with multiple exhaustion markers on CD3/CD28 stimulated human T cells.

(a, b) Time course of SLAMF7 and exhaustion marker expression on Mock or CD3/CD28 *in vitro* stimulated primary human CD8⁺ T cells (a) and CD4⁺ T cells (b). Top, exhaustion marker expression is shown as mean of two replicates of 2-4 healthy donors with the upper and lower 5% bounds of data shaded in. Bottom, representative plots of SLAMF7 expression on Mock and CD3/28 stimulated cells over time. (c, d) Left, SPICE plots showing co-expression of SLAMF7 with exhaustion markers on Mock and CD3/28 stimulated CD8⁺ T cells (c) and CD4⁺ T cells (d). SPICE plots in (c) and (d) each represent two replicate samples from two healthy donors. Right, representative biaxial plots of SLAMF7 co-expression on CD3/28 stimulated T cells after 6 days. Data is representative of 4 total healthy donors from two independent experiments.

Results

SLAMF7 is co-expressed with multiple exhaustion markers on activated T cells.

To examine associations between SLAMF7 and various inhibitory receptors on T cells we used a chronic, polyclonal, *in vitro* T cell activation assay. CD3⁺ human T cells were cultured with only rhIL-2 (Mock) or rhIL-2 + CD3/CD28 Dynabeads and exhaustion markers were assessed over a

period of six days using spectral cytometry (Supplementary Fig. 3a-c). We observed time-dependent increases in expression of LAG3, PD-1, and Tim3 on CD3/28 activated CD8⁺ and CD4⁺ T cells (Fig. 14a and b). SLAMF7 expression was minimal on both CD8⁺ (1.12%) and CD4⁺ (0%) T cells initially, but increased over time with CD3/28 stimulation, more in CD8⁺ than CD4⁺ T cells, and interestingly, was robustly induced in a time-dependent manner in the absence of CD3/28 activation on CD8⁺ T cells (Fig. 14a, b). To assess co-expression patterns of SLAMF7 with LAG3, Tim3, PD-1, and CTLA-4 we utilized SPICE [222] and observed that SLAMF7 is highly co-expressed in cells expressing any combination of exhaustion markers, and is consistently present on CD8⁺ T cells expressing multiple exhaustion markers (Fig. 14c). This effect was also observed on CD4⁺ T cells, but less pronounced, as these cells do not up-regulate SLAMF7 expression to the levels seen on CD8⁺ T cells (Fig. 14d). Additionally, we repeated this assay with mouse splenocytes and observed the same pattern of co-expression (Supplementary Fig. 3d-h).

Activation of SLAMF7 alone on T cells induces inhibitory receptors and exhaustion-associated transcription factors.

Since we identified that SLAMF7 is co-expressed with multiple exhaustion markers, we decided to examine if inducing SLAMF7 signaling in T cells impacts the expression level of T cell inhibitory receptors. We utilized a similar *in vitro* T cell stimulation assay as before, but instead activated the SLAMF 7 receptor on T cells with an agonistic antibody via cross-linking, as previously described [216]. We found that activating the SLAMF7 receptor on human T cells induced expression of PD-1, Tim3, and LAG3 in a time-dependent manner on CD8⁺ T cells (Fig.

15a, b), but to a lesser extent on CD4⁺ T cells (Fig. 15c, d). We also noted considerable numbers of T cells co-expressing multiple exhaustion markers by three and six days (Fig. 15b, d). This finding was not observed when cells were cultured in the absence of IL-2 (data not shown).

To gain a more in-depth understanding of the effects SLAMF7 activation had on T cell exhaustion we employed unbiased, neural-network-based, computational clustering using FlowSOM [223], and dimensionality reduction using tSNE, which revealed six distinct T cell clusters in Mock and SLAMF7 activated samples following six days of stimulation (Fig. 15e). We identified two CD4⁺ T cell clusters (CD4 1-2) and four CD8⁺ T cell clusters (CD8 1-4) (Fig. 15e). Importantly, the CD4 2, CD8 2, and CD8 3 clusters were virtually absent in Mock stimulation and only appeared in SLAMF7 activated samples (Fig. 15f, g). Comparison of these clusters with clusters present during Mock stimulation revealed an inhibitory receptor and transcription factor (TF) expression profile characteristic of exhausted/dysfunctional T cells [224-227] (Fig. 15h and f Supplementary Fig. 4a, d, e). Specifically the CD4 2 cluster had high expression of PD-1 and the epigenetic-reprogramming transcription factors YY1, Blimp1, and EZH2 (Fig. 15h). The two SLAMF7 cross-linking-induced CD8⁺ T cell clusters shared an exhaustion phenotype, but differed in expression of various markers such as EZH2, Tim3, and YY1 (Fig. 15h). Together, this suggests that SLAMF7 activation on human T cells is able to induce expression of inhibitory receptors and transcription factors linked to control of T cell exhaustion, independent of TCR signaling.

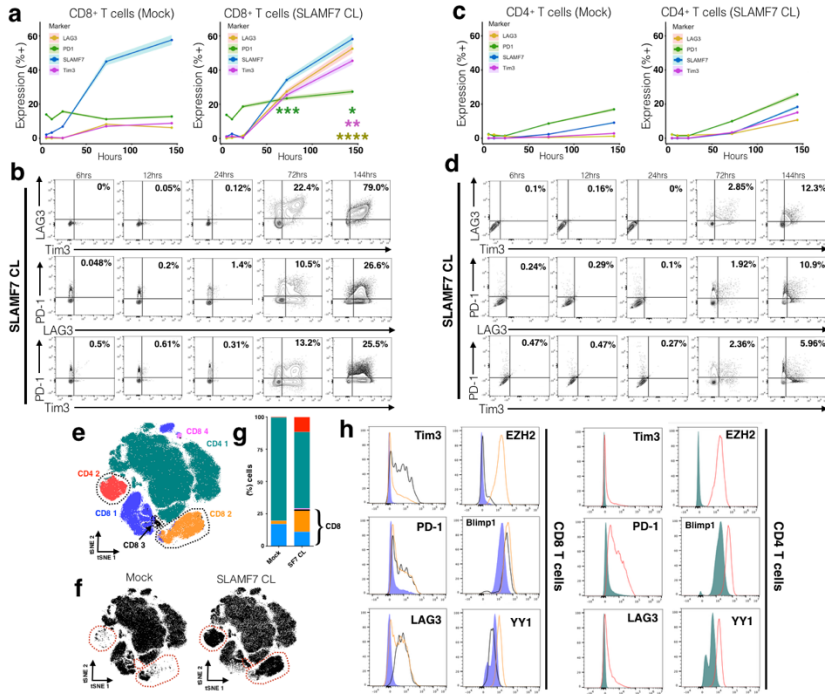


FIGURE 15: SLAMF7 activation induces expression of inhibitory receptors and exhaustion promoting transcription factors in CD8+ and CD4+ T cells.

(a, b) Time course of exhaustion marker expression on CD8⁺ T cells in the presence or absence of *in vitro* SLAMF7 activation. SLAMF7 was activated by receptor cross-linking with an anti-SLAMF7 mAb. Exhaustion marker expression is shown as mean of two replicates of 2-4 healthy donors with the upper and lower 5% bounds of data shaded in (a) or as biaxial plots (b). Asterisks indicate significant differences in marker expression between Mock and SLAMF7 CL conditions at various time points and are colored by marker. (c, d) Time course of exhaustion marker expression on SLAMF7 activated CD4⁺ T cells shown in the same manner as (a, b). (a-d) Representative of (n=5) independent experiments with (n=11) total healthy donors. (e) FlowSOM clustering on Mock and SLAMF7 activated T cells reveals unique clusters of T cells following SLAMF7 activation. Individual cells (n=200,000) are depicted on a tSNE plot and colored according to FlowSOM clusters. Clusters only present, or greatly enriched, during SLAMF7 activation are outlined. (f) tSNE maps of T cells separated by condition with clusters only present during SLAMF7 CL outlined. (g) Cluster composition of Mock and SLAMF7 CL conditions. (h) Comparison of exhaustion markers and T cell exhaustion-linked transcription factors between various FlowSOM clusters. Histograms are colored corresponding to clusters from (e). Results in [A-H] are representative of 4 independent experiments showing similar results with a total of (n=8) healthy donors. Pooled results from (n=2) healthy donors displayed in [A-H]. Groups in (i) compared using a paired student's t-test. *p<0.05. Conditions in (a) compared by fitting a mixed model and with Sidak's multiple comparison test. Mock results from (a) and (c) are duplicated from **Figure 14**.

Due to the fact that regulatory T cells (Tregs) are known to express high levels of certain exhaustion markers [228, 229] we wanted to rule out the possibility that SLAMF7 activation was merely inducing CD4⁺ and CD8⁺ Tregs. FoxP3 staining showed minor, but consistent increases in

FoxP3⁺ CD4⁺ T cells (Supplemental Fig. 4b) and CD8⁺ T cells (Supplementary Fig. 4c) following SLAMF7 activation, but these few cells did not account for the far greater percentage of cells expressing multiple exhaustion markers.

In vitro SLAMF7-activated T cells are distinct from terminally exhausted T cells and are capable of producing cytokines upon re-stimulation.

While the T cells induced following SLAMF7 activation have the appearance of exhausted T cells, we wished to confirm this by performing a functional assay. Primary human T cells were stimulated as described above for six days and then re-stimulated with fresh CD3/28 Dynabeads for an additional three days. We then assessed the ability of these cells to produce pro-inflammatory cytokines following re-stimulation. We found that T cells first stimulated for six days with CD3/28 Dynabeads were unable to produce IL-2, TNF α , and IFN γ upon re-stimulation consistent with their inhibitory marker profile, identifying them as *bona fide* exhausted T cells (Fig. 16a-d). In contrast to these cells, cells receiving Mock stimulation (only IL-2) first were able to produce significant quantities of all three cytokines (Fig. 16a-d). Interestingly though, we found that cells first stimulated with SLAMF7 CL for six days were still able to produce cytokines equivalent to Mock samples (Fig.16a-d). This indicates that while *in vitro* SLAMF7-activated T cells upregulate exhaustion markers, they still retain the ability to produce pro-inflammatory cytokines suggesting they have not reached terminal exhaustion yet.

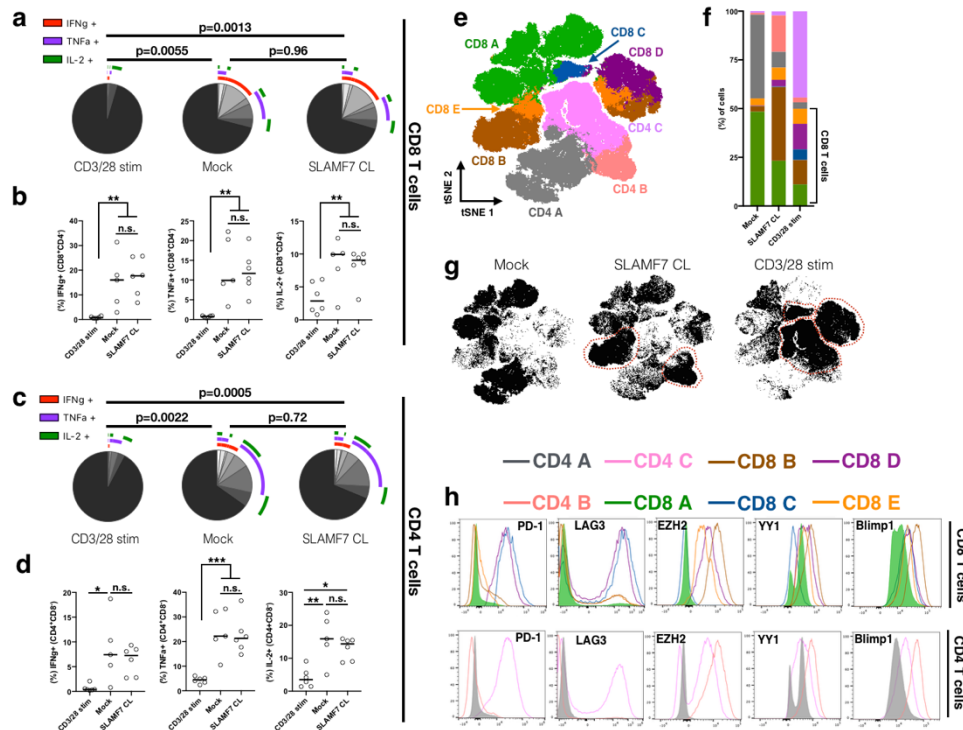


FIGURE 16: SLAMF7-activated T cells are distinct from terminally exhausted T cells and are capable of producing cytokines upon re-stimulation.

(a, b) Primary human T cells were stimulated for 6 days as described previously and re-stimulated on the seventh day with CD3/28 Dynabeads at a 0.2:1 bead:cell ratio for an additional 3 days. Expression of pro-inflammatory cytokines by CD8⁺ T cells was measured by intracellular staining and depicted as SPICE plots in (a) and dot plots in (b).

(c, d) Pro-inflammatory cytokine expression of CD4⁺ T cells.

(e) tSNE map of primary human T cells stimulated for 6 days as described previously with Mock, SLAMF7 CL, or CD3/28 stimulation. Shown are 400,000 cells pooled from 5 healthy donors and colored by FlowSOM clusters.

(f) Comparison of various FlowSOM clusters by stimulation condition.

(g) tSNE maps separated by condition with clusters enriched in each stimulation condition outlined.

(h) Comparison of exhaustion markers and T cell exhaustion-linked transcription factors between various FlowSOM clusters. Histograms are colored corresponding to clusters from (e).

(a-d) Representative of a single experiment with a total of 5 healthy donors.

SPICE plots in (a, c) representative of all samples combined and compared using Permutation test and results in (b, d) compared by fitting a mixed model and with Tukey's multiple comparison test.

[A-H] is representative of a single experiment with 5 healthy donors.

*p<0.05, **p<0.01, ***p<0.001

We next compared the inhibitory receptor and transcription factor profile of SLAMF7-activated

T cells to terminally exhausted T cells (CD3/28 stimulation) in an unbiased manner. FlowSOM

clustering of Mock, SLAMF7 CL, and CD3/28 stimulated T cells (all stimulated for six days)

revealed three CD4⁺ T cell clusters and five CD8⁺ T cell clusters (Fig. 16e). Each of the CD4 T cell clusters was strongly enriched in one of the stimulation conditions with Mock being primarily composed of CD4 A, SLAMF7 CL composed mostly of CD4 B, and CD3/28 stimulation composed primarily of CD4 C (Fig. 16f, g). Similarly, Mock samples primarily contained the CD8 A cluster, while SLAMF7 CL samples contained mostly the CD8 B cluster, and CD3/28 stimulation containing mostly CD8 C and CD8 D clusters (Fig. 16f, g). Comparison of inhibitory receptors and TF's in these clusters revealed important distinctions between SLAMF7-activated T cell clusters and terminally exhausted T cell clusters. We found that exhausted T cell clusters (CD8 C, CD8 D, and CD4 C) have high expression of PD-1 and LAG-3, along with lower expression of the transcription factors YY1, EZH2, and Blimp1 (Fig. 16h). SLAMF7 CL samples still co-expressed multiple inhibitory receptors, but at a low level than exhausted T cells, along with much stronger expression of all three transcription factors (Fig. 16h). Together, this reveals that although *in vitro* SLAMF7-activated T cells resemble exhausted T cells, they are not functionally (terminally) exhausted, yet still have an increased susceptibility to multiple inhibitory signals due to their inhibitory receptor profile. As they show high expression of TF's involved in T cell exhaustion, *in vitro* SLAMF7-activated T cells may be progressing along the path to terminal exhaustion through a pathway independent from TCR activation.

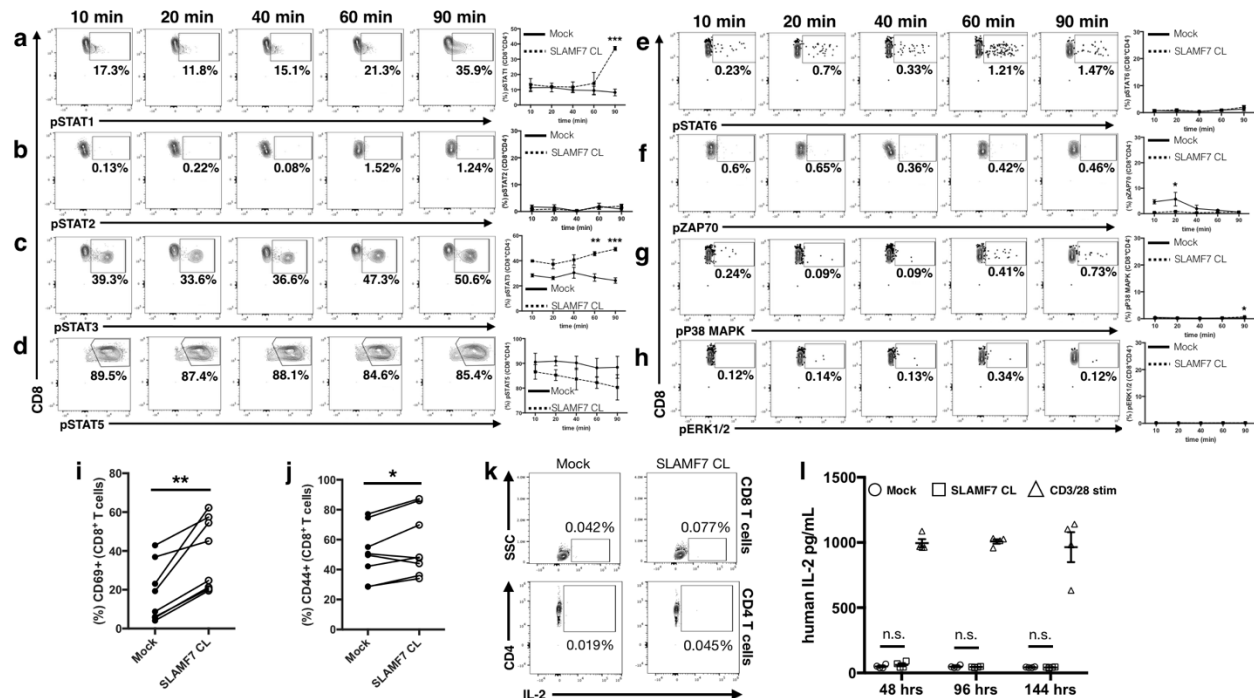


FIGURE 17: Alterations in T cell signaling pathways following SLAMF7 activation

(a-h) Time course of isolated primary human CD8⁺ T cells stimulated *in vitro* by SLAMF7 cross-linking (n=2 donors). Representative biaxial plots are shown for only SLAMF7 CL conditions. Surface expression of CD69 (i) and CD44 (j) was assessed on (n=8) donors following 6 days of *in vitro* stimulation. (k) Biaxial plots showing lack of IL-2 expression in CD8⁺ (top) and CD4⁺ primary human T cells following 3 days of *in vitro* stimulation (n=2), representative of two independent experiments. (l) Secretion of IL-2 by *in vitro* stimulated primary human CD3⁺ T cells was assessed over time by ELISA (n=4). No exogenous IL-2 was added to cultures and results are representative of two independent experiments. (a-h) is representative of two independent experiments with a total of 5 healthy donors and was analyzed by two-way ANOVA with Sidak's multiple comparison test. (i, j) contains pooled samples from 2 independent experiments and was analyzed with a paired students t-test. Two-way ANOVA with Tukey's multiple comparison test used for (l).

SLAMF7 signaling in CD8+ T cells induces STAT1 and STAT3 phosphorylation.

To mechanistically understand how SLAMF7 signaling in CD8⁺ T cells modulates the expression levels of multiple inhibitory receptors and their associated transcription factors, we performed phosphoflow on human T cells utilizing a panel containing common intermediary signaling proteins implicated in T cell responses [230]. We found that SLAMF7 activation induced a progressive increase in STAT3 phosphorylation over time and a burst of STAT1 phosphorylation at 90 minutes post-activation, without affecting numerous other known T cell signaling intermediaries (Fig. 17a-h). Additionally, we observed that SLAMF7 activation induced CD69

expression and minimally altered CD44 expression on CD8⁺ T cells (Fig. 17i, j); an important observation as CD69 has been previously shown to drive inhibitory receptor expression on T cells [231]. SLAMF7 activation on CD8⁺ T cells also shifted the subset distribution away from naive and terminal differentiated effector memory re-expressing CD45RA cells (EMRA) towards effector memory cells (Supplemental Fig. 4f). Finally, as high levels of IL-2 can drive both T cell inhibitory receptor expression [232, 233] and Treg formation [232, 234], we assessed IL-2 production and found that SLAMF7 activation does not stimulate IL-2 production or secretion from T cells (Fig. 17k, l). Together, these findings tie STAT1 and STAT3 phosphorylation to SLAMF7 activation in CD8⁺ T cells, suggesting that these factors might be involved in SLAMF7-dependent T cell signaling.

SLAMF7 expression is correlated with inhibitory receptor expression in clear cell renal cell carcinoma patients and is linked to poor survival.

To begin to identify if the SLAMF7 receptor functions to modulate T cell responses in cancer patients *in vivo*, we assessed co-expression of SLAMF7 mRNA with mRNA from various exhaustion markers in patient tumor samples. Using TCGA RNA-seq data, we first assessed all cancers to see which had the highest levels of CD8⁺ T cells and SLAMF7 expression (Supplementary Fig. 4g, h). We focused our further analyses on clear cell renal cell carcinoma (ccRCC) due to its high levels of CD8⁺ T cells, large sample size, and the knowledge that immune dysfunction in ccRCC occurs primarily via T cell exhaustion [213]. Correlation analyses between SLAMF7 with CTLA-4, LAG3, and PD-1 revealed very strong co-expression in ccRCC (Fig. 18a). Co-expression was weaker with Tim3 (Fig. 18a), an effect possibly due to the expression of Tim3

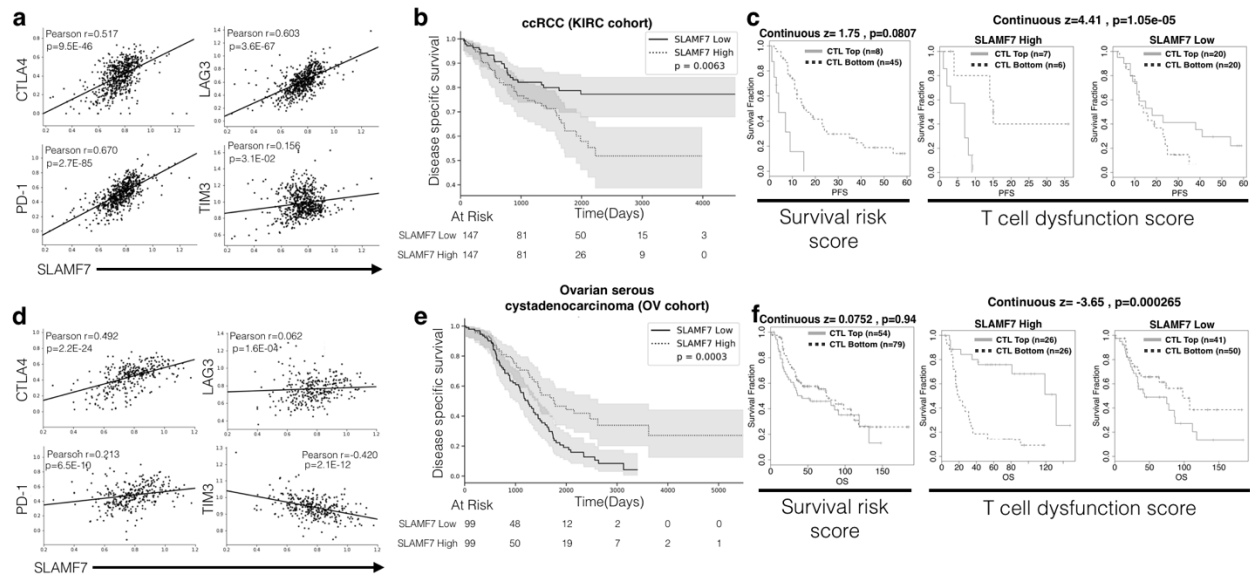


FIGURE 18: SLAMF7 correlates with exhaustion markers and is linked to poor survival in ccRCC.

(a) TCGA data was analyzed to examine co-expression of SLAMF7 with PD-1, CTLA-4, TIM-3, and LAG-3 at the mRNA level in ccRCC. Data was normalized to CD45 (*PTPRC*) to control for differential levels of immune cells. Pearson R and p values are displayed in each figure. (b) Disease specific survival in ccRCC patients from the KIRC cohort (n=603) in the top and bottom SLAMF7 expression quartiles. (c) SLAMF7-specific TIDE analysis of ccRCC patients from the E-MTAB-3267 cohort (n=53). Left, progression free survival of patients with high versus low SLAMF7 mRNA expression, with continuous z-score and associated p value signifying gene-associated death risk from a CoxPH model displayed. Right and middle, SLAMF7 expression effects on progression free survival with patients from the E-MTAB-3267 cohort stratified by CTL levels. Right-most plot displays patients with low SLAMF7 mRNA expression and middle plot shows patients with high SLAMF7 mRNA expression. Kaplan-Meier plots show survival differences based on TIDE-determined CTL levels in each patient. Continuous z-score and associated p value is displayed. (d) SLAMF7 associations with exhaustion markers from patients in the ovarian serous cystadenocarcinoma (OV) cohort from TCGA (n=426) displayed as in (a). (e) Kaplan-Meier plot for patients in the OV cohort stratified by highest and lowest SLAMF7 expression quartiles as in (b). (f) TIDE analysis of ovarian cancer patients from the GSE139@PRECOG cohort (n=203) performed as in (c). Overall survival is used in (f) as opposed to progression free survival used in (c). Log-rank test was used for Kaplan-Meier plots in (b) and (e) and shaded regions represent 95% confidence interval.

on various myeloid cell subsets [235]. Importantly, stratifying ccRCC patients into the highest and lowest SLAMF7 expressing quartiles revealed reduced disease-specific survival in patients with high expression of SLAMF7 (Fig. 18b).

To further determine if SLAMF7 expression in ccRCC was linked to T cell exhaustion and dysfunction, we used the Tumor Immune Dysfunction and Exclusion [TIDE] tool [213]. TIDE analysis of a separate, smaller cohort of ccRCC patients confirmed impaired survival in patients

with high SLAMF7 expression (Fig. 18c). It also showed that high levels of cytotoxic T lymphocytes (CTLs) are moderately protective, except when SLAMF7 expression is high, in which case there is reduced survival (Fig. 5c). Analysis of other cancers in the TCGA revealed this phenomenon was not conserved (Supplemental Fig. 4i-l). In cancers where immune dysfunction is not primarily occurring via T cell exhaustion, such as ovarian cancer (Fig. 18d-f) and squamous cell lung carcinoma (Supplementary Fig. 4k) [213], this trend disappears. Together, these results suggest that high SLAMF7 mRNA expression is linked to poor survival, only in cancers dominated by T cell exhaustion.

SLAMF7 expression patterns in human ccRCC tumors, associations with exhausted T cells, and links to patient survival.

While the correlations and effects on patient survival noted using TCGA data are informative, it does not address immune cell-specific expression patterns of SLAMF7 in the ccRCC TME. To address this we re-analyzed a previously published CyTOF dataset of ccRCC patient tumors, which contained expression data for SLAMF7 [209]. As predicted by CIBERSORT analysis of bulk RNA-seq data (Supplementary Fig. 4g), the ccRCC TME is composed primarily of T cells, followed by myeloid cells (Fig. 19a) [209]. The SLAMF7⁺ compartment largely mimics that seen in the periphery, with major contributions from plasma cells and NK cells (Fig. 19a). Looking at SLAMF7 expression on major immune cell types, as well as various predetermined TAM subsets [209], we observed considerable heterogeneity in SLAMF7 expression on numerous immune cell types across patients (Fig. 19b and Supplementary Fig. 5a). In particular, NK cells,

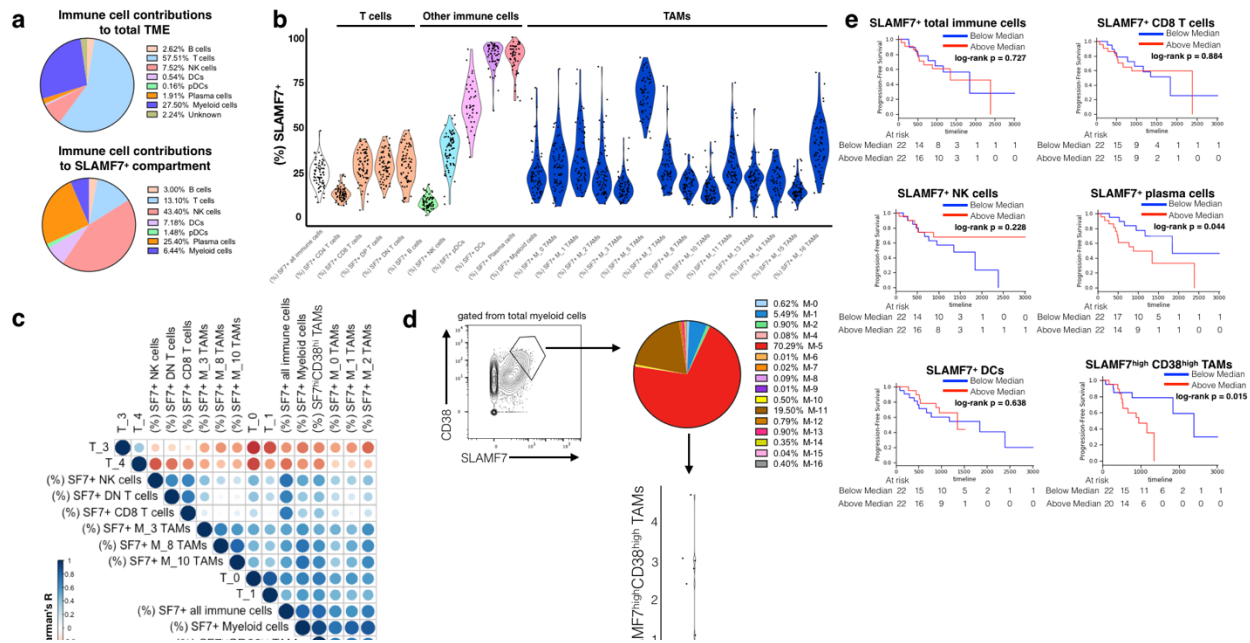


FIGURE 19: SLAMF7 expression in the ccRCC immune niche and associations with T cell phenotypes and patient survival.

(a) Top, relative contributions of various immune cell subsets in the ccRCC TME as assessed by CyTOF. Percentages are calculated from a concatenated sample of (n=73) ccRCC tumor samples using Phenograph-assigned clusters previously determined by Chevrier et al., 2017. Bottom, SLAMF7⁺ cells were gated out from total immune cells and contributions of various Phenograph clustered immune cell subsets was determined. (b) SLAMF7 expression across various immune cell types in the ccRCC TME. Phenograph-assigned clusters were used for immune subset identification with TAMs being further subdivided based on TAM-specific subsets identified by Chevrier et al., 2017. Each dot represents an individual patient tumor sample. (c) Correlation matrix heatmap of SLAMF7 expression on various immune cell types and frequencies of various T cell subsets. T cell frequencies are calculated as the frequency of each T cell subset out of the total T cell compartment of each patient. T cell subsets are identified by Phenograph in Chevrier et al., 2017. Spearman correlation is displayed as a circle scaled by color and size based on the magnitude of the R value. Only the top 10 positive and negative correlations are displayed. (d) Left, gating of SLAMF7^{high}CD38^{high} TAMs from total myeloid cells. Right, breakdown of SLAMF7^{high}CD38^{high} TAMs by Phenograph-determined TAM subsets. Results are from a concatenated sample containing all 73 ccRCC tumor samples. Bottom, frequency of SLAMF7^{high}CD38^{high} TAMs per total immune cells per patient. Red line indicates median (0.052). (e) Kaplan-Meier plots of progression free survival, with ccRCC patients stratified by high or low numbers of various immune cell subsets expressing SLAMF7. For all plots the relative frequency of SLAMF7⁺ cells from each immune subset out of the total immune compartment is considered. Log-rank test is used to compare groups in (e).

plasmacytoid dendritic cells (pDCs), and various TAM subsets show the greatest heterogeneity (Fig. 19b).

To begin to identify which SLAMF7 expressing cell types in the TME might be responsible for activating SLAMF7 on T cells and inducing exhaustion, we performed a correlation analysis of

various SLAMF7⁺ immune cells to all of the predetermined T cell subsets [209] (Fig. 19c). We found strikingly strong positive correlations between subsets of exhausted T cells (T-0, T-1, T-7, T-16, and T-18) [209] and SLAMF7⁺: total immune cells, total myeloid cells, M-0 TAMs, M-1 TAMs, M-2 TAMs, M-3 TAMs, and M-10 TAMs (Fig. 19c and supplementary table 1). Importantly the “exhausted” T cell subsets were labeled as such based on high expression of inhibitory receptors and were never functionally characterized [209]. We also noted relatively strong positive correlations of CD4⁺ Tregs (T-6) [209] to SLAMF7⁺ total immune cells (Spearman $r=0.3$) and SLAMF7⁺ total myeloid cells (Spearman $r=0.38$) (Fig. 19c). Furthermore, we observed strong negative correlations between the above listed SLAMF7⁺ TAM subsets and subsets of effector memory T cells (T-3 and T-4) [209] (Fig. 19c and supplementary table 1). It is recognized that TAMs are responsible for driving tumor infiltrating leukocytes (TILs) towards exhaustion phenotypes [236]. Our results here suggest that SLAMF7-SLAMF7 interactions between TAMs and TILs may be a novel mechanism through which tumors are able to create an inhospitable immune niche, by the induction of T cell exhaustion, Treg formation, and shifts away from beneficial effector memory T cells [237].

Previous analysis of this data set concluded that high CD38 expression marks pathogenic TAMs [209]. We discovered a population of SLAMF7^{high}CD38^{high} TAMs present at varying levels between patients (Fig. 19d). Hypothesizing that this may be a pathogenic TAM subset linked to T cell exhaustion, we correlated the percentage of this cell population per total immune cells in the TME of each patient to T cell subsets in our correlation matrix. Levels of this unique TAM subset showed the strongest positive correlations with the above listed exhausted T cell subsets

and Tregs (Fig. 19c and supplementary table 1). Further analysis of this TAM subset revealed it is composed primarily of M-5 and M-11 TAMs (Fig. 19d), both previously linked to T cell exhaustion and poor survival in this cohort [209]. To identify which SLAMF7 expressing immune cell types were linked to poor survival we performed a series of Kaplan-Meier analyses by splitting patients up based on high or low frequencies of various SLAMF7⁺ cell types. We found that high levels of SLAMF7⁺ total immune cells, CD8⁺ T cells, DCs, and NK cells were not linked to poor survival (Fig. 19e). Patients with high levels of SLAMF7⁺ plasma cells (Fig. 19e) had poor survival, however, as nearly all plasma cells express SLAMF7, further analysis showed this effect was merely due to differences in numbers of plasma cells (Supplementary Fig. 5b).

Unsurprisingly, we also noted that patients with high levels of Tregs (T-6) had markedly worse survival (Supplementary Fig. 5c). Most interestingly, we found that stratifying patients by high levels of the SLAMF7^{high}CD38^{high} TAM subset was the most effective parameter for identifying patients with poor survival (Fig. 19e). This effect was not just due to this population containing high levels of M-5 TAMs (previously linked to T cell exhaustion [209]), as patients with high levels of M-5 TAMs showed no decrease in survival (Supplementary Fig. 5d). Finally, patients in the high and low SLAMF7^{high}CD38^{high} TAM groups were otherwise balanced in available demographic and clinical parameters (Supplementary Fig. 5e). Together, these findings suggest that SLAMF7^{high}CD38^{high} TAMs may be driving T cell dysfunction and immune evasion in the ccRCC TME.

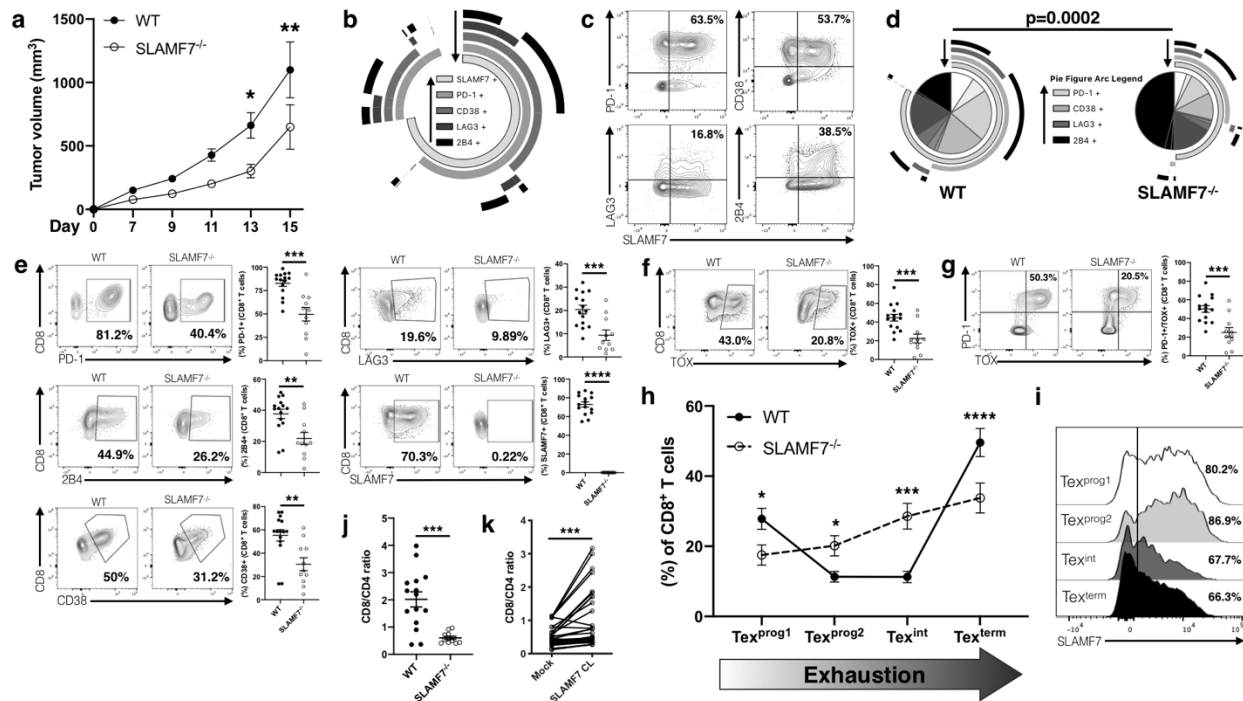


FIGURE 20: SLAMF7 expression in the TME propels CD8+ T cells towards terminal exhaustion and impacts tumor growth.

(a) B16-F10 tumor growth in WT and SLAMF7^{-/-} mice. (b) SPICE plot of inhibitory receptor expression on intra-tumoral CD8⁺ T cells from WT mice; plot shows response from all samples combined. Arrows assist in identifying which arc each marker corresponds too. (c) Biaxial representative plots of SLAMF7 co-expression with various inhibitory receptors on intra-tumoral CD8⁺ T cells from WT mice. (d) SPICE plots comparing exhaustion marker expression on intra-tumoral CD8⁺ T cells from WT and SLAMF7^{-/-} mice. Plots are aggregate from all samples and compared with a Permutation test. Arrows assist in identifying which arc each marker corresponds too. (e) Comparison of individual inhibitory receptors from intra-tumoral CD8⁺ T cells showing both representative biaxial plots and responses of individual mice. (f) Expression of TOX in intra-tumoral CD8⁺ T cells from WT and SLAMF7^{-/-} mice. (g) Co-expression of TOX and PD-1 from intra-tumoral CD8⁺ T cells from WT and SLAMF7^{-/-} mice. (h) Frequency of CD8⁺ intra-tumoral T cells across the four populations that make up the exhaustion developmental trajectory (Beltra et al., 2020). Populations are defined as: Tex^{prog1} (SLAMF6⁺CD69⁻), Tex^{prog2} (SLAMF6⁺CD69⁻), Tex^{int} (SLAMF6⁺CD69⁻), Tex^{term} (SLAMF6⁺CD69⁺). (i) SLAMF7 expression across exhausted CD8⁺ T cell subsets. (j, k) Ratio of CD8⁺ to CD4⁺ T cells from B16-F10 melanomas of WT and SLAMF7^{-/-} mice (j), or PBMCs of healthy human individuals with either mock or SLAMF7 CL stimulation (k). Results from (a) are pooled from two independent experiments using n=14-15 mice per genotype, composed of equal numbers of males and females, and compared with 2-way ANOVA and Sidak's multiple comparison test. Results from (b-i) are pooled results from two independent experiments with n=15 WT and n=11 SLAMF7^{-/-} mice composed of equal numbers of males and females and compared with unpaired two-tailed students t-test. Results in (k) are pooled from seven independent experiments with n=32 and compared with paired two-tailed students t-test. All data are represented as mean ± SEM. **p<0.01; ***p<0.001; ****p<0.0001.

SLAMF7 expression in the TME propels CD8+ T cells towards terminal exhaustion and impacts tumor growth.

In order to validate our findings from human samples *in vivo*, we generated SLAMF7^{-/-} mice and assessed growth of B16-F10 tumors. We found tumor growth to be significantly attenuated in

SLAMF7^{-/-} mice compared to WT mice (Fig. 20a). We also observed high co-expression of SLAMF7 with various inhibitory receptors on CD8⁺ TILs from WT mice (Fig. 20b, c). In comparing WT to SLAMF7^{-/-} TILs, we observed significantly fewer CD8⁺ T cells expressing multiple exhaustion markers (Fig. 20d) and individual markers (Fig. 20e) in SLAMF7^{-/-} mice. To validate if SLAMF7 was modulating levels of *bona fide* exhausted T cells we compared expression of the exhaustion-defining TF, TOX [238-240]. SLAMF7^{-/-} CD8⁺ intra-tumoral T cells expressed significantly fewer TOX⁺ cells (Fig. 20f) and PD-1⁺/TOX⁺ cells (Fig. 20g). Taking a more granular approach, we used the markers SLAMF6 (Ly108) and CD69 to track where CD8⁺ TILs from WT and SLAMF7^{-/-} mice were on the exhaustion developmental trajectory, as recently described [241]. We found that CD8⁺ T cells from WT mice tended to be at either end of the exhaustion spectrum (Tex^{prog1} and Tex^{term}) (Fig. 20h), while SLAMF7^{-/-} CD8⁺ T cells occupied the intermediate stages more often (Tex^{prog2} and Tex^{int}) with significantly less terminally exhausted cells (Fig. 20h). We also observed SLAMF7 expression to be highest on the two progenitor stages (Tex^{prog1} and Tex^{prog2}) (Fig. 20i), which together with the above findings, suggests that SLAMF7 signaling may help to propel CD8⁺ T cells through the exhaustion developmental pathway to terminal exhaustion.

Interestingly, we also noticed a significantly decreased CD8/CD4 T cell ratio in TILs from SLAMF7^{-/-} mice (Fig. 20j). Returning to our *in vitro* human data, we observed a corresponding reverse trend in the presence of SLAMF7 activation (Fig. 20k). Thus, while SLAMF7 appears to drive T cell exhaustion, it may also be playing a role in CD8⁺ T cell survival or ability to maintain tissue residency.

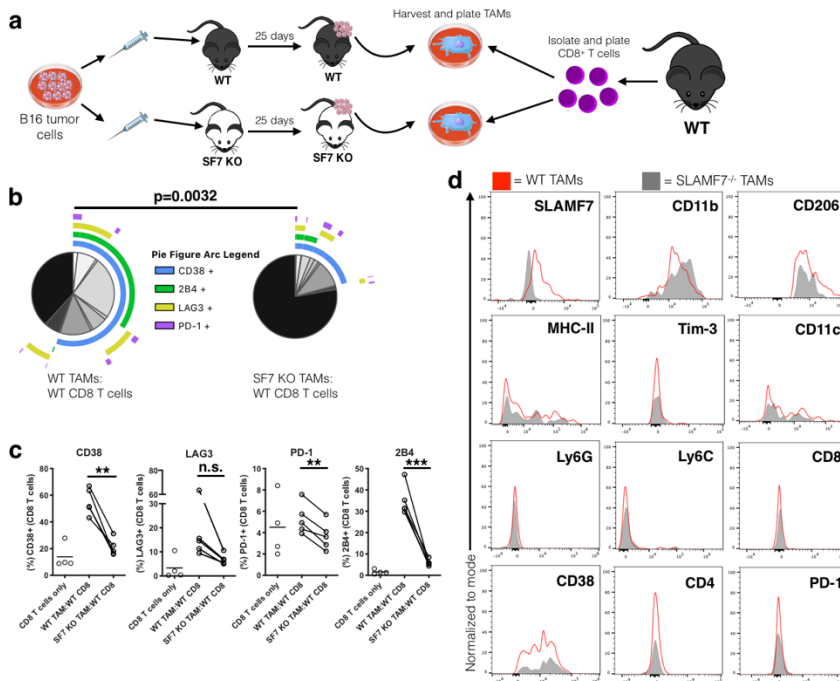


FIGURE 21: SLAMF7 expression on TAMs drives T cell exhaustion.

(a) Experimental approach used for *ex vivo* T cell:TAM co-culture. (b) SPICE plots of CD8⁺ T cells co-cultured with TAMs for 6 days (n=5); plots show response from all samples combined. (c) Changes in expression of exhaustion markers on CD8⁺ T cells from co-culture experiment (n=5). Groups containing CD8⁺ T cells and TAMs compared using a paired student's t-test. (d) Comparison of various markers on TAMs from B16-F10 tumors grown in WT and SLAMF7^{-/-} mice. Results from (b-d) are representative of a single experiment using TAMs pooled from (n=4) mice per genotype and CD8⁺ T cells from splenocytes of (n=5) WT, non-tumor bearing mice. n.s., not significant; **p<0.01; ***p<0.001.

Expression of SLAMF7 on TAMs drives T cells to express inhibitory receptors.

To determine if SLAMF7-SLAMF7 self-ligation between TAMs and tumor-infiltrating T cells induces T cell inhibitory receptor expression, we developed an *ex vivo* TAM-T cell co-culture model (Fig. 21a). B16-F10 tumors were grown in WT and SLAMF7^{-/-} mice, TAMs were isolated from established tumors 25 days at day 25, and co-cultured with CD8⁺ T cells from splenocytes of non-tumor bearing mice (Fig. 21a). We observed that T cells co-cultured with SLAMF7⁺ TAMs expressed multiple inhibitory receptors (Fig. 21b, c). Notably, T cells cultured with SLAMF7^{-/-}

TAMs had significantly fewer cells positive for various exhaustion markers, with dramatic decreases in T cells co-expressing multiple markers appearing similar to CD8⁺ T cells cultured in the absence of TAMs (Fig. 21c). Importantly, this finding is specific to TAMs, as CD8⁺ T cells co-cultured with bone marrow-derived macrophages (BMDMs) from WT or SLAMF7^{-/-} mice do not show alterations in inhibitory receptor expression (Supplemental Fig. 5f, g). Additionally, comparison of TAMs from WT and SLAMF7^{-/-} mice revealed that they have similar expression of numerous markers, except for SLAMF7 (Fig. 21d). This finding suggests that direct SLAMF7-SLAMF7 interactions between TAMs and CD8⁺ T cells are sufficient to induce expression of multiple inhibitory receptors on T cells.

Discussion

The impressive response rates and instances of complete remission following checkpoint inhibitor therapy have catapulted immunotherapy and T cell exhaustion to the forefront of cancer research. While therapies targeting PD-1 (and PD-L1) and CTLA-4 have proven efficacious, there are still a great many patients who do not respond or develop resistance to checkpoint blockade, suggesting the need for a greater understanding of the biological processes regulating T cell dysfunction. To this end, a host of additional inhibitory checkpoint receptors have been identified and found to be expressed on exhausted T cells [196], with blocking antibodies against these receptors now in phase I, II, and III clinical trials for various cancers [196]. However, this approach of targeting additional T cell inhibitory receptors does not address the root problem, which is: what are the TCR-independent mechanisms responsible for inducing inhibitory receptor expression in the TME in the first place [197]. Here, we have

begun to answer this question in ccRCC and provide early evidence that SLAMF7-SLAMF7 self-ligation between CD8⁺ T cells and SLAMF7⁺ TAMs may be driving T cell inhibitory receptor expression and exhaustion.

Based on the temporal expression patterns we observe, it would seem that SLAMF7 is actually one of the first receptors expressed on activated CD8⁺ T cells following any sort of pro-inflammatory stimuli. This observation has been noted at the single-cell level [219] and lends credence to the idea that SLAMF7 may be one of the earliest counter-measures T cells use to rein in over-activation. It accomplishes this by providing an early TCR-independent signal to begin up-regulating expression of multiple inhibitory receptors immediately upon initial activation or entrance into an inflammatory microenvironment. It also appears to reprogram these cells by inducing numerous transcription factors known to positively modulate T cell exhaustion programs. Notably, while SLAMF7 signaling on T cells does not impair their ability to produce cytokines, it does lend them highly susceptible to signaling from multiple inhibitory receptors, which would still result in the induction of non-functional T cells in the TME where these signals are abundant. This is an important subtlety to the biology of SLAMF7 signaling on T cells, and suggests that interruption of this signaling could result in effective anti-tumor responses by T cells.

Already we have taken the first steps at understanding the underlying mechanism by finding that SLAMF7 activation on CD8⁺ T cells induces STAT1 and STAT3 phosphorylation.

Phosphorylated STAT3 in intra-tumoral T cells has been shown to induce PD-1 expression [242],

inhibit effector T cells [242], and promote expansion of Tregs [242]; findings that we also observe following SLAMF7 activation on T cells. Furthermore, there is evidence that EZH2 is able to induce phosphorylation of STAT3 [243] and that CD38 is able to modulate EZH2 activity [244], suggesting SLAMF7 signaling in T cells may be inducing expression of inhibitory receptors via a CD38-STAT3-EZH2 axis.

Contrary to STAT3, the role of STAT1 in modulating CD8⁺ T cell signaling and exhaustion marker expression is less well understood. There is evidence showing the potential for pSTAT1 to induce expression of PD-1 in T cells and other immune cells [245]. Further confirming that SLAMF7-mediated STAT1 phosphorylation is implicated in driving T cell exhaustion is the finding that Tex^{term} CD8⁺ T cells are enriched with open chromatin regions bound by STAT1 [241], and we find that in the absence of SLAMF7 there are fewer of these cells. Additionally, SLAMF7-mediated increases in the expression of the exhaustion-controlling transcription factors YY1 [227], Blimp1 [224, 225], and EZH2 [226, 227], are likely potential mechanisms regulating T cell exhaustion. The choice to study these transcription factors specifically, was made not only because they are linked to T cell exhaustion, but because both Blimp1 and YY1 have been found to control SLAMF7 expression [246, 247], which implies there may be reciprocal regulation involved. Interestingly, Tex^{term} CD8⁺ T cells are enriched in open chromatin regions bound by Blimp-1, we find that SLAMF7 activation induces Blimp-1, and in the absence of SLAMF7, there are fewer Tex^{term} cells, implicating another potential mechanism behind SLAMF7-specific effects on T cells.

The restricted B16-F10 tumor growth in SLAMF7^{-/-} mice can potentially be explained by the CD8⁺ T cell population shifts we see along the exhaustion development spectrum. Tex^{int} cells (which we find significantly more of in the tumors of SLAMF7^{-/-} mice) have been found to have high cytotoxic capacity and lower expression of inhibitory receptors compared to the other subsets recently described [241]. Having more of these cells is likely to provide a beneficial anti-tumor response. How exactly SLAMF7 signaling drives cells away from Tex^{int} towards Tex^{term}, and if SLAMF7 mediates changes in TOX expression remain to be discovered.

Our discovery that high expression of both CD38 and SLAMF7 on TAMs marks a unique subset strongly linked to T cell exhaustion and poor survival, helps to mechanistically explain why a previous study found M-5 TAMs to be so strongly associated with exhausted CD8⁺ T cells [209]. M-5 TAMs have the highest expression of SLAMF7 of any of the other TAM subsets that were identified, and the SLAMF7^{high}CD38^{high} TAM subset is composed of 70% M-5 TAMs [209]. It will be important for future studies to determine if this unique TAM subset is present in the TME of other cancers, and if so, does it also induce T cell inhibitory receptor expression. Along the same lines, the results from our *ex vivo* TAM-T cell co-culture model support this proposed mechanism, but do not provide conclusive, *in vivo* proof.

An important concept to consider as future studies are conducted to both better understand the physiology of SLAMF7 signaling and attempt to therapeutically modulate it, is the sensitivity of SLAMF7 to different methods of activation or inhibition. By targeting SLAMF7 with a ligand attached to a solid surface (such as that of a cell culture plate or a cell membrane) as we have

done here and previously [216], the receptor becomes activated and down-stream signaling is initiated. However, adding soluble SLAMF7 ligands to the system might result in blocking of the receptor and achieve effects directly opposite to that of receptor activation [216]. This makes the study of SLAMF7 signaling very dependent on the experimental methods used and may explain why other studies [248] reached different conclusions from this study.

Our analysis of the roles played by SLAMF7 on both T cells and tumor-associated macrophages, incorporating a combination of multi-parametric spectral cytometry and targeted analysis of existing datasets, provide early evidence implicating a novel immune evasion mechanism employed by tumors.

Acknowledgments. We thank the MSU Transgenic and Genome Editing Facility, Elena Demireva, and Huirong Xie for generating SLAMF7^{-/-} mice. We appreciate assistance performing spectral cytometry provided by Matthew Bernard and the MSU South Campus Flow Cytometry Core Facility. Thanks to Austen N. Grooms for assistance with IL-2 ELISA experiments.

Author contributions. P.O. and Y.A.A. conceptualized the study and designed its experiments. P.O., S.H., and Y.A.A. performed all experiments. S.H. and M.K.B. performed IL-2 ELISA experiments. P.O. performed re-analysis of CyTOF data. S.H. performed analysis of TCGA data. S.G. managed all mouse work, genotyped, and bred mice. A.A. assisted in experimental design and provided funding. P.O. wrote the manuscript, and all authors assisted in editing the manuscript. Y.A.A. supervised the study. The authorship order of the two co-first authors was determined based on differing roles in conceptualization of the study and manuscript

preparation. P.O. contributed mainly through design, planning, analysis, and writing of the manuscript, while S.H. physically performed many of the experiments and performed data analysis.

Abbreviations. SLAMF7, SLAM family member 7; SF7, SLAMF7; TME, Tumor microenvironment; ccRCC, clear cell renal cell carcinoma; TCGA; The Cancer Genome Atlas; TAM, tumor-associated macrophage; CyTOF, Cytometry by time of flight; CL, Cross-linking; tSNE, t-distributed stochastic neighbor embedding.

CHAPTER: 5 Adenoviral delivery of an immunomodulatory protein to the tumor
microenvironment controls tumor growth

Authors: Patrick O'Connell, Maja K. Blake, Yuliya Pepelyayeva, Sean Hyslop, Sarah Godbehere, Ariana M. Angarita, Cristiane Pereira-Hicks, Andrea Amalfitano, Yasser A. Aldhamen

Abstract

The discovery that targeted manipulation of the immune system against tumors is capable of achieving responses in otherwise refractory cancers has spurred efforts aimed at optimizing such strategies. To this end, we have previously investigated cancer immunotherapy approaches utilizing recombinant adenovirus vectors, as well as via manipulation of the self-ligand receptor SLAMF7. Here, we present a viral-based immunotherapy approach employing targeted delivery of a recombinant SLAMF7-Fc fusion protein directly into tumors at high concentrations via a recombinant adenoviral vector (Ad-SF7-Fc). Using multiple murine cancer models, we show Ad-SF7-Fc is able to induce tumor control via augmentation of innate immunity; specifically, type I interferon, dendritic cell, and macrophage responses. Analogously, we find that modulating SLAMF7 signaling via an adenoviral vector expressing its intra-cellular adaptor, EAT-2, is also capable of inducing tumor control. Finally, we employ a novel in vivo prediction approach and dataset integration with machine learning to dissect how Ad-SF7-Fc modulates cell type-specific responses in the TME to achieve tumor control. Our novel combinatorial cancer immunotherapy highlights the benefit of multi-modal immune modulation and lays a framework for combination with complementary approaches capable of inducing adaptive immune responses.

Introduction

Cancer immunotherapy has revolutionized the way we think about cancer from both treatment and research perspectives. [249] Currently, the most clinically successful approaches to antagonize the immune system against tumors rely on the use of monoclonal antibodies which,

for the most part, modulate T cell responses. [250] While highly efficacious in subsets of patients with certain cancers, [249, 250] these antibodies still suffer a number of limitations, not limited to: their non-selective targeting of immune cells systemically, induction of autoimmunity, [251] development of resistance, [252] high production cost, and exaggerated adverse effects when used in combination. [205] As an alternative approach to induce anti-cancer immune responses, recombinant viral vectors have been investigated, including a number of studies and clinical trials using human recombinant adenovirus vectors. [253, 254] These viral approaches function via multiple mechanisms including direct cytolysis of tumor cells and augmentation of anti-tumor immune responses, [254] but have fallen short of the impressive responses produced by monoclonal antibodies. [249, 250] Combining antibody-based and viral-based approaches has the potential to address a number of the issues faced by these individual therapies.

The signaling lymphocytic activation molecule family member 7 (SLAMF7) (CRACC, CD319, CS-1) is a self-ligand receptor, restricted to hematopoietic cells and expressed at varying frequencies on different immune cell subsets. [27, 215, 255] SLAMF7 is capable of mediating both activating and inhibitory signals in immune cells; a distinction largely dependent on the presence of its adaptor protein, Ewing's sarcoma-associated transcript 2 (EAT-2). [159] When SLAMF7 is activated in the presence of EAT-2, EAT-2 binds to SLAMF7's phosphorylated intracellular immunoreceptor tyrosine-based switch motif (ITSM) and mediates immune cell activation, while in the absence of EAT-2, various inhibitory SH2 domain-containing phosphatases are recruited to SLAMF7's ITSM. [91, 159] We recently demonstrated that SLAMF7 activation in

type I interferon stimulated monocytes, which lack EAT-2, results in inhibition of pro-inflammatory chemokine responses. [27] We also found that SLAMF7 signaling on CD8+ T cells reprograms them towards an exhausted phenotype; a finding of particular relevance to cancer immunotherapy. [255]

Extending these findings, we recently demonstrated that targeting SLAMF7 using a SLAMF7-Fc (CRACC-Fc, SF7-Fc) fusion protein enhanced natural killer (NK) cell and dendritic cell (DC) activation. [256] Therefore, we hypothesized that a recombinant adenovirus vector expressing SLAMF7-Fc (Ad-SF7-Fc) may augment anti-tumor responses via localized immune activation from both the adenovirus vector and SLAMF7-Fc, while delivering high levels of SLAMF7-Fc to the tumor microenvironment (TME) in a targeted, cost-effective manner. Through testing Ad-SF7-Fc across multiple murine cancer models, we found this integrated immunotherapy capable of augmenting innate immune responses and concordantly controlling tumor growth. Novel in vivo prediction approaches confirm Ad-SF7-Fc is capable of augmenting pro-inflammatory DC responses and suggest that SLAMF7 activation on plasmacytoid dendritic cells (pDCs) may be particularly efficacious in inducing anti-tumor immunity. Finally, we employ a machine learning-based approach to identify the factors critical to tumor control by Ad-SF7-Fc.

Results

Ad-SF7-Fc induces high expression of SF7-Fc and activates the innate immune system.

While we found that our SF7-Fc fusion protein was able to modulate SLAMF7 signaling and induce innate immune activation, [256] production of large amounts of recombinant proteins

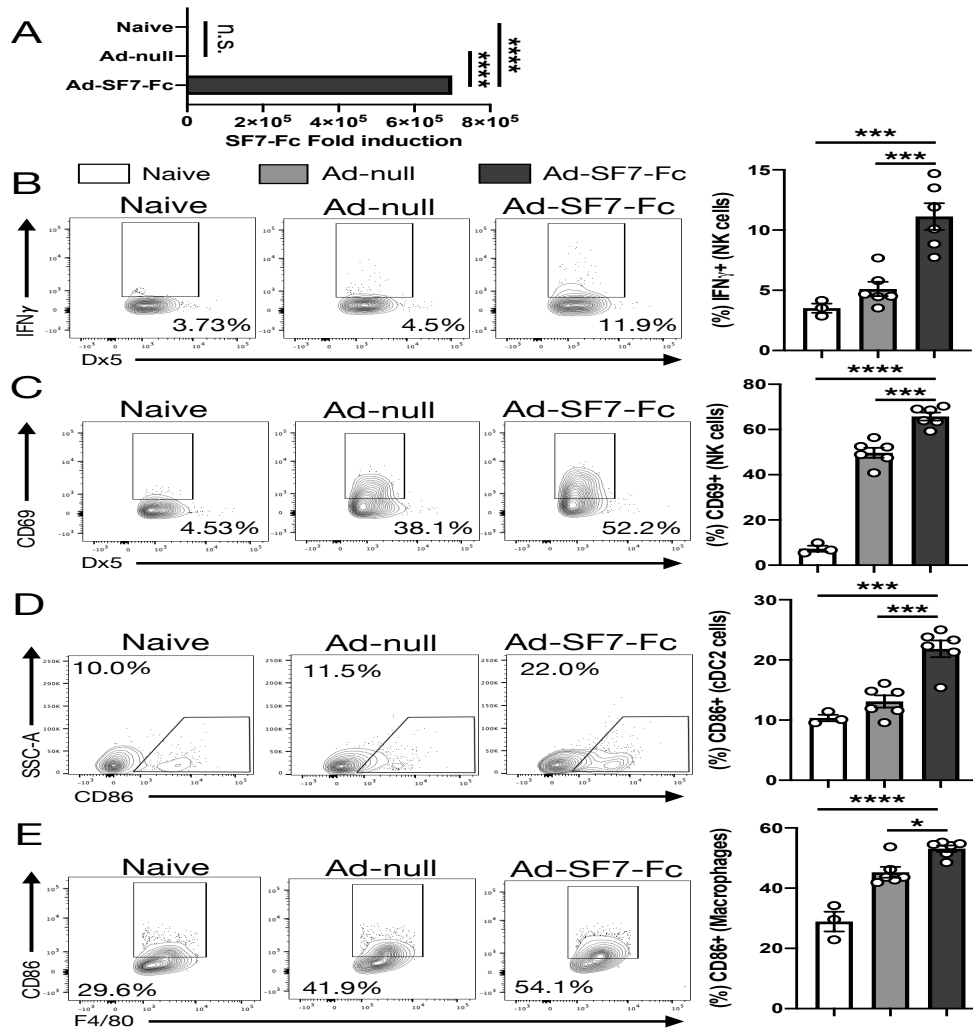


FIGURE 22: Ad-SF7-Fc expresses SF7-Fc and activates NK cells and DCs.

(A) HEK-293-C7 cells (n=3) were control treated with PBS (naive) or infected at an MOI of 1×10^3 with Ad-null or Ad-SF7-Fc overnight and *SLAMF7* gene expression was assessed. Balb/c mice were injected I.V. with 1×10^{10} v.p. of Ad-null (n=6), Ad-SF7-Fc (n=6), or not injected (naïve, n=3), spleens were harvested 10 hours later and immune cell phenotype was analyzed by flow cytometry. (B) IFN γ production by NK cells. (C) CD69 expression on NK cells. (D) CD86 expression on cDC2 cells. (E) CD86 expression on macrophages. All data presented as mean \pm SEM and representative of a single experiment. Groups compared with one-way ANOVA with Tukey's multiple comparison test. * $p < 0.05$; ** $p < 0.01$; *** $p < 0.001$; **** $p < 0.0001$; n.s. not significant.

like SF7-Fc is expensive and delivery to specific locations challenging. [257, 258] To address this, we constructed a recombinant, replication deficient adenovirus vector capable of expressing

SF7-Fc (Ad-SF7-Fc). We first confirmed the ability of Ad-SF7-Fc to express SF7-Fc by infecting HEK293 cells (Fig. 22A).

Previously we found co-administration of SF7-Fc fusion protein and Ad-null increased IFN γ production by NK cells, [256] and here found that treatment with Ad-SF7-Fc increased IFN γ production and CD69 expression on NK cells compared to an empty adenovirus vector (Ad-null) (Fig. 22B, C and Supplementary Fig. 7A). Since we also found that SF7-Fc was capable of activating DCs, [256] we investigated myeloid responses following treatment with Ad-SF7-Fc, and observed increased CD86 expression on DCs (Fig. 22D and Supplementary Fig. 7B) and macrophages (Fig. 22E and Supplementary Fig. 7B). Additionally, Ad-SF7-Fc was able to augment immune cell activation on B cells, CD8⁺ T cells, and CD4⁺ T cells (Supplemental Fig. 6A-C).

Ad-SF7-Fc augments Th1 cytokine and interferon responses.

To investigate the impact of Ad-SF7-Fc on cytokine responses, we evaluated splenic gene expression in mice six hours post-vector injection. We found upregulation of *Ii12*, *Csf2* (GM-CSF), and *Ii6* (Fig. 23A). Interestingly, Ad-SF7-Fc decreased expression of *CXCL10* (IP-10) compared to Ad-null (Fig. 23A), suggesting SF7-Fc may be activating SLAMF7 on monocytes; a result consistent with our previous work. [27] Since NK cell activation is mediated by type I interferons and we previously found SLAMF7 is both an interferon (IFN) responsive gene and modulator of specific IFN responses, we investigated if Ad-SF7-Fc could augment type I IFN

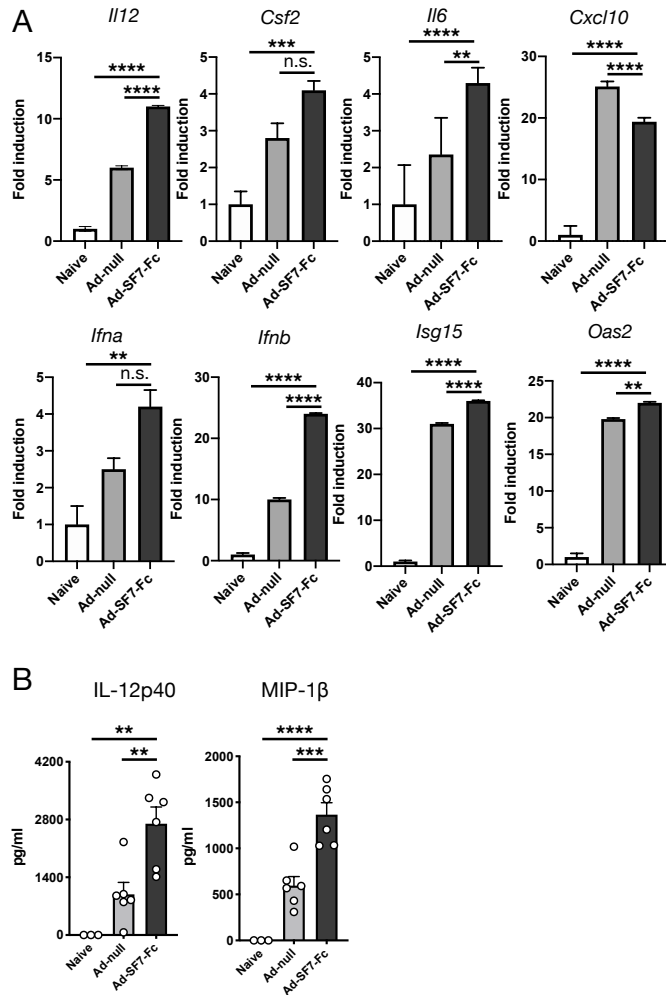


FIGURE 23: Ad-SF7-Fc induces a Th1 cytokine and interferon response.

(A) Balb/c mice were injected I.V. with 1×10^{10} v.p. of Ad-null, Ad-SF7-Fc, or not injected (naive) and six hours later spleens were collected for RNA analysis. Balb/c mice were injected I.V. with 1×10^{10} v.p. of Ad-null, Ad-SF7-Fc, or not injected (naive) and 10 hours later plasma was collected for cytokine analysis. (B) Plasma levels of IL-12(p40) and MIP-1β were compared across treatment groups. All data presented as mean \pm SEM and representative of a single experiment. Groups compared with one-way ANOVA with Tukey's multiple comparison test. ** $p < 0.01$; *** $p < 0.001$; **** $p < 0.0001$; n.s. not significant.

responses. Compared to Ad-null, we found Ad-SF7-Fc increased the expression of *Ifna*, *Ifnb*, *Isg15*, and *Oas2* (Fig. 23A). Furthermore, we confirmed induction of IL-12(p40) and MIP-1β (CCL4) proteins in the plasma of mice following treatment with Ad-SF7-Fc (Fig. 23B).

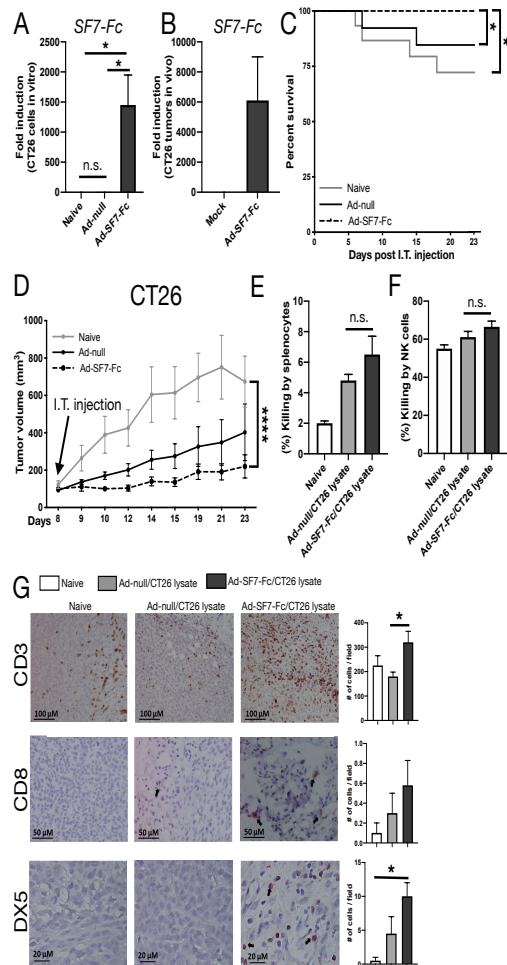


FIGURE 24: Control of CT26 tumor growth by Ad-SF7-Fc in the absence of an increased adaptive immune response.

(A) CT26 cells were untreated (naive) (n=3) or infected at an MOI of 1×10^3 with Ad-null (n=3) or Ad-SF7-Fc (n=3) virus overnight. mRNA was isolated from cells and *SLAMF7* expression was assessed. (B) Balb/c mice were injected S.Q. in the flank with 1.5×10^5 CT26 cells and 14 days later mice were injected I.T. with 1×10^{10} v.p. of Ad-SF7-Fc (n=2) or not injected (naive) (n=2). Tumors were harvested 14 hours later and *SLAMF7* gene expression was assessed. Balb/c mice were injected S.Q. with 1.5×10^5 CT26 cells and eight days later mice were split into three groups: Ad-null (n=14), Ad-SF7-Fc (n=14), and not injected (naive, n=15). All viruses were injected I.T. (C) Kaplan-Meier survival curve of virus treated mice. (D) Tumor volumes in virus treated mice. Splenocytes (E) or NK cells (F) from naïve mice were incubated with CFSE labeled CT26 cells and cultured in presence of plasma from Ad-null/CT26 lysate vaccinated, Ad-SF7-Fc/CT26 lysate vaccinated, or non-vaccinated mice. CT26 viability was assessed by flow cytometry to determine percent killing. (G) CT26 tumors were harvested from mice used in (E and F) and IHC was performed for CD3, CD8, and DX5. All data presented as mean \pm SEM and representative of a single experiment. Groups in (A, E, F, and G) compared with one-way ANOVA with Tukey's multiple comparison test. Log-rank test used to compare groups in (C). Mixed effects analysis with Tukey's post-hoc test used to compare groups in (D). * $p < 0.05$; **** $p < 0.0001$; n.s. not significant.

Ad-SF7-Fc controls CT26 tumor growth in the absence of increased adaptive immune responses.

To examine if Ad-SF7-Fc could function as a cancer immunotherapy in vivo we utilized the CT26 mouse model. We confirmed successful expression of SF7-Fc in CT26 cells in vitro (Fig. 24A) and in vivo (Fig. 24B). We then treated established tumors I.T. with Ad-null, Ad-SF7-Fc, or untreated (naive). We found significantly increased survival in Ad-SF7-Fc treated mice (Fig. 24C) and decreased tumor volume in Ad-SF7-Fc treated compared to naive mice, with a strong trend towards significance when compared to Ad-null (Fig. 24D).

To investigate if the tumor control we observed was due to an increased adaptive immune response we assessed tumor antigen-specific B cell memory responses in the plasma of mice co-vaccinated with various adenovirus vectors and CT26 tumor lysate. We found Ad-SF7-Fc/CT26 lysate co-vaccinated mice produced only slightly higher levels of CT26-specific antibodies compared to Ad-null/CT26 lysate (Supplemental Fig. 8A). Functional ADCC assays using antibodies generated during the aforementioned vaccinations with either total splenocytes (Fig. 24E) or isolated NK cells (Fig. 24F) and CFSE-labeled CT26 cells, showed no significant difference between groups. We also assessed NK and T cell infiltration into CT26 tumors from vaccinated mice, finding a moderate increase in CD3⁺ T cells and DX5⁺ NK cells in mice vaccinated with Ad-SF7-Fc/CT26 lysate compared Ad-null (Fig. 24G). Altogether, this suggests that Ad-SF7-Fc does not increased adaptive immune responses in the CT26 model.

Ad-SF7-Fc controls B16-F10 tumor growth without modulating T cell exhaustion or remodeling the TME.

Since we found that Ad-SF7-Fc augments Th1 cytokine/chemokine responses, and because it is known that Balb/c mice have Th2 skewed immune responses, [259] we reasoned that Ad-SF7-Fc may function better in the B16-F10 tumor model in C57BL/6 mice. We found significantly reduced tumor volumes and improved survival in B16 tumors treated with Ad-SF7-Fc compared to Ad-null (Fig. 25A, B). Considering we recently discovered that SLAMF7 signaling on CD8⁺ T cells reprograms them towards exhaustion, [255] we assessed exhaustion status of CD8⁺ TILs from B16 tumors. We found no change in the frequency of Tox^{high}PD-1^{high} exhausted CD8⁺ TILs, nor any surface markers of T cell exhaustion, or proliferation in Ad-SF7-Fc treated tumors (Fig. 25C-F and Supplemental Fig. 7C, D and Supplemental Fig. 9A-D). Furthermore, we found no changes in the same markers on CD4⁺ TILs (Supplemental Fig. 9E-I). After reconstructing the exhaustion developmental trajectory in CD8⁺ TILs, [241, 255] we found that Ad-SF7-Fc does not impact progression through this trajectory (Fig. 25G).

We also profiled the immune TME of these mice using high dimensional single-cell spectral cytometry. Unbiased clustering revealed 11 distinct immune cell subsets (Fig. 25H), each displaying expected marker expression patterns (Fig. 25I). The frequency of each cell subset did not significantly change between Ad-SF7-Fc and Ad-null treated B16 tumors (Fig. 25J), suggesting that Ad-SF7-Fc does not globally remodel the TME.

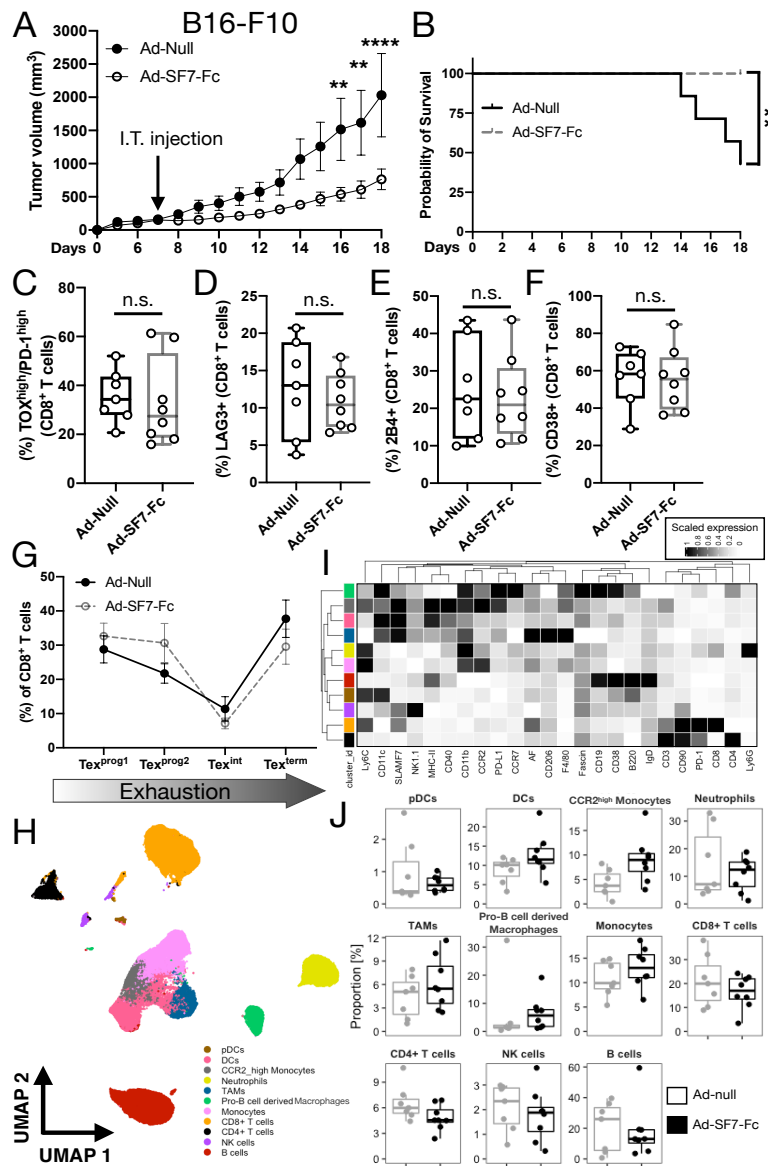


FIGURE 25: Ad-SF7-Fc controls B16 tumor growth without affecting T cell exhaustion or remodeling the TME.

(A) C57BL/6 mice were inoculated with 4×10^5 B16-F10 cells and on day seven were treated I.T. with 1×10^{10} v.p. of either Ad-null or Ad-SF7-Fc. (B) Kaplan-Meier survival curve of virus treated mice. TILs from virus treated B16 tumors were isolated on day 18 and the frequency of TOX^{high}PD-1^{high} CD8⁺ T cells (C), LAG3⁺ CD8⁺ T cells (D), 2B4⁺ CD8⁺ T cells (E), and CD38⁺ CD8⁺ T cells (F) was assessed. (G) The exhaustion developmental trajectory (assessed by co-expression of SLAMF6 and CD69) of CD8⁺ TILs was compared between Ad-null and Ad-SF7-Fc treated tumors. (H) Tumor infiltrating immune cells from Ad-null and Ad-SF7-Fc treated B16 tumors were assessed by high dimensional single-cell spectral cytometry. FlowSOM generated clusters were displayed on a UMAP dimensionally reduction plot. (I) Marker expression across all clusters in (H). (J) Frequency of each immune cell subset from (H and I) compared across Ad-null and Ad-SF7-Fc treated B16 tumors. Data in (A and G) presented as mean \pm SEM. Log-rank test used to compare groups in (B). Two-way ANOVA with Tukey's multiple comparison test used to compare groups in (A and G). Unpaired, two-tailed t test used to compare groups in (C-F). A GLMM was used to compare groups in (J). All data representative of 2 independent experiments showing similar results. **p < 0.01; ***p < 0.0001; n.s. not significant. AF; autofluorescence.

SLAMF7 expression across the TME and tumor-infiltrating myeloid cell phenotypes in Ad-SF7-Fc treated mice.

We next wanted to identify which cell types in the TME express SLAMF7, and thus might be modulated by Ad-SF7-Fc. Utilizing B16 tumor-bearing SLAMF7 deficient (SLAMF7^{-/-}) mice treated with Ad-null, we determined SLAMF7 expression across the TME (Fig. 26A). Because we previously found that Ad-SF7-Fc was able to induce DC activation (Fig. 22D) and IL-12 production (Fig. 23A, B), we wished to further investigate tumor-infiltrating DC phenotypes in our B16 model. Notably, we included markers in our panel allowing the identification of the recently described mregDC subset. [260] We identified seven distinct DC subsets (Fig. 26B, C). Importantly, we found our panel was capable of efficiently identifying mregDCs in an unbiased manner (Fig. 26B, C and Supplemental Fig. 10A). We identified high co-expression of SLAMF7 and CD38 on the DC1 B subset (Fig. 26D) which was intriguing as we recently identified a pathogenic subset of TAMs in clear cell renal cell carcinoma (ccRCC) co-expressing the same markers. [255] Comparison of frequencies of DC subsets across Ad-SF7-Fc treated mice responding or not responding to treatment, we noted that responding mice had more of the DC1 B subset, suggesting that, in contrast to TAMs, DCs co-expressing these markers might be anti-tumorigenic (Fig. 26E). This is not surprising as DCs are known to express EAT-2, [9] suggesting SLAMF7 activation in these cells induces IL-12 and pro-inflammatory responses. Supporting this, we found higher expression of IL-12 and other pro-inflammatory cytokines in the tumors of Ad-SF7-Fc treated B16 tumors compared to Ad-null (Fig. 26F).

We investigated TAM heterogeneity in our model, finding nine TAM subsets (Fig. 26G, H). We found a SLAMF7^{high}CD38^{high} TAM subset similar to the one we previously identified in ccRCC

patients, [255] suggesting this subset may be conserved across tumors and species (Fig. 26G,

H). Ad-SF7-Fc treatment did not alter the frequency of this subset (Supplemental Fig. 10C) We

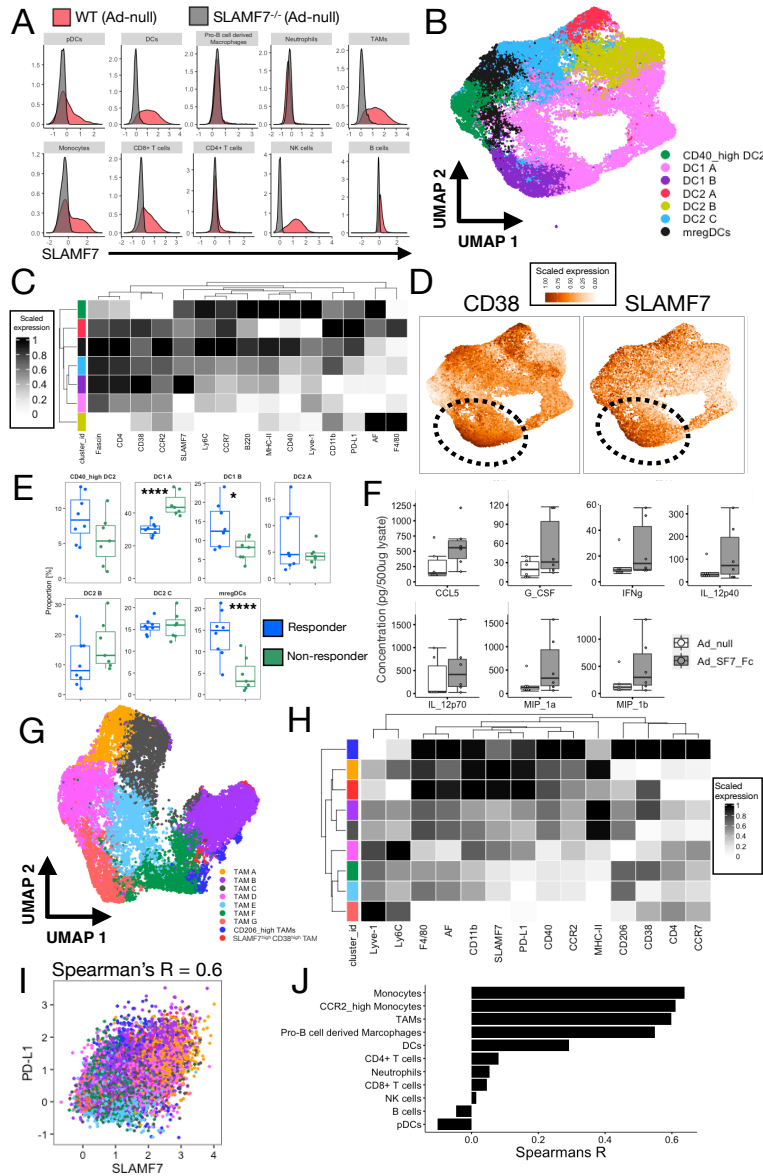


FIGURE 26: SLAMF7 expression across the TME and tumor inflating myeloid cell phenotypes following Ad-SF7-Fc treatment.

(A) SLAMF7 expression across immune cell subsets in B16 tumors following Ad-null treatment. (B) DC subsets in tumors treated with either Ad-null or Ad-SF7-Fc clustered with FlowSOM and displayed with UMAP. (C) Marker expression from clusters in (B). (D) CD38 and SLAMF7 expression displayed on UMAP plot of DCs from (B). (E) Frequency of DC subsets between mice whose B16 tumors respond to I.T. adenovirus treatment or not. (F) Cytokine and chemokine expression from Ad-null and Ad-SF7-Fc treated B16 tumors. (G) TAM subsets in tumors treated with either Ad-null or Ad-SF7-Fc clustered with FlowSOM and displayed with UMAP. (H) Marker expression from clusters in (G). (I) Co-expression of SLAMF7 and PD-L1 on all TAMs (colored by subset). (J) Spearman's correlation coefficient of SLAMF7 and PD-L1 on all immune cell subsets from B16 tumors treated with adenovirus. A GLMM was used to compare groups in (E). Unpaired, two-tailed t test used to compare groups in (F). All data representative of 2 independent experiments showing similar results. AF; autofluorescence.

also found that subsets expressing SLAMF7 also co-expressed PD-L1, with a correlation of 0.6 (Fig. 26I and Supplemental Fig. 10B). We extended this analysis across the TME and found it to be conserved across myeloid cells, except for pDCs and neutrophils (Fig. 26J). [27]

EAT-2 expression in tumor-infiltrating innate immune cells identifies mice able to control B16 tumors.

Since the presence of EAT -2 determines whether SLAMF7 functions as an activating or inhibitory receptor, [159] we examined EAT-2 expression in tumor-infiltrating immune cells in our B16 model. While we found that treatment with Ad-SF7-Fc did not change EAT-2 levels in NK cells or DCs compared to Ad-null (data not shown), we found that B16 tumors responding to adenovirus treatment had significantly higher expression of EAT-2 in NK cells (Fig. 27A), cDC2

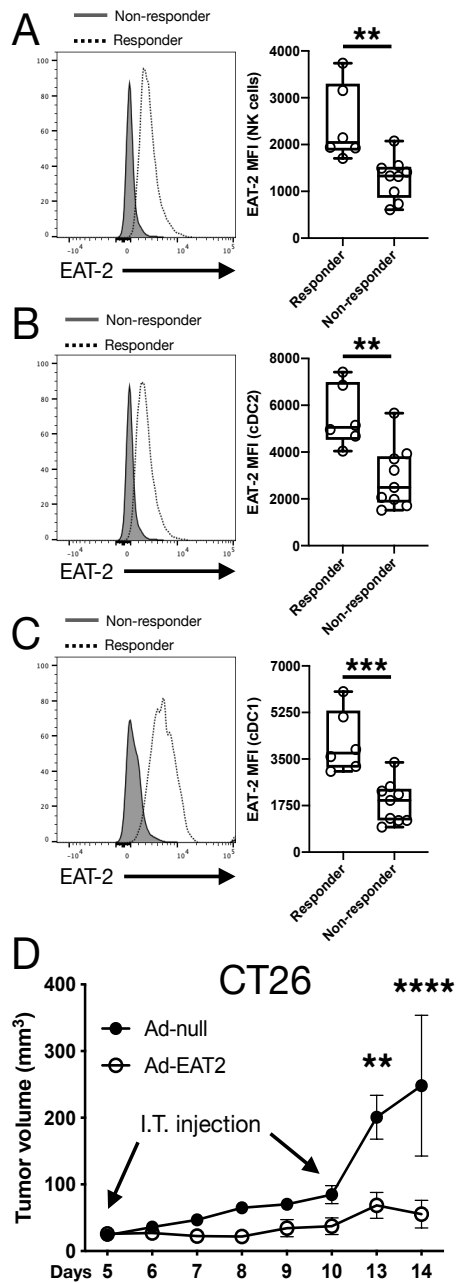


FIGURE 27: EAT-2 expression in immune cells from adenovirus treated B16 tumors as an indicator of response to treatment.

(A) Expression of EAT-2 in B16 tumor-infiltrating NK cells from tumors treated with adenovirus. (B) Expression of EAT-2 in B16 tumor-infiltrating cDC2 cells from tumors treated with adenovirus. (C) Expression of EAT-2 in B16 tumor-infiltrating cDC1 cells from tumors treated with adenovirus. (D) Tumor volumes of CT26 tumors treated I.T. twice with 1×10^{10} v.p. of either Ad-null or Ad-EAT-2. All data presented as mean \pm SEM and representative of a single experiment. Two-way ANOVA with Tukey's multiple comparison test used to compare groups in (D). Unpaired, two-tailed t test used to compare groups in (A-C). ** $p < 0.01$; *** $p < 0.001$; **** $p < 0.0001$.

(Fig. 27B), and cDC1 (Fig. 27C). To confirm this in vivo, we treated CT26 tumors I.T. with a previously described adenovirus expressing EAT-2 [113] and found that mice receiving this virus

displayed superior tumor control compared to Ad-null (Fig. 27D). These findings suggest that modulating SLAMF7 signaling to be solely pro-inflammatory in innate, tumor-infiltrating, immune cells can result in tumor control.

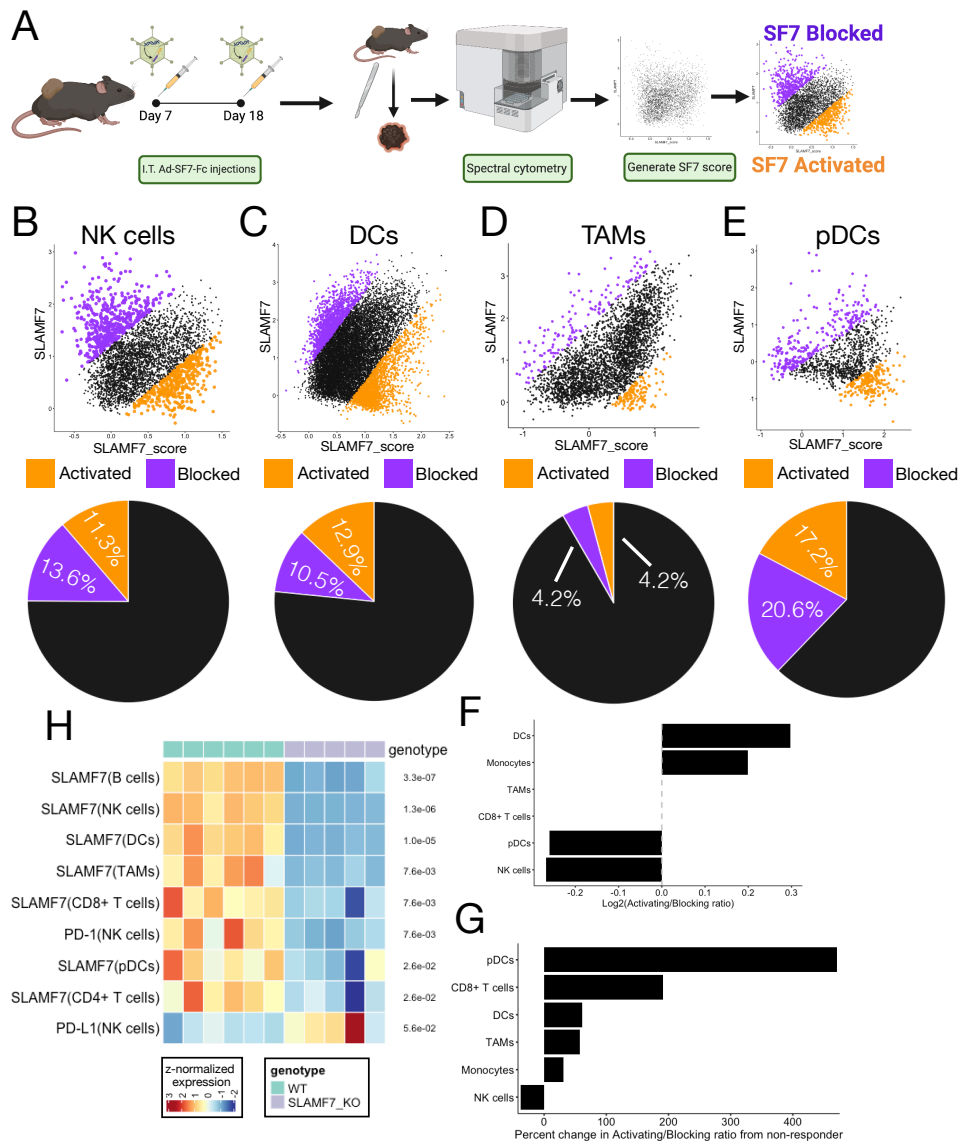


FIGURE 28: Mechanistic predictions of the function of SF7-Fc in B16 tumors.

(A) Schematic overview of experimental design. (B) Dot plot of SLAMF7 and SLAMF7_score for NK cells (See Materials and Methods), with cells predicted to have their SLAMF7 receptor activated colored purple and cells predicted to have their receptor blocked colored orange. Pie charts under each dot plot display frequency of predictions. (C) Same as (B), but for DCs. (D) Same as (B), but for TAMs. (E) Same as (B), but for pDCs. (F) Log_2 transformed ratio of frequency of SLAMF7 activation to blocking for each cell type in the TME with SLAMF7 expression. (G) Percent change in the ratio of predicted SLAMF7 activation to blocking between B16 tumors responding to Ad-SF7-Fc and not responding; plotted for each cell type. (H) Heatmap of differential marker expression across B16 tumor-infiltrating immune cell subsets in Ad-null treated WT and SLAMF7^{-/-} mice. P-value adjusted for multiple comparisons displayed on right of each row. Only markers below a FDR of 0.6 are displayed.

Cell type specific, single-cell predictions of the function of Ad-SF7-Fc in vivo.

Because SLAMF7 is a homotypic receptor, and since SF7-Fc is composed of the extracellular domain of SLAMF7, SF7-Fc can conceivably function to both activate and/or block SLAMF7 signaling depending on local environmental factors and the cell type in question. Additionally, activating or blocking SLAMF7 can have vastly different outcomes on different cell types depending on the presence of EAT-2 [159, 215] which may mechanistically explain how Ad-SF7-Fc achieves tumor control. Therefore, we devised an approach using high dimensional spectral cytometry which allowed us to predict if SF7-Fc was activating or blocking SLAMF7 at the single cell level (Fig. 28A; see Materials and Methods). We found that Ad-SF7-Fc was primarily activating DCs and monocytes, having equally opposing effects on TAMs and CD8⁺ T cells, and primarily blocking pDCs and NK cells (Fig. 28B-F and Supplemental Fig. 11C, D). We next calculated the ratio of SLAMF7 activation versus blocking on each cell type between mice responding or not to Ad-SF7-Fc, finding that responding mice had considerably more pDC activation (Fig. 28G).

Alterations in the immune TME in SLAMF7^{-/-} mice.

We also compared immune cell subsets between the WT (Ad-null treated) and SLAMF7^{-/-} (Ad-null treated) mice used for prediction analyses, finding decreased levels of NK and CD8⁺ T cells in the TME of SLAMF7^{-/-} mice (Supplemental Fig. 11E); the later consistent with our previous work. [255] We investigated TAM subsets in these mice and found a dramatic re-structuring of the TAM landscape in SLAMF7^{-/-} mice (Supplemental Fig. 11F, G). Finally, we identified all

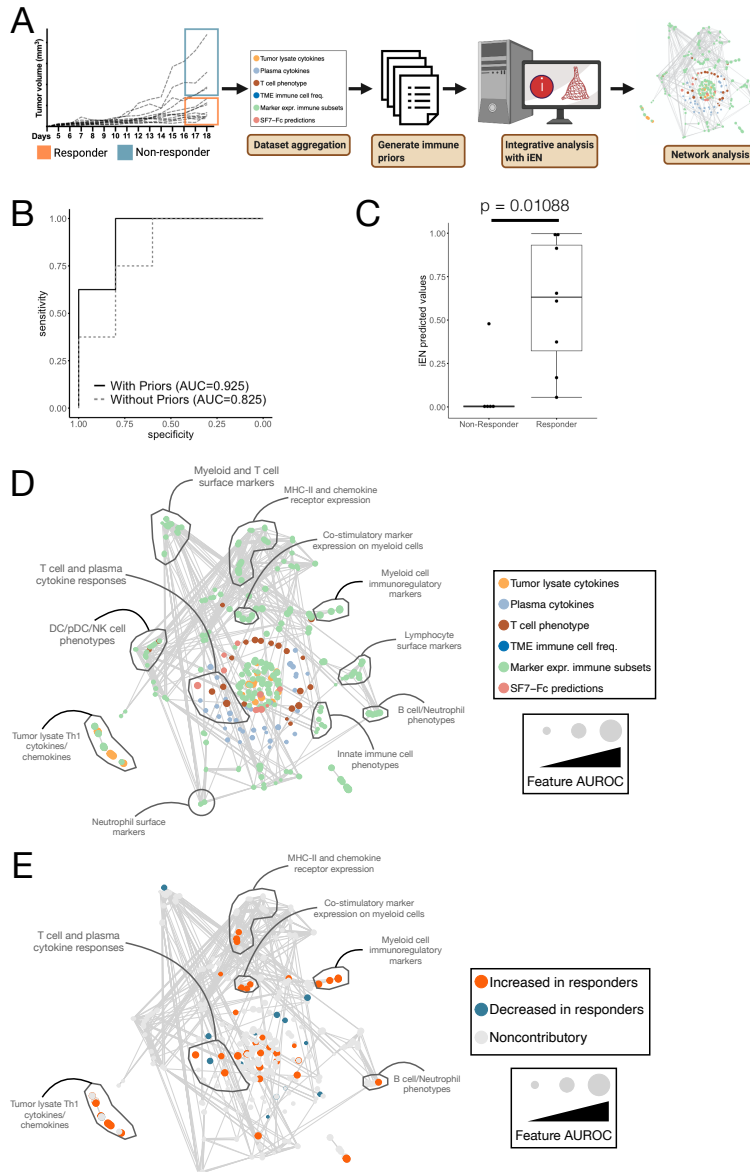


FIGURE 29: iEN machine learning identifies factors underlying tumor response to Ad-SF7-Fc.

(A) Schematic overview of experimental design. (B) ROC curves of iEN model performance with and without inclusion of priors. (C) Comparison of iEN predicted values (arbitrary units) between responders, with statistical comparison performed with Wilcoxon sum rank test. (D) iEN model network where each node is a feature entered into the model and is scaled by its individual AUROC. Edges are significant spearman correlations between features ($p < 0.05$) after bonferroni correction for multiple comparisons. Nodes are colored by the dataset they originate from and communities of shared immunological archetypes are highlighted. (E) The same network from (D), but with nodes colored by iEN model coefficients identifying features increased or decreased in responders and which contributed to model performance. Noncontributory features have a 0 iEN model coefficient. Data analyzed/presented is aggregated from two independent B16 tumor experiments.

markers on all cell subsets statistically different between WT and SLAMF7^{-/-} mice and found decreased PD-1 and increased PD-L1 on NK cells (Fig. 28H). Together, these findings highlight

the broad and diverse roles of SLAMF7 signaling in the TME.

Immunological Elastic Net identifies features underlying tumor response to Ad-SF7-Fc.

In order to determine why some tumors respond with an attenuation of growth to Ad-SF7-Fc and others do not, we employed a machine learning-based approach using the recently described immunological Elastic Net (iEN) algorithm. [261] Into iEN, we input multiple datasets representing a host of systemic and tumor-localized immune measurements, and a table of immune-specific priors (Fig. 29A and Supplemental table 2; see Materials and Methods). We validated that our iEN model is able to discriminate responders from non-responders, and that the addition of our priors improves model performance (Fig. 29B, C). To determine the factors allowing iEN to identify responders, we generated and performed a network analysis (See Materials and Methods) which showed clustering of common immune archetypes (Fig. 29D). Coloring features on the network by those which were increased or decreased in responding B16 tumors, we found many expected changes like: increased CD8⁺ T cells, more Tex^{prog1} CD8⁺ T cells, [241] increased IFN γ in tumors, [262] less neutrophils (MDSCs), [263] less TAMs, and less CD206 expression on TAMs (Fig. 29E and Supplemental table 3). [264, 265] Critically, we found a number of features supporting the ability of SLAMF7 signaling to modulate tumor control, buttressing our hypothesis that SF7-Fc functions to control tumor growth via DC and innate immune cell stimulation. iEN found increased levels of IL-12(p40) in tumors and increased SLAMF7 on TAMs and DCs (Fig. 29E and Supplemental table 3). iEN also found that higher predicted activation of SLAMF7 on TAMs was important in separating responders, which, paired with our earlier data showing high co-expression of SLAMF7 and PD-L1 on TAMs, suggests that

SLAMF7 may be able to modulate this immune suppressive pathway to achieve tumor control (Fig. 29E and Supplemental table 3).

Discussion

The finding that modulation of SLAMF7 signaling in the setting of viral-based immune activation is capable of inducing tumor control is not unexpected, given what is presently known about SLAMF7. Specifically, the ability of Ad-SF7-Fc to induce IL-12 production, putatively by DC activation, is supported by previous findings that in myeloid cells lacking EAT-2, SLAMF7 activation inhibits IL-12 production. [164] As DCs are known to express EAT-2, [9] it is to be expected that SLAMF7 activation in these cells should allow for IL-12 production. Due to the well known importance of IL-12 in inducing anti-tumor immune responses, [266] SLAMF7 modulation of this pathway is likely one mechanism by which Ad-SF7-Fc achieves tumor control. Complementing this IL-12 response is the strong type I IFN response induced by Ad-SF7-Fc. Type I IFN responses can be beneficial in tumor control, and achieve this via multiple mechanisms. [267, 268] Indeed, previous studies have found that IL-12 and type I IFNs can synergize to induce potent immune activation [269] and there is much interest in combination cancer immunotherapies involving IL-12. [270] Since pDCs are one of the primary producers of type I IFNs, [271] express SLAMF7 in the TME, and express EAT-2 (www.immgen.org), it is plausible that SLAMF7 activation on intra-tumoral pDCs drives pDC production of type I IFNs.

Our discovery that Ad-SF7-Fc does not modulate T cell exhaustion in the TME, nor significantly increase adaptive immune responses against tumors, was unexpected based on our previous work. [255, 256] There are a number of explanations for this including: the use of an adenoviral

vector to deliver SF7-Fc, contributions from the TME itself, and the potential for SF7-Fc to both block and activate SLAMF7 simultaneously. The latter we worked to address using our novel in vivo prediction approach which yielded results consistent with our other studies showing that SF7-Fc activates DCs. Our approach also found that B16 tumors responding to Ad-SF7-Fc had more SLAMF7 activation on pDCs, which corresponds with increased type I IFN production by Ad-SF7-Fc. Since Ad-SF7-Fc does appear to both activate and block SLAMF7 on the same cell subsets, our results suggest that targeting SLAMF7 modulation to particular immune cell types could prove more effective.

Our studies utilizing SLAMF7^{-/-} mice have yielded a number of insights into the role of SLAMF7 in the TME. Among these is the decreased frequency of NK and CD8⁺ T cells in the TME of SLAMF7^{-/-} mice, which is consistent with our previous work, [255] and provides evidence that SLAMF7 may function as an adhesion molecule important for lymphocyte egress and residency in the TME. Discovering tumor-infiltrating NK cells from SLAMF7^{-/-} mice do not express PD-1 in contrast to WT mice is particularly interesting given that we recently found SLAMF7 signaling on T cells is able to modulate PD-1 expression, [255] suggesting a similar mechanism may be present in NK cells and may contribute to tumor control as PD-1 signaling is inhibitory on NK cells. [272] Analogously, we found increased PD-L1 expression on NK cells from SLAMF7^{-/-} mice, supporting potentially linked roles for SLAMF7 in the regulation of this receptor pair.

Perhaps most interesting, was the strong co-expression of SLAMF7 and PD-L1 on tumor-infiltrating myeloid cells that we observed. Of the myeloid cell types expressing SLAMF7, DCs

had the lowest co-expression of SLAMF7 with PD-L1, which may be due to the fact that these cells express EAT-2, whereas the other subsets do not. [9] The high co-expression of these two markers may also explain our previous findings that a subset of SLAMF7^{high}CD38^{high} TAMs was linked to poor survival in ccRCC, since these cells have higher PD-L1 expression than other TAM subsets (data not shown). [209, 255] The theory that SLAMF7 may be able to modulate PD-L1 expression on TAMs (or other myeloid cell types) is supported by results from our machine learning analysis of responses to Ad-SF7-Fc. Here, we found that responders counterintuitively had higher expression of PD-L1 on TAMs, but also had more SLAMF7 on TAMs, and critically, more predicted SLAMF7 activation on TAMs. Taken together, this implies that either modulation of SLAMF7 with SF7-Fc induces anti-tumor responses in TAMs, or the strong innate immune response of Ad-SF7-Fc is capable of overcoming coincidentally induced pro-tumor TAM responses.

By combining modulation of SLAMF7 signaling with delivery and immune stimulation via a recombinant adenovirus vector, we provide proof-of-concept that such an approach is capable of achieving superior tumor control compared to an empty viral vector. While our approach functions primarily by augmentation of the innate immune system, future derivations of this paradigm, capable of inducing adaptive immune responses, should prove highly effective as cancer immunotherapeutics.

Methods

Adenovirus Vector construction. All adenovirus used in this study are of human serotype 5. Ad-null was constructed and purified as previously described. [273] Ad-SF7-Fc was constructed and purified in a similar manner, where the SLAMF7 extracellular domain fused to mIgG1-Fc (SLAMF7/mIgG-Fc) (NCBI Reference Sequence: NM_144539.5) was excised using primers flanked by *EcoRI* and *HindIII* restriction endonucleases (NEB, Ipswich, MA) from a plasmid (Biomatik, Delaware, USA) and sub-cloned into the pShuttle vector, containing a CMV expression cassette. The resulting pShuttle-SF7-Fc plasmid was linearized with *PmeI* restriction enzyme and homologously recombined with the pAdEasy1 Ad vector genome yielding Ad-SF7-Fc. HEK293 cells were transfected with *PacI* linearized plasmid and viable virus was obtained and amplified after several rounds of expanding infection. Ad-SF7-Fc virus was purified using a CsCl₂ gradient. The number of viral particles was quantified using optical density measurement at 260 nm, as previously described. [256] All viruses were found to be replication incompetent (RCA free) by both RCA PCR (E1 region amplification) and direct sequencing methods, as described previously. [113, 256]

Tumor models. All animal procedures were approved by the Michigan State University Institutional Animal Care and Use Committee (<http://iacuc.msu.edu/>). SLAMF7^{-/-} mice were generated as previously described. [255] CT26 model: 8-week-old male Balb/c mice were injected subcutaneously (S.Q.) in the flank with 1.5x10⁵ CT26.CL25 (ATCC, CRL-2639) cells in 100 μL of PBS. Eight days later, once visible tumors formed, mice were split randomly into three groups and were either injected intra-tumorally (I.T.) with 10¹⁰ viral particles (v.p.) of Ad-null

(n=15), Ad-SF7-Fc (n=15), or not injected (n=14). Mice were monitored every 2-3 days and their tumor size was assessed with calipers. Tumor size was calculated with the following formula: $0.5 \times (\text{Length} \times \text{Width}^2)$. B16-F10 model: 4×10^5 B16 tumor cells were injected into the hind flanks of 8-12 week old male C57BL/6J mice as previously described. [255] At day seven post-tumor implantation I.T. injection of Ad-null or Ad-SF7-Fc (n=7-12 per treatment) was performed using 10^{10} viral particles of respective virus.

Cell culture. CT26 and B16-F10 tumor cell lines were cultured in modified RPMI-1640 media (ATCC, 30-2001) supplemented with 10% heat inactivated FBS, and 1X penicillin, streptomycin and fungizone (PSF) (Invitrogen). HEK-293C7 cells were cultured in DMEM media, supplemented with 10% FBS, 1X PSF, and hygromycin.

ADCC assays were performed as described previously. [114] Briefly, CFSE-stained CT26 cells were plated at 1×10^5 cells/well in U-bottom 96-well cell culture plates. Total splenocytes from naïve mice were incubated with CFSE-CT26 cells (20:1 Effector:Target) and cultured for 18 hours in presence of plasma (1:200 dilution) from Ad-null/CT26 lysate, Ad-SF7-Fc/CT26 lysate vaccinated, or non-vaccinated mice. Alternatively they were cultured with Dx5+ NK cells isolated via magnetic beads (Miltenyi kit: 130-052-501) from naïve mice and incubated with CFSE-CT26 cells (1:1 E:T ratio) overnight in presence of plasma (1:50 dilution) from vaccinated mice. Cultures contained 2 ng/mL of murine IL-2 (R&D). Trypsinized cells were stained with a viability dye and analyzed by flow cytometry on a BD LSR II cytometer.

Vaccination studies. 6-week-old Balb/c male mice were injected twice intramuscularly (I.M.) (n=6) over a period of 1 month (days 0 and 12) with 200 µg of CT26 tumor lysate, tumor lysate +

10^{10} v.p./mouse of Ad-null, tumor lysate + 10^{10} v.p./mouse of Ad-SF7-Fc, or not injected (naive, n=4). On day 27, mice were sacrificed, tumors were harvested, and IHC was performed.

Tumor lysate preparation. Tumor lysates were prepared using five freeze-thaw cycles, followed by sonication and centrifugation as described previously. [274] Sample concentration was determined using BCA protein kit (Sigma-Aldrich) per manufacturer's protocol and as previously described, [275] after which the samples were stored in -80°C until use.

Innate immune study. 6-week-old Balb/c male mice were injected I.V. with 10^{10} v.p. of Ad-null (n=6), Ad-SF7-Fc (n=6), or not injected, naïve (n=3). After 10 hours, plasma and spleens were collected for Bioplex and flow cytometry analysis.

Flow cytometry and spectral cytometry. Cells were prepared and stained as previously described. [255] All antibodies used are listed in (Supplemental table 4). Intracellular staining was performed with the Cytofix/Perm kit (BD Biosciences) per manufacturer's instructions. Viability staining was performed with Zombie NIR Fixable Viability dye (BioLegend). Fc receptors were blocked in all samples during staining with mouse Fc block (BD Biosciences). When staining cells from B16 tumors, BD Brilliant Stain buffer (cat: 563794) was used per manufacturer's instruction. Samples were acquired on either a 5-laser Cytex Aurora Spectral Cytometer or 3-laser BD LSR II cytometer and data was analyzed using FlowJo version 10.6.1 (Tree Star) and/or R. All gating schemes can be found in (Supplemental Fig. 7). High dimensional single-cell spectral cytometry was performed in R by first cleaning up the data in FlowJo (Supplemental Fig. 7). Data was exported as FCS files which were loaded into R. The CATALYST package was used to perform all analyses with a cell annotation and dimensionality reduction

approach as previously described. [255, 276] An arcsinh transformation of 6000 was used for all spectral cytometry data. Analysis was performed on cells pooled from all conditions as previously described. [276]

Cytokine and Chemokine analysis. Mouse 23-analyte multiplex-based assay was used to determine cytokine/chemokine concentrations via Luminex 100 per manufacturer's protocol (Bio-Rad), as previously described. [27, 256] (plasma was used at 1:4 dilution and 500 µg of tumor lysate was loaded).

ELISA analysis. 6-week-old Balb/c male mice were given three doses of 200 µg of CT26 tumor lysate and 10^{10} v.p. of Ad-null or Ad-SF7-Fc intraperitoneally (I.P.), or not injected over a period of 5 weeks at which point they were injected with 2.5×10^5 CT26 tumor cells. At 41 days post tumor challenge, plasma from Ad-null (n=6), Ad-SF7-Fc (n=7), and naive (n=2) mice was collected. ELISA assessing levels of CT26-specific antibodies in the plasma was assessed as described previously, [31] where 100 µg of CT26 lysate was plated per well in a high-binding 96-well flat-bottom plate (Corning), incubated at 4°C overnight, and plasma was plated at 1:100, 1:200, and 1:500 dilutions.

Quantitative RT-PCR. 6-week-old Balb/c male mice were injected I.V. with 10^{10} v.p. of Ad-null (n=6), Ad-SF7-Fc (n=6) or not injected, naïve (n=3). Six hours later, spleens were harvested and snap frozen in liquid nitrogen. RNA was extracted using Trizol reagent (Life Technologies), per manufacturer's protocol. cDNA was generated using SuperStrand First Strand Synthesis Kit III (Invitrogen) from Trizol-isolated RNA per the manufacturer's protocol. Quantitative RT-PCR was performed using SYBR green PCR Mastermix (Life Technologies) and analyzed on a

QuantStudio7 system (Thermofisher). The following primers were used: *Isg15*: For: 5'GGTGTCCGTGACTAACTCCAT3', Rev: 5'TGGAAAGGGTAAGACCGTCCT3'; *Oas2*: For: 5'TTGAAGAGGAATACATGCGGAAG3', Rev: 5'GGGTCTGCATTACTGGCACTT3'; *Ifna*: For: 5'GCCTTGACACTCCTGGTACAAATGAG3', Rev: 5'CAGCACATTGGCAGAGGAAGACAG3'; *Ifnb*: For: 5'TGGGTGGAATGAGACTATTGTTG3', Rev: 5'CTCCCACGTCAATCTTTCCTC3'; *Il6*: For: 5'TAGTCCTTCTACCCCAATTTCC3', Rev: 5'TGGTCCTTAGCCACTCCTTC3'; *Il12*: For: 5'TGGTTTGCCATCGTTTTGCTG3', Rev: 5'ACAGAGGTTCACTGTTTCT3'; *csf2*: For: 5'GGCCTTGAAGCATGTAGAGG3', Rev: 5'GGAGAACTCGTTAGAGACGACTT3'; *mGapdh*: For: 3'AGAACATCATCCCTGCATCC3', Rev: 5'CACATTGGGGGTAGGAACAC3'.

HEK-293-C7 cells were plated at 2×10^6 cells/mL in 12-well plates in 500 μ L of complete RPMI media. Ad-null and Ad-SF7-Fc viruses were added at multiplicity of infection (MOI) of 10^4 v.p./cell. Mock treated cells were treated with PBS. After 12 hours, RNA was extracted using Trizol. Primers used: *Slamf7*: For: 5'GGCACATGCGTGATCAATCT3', Rev:

5'ATCGCCAAGCGATACTCAGA3'; *hGAPDH*: For: 5'GGGTGTGAACCATGAGAAGTATGAC3', Rev: 5'GCCATCCACAGTCTTCTGGGT3'. The $\Delta\Delta C_t$ method was used to compare gene expression across conditions and all genes were normalized to *GAPDH* in all experiments.

Immunohistochemistry. Samples were fixed in 10% Neutral Buffered Formalin, embedded in paraffin, and sectioned on a rotary microtome at 4 μ m. Sections were placed on positively charged slides and dried at 56°C overnight. Following deparaffinization in Xylene, slides underwent heat induced epitope retrieval in a steamer utilizing Scytek Citrate Plus Retrieval pH

6.0 followed by several rinses in distilled water. Endogenous Peroxidase was blocked via a 3% Hydrogen Peroxide/Methanol bath for 30 minutes. After blocking for non-specific protein with Rodent Block M (Biocare) for 10 or 20 minutes; sections were incubated with appropriate primary antibodies as described in (Supplemental table. 5). Micro-Polymer (Biocare) reagents were subsequently applied for specified incubations followed by reaction development with Romulin AEC™ (Biocare) and counterstained with Cat Hematoxylin. The number of positive cells was manually counted under magnification 10X for CD3-stained, 20X for CD8-stained and 40X for DX5-stained slides, where 5 areas per sample, and at least 2 sections per sample were used.

Intra-tumor immune cell isolation. Tumors were surgically removed from mice and placed in ice cold PBS. Tumors were minced and non-tumor tissue was removed. Cell suspension was pelleted and resuspended in RPMI with 0.5 mg/mL Collagenase IV (Millipore-Sigma) and 1×10^3 IU/mL DNaseI (Millipore-Sigma) under constant, gentle agitation at 37°C for 1 hr. Digestion was stopped with EDTA and RPMI-1640 supplemented with 10% FBS and cell suspension was filtered through a 40µm cell strainer. Cells were then subject to a Ficoll-Paque gradient centrifugation step to enrich for immune cells. [277]

SLAMF7 activating and blocking predictions. 24 hrs after a second I.T. injection of Ad-null or Ad-SF7-Fc tumors were harvested, cells were stained, and analyzed on a Cytex Aurora spectral cytometer, all as described above. We also confirmed that acute administration of adenovirus does not remodel the TME (Supplemental Fig. 11B). Cells were clustered and annotated as described above. To perform predictions, first we obtain a signature for what a cell with SLAMF7 signaling looks like. To get this we first subset to just a single immune cell type, calculate the median expression of each marker in that cell type in WT (Ad-null treated) and

SLAMF7^{-/-} (Ad-null treated), and subtract the SLAMF7^{-/-} marker expression values from WT. We then select the markers with the most positive and most negative difference to use as a signature. This is done via manual inspection and typically the top 3-4 and bottom 4-5 markers were chosen. Markers that would never be expected to be expressed on a particular cell type are excluded. This yields a SLAMF7 signature of both up-regulated and down-regulated markers on a cell type-specific basis.

We then subset the same cell type from WT (Ad-SF7-Fc treated) mice and use the previously calculated signature to generate a SLAMF7_score for each cell. The score is calculated using a previously-published formula used to obtain signature scores from scRNA-seq data. [278] Importantly, our prior work has shown that activation of SLAMF7 with SF7-Fc leads to its down-regulation [27] and we confirmed that blocking SLAMF7 with SF7-Fc leads to its up-regulation (Supplemental Fig. 11A). [27] Therefore, for each cell type we plot the SLAMF7_score by SLAMF7 expression as a dot plot and expect that cells where SLAMF7 is being blocked should have high SLAMF7 expression (Supplemental Fig. 11A) and a low SLAMF7_score, while cells where SLAMF7 is being activated should have low SLAMF7 expression [27] and a high SLAMF7_score. Cells where SLAMF7 is being activated or inhibited naturally come off the diagonals so we select the cells at either extreme of the appropriate diagonals as being blocked or activated.

To calculate outliers in an unbiased manner we identify the points on the plot representing the intersection of the 25th percentile of SLAMF7 expression and the 75th percentile of SLAMF7_score for defining the boundary of cells getting SLAMF7 blocked. We do the reverse for cells getting SLAMF7 activated. We now calculate the slope of the diagonal lines passing through each point with a linear model where the y-intercept for each line is the model coefficient. To identify the points on either extreme of these lines we calculate and use the corresponding residuals. This approach was performed only for cell types with considerable levels of SLAMF7 expression (ie. not CD4⁺ T cells and B cells, which express SLAMF7 at very low levels).

iEN machine learning analysis of tumor response to Ad-SF7-Fc. We first separate mice inoculated with B16 tumors and treated with Ad-SF7-Fc into those who responded and those who did not based on final tumor volume at time of sacrifice (Fig. 29A). Next, we pool together all immune measurements made on these mice across various assays. We then generate a table containing prior immunological knowledge about known responses to adenovirus vectors [31, 113, 279-285] and expected marker expression across different cell types (other immune measurements were not weighted in our priors so as to not bias the algorithm) (Supplemental table 2). We input all immune measurements into the immunological Elastic Net (iEN) algorithm along with our priors and perform 10-fold cross validation. [261] Model validation is performed by calculating the AUROC. Networks were generated as previously described. [261] Briefly, each node is a feature entered into the iEN model and node sizes are scaled by their individual

AUROC. Edges are significant spearman correlations between features ($p < 0.05$) after bonferroni correction for multiple comparisons. Imbedding in 2-D space was performed with tSNE.

Statistical analysis. Data in all graphs is presented as mean \pm SEM. Statistical analysis are listed in all figure legends and were performed in either GraphPad Prism V8 or the R computing environment. Cell subset frequency comparisons and differential marker expression on cell subsets from experiments employing high dimensional spectral cytometry were statistically compared with a GLMM implemented through the diffcyt R package. [286] All heatmaps were locally scaled. No samples/mice were excluded from any analysis except for one Ad-null treated WT and one Ad-SF7-Fc treated WT mouse from the same B16 tumor growth experiment, where an outlier test identified the tumor volume in each mouse as a statistically significant outlier.

Data availability. Raw data and code used is available from authors upon reasonable request.

Acknowledgements. We would like to thank the MSU genomics core for assistance with qRT-PCR and the MSU histology core for sample preparation and immunohistochemistry. We also thank Dr. David L. Carlson for assistance with SF7-Fc prediction analysis and Anthony Culos for assistance analyzing iEN models. The data presented herein were obtained using instrumentation in the MSU Flow Cytometry Core Facility with support of Core staff. The facility is funded through user fees and the financial support of Michigan State University's Office of Research & Innovation, College of Osteopathic Medicine, and College of Human Medicine. Y.A.A. and A.A. hold a patent on the SF7-Fc protein. Y.A.A. was supported by the US National

Institute of Health grant (1R21AI122808-01) and the Michigan State University Clinical and Translational Sciences Institute (MSU-CTSI). A.A. is supported by the MSU Foundation and the Osteopathic Heritage Foundation. P.O. is supported by the John A. Penner Endowed Research Fellowship.

Author contributions. P.O. designed all B16 experiments and Y.P. designed all CT26 experiments. P.O., M.K.B., Y.P., and S.H. performed all experiments. M.K.B. performed all bioplex assays. Y.P. analyzed all data related to CT26 experiments and P.O. analyzed all data related to B16 experiments. C.P.H. manage all cell lines. S.G. and C.P.H. prepared all adenoviruses. S.G. managed all mouse work. Y.A.A. conceptualized Ad-SF7-Fc and Ad-EAT-2 and designed the vectors. A.M.A. performed IHC analysis. P.O. performed all high dimensional single-cell spectral cytometry and analyzed all associated data. P.O. conceptualized and performed all computational analyses. P.O. generated all figures and wrote the manuscript, with input and revisions from all authors. Y.A.A. and A.A. supervised the study and provided funding.

Conflicts of interest. The authors declare no conflicts of interest exist.

CHAPTER: 6 The immune cell receptor SLAMF7 is linked to susceptibility to CNS autoimmunity
via modulation of B cell responses

Authors: Patrick O'Connell, Maja K. Blake, Sarah Godbehere, Andrea Amalfitano, Yasser A. Aldhamen

Abstract

Background: Multiple sclerosis (MS) is a chronic, debilitating condition resulting from autoimmunity against the CNS. The etiology of MS is complex, involving both environmental and genetic factors, and is not yet fully understood. The body of research into MS points to dysregulation of the immune system as the most likely culprit in driving disease susceptibility, however, we still lack an understanding of how the many MS-associated genes contribute to MS-driving immune disruption. We undertook a series of studies using the murine model of CNS autoimmunity, experimental autoimmune encephalomyelitis (EAE), in order to determine why the *SLAMF7* gene has been linked to MS.

Methods: We subjected WT and *SLAMF7*^{-/-} mice to EAE induced with the rmMOG₁₋₁₂₅ antigen, compared disease severity between genotypes, and comprehensively profiled the CNS immune landscape of these mice. We employed high dimensional single-cell spectral cytometry on CNS immune cells of these mice allowing identification of all *SLAMF7* expressing CNS immune cells and comparison of the entire CNS immune niche. Studies were repeated with WT and *SLAMF7*^{-/-} mice on an IL-10^{GFP} background allowing us to determine if *SLAMF7* altered IL-10 production in the setting of EAE. We performed deep phenotyping of B cells using a targeted high dimensional B cell spectral cytometry panel. Adoptive transfer studies involving the transfer of WT and *SLAMF7*^{-/-} B cells into B cell deficient mice (μ MT) were also performed.

Results: We found *SLAMF7*^{-/-} mice to be more susceptible to EAE compared to WT mice and found *SLAMF7* to be expressed on numerous CNS immune cell subsets, but notably absent on

microglia and exhibiting downregulation during EAE only on B cells. The absence of SLAMF7 did not grossly alter the CNS immune landscape, but allowed for increased CNS B and CD4⁺ T cell infiltration during EAE. We confirmed that SLAMF7 does not alter CNS-specific immune cell IL-10 responses during EAE. Deep phenotyping of B cells from revealed disease and microenvironment-specific SLAMF7 changes on plasma cells along with increased plasma cell activation in SLAMF7^{-/-} mice. Adoptive transfer studies revealed that the increased susceptibility of SLAMF7^{-/-} mice to EAE is partly B cell dependent which correlated with studies showing SLAMF7 drives B cell maturation.

Conclusions: Our investigations on the genetic linkage between SLAMF7 and MS have identified novel roles for SLAMF7 in CNS immune regulation and revealed a new role for SLAMF7 in the control of B cell maturation, particularly during CNS autoimmunity.

Introduction

Autoimmune diseases represent some of the most pathologically complex conditions in modern medicine, both in terms of their causes and response to therapies. Multiple sclerosis (MS) is no exception, and takes a significant toll on all those it affects as it often appears early in life, progressively gets worse, and consequently, leads to many years of disability and hardship [287]. Since the disease MS was first termed in 1868 [288], efforts have been underway to identify both the underlying causative mechanisms and effective treatments. Our current understanding of MS has identified both environmental and genetic links to MS susceptibility [289], with immune dysfunction emerging as a unifying feature [4]. However, the immune

system is recognized as one of the human body's most complex organ systems, and we still have much to learn regarding how complex immune interaction networks maintain health and drive disease susceptibility [290, 291].

While there are a considerable number of available therapies for MS, most of them targeting the immune system [292-294], many patients, particularly those with more aggressive forms of the disease, fail to respond to these [8]. An example is the newer B cell depleting antibodies (Ocrelizumab, Ofatumumab, etc) which have shown remarkable success in inducing remissions in MS patients with the relapsing remitting subtype [294, 295], yet fail on patients with the more severe primary progressive subtype [8]. To develop better MS therapeutics, we must first understand how many of the genes linked to MS contribute to disease pathogenesis, allowing for the construction of a unified framework linking specific disruptions in immune networks to pathogenesis.

The International Multiple Sclerosis Genetics Consortium has made great strides in identifying the plethora of genes linked to MS [4], yet few of these genes have been investigated in depth to determine mechanistically how they contribute to susceptibility to CNS autoimmunity. Here, we investigated the link between the *SLAMF7* gene and MS [4, 116, 117]. *SLAMF7* is a member of the signaling lymphocytic activation molecule [SLAM] family of genes and is expressed only on hematopoietic cells [9, 215]. *SLAMF7* can drive either activating, proinflammatory signaling in a cell or inhibitory signals, and which type of signaling *SLAMF7* induces depends on the presence of its intracellular adaptor, Ewing sarcoma-associated transcript 2 (EAT-2) [215]. In

general, in cells with EAT-2, SLAMF7 signaling is activating and in the absence of EAT-2, it is inhibitory [27, 215]. We have previously defined roles for SLAMF7 in a number of conditions including HIV infection [27] and cancer [255], and have also worked to modulate SLAMF7 signaling for therapeutic benefit (O'Connell, P., et al. *Under Review*) [31, 80, 81, 112-114]. Using the mouse model of MS, experimental autoimmune encephalomyelitis (EAE), we find SLAMF7^{-/-} mice to be more susceptible to CNS autoimmunity and we characterize SLAMF7 expression across the CNS immune landscape. We further define CNS immune cell-specific changes driven by SLAMF7 and identify a role for SLAMF7 in the modulation of B cell responses. Deep phenotyping studies highlight specifically how SLAMF7 alters B and plasma cell responses, while adoptive transfer studies confirm that a lack of SLAMF7 signaling on B cells contributes to EAE susceptibility. These studies identify a novel role for SLAMF7 in the modulation of B cell responses and provide early mechanistic evidence supporting the genetic link between *SLAMF7* and MS.

Results

SLAMF7 is protective against CNS autoimmunity and displays unique cell type expression patterns.

To assess the global impact of SLAMF7 signaling on neuroinflammation, we subjected WT and SLAMF7^{-/-} mice to EAE induced with the rmMOG₁₋₁₂₅ protein [132]. We found SLAMF7^{-/-} mice to be significantly more susceptible to EAE compared to WT mice (Fig. 30A, B). Since SLAMF7 is only expressed on immune cells [9] and since immunological determinants are one of the

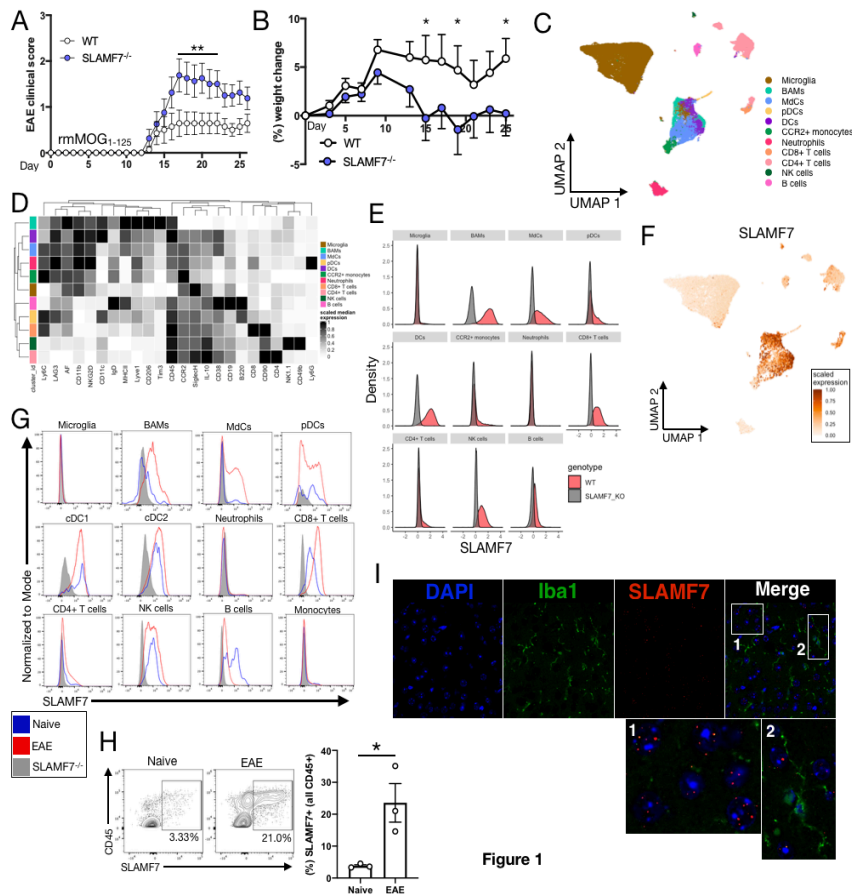


Figure 1

FIGURE 30: SLAMF7 displays unique expression patterns in the CNS and protects from EAE.

(A) Clinical scores of WT (n=14) and SLAMF7^{-/-} mice (n=16) subjected to EAE induced with rmMOG₁₋₁₂₅. (B) Change in baseline weight for mice in (A). (C) UMAP of the entire CNS immune landscape in WT and SLAMF7^{-/-} mice subjected to EAE. The complete CNS immune landscape was assessed via high dimensional single-cell spectral cytometry. (D) Marker expression on CNS immune cell subsets from (C). (E) Density plots of SLAMF7 expression across CNS immune subsets from (C). (F) Scaled SLAMF7 expression plotted on the UMAP projection of all CNS immune cells from (C). (G) Histograms of SLAMF7 expression on CNS immune cell subsets at steady state and during active EAE neuroinflammation. (H) SLAMF7 expression on all CNS immune cells at steady state and during EAE. (I) Conical imaging of SLAMF7 and Iba1 on mouse brain tissue during peak EAE. Magnifications 1 and 2 highlight regions with SLAMF7⁺ Iba1⁻ non-microglial cells and SLAMF7⁺ Iba1⁺ microglia, respectively. Groups in (A) compared with a two-way ANOVA with Sidak's multiple comparison test, displayed with mean ± SEM, and representative of two independent experiments showing similar results. Groups in (B) compared with a two-way ANOVA with Fisher's LSD test. Groups in (H) compared with an unpaired two-way t-test and representative of a single experiment. *p<0.05, **p<0.01. BAMS, border-associated macrophages; MdCs, myeloid-derived cells; AF, autofluorescence.

primary factors controlling EAE susceptibility [4], we profiled the entire CNS of mice during EAE to both determine which cells express SLAMF7 and how SLAMF7 expression changes during neuroinflammation. Employing high dimensional single-cell spectral cytometry [193, 255, 296]

we reconstruct the entire CNS immune landscape during EAE and identify 11 immune cell subsets (Fig. 30C, D and Supplementary Fig. 12A). We find SLAMF7 is expressed on many of the same cell types in the CNS as in the periphery including: macrophages (termed border-associated macrophages [BAMs] in the CNS), myeloid-derived cells (MdCs), pDCs, DCs, CD8⁺ T cells, NK cells, and B cells, with minimal expression on a few other subsets (Fig. 30E, F). Comparing SLAMF7 expression on various CNS immune cell subsets during steady state or active neuroinflammation with EAE we found that SLAMF7 expression increased on BAMs, CD8⁺ T cells, and CD4⁺ T cells (Fig. 30G), while decreasing on B cells (Fig. 30G). We also observed a significant increase in the total frequency of SLAMF7⁺ cells in the CNS during EAE compared to steady state (Fig. 30H). This is to be expected since many of the infiltrating immune cells into the CNS during EAE also express SLAMF7. Finally, while we found SLAMF7 expressed on a number of CNS myeloid cell types, we did not observe any SLAMF7 expression on the most populous CNS myeloid cell type, microglia (Fig. 30E, G). To confirm that microglia truly do not express SLAMF7 we imaged brain of WT mice during EAE with confocal microscopy and found punctate SLAMF7 staining on Iba1⁻ CNS immune cells and no SLAMF7 staining on any Iba1⁺ microglial cells (Fig. 30I). Together, these results highlight that SLAMF7 is broadly expressed in the CNS at steady state and during neuroinflammation and plays some role in the regulation of the latter.

SLAMF7-mediated changes in the CNS immune landscape during EAE.

We next compared the frequency of all CNS immune cell subsets (identified using our high dimensional spectral cytometry approach) during EAE between WT and SLAMF7^{-/-} mice and

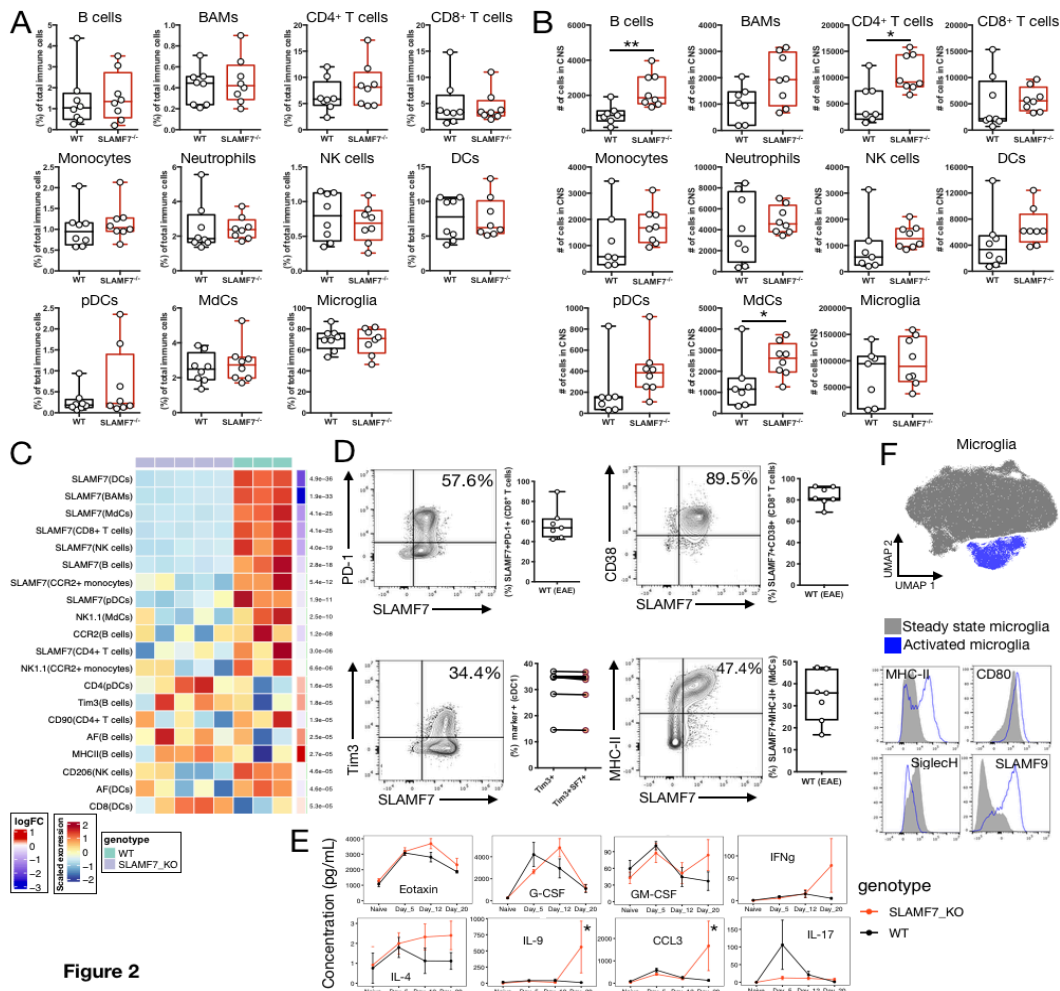


Figure 2

FIGURE 31: SLAMF7-induced changes in the CNS immune cell landscape and elsewhere during EAE.

(A) Frequency of various CNS immune cell subsets between WT (n=8) and SLAMF7^{-/-} mice (n=8) during EAE induced with rmMOG₁₋₁₂₅. (B) Total number of various immune cell subsets in the CNS of WT (n=8) and SLAMF7^{-/-} mice (n=8) during EAE induced with rmMOG₁₋₁₂₅. (C) Heatmap of differential marker expression on all CNS immune cell subsets from WT and SLAMF7^{-/-} mice during EAE with a FDR < 0.05. Adjusted p-value displayed on the right of each row. (D) Interesting co-expression patterns of SLAMF7 with other regulatory markers on various CNS immune cell subsets during EAE. Top left, co-expression of SLAMF7 and PD-1 on CD8⁺ T cells; Top right, SLAMF7 co-expression with CD38 on CD8⁺ T cells; Bottom left, co-expression of SLAMF7 and Tim-3 on cDC1 cells; Bottom right, co-expression of MHC-II and SLAMF7 on MdCs. (E) Temporal expression of various cytokines/chemokines in WT (n=6) and SLAMF7^{-/-} mice (n=8) during EAE induced with rmMOG₁₋₁₂₅. (F) Top, UMAP of all CNS microglia in WT mice during EAE with FlowSOM-defined clusters differentially colored. Bottom, histograms of activation marker expression on microglia subsets from above. Notably, activated microglia have very high protein-level expression of SLAMF9. Groups in (A, B) compared using unpaired two-way t-tests and representative of two independent experiments showing similar results. Groups in (C) compared using a GLMM and representative of a single experiment. Groups in (E) compared using a mixed effects model with Sidak's post-hoc test implemented through GraphPad Prism and representative of a single experiment. *p<0.05, **p<0.01. BAMS, border-associated macrophages; MdCs, myeloid-derived cells.

found no significant changes (Fig. 31A). However, comparing the total number of various CNS immune cell subsets in WT and SLAMF7^{-/-} mice during EAE we found increased numbers of B

cells, CD4⁺ T cells, and MDCs in SLAMF7^{-/-} mice (Fig. 31B). Interesting findings, considering both B cell and CD4⁺ T cells play critical roles in the pathogenesis of EAE and MS [5, 132, 133, 294, 297]. We also compared all significantly differentially expressed markers on all CNS immune cell subsets between WT and SLAMF7^{-/-} mice during EAE and found multiple changes on B cells (Fig. 31C). Specifically, SLAMF7^{-/-} B cells had higher MHC-II expression, Tim3 expression, and autofluorescence (Fig. 31C), suggesting these cells are highly-activated. We also observed a number of interesting instances of SLAMF7 co-expressing with other regulatory receptors on CNS immune cells during EAE including: PD-1 on CD8⁺ T cells [255] (Fig. 31D), CD38 on CD8⁺ T cells (Fig. 31D), Tim3 on cDC1 cells (Fig. 31D), and MHC-II on MDCs (Fig. 31D). After observing that SLAMF7 was capable of modulating the phenotype of various CNS immune cells, we wished to determine if SLAMF7 is also capable of modulating cytokine and chemokine responses in mice during the course of EAE. We serially profiled plasma levels of multiple cytokines and chemokines in WT and SLAMF7^{-/-} mice and found a pattern of increased soluble inflammatory mediators later in the disease course in SLAMF7^{-/-} mice compared to WT mice (Fig. 31E). Notably, while WT mice displayed a spike in plasma IL-17 levels at day five post-EAE induction (Fig. 31E), SLAMF7^{-/-} mice did not have increased levels of IL-17 (Fig. 31E). This suggests that the increased susceptibility to EAE in SLAMF7^{-/-} mice is independent of Th17 responses, which are known to be a critical inflammatory pathway in the pathogenesis of EAE/MS [298].

As an aside, we also measured the expression of a receptor related to SLAMF7, SLAMF9, on microglial cells during EAE. SLAMF9 is one of the least studied members of the SLAM family, yet

it has been linked to modulation of EAE susceptibility via control of pDC responses [38] and has been identified at the mRNA level as being a specific marker of disease-associated microglia (DAMs) [299]. Using high dimensional spectral cytometry and unbiased clustering with FlowSOM, we identified a population of activated microglia in WT mice during EAE which expressed high levels of MHC-II, CD80, and SLAMF9, while expressing low levels of SiglecH; all markers of microglia activation (Fig. 31F) [193]. By validating that SLAMF9 is expressed on the cell surface of microglia at the protein level, this opens up the opportunity to both use SLAMF9 as a marker of DAMs and as a potential therapeutic target [300].

SLAMF7 does not alter the CNS-resident IL-10 immune niche during EAE.

A common mechanism of altered susceptibility to CNS autoimmunity is dysregulated immune suppressive mechanisms, primarily IL-10-mediated [301-304]. Importantly, our previous work found that SLAMF7 signaling was capable of driving STAT3 phosphorylation [255], which is a critical driver of IL-10 production [305, 306]. Therefore, we hypothesized that lack of SLAMF7 signaling may be preventing appropriate pSTAT3-mediated IL-10 suppressive responses. To examine this, we cross our SLAMF7^{-/-} mice to IL-10^{GFP} mice [307] allowing us to accurately measure IL-10 across all cell types. We induced EAE with rmMOG₁₋₁₂₅ in WT-IL-10^{GFP} and SLAMF7^{-/-}-IL-10^{GFP} mice and assessed the resident CNS immune landscape. We also performed

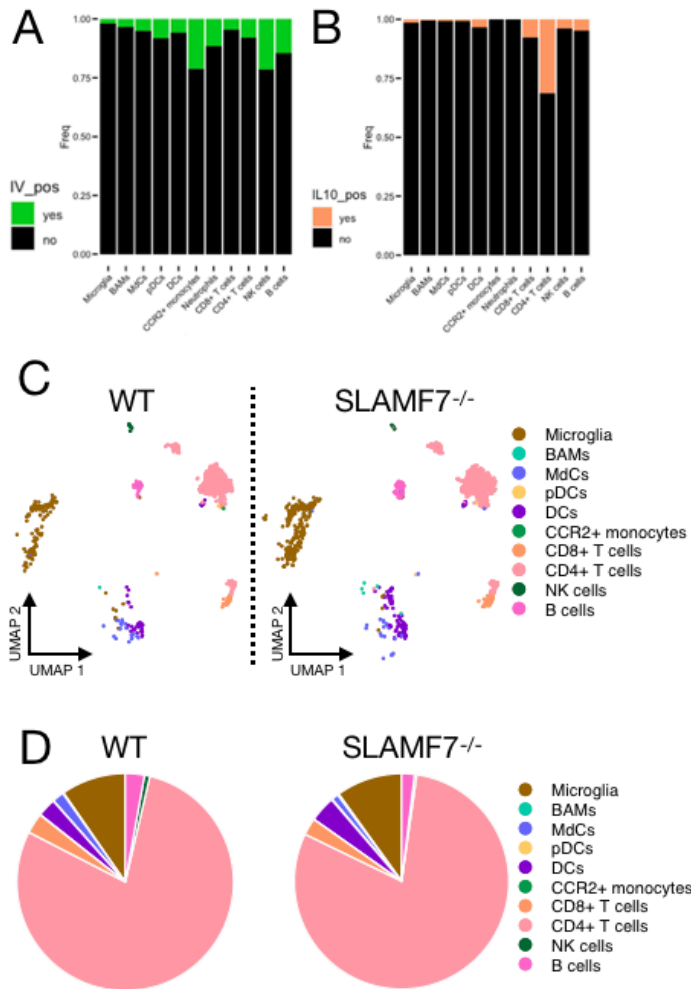


FIGURE 32: The resident CNS il-10 immune niche in WT and SLAMF7^{-/-} mice during EAE.

(A) Frequency of resident [IV⁻] versus circulating (IV⁺) CNS immune cells in WT-IL-10^{GFP} (n=3) and SLAMF7^{-/-}-IL-10^{GFP} (n=5) mice during EAE induced with rmMOG₁₋₁₂₅. (B) Frequency of IL-10 producing cells in the CNS of WT-IL-10^{GFP} (n=3) and SLAMF7^{-/-}-IL-10^{GFP} (n=5) mice during EAE induced with rmMOG₁₋₁₂₅. (C) UMAP of all CNS-resident IL-10⁺ immune cells in WT-IL-10^{GFP} and SLAMF7^{-/-}-IL-10^{GFP} mice during EAE. (D) Pie charts of all CNS-resident IL-10⁺ immune cells in WT-IL-10^{GFP} and SLAMF7^{-/-}-IL-10^{GFP} mice during EAE. Groups in (D) compared with a GLMM. Data in (A-D) representative of a single experiment. BAMS, border-associated macrophages; MdCs, myeloid-derived cells.

in vivo labeling before harvest of CNS tissue to allow for identification of bona fide resident CNS immune cells (O'Connell, P., et al. *Under Review*). We found the majority of immune cells from most cell types were CNS resident, particularly for microglia and BAMS, while cell types such as

CCR2⁺ monocytes and NK cells were slightly more likely to be non-resident (Fig. 32A and Supplementary Fig. 12B). We performed all downstream analyses using only resident CNS immune cells. Comparing the frequency of IL-10⁺ cells per immune subset we found CD4⁺ T cells to have the largest fraction of IL-10⁺ cells (Fig. 32B). We next reconstructed the CNS resident IL-10 immune landscape (Fig. 32C) and found CD4⁺ T cells and microglia to be the predominant sources of IL-10 during EAE, and that this was consistent between IL-10^{GFP} and SLAMF7^{-/-}-IL-10^{GFP} mice (Fig. 32D). These results suggest that SLAMF7 does not alter the CNS IL-10 immune niche during EAE and argue in favor of alternative mechanisms explaining SLAMF7^{-/-} mice susceptibility to EAE.

SLAMF7 induced changes in B cell maturation.

We next decided to look closer at how SLAMF7 signaling modulated B cell responses in our model due to the fact that we were using a B cell-dependent model of EAE [rmMOG₁₋₁₂₅ protein [308-311]], since we noted increased numbers of B cells in the CNS of SLAMF7^{-/-} mice during EAE (Fig. 31B), and because B cells were the only CNS immune cell subset where SLAMF7 expression was decreased during EAE compared to steady state (Fig. 30G). Comparing splenic B cells from WT and SLAMF7^{-/-} mice during EAE we noted SLAMF7^{-/-} mice had fewer B220^{low}IgD^{low} mature B cells (Fig. 33A) [312]. We also found that in vitro activation of the SLAMF7 receptor on B cells via antibody cross-linking [27, 255] resulted in an increased frequency of mature B cells (Fig. 33B), together suggesting that SLAMF7 receptor signaling is important for B cell maturation to some degree. A lack of mature B cells, and more immature B cells in SLAMF7^{-/-} mice, may explain the increased susceptibility to EAE since these mature B220^{low}IgD^{low} B cells

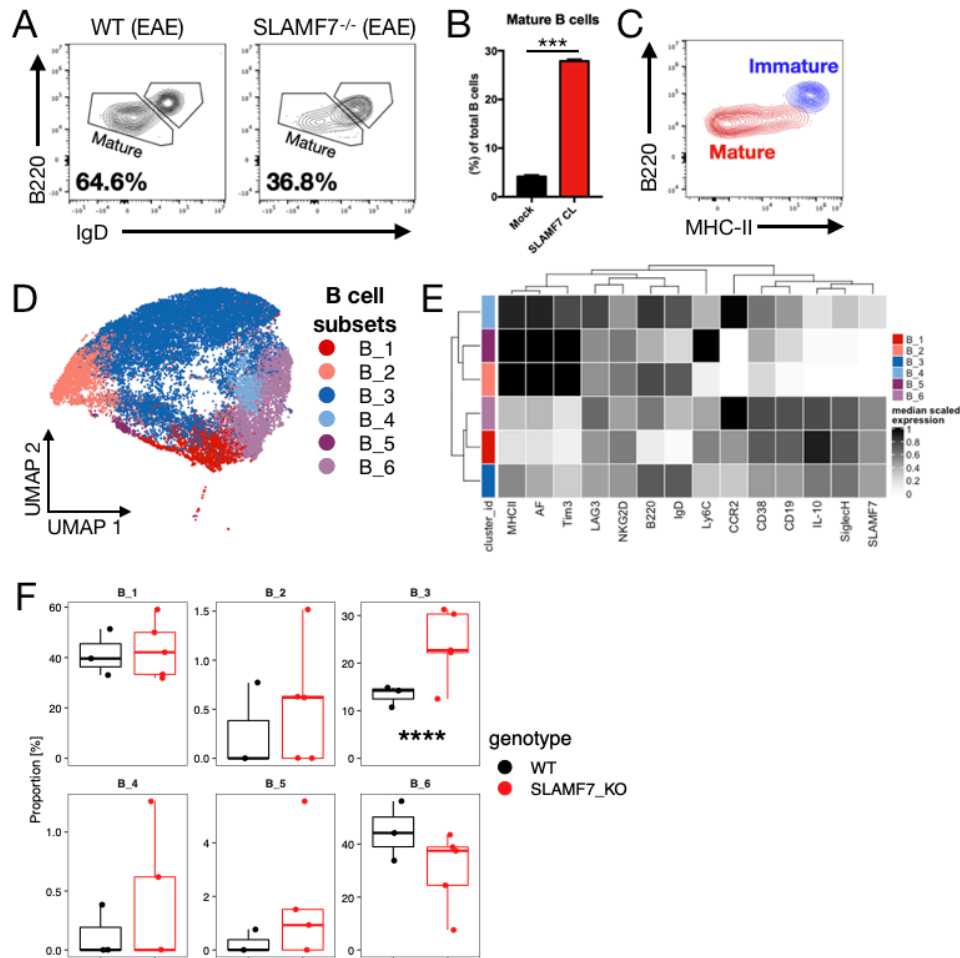


FIGURE 33: SLAMF7 modulation of B cells and CNS B cell differences between WT and SLAMF7^{-/-} mice.

(A) Bivariate FACS plots of splenic mature and immature B cells in WT and SLAMF7^{-/-} mice during EAE. Mature B cells are B220^{low}IgD^{low} per Ray et al., 2019. (B) Comparison of the frequency of mature B cells after 10hrs in vitro culture of WT B cells in the presence or absence of SLAMF7 activation (CL). (C) FACS plot identifying immature B cells as being MHC-II^{high} and mature B cells being MHC-II^{neg-low}. (D) UMAP of sub-clustering of resident-CNS B cells in WT and SLAMF7^{-/-} mice during EAE. (E) Marker expression of B cell subsets from (D). (F) Comparison of the frequency of CNS B cell subsets to total CNS B cells in WT and SLAMF7^{-/-} mice during EAE. Groups in (B) compared with a two-way unpaired t-test and representative of a single experiment. Groups in (F) compared using a GLMM and representative of a single experiment. ***p<0.001, ****p<0.0001. AF, autofluorescence.

are known to play an important IL-10-independent regulatory role during EAE [312].

Additionally, the immature B cell subset (which SLAMF7^{-/-} mice have more of) has high MHC-II expression (Fig. 33C) indicating a potential to activate CD4⁺ T cells [297]. We next looked at CNS B cells more in depth using our high dimensional spectral profiling approach and identified six B

cell subsets in an unbiased manner (Fig. 33D and Supplemental Fig. 13A). Our approach identified a putative Breg cluster expressing high levels of IL-10 (B_1) (Fig. 33E), but we did not observe changes in this subset between WT and SLAMF7^{-/-} mice during EAE (Fig. 33F), consistent with an IL-10-independent mechanism. We did however, find an increased frequency of the B_3 subset SLAMF7^{-/-} mice which had higher expression of B220 and IgD (Fig. 33E), consistent with a more immature B cell subset and aligning with our previous data from splenic B cells. These findings identify a defect in B cell maturation in the absence of SLAMF7 signaling which may implicate B cells as responsible for the association of SLAMF7 with increased susceptibility to CNS autoimmunity.

Deep phenotyping of B cells at steady state and during EAE reveals plasma cell alterations in SLAMF7^{-/-} mice.

In order to more comprehensively investigate B cells in our model we developed a high dimensional spectral cytometry B cell profiling panel (Supplementary Fig. 14A and Supplementary table 6) and analyzed both splenic and CNS B cells from WT and SLAMF7^{-/-} at steady state and during EAE. We found interesting changes in SLAMF7 expression across various B and plasma cell subsets in the CNS, observing decreased SLAMF7 expression on mature plasma cells and T1 B cells during EAE (Fig. 34A). However, in the spleens of the same mice we noted increased SLAMF7 expression on immature and mature plasma cells during EAE (Fig. 34B). Comparing the frequency of each of the 12 splenic B cell subsets we identified between WT and SLAMF7^{-/-} mice, we only observed a minor decrease in T2 B cells in SLAMF7^{-/-} mice during EAE compared to WT mice (Fig. 34C). Similarly, in the CNS we only observed a small

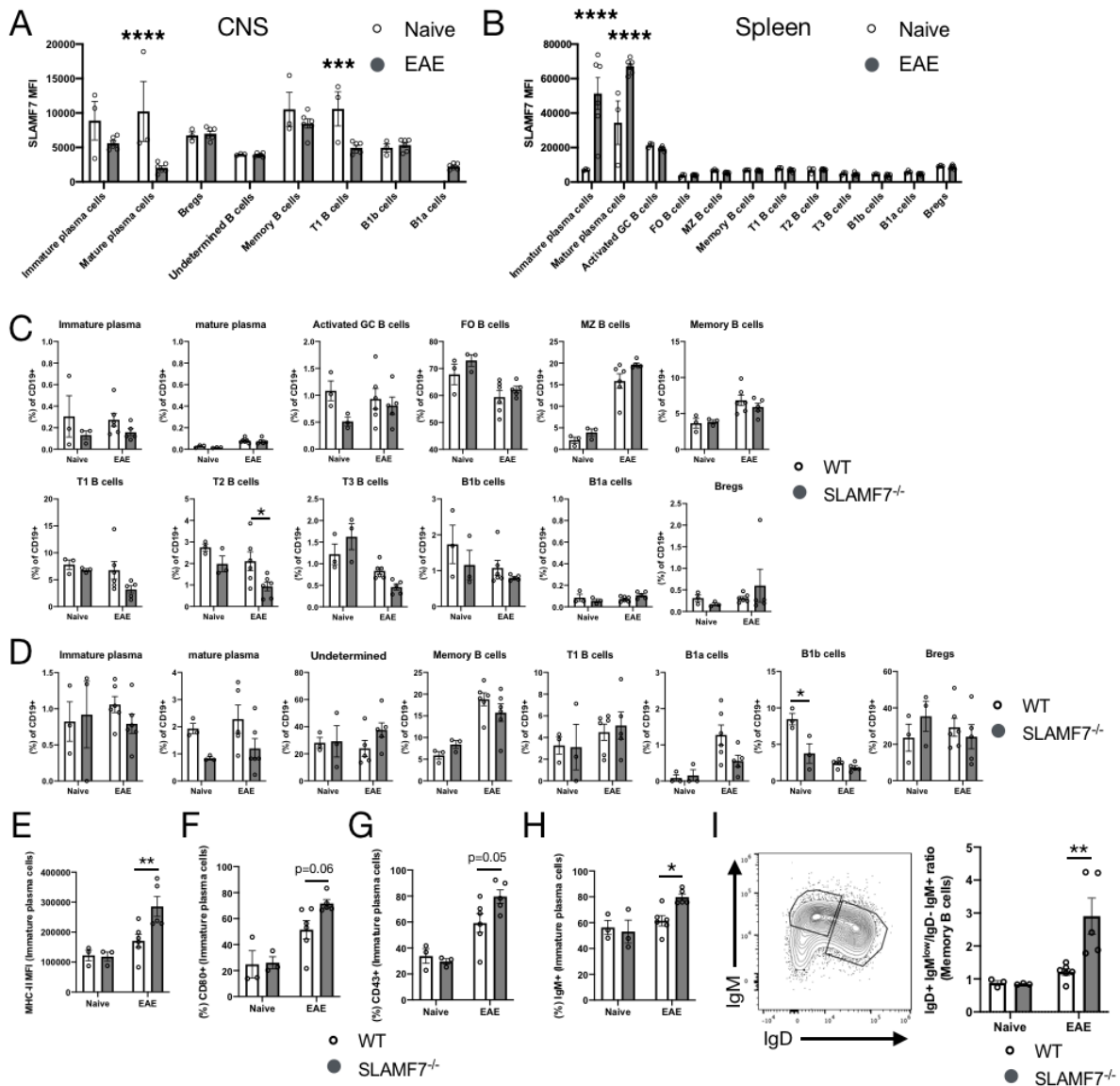


FIGURE 34: Deep phenotyping of splenic and CNS B cell subsets in WT and SLAMF7^{-/-} mice.

(A, B) SLAMF7 expression level across CNS (A) and splenic (B) B cell subsets at steady state and during active EAE neuroinflammation in WT mice. (C) Frequency of various B cell subsets from total splenic B cells in WT and SLAMF7^{-/-} mice at steady state and during EAE. (D) Frequency of various B cell subsets from total CNS B cells in WT and SLAMF7^{-/-} mice at steady state and during EAE. (E) MHC-II expression on splenic immature plasma cells. (F) CD80 expression on splenic immature plasma cells. (G) CD43 expression on splenic immature plasma cells. (H) IgM expression on splenic immature plasma cells. (I) Changes in the ratio of IgD⁺IgM^{low} memory B cells to IgD⁺IgM⁺ memory B cells in WT and SLAMF7^{-/-} mice at steady state and during EAE. Data in (A-I) representative of a single experiment. Groups in (A, B) compared with multiple unpaired two-way t-tests with a Holm-Sidak correction for multiple comparisons. Groups in (C-I) compared with a two-way ANOVA with Sidak's test for multiple comparisons. FO, follicular; MZ, marginal zone; Bregs, regulatory B cells.

decrease in the frequency of B1b cells in SLAMF7^{-/-} mice at steady state compared to WT mice (Fig. 34D). Together, these suggest that SLAMF7 expression does not globally remodel either

the CNS or splenic B cell compartments at steady state or during active neuroinflammation.

Further investigations into these various B and plasma cell subsets uncovered interesting phenotypic differences between WT and SLAMF7^{-/-} mice. We found increased expression of the activation markers MHC-II (Fig. 34E), CD80 (Fig. 34F), and CD43 (Fig. 34G) on immature plasma cells of SLAMF7^{-/-} mice only during EAE compared to WT. We also observed increased expression of IgM on SLAMF7^{-/-} immature plasma cells only during EAE (Fig. 34H) which is intriguing since IgM⁺ plasma cells are known to retain a functional BCR and are potent cytokine producers [313]. Furthermore, we observed two subsets of memory B cells which could be separated by IgD and IgM expression into IgD⁺IgM^{low} and IgD⁻IgM⁺ subsets (Fig. 34I) which have previously been described [314, 315].

We also noted a number of phenotypic differences on T2 and MZ B cells including: decreased CD1d expression on MZ (Supplementary Fig. 3B) and T2 (Supplementary Fig. 3C) B cells from SLAMF7^{-/-} mice and increased MHC-II (Supplementary Fig. 14D) and GL7 (Supplementary Fig. 14E) on T2 B cells from SLAMF7^{-/-} mice during EAE. Since T2 B cells are recognized as a precursor to MZ B cells [316, 317], the latter of which expand greatly during EAE, our findings of increased activation in these cells suggests SLAMF7 may affect responses in this cell lineage early in their development.

Discussion

The increased susceptibility to EAE we observe in *SLAMF7*^{-/-} mice links well to GWAS studies showing an association of polymorphisms in *SLAMF7* with MS [4, 116, 117]. It supports a role for *SLAMF7* in dampening over-zealous, pathology-inciting immune responses, which when perturbed, lead to MS susceptibility. This fits with our current understanding of *SLAMF7*, since most immune cells which express *SLAMF7* do not express EAT-2, meaning that *SLAMF7* signaling on most immune cells should be anti-inflammatory [9, 27].

After profiling the expression of *SLAMF7* across the entire CNS immune landscape, we found *SLAMF7* expression to closely mirror that seen in the periphery [9, 215], with the notable exception of B cells where a decrease in *SLAMF7* expression is observed during EAE. This decrease in *SLAMF7* expression in the setting of a highly inflammatory environment is out of character for *SLAMF7*, as this receptor is quite responsive to inflammatory stimuli and usually increases in expression in these settings [27, 164, 255]. This points to a potentially unique role for *SLAMF7* in B cells, of which we have only scratched the surface of here.

How exactly *SLAMF7* controls B/plasma cell responses remains to be seen, however, our semi-targeted high dimensional approach found particularly interesting changes in the maturation state of these cells. In particular, the changes we see in immature plasma cells, coupled with the lack of mature B cells in *SLAMF7*^{-/-} mice, and that *SLAMF7* activation on B cells causes maturation, points to a role for *SLAMF7* in B/plasma cell maturation. While further studies are needed to confirm this, the fact that the Blimp-1 transcription factor is critical to plasma cell

differentiation [318] and considering we recently published that SLAMF7 signaling drives Blimp-1 expression [255], suggests this pathway (and/or others) may be responsible. These defects in B cell maturation may be linked to the increased susceptibility to EAE in SLAMF7^{-/-} mice, considering recent work showing that a mature B220^{low}IgD^{low} population of B cells suppressed immune responses in an IL-10-independent manner and protects from EAE [312].

In a similar vein, the changes we observed on plasma cells between the CNS and spleen point to the presence of an unknown factor in the CNS responsible for decreases in SLAMF7 expression in a microenvironment-specific manner. This is evidenced from the decreases in SLAMF7 expression on plasma cells in the CNS compared to the spleen at steady state (Fig. 34A, B). This factor may be increased in the CNS during EAE, which would explain why mature plasma cells in the CNS decrease their SLAMF7 expression during EAE compared to steady state (Fig. 34A). This unknown factor must be B/plasma cell specific since other cell types (ie. CD8⁺ T cells) increase SLAMF7 expression during EAE. Supporting the theory that this factor must be CNS-specific comes from the fact that in the spleen, plasma cells increase SLAMF7 expression during EAE (Fig. 34B); however, more research is certainly warranted regarding the identity of this unknown factor.

That our large, unbiased phenotyping panels detected changes in B cells in SLAMF7^{-/-} mice during EAE over other cell types, provides strong evidence that B cells are responsible for the increased susceptibility to EAE in SLAMF7^{-/-} mice. This is supported by our adoptive transfer studies and is particularly exciting considering how the new B cell depleting monoclonal

antibodies are changing the way we treat MS [294, 319]. How B cells contribute to MS pathogenesis is one of the most pressing questions in the MS field, and a number of theories have been proposed and studied, yet none has emerged as a unifying mechanism [5, 319]. Interestingly, there is also an FDA-approved therapy targeting SLAMF7, Elotuzumab [320]. Elotuzumab is approved for the treatment of multiple myeloma and functions primarily via antibody-dependent cellular cytotoxicity, but has also been shown to have SLAMF7 agonistic activity [321]. Considering our results in a pre-clinical model of MS, it would be interesting to see how a SLAMF7 agonist would perform in MS patients, especially in combination with other immuno-modulatory agents.

The discovery that microglia do not express SLAMF7 was unexpected considering most other myeloid subsets express SLAMF7. There are a number of possible explanations for this, one of which concerns the origin of microglia. Unlike other myeloid cells, microglia have a unique ontogeny, arising from the yolk sac during development [322, 323], which may play a role in the unique cellular programs present in microglia compared to other myeloid cells. Whether this effect is conserved for other SLAM receptors and potential functional consequences of this are interesting questions for future investigations. Additionally, recent work has shown that a subset of CNS-resident border-associated macrophages (BAMs) are yolk sac-derived [324, 325], yet BAMs express SLAMF7. If different subsets of BAMs, from differing ontogenies, differentially express SLAMF7 and other SLAM receptors, and what programs are responsible for this will be important questions to answer as we begin to define the roles of SLAM receptors across the CNS.

Acknowledgements

The data presented herein were obtained using instrumentation in the MSU Flow Cytometry Core Facility with support of Core staff. The facility is funded through user fees and the financial support of Michigan State University's Office of Research & Innovation, College of Osteopathic Medicine, and College of Human Medicine. PO was supported by the John A. Penner Endowed Research Fellowship. Funding provided by the Osteopathic Heritage Foundation Endowed Chair (A.A.). We thank Dr. A.J. Robison for advice and assistance performing confocal microscopy.

Author Contributions

P.O. and Y.A.A. conceived the project. P.O. and Y.A.A. designed experiments. P.O., M.K.B., and Y.A.A. performed all experiments. S.G. managed all mouse work. P.O. analyzed data. P.O. wrote the manuscript, with input and revisions from all authors. Y.A.A. and A.A. supervised the study and A.A. provided funding.

Conflicts of interest

The authors declare no conflicts of interest exist.

Materials and Methods

EAE model

All animal procedures were approved by the Michigan State University Institutional Animal Care and Use Committee (<http://iacuc.msu.edu/>). SLAMF7^{-/-} mice were generated as previously described [255]. On day -2, mice were injected with 33ug full-length recombinant murine MOG

(rmMOG₁₋₁₂₅) (Anaspec) with equal parts complete Freund's adjuvant (CFA) as previously described [326]. 400ng of pertussis toxin (MilliporeSigma) was injected intraperitoneally on days -2 and 0. Mice were scored daily on a scale of 0-5 as previously described [326], with a score of 0 = no symptoms, 1 = tail paresis, 2 = partial hindlimb paresis, 3 = complete hindlimb paresis, 4 = complete hindlimb paresis and front limb involvement, 5 = moribund or dead. Mice were humanely euthanized if a score of 4 or 5 was reached. Investigators were blinded to genotypes of mice during the 1st experiment comparing WT and SLAMF7^{-/-} mice (presented in Fig. 30). The WT mice used in experiments depicted in (Fig. 30A, B) were from a combined experiment, the remainder of which is available elsewhere (O'Connell, P., et al. *Under review*).

Adoptive transfer study

Splenocytes were collected from WT and SLAMF7^{-/-} mice as previously described [124]. B cells were isolated per manufacturer's guidelines using the murine B cell isolation kit (Miltenyi Biotec) and injected I.V. retro-orbitally (2×10^7 cells) into μ MT mice (The Jackson Laboratory). Five days after transfer, EAE was induced in mice with rmMOG₁₋₁₂₅ as described above.

CNS immune cell isolation

Mice were anesthetized and trans-cardiac perfusion with 15-20mL of sterile PBS was performed. Brains were then removed, placed in ice-cold 1X HBSS and minced using a scalpel. Brains were digested using a digestion cocktail for 45 minutes at 37°C as previously described [327]. Samples were then homogenized with a dounce homogenizer and the digestion reaction was stopped using EDTA and 1X HBSS containing 10% FBS. The lysate was then subjected to

gradient centrifugation using Percoll as previously described [328]. Isolated immune cells were resuspended in FACS buffer and stained for spectral cytometry. For experiments involving in vivo circulating immune cell labeling, before trans-cardiac perfusion, 5mg of anti-CD45 SparkBlue 550 antibody was injected trans-cardiac through the left ventricle and allowed to circulate for three minutes. The mouse was then trans-cardiac perfused with PBS as described above.

Spectral cytometry

Cells were isolated from the CNS and spleen as previously described [31]. Cells were stained with various antibodies (Supplementary table 6) utilizing BD Brilliant Stain Buffer (50uL per sample) whenever multiple Brilliant dyes were used in combination. Viability staining was performed with Zombie NIR (BioLegend) and Fc receptors were blocked with murine Fc block (BD Biosciences). Samples were acquired on a 5 laser Cytex Aurora Spectral Cytometer and data was analyzed using FlowJo version 10.6.1 (Tree Star) and the R computing environment. High dimensional single-cell spectral cytometry was performed in R. The CATALYST package was used to perform all analyses with a cell annotation and dimensionality reduction approach as previously described (O'Connell, et al., *under review*) [276]. After data clean up in FlowJo, files were exported as FCS files, loaded into R, and an arcsinh transformation of 6000 was applied to all spectral cytometry data. Unbiased clustering was performed with FlowSOM [223], and clusters were annotated and manually merged as necessary down to functionally distinct immune cell subsets.

For experiments using IL-10^{GFP} mice and/or in vivo labeling, IL-10-GFP⁺ and negative (and IV⁺ and negative) cells were combinatorially boolean gated in FlowJo allowing for absolute positive/negative discrimination in high dimensional analyses performed in R. In all analyses where IV labeling was performed, IV⁺ cells were removed before final generation of figures and statistical analysis. Additionally, high dimensional spectral cytometry analysis performed in (Fig. 30A, B) was done entirely in FlowJo employing an exhaustive manual gating scheme allowing identification of nearly all immune cells (Supplementary Fig. 12A), the accuracy of which was confirmed by unbiased FlowSOM clustering also performed in FlowJo (data not shown).

Confocal microscopy

EAE was induced in WT mice as described above and during the peak of EAE severity, mice were sacrificed and brain tissue was harvested. Mice were perfused with 10% formalin before collection of brain tissue which was stored in 10% formalin for approximately 24hrs before being transferred into a 30% sucrose solution for approximately 72hrs. Brains were sectioned at 4 μ m on a cryotome. Tissue was blocked with 3% normal donkey serum and 0.3% Triton X for 40min at 4°C. Primary staining with anti-SLAMF7 (1:500) and anti-Iba1 (1:1000) was performed over night at 4°C in buffer containing 3% normal donkey serum and 0.3% Tween-20. Sections were washed with PBST and PBS before secondary staining with Alexa 555 anti-rabbit (1:1000) and Alexa 488 anti-goat (1:1000) at room temperature for 5.5hrs. Sections were rinsed in PBS, mounted on slides, and counter stained with DAPI using ProLong Gold antifade reagent (Invitrogen). Sections were imaged with an Olympus FluoView 1000 CSLM.

Multiplex cytokine/chemokine analysis

Mouse 23-analyte multiplex-based assay was used to determine cytokine/chemokine concentrations via Luminex 100 per manufacturer's protocol (Bio-Rad), as previously described using a 1:4 dilution of plasma [27, 112].

In vitro B cell stimulation

Splenic B cells were isolated from WT mice as described above. B cells were plated at 3×10^5 cells/well for 10hrs. SLAMF7 cross-linking was performed by coating plates with $6 \mu\text{g/mL}$ of anti-SLAMF7 mAb (clone: 4G2) (Biolegend) as previously described [27, 255]. Cells were analyzed by spectral cytometry for expression of B220 and IgD as a proxy for B cell maturation status.

Statistical analysis

Statistical analyses are listed in all figure legends and were performed in either GraphPad Prism V8 or the R computing environment. Cell subset frequency comparisons and differential marker expression on cell subsets from experiments employing high dimensional spectral cytometry were statistically compared with a GLMM implemented through the diffcyt R package [286]. All heatmaps were locally scaled.

Data and code availability

All raw data is available upon reasonable request. Analysis code can be found at:

https://github.com/poconnel3/OConnell_et_al_SLAMF7_EAE_paper_code.

CHAPTER: 7 Absence of ERAP1 in B cells increases susceptibility to CNS autoimmunity, alters B cell biology, and mechanistically explains genetic associations between ERAP1 and Multiple Sclerosis

Authors: Patrick O'Connell, Maja K. Blake, Sarah Godbehere, Andrea Amalfitano, Yasser A. Aldhamen

Abstract

Hundreds of genes have been linked to Multiple Sclerosis (MS), yet the underlying mechanisms behind these associations have only been investigated in a fraction of cases. One such gene is *ERAP1*, an endoplasmic reticulum-localized aminopeptidase with important roles in trimming peptides destined for MHC-I and regulation of innate immune responses. As such, genetic polymorphisms in *ERAP1* have been linked to multiple autoimmune diseases including MS. Here, we present the first mechanistic studies performed to uncover why polymorphisms in *ERAP1* are associated with increased susceptibility to MS. Combining multiple mouse models of CNS autoimmunity (EAE) with high dimensional single-cell spectral cytometry, adoptive transfer studies, and integrative analysis of human single-cell RNA-seq datasets, we identify an intrinsic defect in B cells as being primarily responsible for ERAP1-mediated EAE susceptibility. Not only are mice lacking ERAP1 more susceptible to CNS autoimmunity, but adoptive transfer of B cells lacking ERAP1 into B cell-deficient mice recapitulates this susceptibility. We find B cells lacking ERAP1 display decreased proliferative capacities in vivo, while expressing higher levels of activation/co-stimulatory markers, yet produce equivalent levels of IL-10 compared to WT B cells. Through our studies using IL-10-GFP mice to study ERAP1's ability to modulate IL-10 production from various immune cell subsets, we also generated the first murine protein-level map of the CNS IL-10⁺ immune compartment at steady state and during neuroinflammation. Integrative analysis of scRNA-seq of human B cells from 36 individuals revealed subset-conserved differences in gene expression and pathway activation in individuals harboring the MS-linked K528R *ERAP1* SNP. Together, these studies identify a novel role for ERAP1 in the

modulation of B cells and highlight this as one reason why polymorphisms in this gene are linked to MS.

Introduction

Nearly 2.5 million people are living with Multiple Sclerosis (MS) worldwide, and despite new therapies for MS, the chronic neuroinflammatory disease remains incurable and severely debilitating for many [329, 330]. Known risk factors for MS include both genetic and non-genetic components, with the role of innate inflammation becoming ever more important [289, 329, 331]. Various immune cells contribute to disease pathogenesis with characteristic brain lesions containing: monocytes, CD4⁺ T cells, CD8⁺ T cells, and B cells, amongst others [297, 332]. Therapies targeting the immune response in MS patients have been developed to modulate inflammatory signals and include interferon-beta [292] and specific immune cell targeting monoclonal antibodies [293]. More recently, B cells have been targeted for depletion, revealing them as a critical driver of MS [294]. Despite great clinical benefit, these therapies are not effective for disease prevention or reducing lesions, especially in more severe MS subtypes, as well can result in significant immune-suppressive side-effects, highlighting the need to better understand mechanisms underlying MS pathogenesis.

Early studies of monozygotic twins revealed that approximately 30% of all MS risk can be attributed to genetics [333], with subsequent genome-wide association studies identifying over 500 genetic regions highly linked to MS [4, 116]. Interestingly, one specific single nucleotide polymorphism (SNP) located within an important immune regulatory gene, *ERAP1*, has been

linked with MS in large genome-wide association studies [4, 334]. Endoplasmic reticulum aminopeptidase 1 (ERAP1) is a ubiquitously expressed protein located in the ER which trims peptides prior to loading onto MHC-I molecules, which are then presented on the cell surface for antigen identification [335]. Given these roles, it is not surprising that ERAP1 plays an important role in adaptive immunity; however, it is also a well-known mediator of the innate immune responses [129, 130]. ERAP1 also plays a pivotal role in TLR regulation [129, 130], and may be involved with the NLRP3 inflammasome as well (Blake, M.K., et al. *In Preparation*) [130]. Critically, it has been shown that mice lacking ERAP1 spontaneously develop an autoimmune disease phenotype similar to that of Ankylosing Spondylitis, which various ERAP1 SNPs are also genetically linked to [131].

Here, we investigated the mechanistic underpinnings of the genetic association of ERAP1 with MS which was accomplished using the well-studied experimental autoimmune encephalomyelitis (EAE) mouse model of CNS autoimmunity [132]. We discovered that ERAP1^{-/-} mice had exaggerated EAE severity and that this was partly B cell dependent. We also found that B cells lacking ERAP1 exhibit impaired proliferation in vivo, express higher levels of multiple activation markers, and have a specific deficit in the B1 cell compartment across the CNS and spleen. Correlating with these findings, integrated analysis of human B cells from multiple scRNA-seq datasets containing 36 individuals revealed that B cells containing the MS-linked K528R ERAP1 SNP exhibit over-activation of eIF2 signaling. Finally, we also present the first single-cell protein-level reference map of the murine CNS resident IL-10⁺ immune compartment, and uncover ERAP1-specific modulations of the same. Together, our results link

the genetic association between ERAP1 and MS to an intrinsic effect on B cells, uncovering a novel immuno-modulatory role for ERAP1.

Results

ERAP1^{-/-} mice have increased neuroinflammation and an altered CNS immune landscape following EAE induction.

While polymorphisms in the ERAP1 gene in humans have been linked to MS, no studies have been performed to date examining if mice lacking ERAP1 are differentially susceptible to MOG-induced EAE (a well-established model for inducing CNS autoimmunity in mice [132]). WT and ERAP1^{-/-} mice had EAE induced with rmMOG₁₋₁₂₅. We found that ERAP1^{-/-} mice were significantly more susceptible to EAE compared to WT mice (Fig. 35A), suggesting that ERAP1 function is important in regulating CNS autoimmunity. We next profiled of the CNS immune compartment via high dimensional spectral cytometry. We utilized a panel capable of identifying all CNS immune cell subsets and compared the CNS immune landscape of WT and ERAP1^{-/-} mice during active EAE (Fig. 35B and Supplemental Fig. 15A). We found our panel capable of identifying all known CNS resident immune cell subsets, comparable to a previously published reference map [193], with the CNS being dominated by microglia, and significant lymphoid and myeloid cell infiltrates, indicative of active neuroinflammation (Fig. 35B). Comparison of immune cell subset frequencies between WT and ERAP1^{-/-} mice revealed decreased border-associated macrophages (BAMs), increased NK cells, and increased myeloid-derived cells (MdCs) in the ERAP1^{-/-} CNS (Fig. 35C). We also found that ERAP1^{-/-} mice had increased total numbers of: B cells, BAMs, CD4⁺ T cells, Ly6C⁺ monocytes, NK cells, NKT cells,

and MdCs (Fig. 35D); correlating with exaggerated EAE clinical symptoms in ERAP1^{-/-} mice.

Interestingly, we observed strong increases in the expression of Tim3 on multiple CNS myeloid

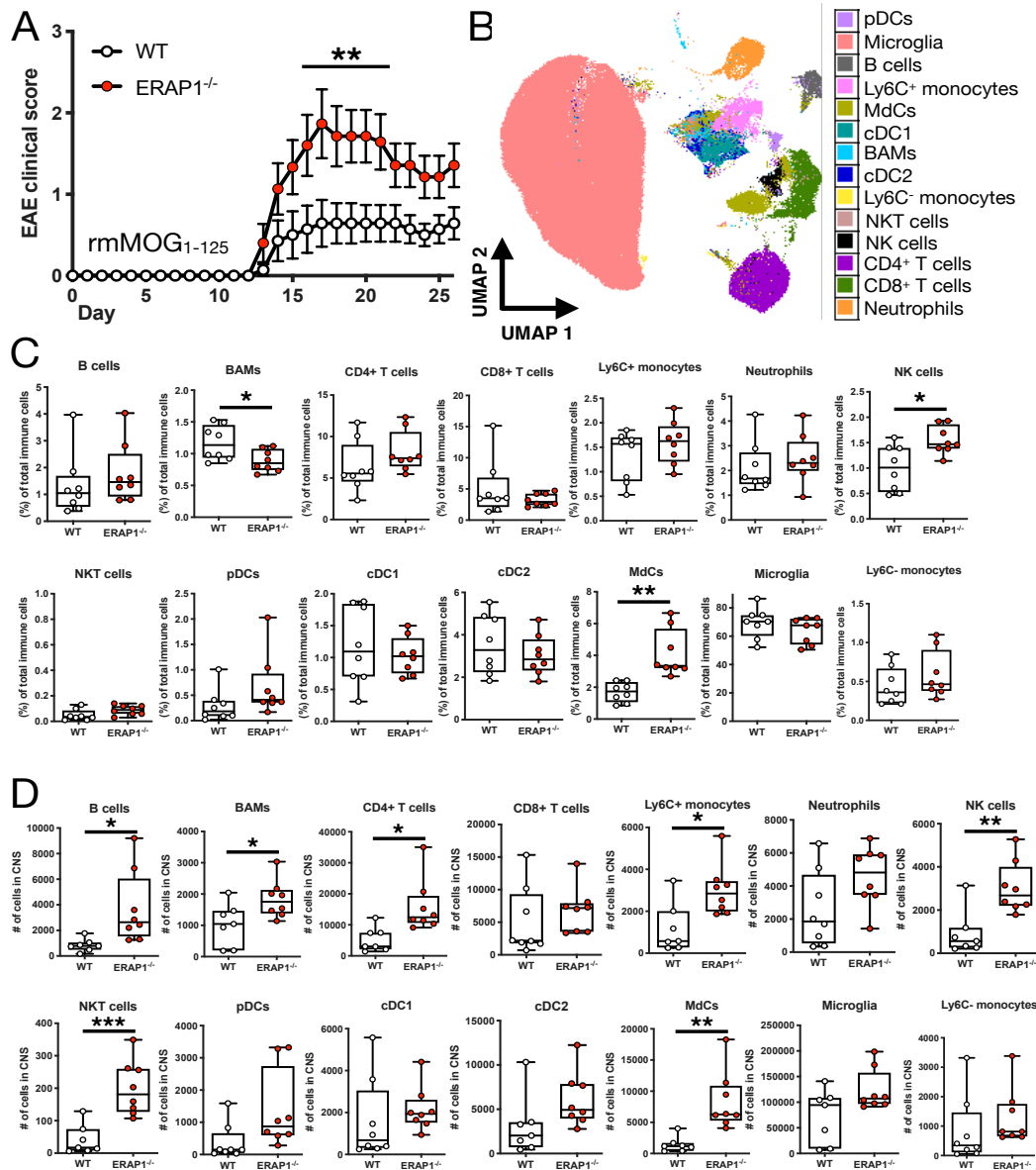


FIGURE 35: ERAP1^{-/-} mice are more susceptible to EAE and exhibit alterations in the CNS immune landscape.

(A) Clinical scores of WT and ERAP1^{-/-} mice subjected to EAE induced with rmMOG₁₋₁₂₅. (B) UMAP projection of the entire CNS immune landscape in WT and ERAP1^{-/-} mice subjected to EAE. The complete CNS immune landscape was assessed via high dimensional single-cell spectral cytometry. (C) Frequency of all CNS immune cell subsets from (B) between WT and ERAP1^{-/-} mice. (D) Total number of various immune cell subsets in the CNS of WT and ERAP1^{-/-} mice subjected to EAE. Groups in (A) compared with a two-way ANOVA with Tukey's multiple comparison test, displayed with mean ± SEM, and representative of two independent experiments showing similar results. Groups in (B, C) compared with unpaired two-way t-test and representative of two independent experiments showing similar results. *p<0.05, **p<0.01, ***p<0.001.

cell types, suggesting that ERAP1 may be able to modulate this emerging myeloid cell modulatory receptor (Supplementary Fig. 16A-D) [336-338]. Together these results imply the association of ERAP1 with MS is conserved in mice and that mice lacking ERAP 1 exhibit enhanced neuroinflammation.

Exhaustive profiling of the resident CNS IL-10 immune compartment.

We previously published that mice lacking ERAP1 have decreased numbers of an important regulatory immune cell type (Tr1 cells), known to modulate immunity via production of IL-10 [131, 339, 340]. Since IL-10 is known to play an important role in MS/EAE pathogenesis [301-304], we examined IL-10 expressing cells in our EAE model. First, however, we combined our high dimensional single-cell spectral cytometry approach with IL-10-GFP mice [307], in order to generate a reference map of the CNS IL-10 immune compartment at steady state and during EAE. In addition to accurate detection of IL-10⁺ cells using our reporter mouse, we employ *in vivo* cell labeling to discriminate bona fide resident from circulating immune cells (Fig. 36A, B). We first generated a reference map of all CNS immune cell subsets at steady state and during EAE, where cells are colored by FlowSOM-defined clusters (Fig. 36C). These cell subsets express markers as typically expected (Fig. 36D). The importance of IV labeling to discriminate resident from circulating cells can be appreciated when examining the fraction of each cell cluster staining IV⁺ at steady state (Fig. 36E, and Supplemental Fig. 17A) and during EAE (Fig. 36F); non-resident cells were removed from downstream analysis. We found very few cells making IL-10 at steady state (Fig. 36G, and Supplemental Fig. 17B), but during active EAE one can appreciate a considerable portion of CD4⁺ T cells now making IL-10 (Fig. 36H). By restricting our analysis to

just IL-10⁺ cells, we find that at steady state in WT mice, microglia are the primary cell type responsible for IL-10 production (Fig. 36I). In contrast, during EAE, CD4⁺ T cells dominate the

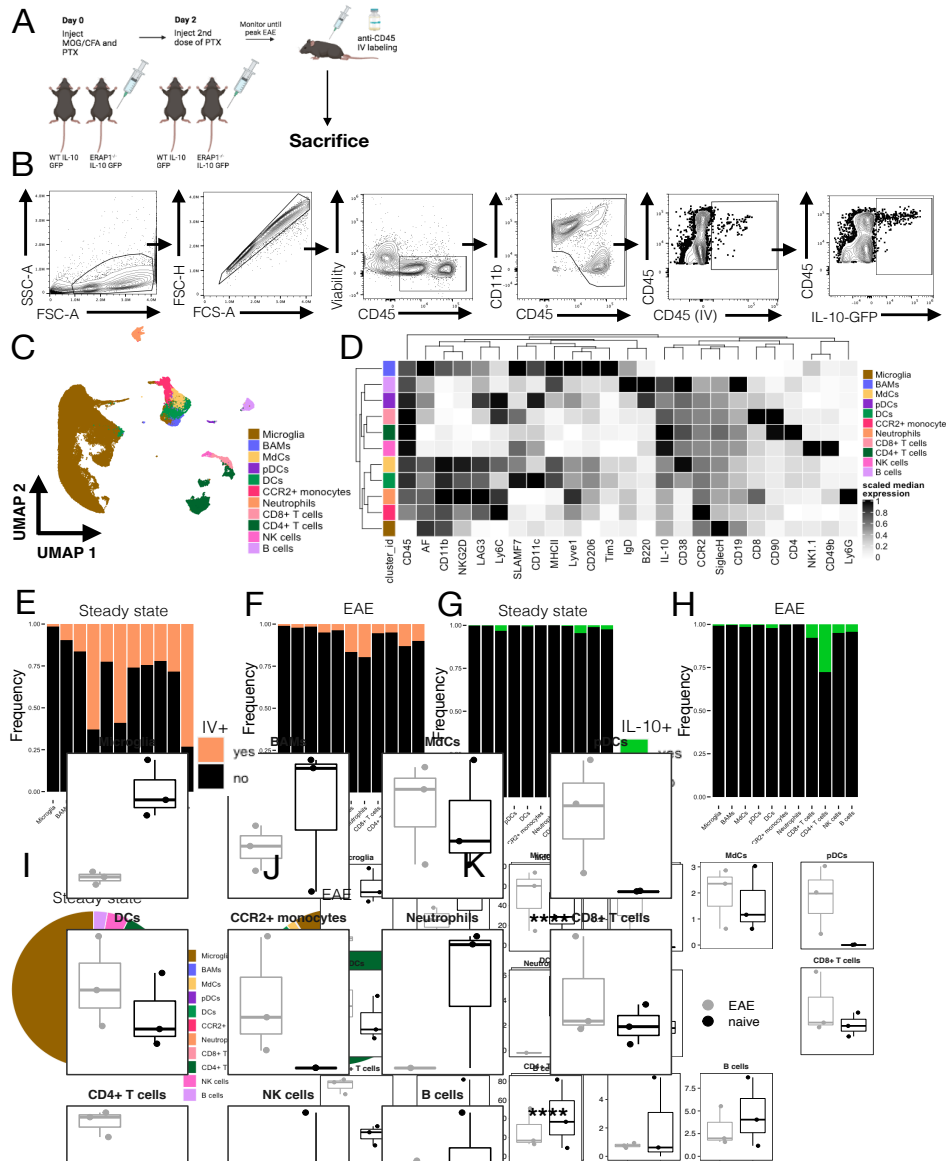


FIGURE 36: Single-cell profiling of the CNS resident IL-10⁺ immune compartment.

(A) Graphical overview of experimental design. (B) CNS immune cell gating scheme. All combinations of IV⁺/IV⁻ and IL-10⁺/IL-10⁻ were boolean gated and exported for high dimensional analysis. (C) UMAP projection of the entire CNS immune cell landscape from WT mice at steady state and with EAE, where cells are colored according to FlowSOM-defined clusters. (D) Heatmap of marker expression from all clusters in (C). (E, F) Frequency of non-resident (IV⁺) immune cells across various subsets in WT mice at steady state (E) and during EAE (F). (G, H) Frequency of IL-10⁺ cells across various immune subsets in WT mice at steady state (G) and during EAE (H). (I, J) Contributions of various IL-10⁺ immune cells subsets to the entire CNS resident IL-10⁺ immune compartment for WT mice at steady state (I) and during EAE (J). (K) Changes in contributions to the CNS resident IL-10⁺ compartment between steady state and EAE in WT mice. Groups in (K) compared with a GLMM. Results in (B-K) representative of a single experiment. **** $p < 0.0001$. AF: autofluorescence.

CNS IL-10⁺ compartment (Fig. 36J, K).

Comparison of CNS immune cell states and IL-10 production between WT and ERAP1^{-/-} mice.

We next compared the CNS immune landscape of WT/IL-10^{GFP} and ERAP1^{-/-}/IL-10^{GFP} mice at steady state and during MOG-induced EAE. Global dimension reduction with MDS reveals samples clustering by disease status across the first MDS dimension and by genotype across the second MDS dimension (Fig. 37A). Comparing the composition of the CNS resident compartment at steady state, we find that while microglia make up about 80% of IL-10⁺ cells in WT mice, and in ERAP1^{-/-} mice there are significantly less IL-10⁺ microglia and more CD4⁺ T cells (Fig. 37B). We also find there are significantly less total IL-10⁺ cells in the ERAP1^{-/-} CNS at steady state (Fig. 37C). Interestingly, during EAE, the CNS resident IL-10 compartment of WT and ERAP1^{-/-} mice is equivalent (Fig. 37D), as are total numbers of CNS IL-10⁺ cells (Fig. 37E). These findings may point to the potential for ERAP1 to be important in early processes controlling the development of CNS autoimmunity, and not during later stages. We next compared all significantly differentially expressed markers across all CNS immune subsets between WT and ERAP1^{-/-} mice at steady state (Fig. 37F) and during EAE (Fig. 37G). We found decreased

expression of CD90 of multiple lymphoid cell types in ERAP1^{-/-} mice at steady state (Fig. 37F) and decreased CD90 on multiple myeloid subsets in ERAP1^{-/-} during EAE (Fig. 37G).

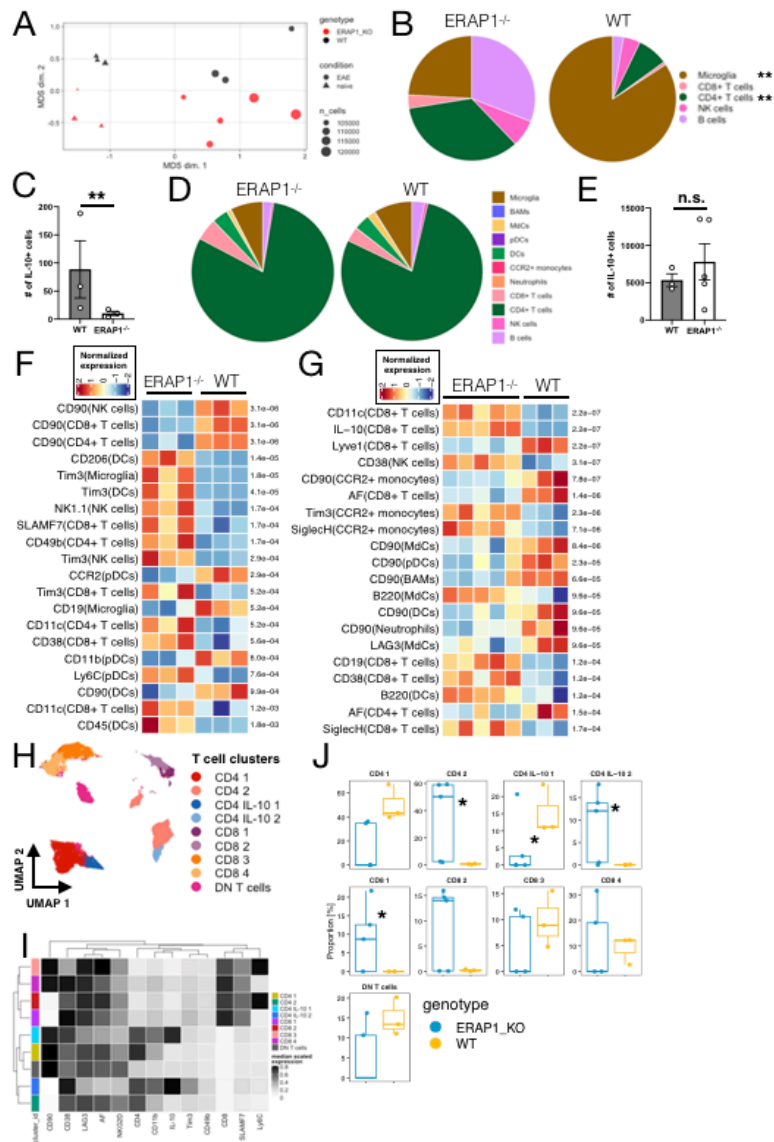


FIGURE 37: In depth comparison of resident CNS immune cell states and IL-10 production between WT and ERAP1^{-/-} mice.

(A) MDS plot of CNS immune cells from WT and ERAP1^{-/-} mice at steady state and during EAE. (B) Comparison of the CNS resident IL-10⁺ immune cell compartment between WT and ERAP1^{-/-} mice at steady state. (C) Number of total IL-10⁺ immune cells in the CNS of WT and ERAP1^{-/-} mice at steady state. (D) Comparison of the CNS resident IL-10⁺ immune cell compartment between WT and ERAP1^{-/-} mice during EAE. (E) Number of total IL-10⁺ immune cells in the CNS of WT and ERAP1^{-/-} mice during EAE. (F, G) Heatmap of all statistically significant (FDR<0.05) differentially expressed markers between WT and ERAP1^{-/-} mice at steady state (F) and during EAE (G). Adjusted p-values are listed next to each row. (H) UMAP of resident CNS T cell subsets colored by FlowSOM-defined clusters. (I) Marker expression on clusters from (H). (J) T cell subset frequency differences between WT and ERAP1^{-/-} mice during EAE. Groups in (B, D, J) compared with a GLMM. Groups in (C, E) compared with an unpaired two-way t-test. Differentially expressed markers shown in (F, G) determined via a GLMM. Results in (A-K) representative of a single experiment. *p<0.05, **p<0.01, n.s. not

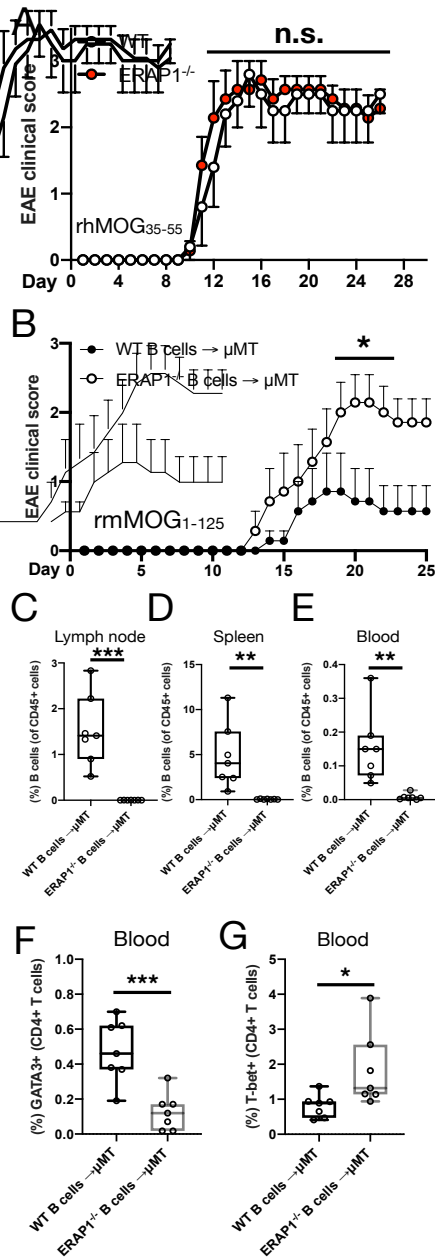


FIGURE 38: Loss of ERAP1 in B cells renders mice more susceptible to EAE.

(A) Clinical scores of WT and ERAP1^{-/-} mice subjected to EAE induced with rhMOG₃₅₋₅₅. (B) Clinical scores of μMT mice reconstituted with 1x10¹⁰ of WT or ERAP1^{-/-} B cells five days before EAE induction with rmMOG₁₋₁₂₅. (C-E) Percent adoptively transferred B cells of total CD45⁺ cells from mice in (B) in the inguinal lymph nodes (C), spleen (D), and blood (E). (F) Percent GATA3⁺ CD4⁺ T cells (Th2 cells) in the blood of mice from (B). (G) Percent Tbet⁺ CD4⁺ T cells (Th1 cells) in the blood of mice from (B). Groups in (A, B) compared with a two-way ANOVA with Tukey's multiple comparison test, displayed with mean ± SEM, and representative of two independent experiments showing similar results. Groups in [A] compared with an unpaired two-way t-test and are representative of two independent experiments showing similar results.

Increases in Tim3 across myeloid cell subsets in ERAP1^{-/-} mice are again observed, both at steady state (Fig. 37F) and during EAE (Fig. 37G). We also observe alterations in CD8⁺ T cell

phenotypes, with ERAP1^{-/-} CD8⁺ T cells expressing more SLAMF7 [255], more CD38 [255], more CD11c [341], and more IL-10 (Fig. 37F, G).

Due to the important role of various T cell subsets in MS/EAE, we narrowed our analysis to T cells and performed sub-clustering to investigate these cells on a more granular level. We identified nine T cell subsets (Fig. 37H and Supplemental Fig. 18A) including two IL-10⁺ CD4⁺ T cell subsets (Fig. 37H, I and Supplemental Fig. 18B). While none of these IL-10⁺ CD4⁺ T cell subsets displayed characteristic Tr1 cell markers [340] (data not shown), they were generally separable by their expression of CD90 (Fig. 37I). We found that during EAE, ERAP1^{-/-} mice lack the CD90⁺IL-10⁺CD4⁺ T cell subset compared to WT mice and show significant changes in other T cell subsets (Fig. 37J). Altogether, these results identify important differences in the CNS immune compartment in mice lacking ERAP1, but do not reveal a defect in Tr1 cells per se. This implies that mechanisms underpinning the susceptibility of ERAP1^{-/-} mice to EAE, as well as AS, may not be primarily due to intrinsic defects in Tr1 cells [131].

ERAP1^{-/-} susceptibility to EAE is B cell-dependent.

In an effort to better identify the specific, non-Tr1 cells that may be mediating EAE susceptibility in ERAP1^{-/-} mice, we also induced EAE in WT and ERAP1^{-/-} mice using the rhMOG₃₅₋₅₅ peptide, known to induce a CD4⁺ T cell-dependent, B cell-independent form of EAE [132, 308]. Surprisingly, we observed identical EAE susceptibility using this antigen (Fig. 38A). This result, combined with the fact that EAE induced with rmMOG₁₋₁₂₅ protein is known to be B cell-dependent [308-311], led us to hypothesize that an intrinsic defect in ERAP1^{-/-} B cells may be

responsible for their increased susceptibility to EAE. To test this we adoptively transferred WT or ERAP1^{-/-} B cells into mice genetically deficient in B cells (μ MT mice [342]), confirmed equivalent transfer of cells (Supplemental Fig. 19A), and then induced EAE with rmMOG₁₋₁₂₅. Indeed, mice receiving ERAP1^{-/-} B cells were significantly more susceptible to EAE compared to mice receiving WT B cells, confirming this intrinsic defect in ERAP1^{-/-} B cells (Fig. 38B).

During the late phase of EAE in these mice (day 38 post-EAE induction) we profiled the inguinal lymph nodes, spleen, and blood to assess B cell reconstitution and T cell phenotypes.

Interestingly, we found that while WT B cells reconstituted the spleen and lymph nodes effectively (and to a lesser extent the peripheral blood), ERAP1^{-/-} B cells were absent from all three locations (Fig. 38C-E). The observed decreases in B cells were not due to NK cell-mediated killing (Supplemental Fig. 19B). Assessing T cell phenotypes in the peripheral blood, mice reconstituted with ERAP1^{-/-} B cells showed a skewing of CD4⁺ T cells away from GATA3⁺ Th2 cells towards Tbet⁺ proinflammatory Th1 cells (Fig. 38F, G), consistent with their more severe EAE phenotype [343, 344]. Looking to other CD4⁺ T cell subsets important in EAE/MS pathogenesis (Th17 and Treg) we did not find any significant changes (Supplementary Fig. 19C-E). Together, these findings not only point to an ERAP1-mediated dysfunction in B cells as responsible for the EAE phenotype we originally observed in MOG protein treated ERAP1^{-/-} mice, but identify a further defect in the ability of ERAP1^{-/-} B cells to reconstitute secondary lymphoid organs and a potential for them to bias CD4⁺ T cell polarization.

Deep phenotyping of B cells during EAE reveal increased activation and specific decreases in B1 B cells in ERAP1^{-/-} mice.

To better understand how ERAP1 modulates B cells, we designed an exhaustive B cell phenotyping panel to allow us to comprehensively profile all B cell subsets across the spleen and CNS. In the spleens of WT and ERAP1^{-/-} mice at peak EAE, we identified 12 different B and plasma cell subsets via unbiased FlowSOM clustering (Fig. 39A), all expressing expected markers (Fig. 39B). Notably, using mice on an IL-10-GFP background allowed measurement of IL-10 across all B cell subsets, however, the distinct regulatory B cell [Breg] subset (CD1d⁺CD5⁺) we identified was clustered independently of IL-10 expression (Fig. 39A, B). We also used the same panel to profile the CNS B cell compartment of the same mice, revealing many of the same B cell subsets, except for the absence of follicular B cells, and the discovery of an undetermined subset (Fig. 39C, D). As these undetermined cells are IgD⁺B220⁺CD21⁻CD23⁻, make up the majority of B cells in the CNS, and since it has been shown previously that most CNS B cells are class-switched memory B cells [345], this unknown population likely represents these cells. Comparison of the frequency of B cell subsets across the spleen and CNS in WT mice revealed compartment-specific differences in follicular, undetermined, B1b, and marginal zone subsets (Fig. 39E). Comparing the frequency of splenic B cell subsets between WT and ERAP1^{-/-} mice during EAE, we found significant decreases in both B1 cell subsets, and a minor decrease in

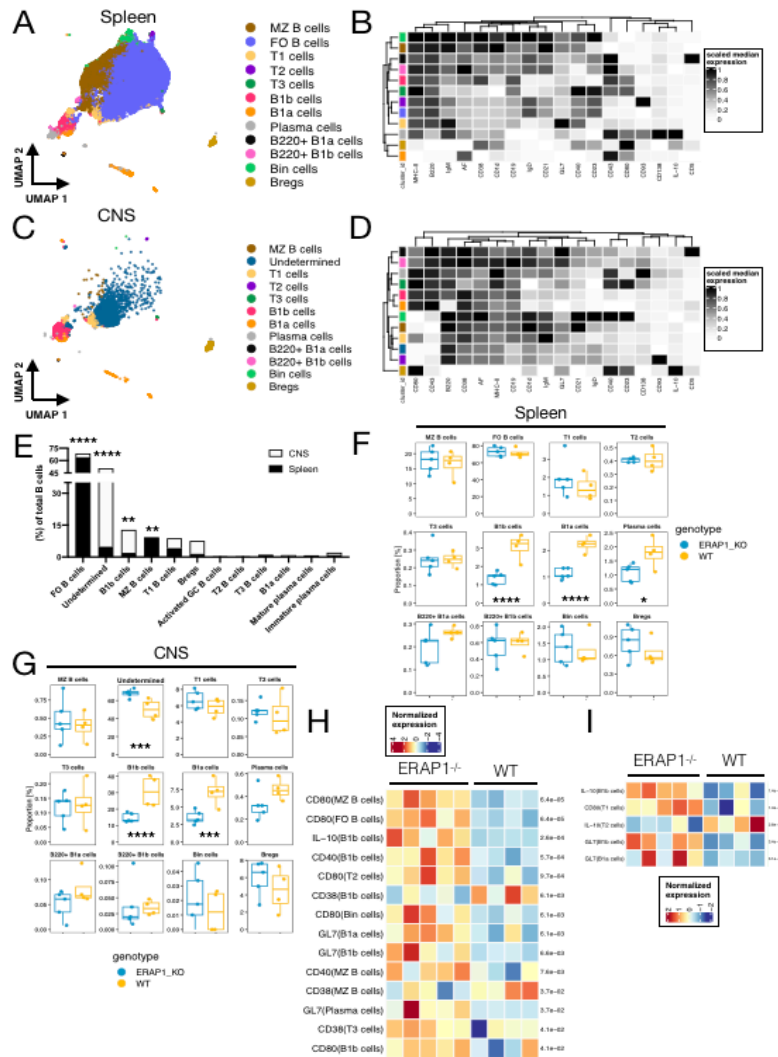


FIGURE 39: Reconstruction of the splenic and CNS B cell compartments during EAE reveal specific decreases in B1 cells and increased activation of ERAP1^{-/-} B cells.

(A) UMAP projection of all splenic B cells from WT mice during EAE with cells colored by FlowSOM-defined clusters. (B) B cell subset marker expression in cells from (A). (C) UMAP projection of all CNS B cells from WT mice during EAE with cells colored by FlowSOM-defined clusters. (D) B cell subset marker expression in cells from (C). (E) Comparison of B cell subset frequency across the spleen and CNS during EAE in WT mice. (F) Frequency of all immune cell subsets in the spleen of WT and ERAP1^{-/-} mice during EAE. (G) Frequency of all immune cell subsets in the CNS of WT and ERAP1^{-/-} mice during EAE. (H) Heatmap of all statistically significant (FDR<0.05) differentially expressed markers on splenic B cells during EAE between WT and ERAP1^{-/-} mice. (I) Heatmap of all statistically significant (FDR<0.05) differentially expressed markers on CNS B cells during EAE between WT and ERAP1^{-/-} mice. Groups in (E) compared with a two-way ANOVA with Sidak's multiple comparison test and representative of a single experiment. Groups in (F-G) compared with a GLMM and are representative of a single experiment. Differentially expressed markers shown in (H, I) determined via a GLMM. *p<0.05, ***p<0.001, ****p<0.0001, n.s. not significant. FO: follicular, MZ: marginal zone, Bin: B cells in inflamed nodes, Bregs: regulatory B cells.

plasma cells (Fig. 39F). Similarly, in the CNS we also found decreases in both B1 cell subsets in ERAP1^{-/-} mice (Fig. 39G). Comparison of differentially expressed markers across all B cell subsets

in the spleen uncovered higher expression of activation markers such as CD80, CD40, and GL7 on numerous ERAP1^{-/-} B cell subsets (Fig. 39H). This was also observed in the CNS, but to a lesser extent (Fig. 39I). Together, this demonstrates that a lack of ERAP1 expression in B cells results in excessive B cell activation and a specific decrease in the innate-like B1 cell subsets during EAE.

Lack of ERAP1 in B cells leads to reduced proliferation in vivo and lack of B cell engraftment during EAE.

B cells are known to have different roles in the modulation of EAE during different stages of the disease [140, 346]. Therefore, to help explain why μ MT mice receiving ERAP1^{-/-} B cells showed increased susceptibility to EAE, and to help identify why ERAP1^{-/-} B cells could not be detected in these animals, we developed a unique in vivo assay (Fig. 40A). Here, we differentially labeled WT and ERAP1^{-/-} B cells with CFSE and CellTrace Violet, mixed them in a 1:1 ratio, adoptively transferred them into μ MT mice, induced EAE with rmMOG₁₋₁₂₅, and monitored B cell survival and proliferation at various timepoints during the EAE disease course (Fig. 40A). We found minor increases in the ratio of WT:ERAP1^{-/-} B cells at day 2, with larger, more significant increases on day 5, 10, and especially day 20, reflecting a higher survival rate for WT B cells relative to ERAP1^{-/-} B cells in mice experiencing EAE (Fig. 40B and Supplemental Fig. 20A). By day 20, a consistent two-fold increase in the ratio of WT:ERAP1^{-/-} B cells was evident across multiple environments, with very few ERAP1^{-/-} B cells present overall (Fig. 40B). We found that the decreases in the numbers of ERAP1^{-/-} B cells only occurred in mice with EAE, and did not occur when ERAP1^{-/-} B cells were transferred into μ MT mice that did not have EAE (Fig. 40C-E).

Finally, since we labeled our cells with commonly used proliferation dyes, we were able to assess B cell proliferation in vivo. We found equivalent levels of WT and ERAP1^{-/-} B cell

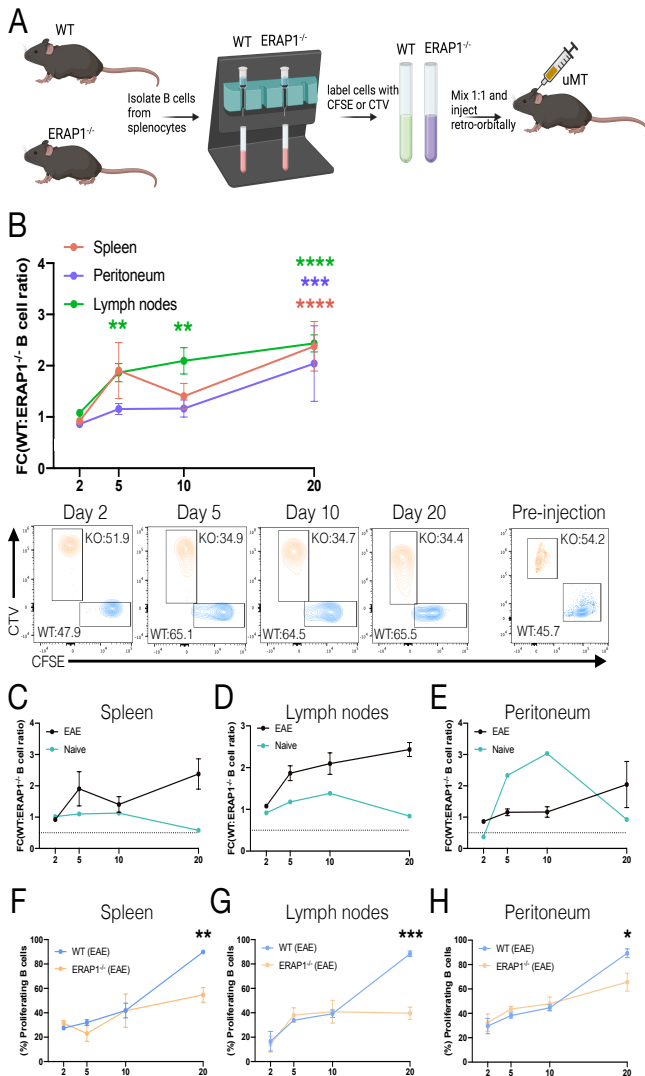


FIGURE 40: ERAP1^{-/-} B cells display impaired proliferation in vivo during EAE.

(A) Graphical overview of experimental design. (B) Top, Fold change in the ratio of WT to ERAP1^{-/-} B cells transferred into the same μ MT mouse and assessed across various lymphoid organs at multiple timepoints following induction of EAE with rmMOG₁₋₁₂₅. Bottom, representative FACS plots of differentially labeled WT and ERAP1^{-/-} B cells at various timepoints during EAE. (C-E) Fold change in the ratio of WT to ERAP1^{-/-} B cells transferred into the same μ MT mouse over time in mice subjected to EAE or left untreated. (F-H) Frequency of adoptively transferred B cells actively proliferating from the previous timepoint in mice subjected to EAE. Data in (B-H) representative of a single experiment with three mice analyzed per timepoint in the EAE group and one mouse per timepoint in the naive group. Groups in (B, F) compared with a two-way ANOVA with Sidak's multiple comparison test. Comparisons in (B) were performed by comparing the fold change from baseline between WT and ERAP1^{-/-} B cells. Groups in (G, H) compared with a mixed-effects analysis. *p<0.05, **p<0.01, ***p<0.001, ****p<0.0001.

proliferation across all locations up until day 10. By day 20, *ERAP1*^{-/-} B cells exhibited a significant reduction in the ability to proliferate compared to WT B cells across all locations (Fig. 40F-H). These findings suggest that B cells lacking *ERAP1* are not able to cope well in settings of prolonged immune activation, and that they reach a threshold at which point they can no longer proliferate and survive.

Human B cell subset dysregulation in individuals carrying the *ERAP1* K528R SNP.

While murine B cells completely lacking the *ERAP1* gene show considerable differences from their WT counterparts, in humans the presence of specific SNPs in *ERAP1* results in dysfunction of the protein and are linked to multiple autoimmune diseases [121, 334]. The most pathogenic of these, the K528R SNP, genetically associated with MS [4, 334], and shows the strongest associations with other autoimmune diseases [122, 347]. We have previously shown that the presence of this SNP also induces the strongest changes in immune cells and activation of the NLRP3 inflammasome compared to other *ERAP1* variants [130]. Therefore, we wanted to determine if human B cells carrying this pathogenic SNP exhibit dysregulated phenotypes. We accomplished this by sourcing data from multiple published scRNA-seq datasets. We collected data from PBMCs of 36 healthy individuals across six datasets encompassing a total of 24,795 B cells (see Materials and Methods) (Fig. 41A). Critically, using the raw sequencing data, we were able to determine which individuals carry the *ERAP1* K528R SNP, identifying seven out of the 36 individuals as having at least one copy of this SNP.

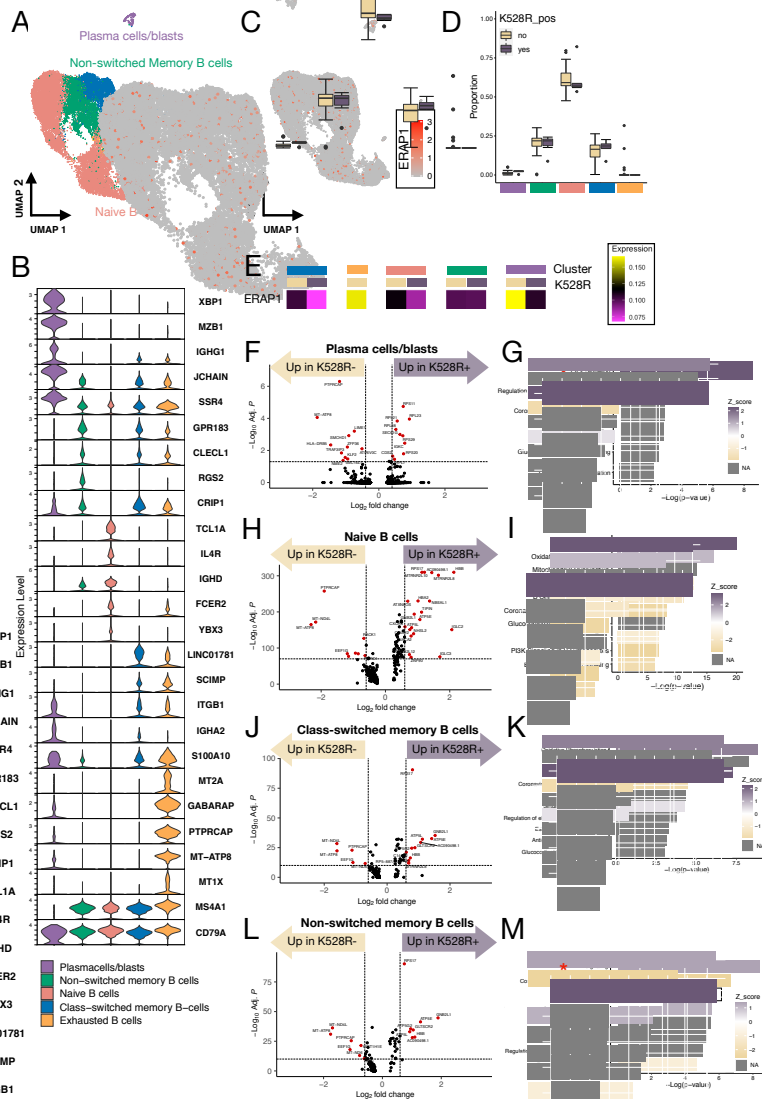


FIGURE 41: Integrated scRNA-seq analysis of human B cells reveal subset-conserved dysregulation in B cells carrying the K528R ERAP1 SNP.

(A) UMAP of plasma cells/blasts and B cell subsets from an integrated analysis of six healthy human scRNA-seq datasets incorporating 36 individual samples and 24,795 cells. Cells are colored based on cluster-level annotations obtained using SingleR. (B) Stacked violin plots of expression of cluster-defining markers. (C) UMAP of the expression of ERAP1 on B cell subsets revealing equal distribution across clusters. (D) Proportion of various B cell subsets in individuals based on the presence or absence of the K528R SNP. (E) Heatmap of ERAP1 expression on B cell subsets split by cells containing the K528R SNP or not. The exhausted B cell subset contains only cells without the K528R SNP. (F) Volcano plot of differentially expressed genes (DEGs) in plasma cells/blasts based on the presence of the K528R ERAP1 SNP. (G) IPA canonical pathway analysis using DEGs from (F) with bars colored based on whether the pathway is up- or down-regulated in cells with the K528R SNP. Gray bars indicate no pathway directionality data is available. (H, I) Same as (F, G), but for Naive B cells. (J, K) Same as (F, G), but for Class-switched memory B cells. Same as (F, G), but for non-switched memory B cells. Differential expression in (B, F, H, J, and L) performed with MAST.

Unbiased clustering (See Materials and Methods) identified five distinct B and plasma cell subsets (Fig. 41A) expressing numerous subset-defining genes (Fig. 41B). Each of the six studies

contributed evenly to these subsets with the exception of the "Exhausted B cell" subset which was almost entirely from Kang, H.M., et al. (Supplementary Fig. 21A-C) [348]. We found that B cells expressing high levels of ERAP1 were evenly distributed across all subsets (Fig. 41C) and that the proportion of each subset per individual did not differ based on the presence of the K528R SNP (Fig. 41D). However, individuals carrying K528R had decreased expression of ERAP1 in their naive B cells, class-switched memory B cells, and plasma cells/blasts (Fig. 41E). For each B cell subset we identified differentially expressed genes (DEGs) and pathways between cells with the K528R SNP and those without. We observed consistent findings across all cell subsets noting decreased expression of: *PTPRCAP*, *EEF1G*, *MT-ATP8*, and *MT-ND4L* (Fig. 41F, H, J, L), and increased expression of: numerous ribosomal protein genes, *ATP5E*, and *TIPIN* (Fig. 41F, H, J, L) in K528R containing B cells. Most interesting were the conserved pathways enriched in B cell subsets carrying the K528R SNP, most notably upregulation of eIF2 signaling and oxidative phosphorylation (Fig. 41G, I, K, M). These results suggest that the presence of the K528R *ERAP1* SNP in human B cells correlates with an up-regulation of ribosomal translation machinery and altered metabolism; both of which are known to affect immune cell function [349-351].

Discussion

Hundreds of genes have been linked to MS [4], yet we still understand little of the mechanisms underlying each of these associations. Through incremental discoveries of these mechanisms, we can hope to reveal conserved master pathogenesis archetypes responsible for MS, that can then be therapeutically targeted. To this end, we sought to understand the mechanism(s) linking SNPs in the *ERAP1* gene to MS. Identifying mechanisms underlying *ERAP1*'s link to MS is

significant as ERAP1 is linked to many other autoimmune diseases [121, 122]. An understanding of the relationship between ERAP1 and MS may also identify key commonalities across multiple human autoimmune diseases to which ERAP1 has also been linked, including: AS, Psoriatic Arthritis, and Behcet's disease.

Our finding that mice lacking ERAP1 are at increased susceptibility to a rodent form of autoimmune neuroinflammation that mirrors MS supports the link between human ERAP1 SNPs and susceptibility to MS. Specifically, since we and others have shown that these ERAP1 SNPs can drastically alter its enzymatic function to cause disruption of peptide trimming in the ER, resulting in loss of cell surface MHC I/antigen complexes, and impact global innate and adaptive immune responses [123-125, 130, 131].

In this study we confirm that lack of ERAP1 function leads to decreased numbers of IL-10⁺ immune cells at steady state [131]. Yet our finding that CNS levels of IL-10-producing CD4⁺ T cells remain unchanged in ERAP1^{-/-} mice is interesting and suggests that like our previous work showed [131], ERAP1 does modulate regulatory cells, but perhaps in a context-specific manner.

The localization of ERAP1's contribution to CNS autoimmunity via B cells links well with current theories regarding MS pathogenesis since B cell depleting monoclonal antibodies are now a mainstay of MS treatment [293]. Why depleting B cells leads to robust clinical responses in some MS patients is currently a heavily investigated topic, with a number of potential mechanisms postulated, including: B cell antigen presentation [319], B cell cytokine production

[5], B cell-mediated T cell co-stimulation [319], Epstein-Barr virus infection of B cells [352], and contributions from Bregs [319]. Importantly, B cell depletion therapies are far from a cure, and show limited efficacy in MS patients with more severe forms of MS such as primary progressive MS [8]. Accordingly, groups have been vigorously researching how B cells contribute to MS [5, 319], and if more targeted B cell therapies can achieve superior responses [319]. Our results show that B cells lacking ERAP1 have both exaggerated expression of T cell co-stimulatory/activation markers and fail to proliferate in vivo. Both of these may explain why mice lacking ERAP1 are more susceptible to EAE since increased B cell activation during the initiation phase of EAE and impaired B cell regulatory responses during the chronic phase of EAE are linked to more severe pathology [319]. Such findings tie in with the currently appreciated divergent roles for B cells during the pathogenesis of CNS autoimmunity, where B cells are capable of harboring both disease-inducing roles early on and protective roles later during the resolution phase [140, 346].

Intriguingly, mice lacking ERAP1 also have drastically reduced numbers of the innate-like B1 cell subsets. This effect is likely due to an intrinsic defect, but we cannot fully rule out an extrinsic one, such as NK cell-mediated depletion, however, our ex vivo studies argue against such a possibility. While B1 cells are understudied, they are known to be able to secrete auto-antibodies, function as APCs, secrete cytokines, and respond to pathogen infection in an innate manner [353]. They have also been linked to a number of autoimmune diseases including MS, however their precise role in the pathogenesis of MS is unclear, as B1 cells have been shown to have both protective and pathogenic roles in EAE depending on the stage of disease [354, 355].

If this lack of B1 cells contributes to diseases susceptibility in mice lacking ERAP1, or if it is just a consequence of ERAP1's ability to broadly dysregulate B cells, remains to be seen and is an interesting area of future investigation.

In a further effort to tie our B cell findings back to humans carrying the actual MS-linked ERAP1 SNP, we took advantage of publicly available scRNA-seq datasets and found well conserved transcriptional changes across multiple B cell subsets. A consistent decrease in the expression of *PTPRCAP* (CD45-associated protein [CD45-AP]) in B cells carrying the ERAP1 K528R SNP stood out. CD45-AP is an understudied protein known to interact with CD45 and modulate its behavior in a number of ways, but generally thought to augment CD45 signal transduction [356]. How a lack of normal ERAP1 function causes altered expression of CD45-AP in B cells, and how that might affect cellular function is a more complicated manner, as CD45 plays complex roles in B cells [357]. As CD45-AP increases CD45 signaling and CD45 signaling activates Src kinases which leads to B cell proliferation [356, 357], B cells carrying the K528R SNP would be expected to have decreased CD45 signaling due to less CD45-AP and consequently may have impaired capacity to proliferate. This fits with our data showing murine B cells lacking ERAP1 have impaired proliferation when transferred into B cell deficient hosts. Additionally, CD45 signaling is known to inhibit cytokine secretion [357], thus B cells with K528R may also have an increased propensity for cytokine secretion which can be deleterious in an autoimmune disease like MS [358]. ERAP1 direct and indirect effects on CD45-AP is another area for future investigation and potential therapeutic targeting in ERAP1-linked autoimmune diseases.

Similarly, we also found upregulation of eIF2 signaling and oxidative phosphorylation pathways in all B cell subsets bearing the K528R SNP, suggesting ERAP1's ability to modulate these pathways is conserved across B cells. As ERAP1 is an endoplasmic reticulum-localized peptidase, it is possible that dysfunctional ERAP1 variants may lead to issues with protein processing/production, thus requiring the cell to up-regulate translation machinery to maintain protein production. Importantly, many of the genes we see upregulated in the eIF2 signaling pathway in cells with K528R are involved in translation. Since endoplasmic reticulum function is tied to cell metabolism and immune responses [359, 360], this may explain the concerted dysregulation of these pathways in B cells in particular [361, 362], and possibly the increased susceptibility to MS, although there is a paucity of studies regarding the effects of ER dysfunction in B cells as it relates to autoimmunity [363]. It is also important to note that all of these findings are from healthy individuals at baseline and that these DEGs and pathways may be exacerbated during settings of inflammation/immune activation.

We also observed some interesting CNS T cell phenotypes, such as a subset of IL-10⁺CD4⁺CD90⁻ T cells only in mice lacking ERAP1. CD90 has been found to affect T cells in a number of ways including: modulation of proliferation, cytokine production, cell-adhesion, apoptosis, and more [364, 365]. It is tempting to speculate how these IL-10⁺CD4⁺CD90⁻ T cells, found in the CNS of mice lacking ERAP1, may be functioning compared to their CD90⁺ counterparts found in the WT CNS, and how this may relate to B cell-dependent EAE phenotypes, but proper functional studies will be required for this.

An alternative hypothesis not investigated here concerns ERAP1's canonical role in antigen presentation. While ERAP1's ability to shape the immuno-peptidome is well understood [123], this particular function has not been shown to be the sole cause of ERAP1's genetic associations with multiple autoimmune diseases [347]. This is critical when considering the linkage to MS, since no set of conserved immunogenic epitopes has been confirmed to underlie susceptibility to all cases of MS [366, 367], unlike related neuroinflammatory diseases such as anti-MOG associated encephalitis [136] and neuromyelitis optica spectrum disorder [368]. This implies that polymorphisms in ERAP1 may be causing increased susceptibility to MS via alternative mechanisms, some of which we have previously identified [124, 129-131]. It has recently been shown that B cells present a unique repertoire of self-peptides on HLA-DR15 (MHC-II), a gene accounting for almost half of all genetic risk for MS [367]. Critically, memory CSF CD4⁺ T cells responded to these self-peptides, the most reactive of which, have been previously linked to MS [367]. It is therefore, conceivable, that since ERAP1 plays an important role in processing self-peptides for presentation on MHC-I [347], and that since the K528R SNP is known to modulate this trimming ability and alter the immunopeptidome [369], that B cells carrying the K528R SNP may be more likely to present CNS autoimmunity-driving auto-antigens on HLA-DR15. While it is commonly believed that ERAP1 only trims peptides presented on MHC-I [347], there is no conclusive evidence showing that ERAP1 does not affect the MHC-II immunopeptidome. Studies ruling out possible MHC-II involvement by ERAP1 only looked at MHC-II surface expression and CD4⁺ T cell responses to a handful of antigens [370]. Since it is now recognized that B cells can actually present self-antigens on MHC-II [367], and that this

may drive MS, further investigations into if and how ERAP1 shapes the MHC-II immunopeptidome are certainly warranted.

Finally, our studies here lead to the creation of the first map of the CNS resident IL-10⁺ immune compartment at the protein level in mice; an important resource for those investigating CNS regulatory mechanisms. Our map is similar to that determined using scRNA-seq [371], but with a couple of important differences potentially related to both the technology and animal models used. While we found microglia to be the primary source of IL-10 at steady state and CD4⁺ T cells the dominant source during EAE, Shemer, A., et al. claim microglia are unable to make IL-10 and that with LPS stimulation NK cells and neutrophils are the primary sources of IL-10 in the CNS [371]. Our protein level assessment of IL-10 using a highly specific reporter mouse [307] contradicts the idea that microglia do not make IL-10 and our results are consistent with other published work [372]. One reason for the discrepancy between our datasets is likely due to Shemer, A., et al. only measuring IL-10 at the mRNA level, while we measure it at the protein level. Measurements at the protein level are critical for a cytokine such as IL-10, as its mRNA is subject to multiple post-transcriptional regulation mechanisms [373] and because IL-10 protein negatively regulates its own mRNA [374]; autocrine signaling which may explain the discrepancy between our results. Lastly, while we employ the EAE model of neuroinflammation, Shemer, A., et al. use the LPS model, which may further explain why we identify different immune cell subsets are making IL-10, notably neutrophils [375]. While it has been reported that this strain of IL-10-GFP mouse is unsuitable for IL-10 detection in myeloid cell during inflammation [376], through the use of spectral cytometry we are able to detect and subtract

out autofluorescence signals from microglia, thus allowing accurate IL-10 detection even on highly autofluorescent cells such as microglia [296].

In total, our efforts to investigate the genetic association between polymorphisms in the *ERAP1* gene and MS have begun to unravel this mystery and focus attention on B cell biology as a potential key regulator in autoimmune neuroinflammation. This correlates with the current clinical treatment of MS using non-discriminate, B cell-depleting regimens. Our work suggests that there may be an opportunity to further target these interventions to specific B cell subsets, both to enhance efficacy, as well as prevent known complications to these approaches, such as global immune-suppression.

Materials and Methods

EAE model

All animal procedures were approved by the Michigan State University Institutional Animal Care and Use Committee (<http://iacuc.msu.edu/>). On day -2, mice were injected with 300µg recombinant human MOG peptide (rhMOG₃₅₋₅₅) (SigmaAldrich) or 33µg full-length recombinant murine MOG (rmMOG₁₋₁₂₅) (Anaspec) with equal parts complete Freund's adjuvant (CFA) as previously described [326]. 400ng of pertussis toxin (MilliporeSigma) was injected intraperitoneally on days -2 and 0. Mice were scored daily on a scale of 0-5 as previously described [326], with a score of 0 = no symptoms, 1 = tail paresis, 2 = partial hindlimb paresis, 3 = complete hindlimb paresis, 4 = complete hindlimb paresis and front limb involvement, 5 = moribund or dead. Mice were humanely euthanized if a score of 4 or 5 was reached.

Investigators were blinded to genotypes of mice during the 1st attempt at each experiment (these are presented as representative in figures).

Adoptive transfer studies

Splenocytes were collected from WT and ERAP1^{-/-} mice as previously described [124]. B cells were isolated per manufacturer's guidelines using the murine B cell isolation kit (Miltenyi Biotec) and injected I.V. retro-orbitally (1×10^7 cells) into μ MT mice (The Jackson Laboratory). Mice were bled to confirm B cell adoptive transfer two days later via FACS. Five days after transfer, EAE was induced in mice with rmMOG₁₋₁₂₅ as described above. For co-transfer of both WT and ERAP1^{-/-} B cells into the same mouse, WT B cells were first isolated and labeled with CFSE [377] and ERAP1^{-/-} B cells were labeled with CellTrace Violet [377] per manufacturer's guidelines. Cells were mixed in a 1:1 ratio and a total of 1×10^7 cells were injected I.V. into each μ MT mouse.

CNS immune cell isolation

Mice were anesthetized and trans-cardiac perfusion with 15-20mL of sterile PBS was performed. Brains were then removed, placed in ice-cold 1X HBSS and minced using a scalpel. Brains were digested using a digestion cocktail for 45 minutes at 37°C as previously described [327]. Samples were then homogenized with a dounce homogenizer and the digestion reaction was stopped using EDTA and 1X HBSS containing 10% FBS. The lysate was then subjected to gradient centrifugation using Percoll as previously described [328]. Isolated immune cells were resuspended in FACS buffer and stained for spectral cytometry. For experiments involving in

vivo circulating immune cell labeling, before trans-cardiac perfusion, 5 μ g of anti-CD45 SparkBlue 550 antibody was injected trans-cardiac through the left ventricle and allowed to circulate for three minutes. The mouse was then trans-cardiac perfused with PBS as described above.

Flow cytometry and spectral cytometry

Cells were isolated from the CNS, spleen, blood, and inguinal lymph nodes as previously described [31]. Cells were stained with various antibodies (Supplementary table 7) utilizing BD Brilliant Stain Buffer (50 μ L per sample) whenever multiple Brilliant dyes were used in combination. Viability staining was performed with Zombie NIR (BioLegend) and Fc receptors were blocked with murine Fc block (BD Biosciences). Intranuclear staining was performed with the BD Transcription Factor Buffer Set kit (BD Biosciences) per manufacturer's instructions. Samples were acquired on a 5 laser Cytex Aurora Spectral Cytometer or a 3 laser BD LSR II and data was analyzed using FlowJo version 10.6.1 (Tree Star) and the R computing environment. High dimensional single-cell spectral cytometry was performed in R. The CATALYST package was used to perform all analyses with a cell annotation and dimensionality reduction approach as previously described (O'Connell, et al., *under review*) [276]. After data clean up in FlowJo, files were exported as FCS files, loaded into R, and an arcsinh transformation of 6000 was applied to all spectral cytometry data. Unbiased clustering was performed with FlowSOM [223], and clusters were annotated and manually merged as necessary down to functionally distinct immune cell subsets.

For experiments using IL-10-GFP mice and/or in vivo labeling, IL-10-GFP⁺ and negative (and IV⁺ and negative) cells were combinatorially boolean gated in FlowJo allowing for absolute positive/negative discrimination in high dimensional analyses performed in R. In all analyses where IV labeling was performed, IV⁺ cells were removed before final generation of figures and statistical analysis. Additionally, high dimensional spectral cytometry analysis performed in (Fig. 35) was done entirely in FlowJo employing an exhaustive manual gating scheme allowing identification of nearly all immune cells (Supplementary fig. 14A), the accuracy of which was confirmed by unbiased FlowSOM clustering also performed in FlowJo (data not shown).

For the in vivo analysis of B cell proliferation, proliferation was measured via CFSE or CTV dye dilution. Specifically, we analyzed the proportion of cells actively proliferating from the previous measurement. This was done since the baseline population will shift over time since all cells are proliferating to some degree over this extended time period. By shifting the baseline from previous timepoints we are able to assess which cells are continuing to proliferate at substantial levels.

Integrated scRNA-seq analysis

We first searched for scRNA-seq datasets containing publicly available raw sequencing data of PBMCs from healthy individuals. We identified seven datasets [345, 348, 378-382] meeting these criteria, six of which used the 10X Genomics platform [345, 348, 378-381], and one which used Seq-well [382]. For 10X datasets, we downloaded the raw FASTQ files, processed them through the CellRanger pipeline and aligned reads to the GRCh38-3.0.0 human reference

genome. Resulting count matrices were saved for later analysis with the Seurat package [383].

We then used the output .bam file from Cell Ranger to call each individual sample for the presence or absence of the ERAP1 K528R SNP. This was accomplished by running mpileup from BCFtools with the following command: `-Ou -A -r 5:96700273-96995983 -f ~/hg38_ref_fasta/Homo_sapiens.GRCh38.dna.primary_assembly.fa`. SNPs were called from the resulting .bcf file using the call command from BCF tools with the following command: `-mv -Ob -o snp_calls_XX.bcf`. BCFtools was then used to index the .bcf file and a list of all SNPs in the ERAP1 region was generated using the BCFtools query command as follows: `-f '%CHROM %POS %REF %END %ALT\n' -r 5:96760273-96935983 snp_calls_XX.bcf > ERAP1_snps_XX.txt`. Resulting SNPs were run through a custom R script to identify the presence of the K528R SNP for each individual. Notably, for a few individuals, we tested if applying Q30 phred-score filtering affected our ERAP1 SNP calls and found that it did not (data not shown).

Seq-well data was downloaded as SRA files which were converted to FASTQ files using faster-dump from SRAtoolkit. Reads were aligned to GRCh38-3.0.0 using STAR, indexed with SAMtools, and SNPs were called as described above. Count matrices were downloaded from publicly available pre-processed data from the original authors [382].

All count matrices were loaded into R as Seurat objects using Seurat V4.0.3 and 10X datasets were merged together. Metadata containing K528R SNP info, study info, sample_ID info, etc was appended to all cells. Seq-well data was read into R and merged together into a Seurat object using the EpicTools package (<https://github.com/ajwilk/EpicTools>). Metadata was

appended to these files and all 10X data was merged with Seq-well data. Cells with < 200 features, > 4100 features, or > 20% of transcripts being mitochondrial were removed.

For dataset integration the harmony R package was used [384]. Briefly, the Seurat object containing all cells from all datasets was processed with SCTransform, the percent of mitochondrial transcripts was regressed out, and 30 PCA dimensions were calculated. Harmony was then run on the SCT assay of this Seurat object and both study and individual donor variability were regressed out of the integration. The standard SCTransform Seurat workflow was then continued and putative B cells were identified from UMAP plots and DEGs across cell clusters. Putative B cells were subsetted out from the rest of cells. Visual inspection of data revealed that there were very few cells from the Seq-well technology, and that these cells exhibited technology-specific clustering; hence, they were removed from downstream analysis.

B cells still exhibited study-specific clustering so the B cells were subjected to further dataset integration using the SCTransform integration approach embedded in Seurat V4.0.3. Briefly, SCTransform was rerun on all cells after splitting them up by study and the SCT assay was used to find integration anchors and to integrate the data. Visual inspection of this data now revealed minimal technology-specific clustering confirming efficient integration.

Re-clustering and differential marker analysis identified a few clusters of non-B cells/plasma cells which were removed. Data was re-clustered again and dimensionality reduction was also performed again. Clusters were annotated in an unbiased manner using the SingleR package

[385]. Here, we performed cluster-level annotation using three reference datasets (HPCA, Blueprint, and Monaco). SingleR effectively annotated all of our clusters with high confidence into five distinct B cell/plasma cell clusters. These clusters exhibit no study-specific biases, with the exception of the “Exhausted B cell” cluster which is composed almost entirely of cells from Kang, et al. (Supplementary fig. 21B) [348].

DEG's and data visualization of the resulting high-quality single-cell dataset were performed using the normalized RNA counts (and not SCTransformed or integrated data) as recommended by the Seurat development team. DEGs were called using MAST [386] and these DEGs were validated using a second approach (Wilcoxon rank sum test) showing very high concordance (data not shown). Pathway-level analyses were performed using IPA (Qiagen) on statistically significant DEGs from various B cell subsets. Bar plots of enriched pathways are colored according to the directionality of the changes in that pathway with more purple color indicating increased pathway activation and more tan color indicating less pathway activation in cells containing the K528R ERAP1 SNP.

Statistical analysis

Statistical analyses are listed in all figure legends and were performed in either GraphPad Prism V8 or the R computing environment. Cell subset frequency comparisons and differential marker expression on cell subsets from experiments employing high dimensional spectral cytometry were statistically compared with a GLMM implemented through the diffcyt R package [286]. All heatmaps were locally scaled.

Data and code availability

All raw data is available upon reasonable request. Analysis code can be found at:

https://github.com/poconnel3/OConnell_et-al_ERAP1_MS_manuscript

CHAPTER: 8 Summary/Discussion

Our multifaceted work presented in this thesis has helped to broaden our understanding as to how genetic association studies of MS have identified two genes, SLAMF7 and ERAP1 that not only predispose to this condition, but may also that may modulate key immunoregulatory mechanisms common to autoimmune diseases generally. Our investigations into SLAMF7's biological functions have expanded the scope of SLAMF7's known roles across immune cell types and diseases. Specifically, we described for the first time roles for SLAMF7 in the setting of chronic HIV infection as well as in T cell-mediated cancer responses [27, 255]. We also defined new cell type-specific functions for SLAMF7 on monocytes and T cells [27, 255]. In particular, we showed the ability of SLAMF7 to counteract type I IFN responses of monocytes; responses important during chronic HIV infection, as well as a number of other diseases [27, 387, 388]. As aberrant type I IFN responses have been identified to play important roles across a wide array of pathologies/conditions [387, 389], it will be interesting to see if SLAMF7 modulation of these responses can prove beneficial in these conditions. Indeed, as type I IFNs play an important role in the body's response to the current pandemic-causing virus, SARS-CoV-2 [390, 391], there have already been reports discussing a potential role for SLAMF7 in the pathogenesis of this infection [392-394]. Likewise, while we focused our studies of SLAMF7's role in T cell exhaustion to cancer [255], T cell exhaustion also plays roles in a number of other pathological states [115, 395]. It will be interesting for future studies to not only investigate this function of SLAMF7 more thoroughly, but also to see if modulation of this pathway can have beneficial outcomes in other disease models where T cell exhaustion is known to be involved.

As our group always has the end goal of improving patient outcomes in mind, we have already

begun to take our newfound knowledge of SLAMF7's diverse biological functions and translating them into potential therapeutics. A prime example of this is our work constructing and testing Ad-SF7-Fc, where we designed an adenovirus which expresses a recombinant protein composed of the extracellular domain of SLAMF7 attached to IgG1 (Chapter 5, this work). Our work here has shown it is possible to modulate this receptor in vivo to achieve positive disease outcomes, but has also highlighted the difficulty of such an approach. This difficulty comes from the nature of SLAMF7 being a homotypic receptor and also that it has differing functions on different immune cell types [27, 215, 255]. This means that a broad-based SLAMF7 targeting approach like the one we employed can actually be partially self-defeating, as it can induce cell type responses with opposing effects on the biological outcome desired. When modulating a receptor like SLAMF7, what is really needed is a targeted, precision approach tailored to the disease in question. Such an approach is currently feasible with currently available technologies such as bi-specific antibodies [396].

Our investigations into the role of SLAMF7 in CNS immunoregulation have uncovered multiple new areas for future investigation. They have also unexpectedly revealed similar mechanisms underlying this genes' association to MS with that of ERAP1; being through modulation of B cell responses. This highlights the importance of B cells in controlling CNS autoimmunity and suggests that B cells are particularly sensitive to any type of perturbation in regards to their ability to drive CNS autoimmunity, both genetic and environmental. This may help explain why so many genes have thus far been linked to MS susceptibility as B cells are a diverse group of immune cells with multiple function [4]. Such findings provide hope that in the future, once

more is known about master regulatory pathways controlling B cells and how changes in these cause autoimmunity, therapeutics may be developed to stabilize B cells against such perturbations. Such therapeutics should, in theory, prove superior to the current, blunt approach of merely depleting all B cells in individuals with MS or other autoimmune diseases.

Our work on another GWAS associated susceptibility gene for MS, ERAP1, demonstrates how ERAP1 modulates immune responses to potentially increase susceptibility to autoimmune conditions in a parallel manner to SLAMF7. Like SLAMF7, ERAP1 is able to modulate the immune system via multiple mechanisms [121], making it a potential master regulator of the immune system. However, unlike SLAMF7 which can affect different immune cell types in vastly different ways [27, 215, 255], ERAP1 appears, in general, to have similar effects on most immune cells; that is, it functions to dampen pro-inflammatory responses [121]. Our work showing ERAP1 increases susceptibility to EAE via a B cell-dependent mechanism is intriguing, since there has never before been published studies showing a mechanistic role for ERAP1 in B cells driving disease (Chapter 7, this work). Based upon these efforts, our group has expanded ERAP1's known functions to include modulation of innate immune functions as well, as well as now B cells specifically [129-131]. It is certainly possible (and highly likely) that ERAP1 has yet more undiscovered roles in the regulation of the immune system which await discovery. Studies investigating the intracellular interaction partners of ERAP1 will be critical, not only in uncovering these, but also at helping to provide more detailed mechanistic evidence for ERAP1's other non-canonical functions. In total, our efforts here have advanced mankind's knowledge of how two proteins, SLAMF7 and ERAP1, modulate immune responses, how this

can alter diseases susceptibility/progression, and ways in which we might be able to therapeutically modulate such responses for clinical benefit.

The combined efforts from our studies of ERAP1 and SLAMF7 in MS/EAE align well with current research in the field of autoimmunity showing that B cells play a much more critical role than once thought. For decades much of the research into causes underlying autoimmune diseases focused on immune suppressive factors (ie. IL-10), which while an important factor in many cases, have emerged as secondary to other master regulatory mechanisms. Now that the immunological community has recognized the critical roles B cells play in orchestrating immune responses, beyond their well-known role in antibody production, new efforts are underway to characterize the full extent of the roles B cells play in immunoregulation. For example, recent work from Marco Colonna and Jonathan Kipnis on CNS B cells has revealed surprising CNS B cell heterogeneity and novel cranial bone marrow reservoirs for CNS B cells [397, 398]. The impetus for such in depth studies was likely driven by the recently appreciated critical roles B cells play in CNS autoimmunity.

Taken together with our studies here, a new picture of autoimmunity is emerging; one in which B cell-mediated orchestration of the global immune system is key to autoimmune disease susceptibility. It is also clear that we have much to learn regarding the precise B cell-specific mechanisms important in controlling these processes. With this knowledge we can begin to move away from our current hard-handed clinical B cell targeting approach (pan-depletion) and move on to more elegant, targeted B cell therapeutics.

CHAPTER: 9 Future work

All of the work presented here could benefit from additional follow-up studies providing more mechanistic evidence supporting and expanding upon our multiple findings. In regards to our studies of SLAMF7 in the setting of HIV [27], some additional studies important to perform include experiments to fully define the mechanism by which SLAMF7 is able to suppress alpha chemokine production from IFN α -stimulated monocytes. In particular, RNA-seq studies paired with SLAMF7 IP-LC MS/MS, followed by integrated analysis using Ingenuity Pathway Analysis software (Qiagen) would provide a powerful combination to help identify potential transcriptional gene networks for more in-depth biochemical studies. Additionally, modulating SLAMF7 in vivo in a mouse (via cre-lox conditional targeting or SLAMF7-targeting antibodies) or using a non-human primate model of HIV-1 infection would provide important proof-of-concept that targeting of the SLAMF7 receptor can have positive disease outcomes. These studies would require appropriate therapeutic modalities to specifically target SLAMF7, which would need to be developed first, such as bi-specific adaptations of our recently developed SLAMF7-Fc protein [112]. It would also be interesting to further investigate how precisely SLAMF7 activation on monocytes is able to inhibit their infection with HIV-1 and if this effect is also true in vivo.

Our work examining how SLAMF7 signaling on CD8⁺ T cells drives them towards exhaustion could also benefit from mechanistic work looking to understand this process at the molecular level. This could be accomplished via a large integrated experiment where CD8⁺ TILs are sorted out from B16 tumors grown in WT or SLAMF7^{-/-} mice. The sorted cells are then subjected to combined scRNA-seq, scATAC-seq, and scTCR-seq [399]. This would not only identify gene transcription networks, but also allow for analysis of epigenetic changes on these cells, which is

critical because of the important role of epigenetics in T cell exhaustion [400, 401], and how we found SLAMF7 modulated the important epigenetic remodeling transcription factors YY1, TOX, and Blimp-1 in T cells [255]. There are of course other ways this could be accomplished, including in vitro stimulation studies of SLAMF7-stimulated T cells paired with SLAMF7-specific cite-seq to help target analyses to just T cells which have had their SLAMF7 receptor activated (this takes advantage of the knowledge that once SLAMF7 is activated it becomes down-regulated at the protein level (O'Connell, 2018 #1639) so comparing protein and RNA expression of SLAMF7 can allow identification of cells w/ bona fide SLAMF7 activation). It would also be important to confirm the enhanced tumor control in SLAMF7^{-/-} mice is due to defects in CD8⁺ T cells, since our work used a whole mouse knockout. This can be easily accomplished using a CD8-cre driver line crossed to a SLAMF7^{fl/fl} mouse (which our group has recently generated, shown to be non-embryonically lethal, and specifically deletes SLAMF7 on CD8⁺ T cells [data not shown]).

A few important questions remain from our work developing the Ad-SF7-Fc virus. Specifically, work confirming that SLAMF7 signaling can alter pDC production of type I IFNs, can induce IL-12 from DCs, and/or can modulate TAM PD-L1 expression, would all help to bolster the conclusions from that work. Much of this could be accomplished with simple in vitro assays utilizing cells from SLAMF7^{-/-} mice and also crosslinking of the SLAMF7 receptor in cells from WT mice. Combining studies utilizing SLAMF7^{-/-} mice and SLAMF7 activation on WT mice should allow for a more robust assessment of the impacts of SLAMF7 signaling, as factors modulated in one direction in SLAMF7^{-/-} immune cells should be modulated in the opposite direction when

SLAMF7 is activated on WT immune cells. It would also be interesting to investigate if SLAMF7 signaling on TAMs alters just PD-L1 expression, or if it alters TAMs in any other way, so transcriptome-wide studies may be useful here. Such studies would provide a global view of how SLAMF7 signaling alters TAMs and would provide information on potential mechanisms linking SLAMF7 signaling to PD-L1 expression.

Perhaps the study prompting the most follow-up work is our investigation into the role of SLAMF7 in MS. Our early work has determined that the mechanism is independent of IL-10, which is important since our work showing SLAMF7 can modulate STAT3 phosphorylation [255], and the knowledge that pSTAT3 drives IL-10 [305, 402], made this a logical potential mechanism. Preliminary data suggests that SLAMF7 signaling on B cells may be responsible for this increased EAE susceptibility, possibly via IL-10-independent regulatory mechanisms, but adoptive transfer and/or conditional targeting studies will be needed to confirm this.

Importantly, our group has both the protocol and μ MT mice in place for adoptive transfer studies, and we also have SLAMF7^{fl/fl} mice available for breeding to CD19-Cre driver lines. Molecular-level mechanism studies could be undertaken with RNA-seq and SLAMF7 IP LC-MS/MS experiments as described above. As there is very little in the literature regarding the role of SLAMF7 on B cells, any results of these investigations would prove important in the SLAM receptor field.

Because we have narrowed down the culprit cell to B cells as being intrinsically susceptible to loss of ERAP1 functions to promote EAE, and that current MS therapies focus on B cell depletion

strategies, future investigations are more straight forward here. The most pressing studies will be ones investigating the molecular mechanism using ERAP1^{-/-} deficient B cells largely accomplished via RNA-seq of WT and ERAP1^{-/-} B cells from mice with EAE and at steady state. Potentially interesting transcriptional networks identified as underlying mechanisms can be validated (reversed) in vitro, and in vivo to determine if they can reverse the EAE phenotype of ERAP1^{-/-} mice. Potentially interesting mechanisms can be validated in vitro, or even in vivo to see if they can reverse the EAE phenotype in ERAP1^{-/-} mice. Moreover, from RNA-seq data, we can calculate an ERAP1^{-/-} gene signature, convert these genes to their human homologues, and map this signature back to our human scRNA-seq dataset. This would allow us determine whether individuals carrying the ERAP1 K528R SNP have more B cells with a high risk ERAP1^{-/-} signature, as would be expected and would help link our murine findings back to humans. By focusing on factors and pathways similarly dysregulated in murine ERAP1^{-/-} B cells and human B cells carrying the K528R SNP, we could then begin functional studies aimed at determining precisely how ERAP1 modulates B cell functions to predispose to autoimmunity. With this functional knowledge of how ERAP1 modulates B cells, translational studies on B cells from MS patients (and patients with other ERAP1-linked autoimmune diseases) could be undertaken. Such studies could investigate if these ERAP1-mediated functional defects in B cells from MS patients are only present in individuals carrying the ERAP1 K528R SNP, or if they are conserved in B cells from individuals with MS not carrying the K528R SNP. If the latter is true, this would point to a conserved pathway in B cells underlying MS susceptibility, (as well additional autoimmune diseases ERAP1 has been linked to) which ERAP1 and other genes may independently be able to contribute too.

REFERENCES

REFERENCES

1. Filippi, M., et al., *Multiple sclerosis*. Nat Rev Dis Primers, 2018. **4**(1): p. 43.
2. DynaMed, *Multiple Sclerosis (MS)*. EBSCO Information Services.
3. Hosseiny, M., S.D. Newsome, and D.M. Yousem, *Radiologically Isolated Syndrome: A Review for Neuroradiologists*. AJNR Am J Neuroradiol, 2020. **41**(9): p. 1542-1549.
4. International Multiple Sclerosis Genetics, C., *Multiple sclerosis genomic map implicates peripheral immune cells and microglia in susceptibility*. Science, 2019. **365**(6460).
5. Michel, L., et al., *B Cells in the Multiple Sclerosis Central Nervous System: Trafficking and Contribution to CNS-Compartmentalized Inflammation*. Front Immunol, 2015. **6**: p. 636.
6. Hauser, S.L., et al., *B-cell depletion with rituximab in relapsing-remitting multiple sclerosis*. N Engl J Med, 2008. **358**(7): p. 676-88.
7. Lee, D.S.W., O.L. Rojas, and J.L. Gommerman, *B cell depletion therapies in autoimmune disease: advances and mechanistic insights*. Nat Rev Drug Discov, 2021. **20**(3): p. 179-199.
8. Montalban, X., et al., *Ocrelizumab versus Placebo in Primary Progressive Multiple Sclerosis*. N Engl J Med, 2017. **376**(3): p. 209-220.
9. Cannons, J.L., S.G. Tangye, and P.L. Schwartzberg, *SLAM family receptors and SAP adaptors in immunity*. Annu Rev Immunol, 2011. **29**: p. 665-705.
10. Veillette, A., *SLAM-family receptors: immune regulators with or without SAP-family adaptors*. Cold Spring Harb Perspect Biol, 2010. **2**(3): p. a002469.
11. Tangye, S.G., *XLP: clinical features and molecular etiology due to mutations in SH2D1A encoding SAP*. J Clin Immunol, 2014. **34**(7): p. 772-9.
12. Felberg, J., et al., *Subdomain X of the kinase domain of Lck binds CD45 and facilitates dephosphorylation*. J Biol Chem, 2004. **279**(5): p. 3455-62.
13. Wu, N. and A. Veillette, *SLAM family receptors in normal immunity and immune pathologies*. Curr Opin Immunol, 2016. **38**: p. 45-51.
14. van Driel, B.J., et al., *Responses to Microbial Challenges by SLAMF Receptors*. Front Immunol, 2016. **7**: p. 4.

15. Bortoluci, K.R. and R. Medzhitov, *Control of infection by pyroptosis and autophagy: role of TLR and NLR*. Cell Mol Life Sci, 2010. **67**(10): p. 1643-51.
16. Iwasaki, A. and R. Medzhitov, *Regulation of adaptive immunity by the innate immune system*. Science, 2010. **327**(5963): p. 291-5.
17. Mogensen, T.H., et al., *Innate immune recognition and activation during HIV infection*. Retrovirology, 2010. **7**: p. 54.
18. Veazey, R.S., et al., *Gastrointestinal tract as a major site of CD4+ T cell depletion and viral replication in SIV infection*. Science, 1998. **280**(5362): p. 427-31.
19. Veazey, R.S., et al., *Identifying the target cell in primary simian immunodeficiency virus (SIV) infection: highly activated memory CD4(+) T cells are rapidly eliminated in early SIV infection in vivo*. J Virol, 2000. **74**(1): p. 57-64.
20. Kahn, J.O. and B.D. Walker, *Acute human immunodeficiency virus type 1 infection*. N Engl J Med, 1998. **339**(1): p. 33-9.
21. Grossman, Z., et al., *Pathogenesis of HIV infection: what the virus spares is as important as what it destroys*. Nat Med, 2006. **12**(3): p. 289-95.
22. Boasso, A. and G.M. Shearer, *Chronic innate immune activation as a cause of HIV-1 immunopathogenesis*. Clin Immunol, 2008. **126**(3): p. 235-42.
23. Ferrari, G., et al., *Humoral and Innate Antiviral Immunity as Tools to Clear Persistent HIV Infection*. J Infect Dis, 2017. **215**(suppl_3): p. S152-S159.
24. Rethi, B., et al., *SLAM/SLAM interactions inhibit CD40-induced production of inflammatory cytokines in monocyte-derived dendritic cells*. Blood, 2006. **107**(7): p. 2821-9.
25. Bleharski, J.R., et al., *Signaling lymphocytic activation molecule is expressed on CD40 ligand-activated dendritic cells and directly augments production of inflammatory cytokines*. J Immunol, 2001. **167**(6): p. 3174-81.
26. Wang, N., et al., *The cell surface receptor SLAM controls T cell and macrophage functions*. J Exp Med, 2004. **199**(9): p. 1255-64.
27. O'Connell, P., et al., *SLAMF7 Is a Critical Negative Regulator of IFN-alpha-Mediated CXCL10 Production in Chronic HIV Infection*. J Immunol, 2018.
28. Agod, Z., et al., *Signaling Lymphocyte Activation Molecule Family 5 Enhances Autophagy and Fine-Tunes Cytokine Response in Monocyte-Derived Dendritic Cells via Stabilization of Interferon Regulatory Factor 8*. Front Immunol, 2018. **9**: p. 62.

29. Wang, G., et al., *Cutting edge: Slamf8 is a negative regulator of Nox2 activity in macrophages*. J Immunol, 2012. **188**(12): p. 5829-32.
30. Dollt, C., et al., *The novel immunoglobulin super family receptor SLAMF9 identified in TAM of murine and human melanoma influences pro-inflammatory cytokine secretion and migration*. Cell Death Dis, 2018. **9**(10): p. 939.
31. Aldhamen, Y.A., et al., *Vaccines expressing the innate immune modulator EAT-2 elicit potent effector memory T lymphocyte responses despite pre-existing vaccine immunity*. J Immunol, 2012. **189**(3): p. 1349-59.
32. Brenchley, J.M., et al., *Microbial translocation is a cause of systemic immune activation in chronic HIV infection*. Nat Med, 2006. **12**(12): p. 1365-71.
33. Berger, S.B., et al., *SLAM is a microbial sensor that regulates bacterial phagosome functions in macrophages*. Nat Immunol, 2010. **11**(10): p. 920-7.
34. van Driel, B., et al., *The cell surface receptor Slamf6 modulates innate immune responses during Citrobacter rodentium-induced colitis*. Int Immunol, 2015. **27**(9): p. 447-57.
35. Boasso, A., *Type I Interferon at the Interface of Antiviral Immunity and Immune Regulation: The Curious Case of HIV-1*. Scientifica (Cairo), 2013. **2013**: p. 580968.
36. Cha, L., et al., *Interferon-alpha, immune activation and immune dysfunction in treated HIV infection*. Clin Transl Immunology, 2014. **3**(2): p. e10.
37. Doyle, T., C. Goujon, and M.H. Malim, *HIV-1 and interferons: who's interfering with whom?* Nat Rev Microbiol, 2015. **13**(7): p. 403-13.
38. Sever, L., et al., *SLAMF9 regulates pDC homeostasis and function in health and disease*. Proc Natl Acad Sci U S A, 2019. **116**(33): p. 16489-16496.
39. Maranon, C., et al., *Dendritic cells cross-present HIV antigens from live as well as apoptotic infected CD4+ T lymphocytes*. Proc Natl Acad Sci U S A, 2004. **101**(16): p. 6092-7.
40. Kis-Toth, K. and G.C. Tsokos, *Engagement of SLAMF2/CD48 prolongs the time frame of effective T cell activation by supporting mature dendritic cell survival*. J Immunol, 2014. **192**(9): p. 4436-42.
41. Moir, S. and A.S. Fauci, *B-cell responses to HIV infection*. Immunol Rev, 2017. **275**(1): p. 33-48.
42. Wong, E.B., et al., *B cell-intrinsic CD84 and Ly108 maintain germinal center B cell tolerance*. J Immunol, 2015. **194**(9): p. 4130-43.

43. Simon, V., N. Bloch, and N.R. Landau, *Intrinsic host restrictions to HIV-1 and mechanisms of viral escape*. Nat Immunol, 2015. **16**(6): p. 546-53.
44. Pallikkuth, S., et al., *T Follicular Helper Cells and B Cell Dysfunction in Aging and HIV-1 Infection*. Front Immunol, 2017. **8**: p. 1380.
45. Veenhuis, R.T., et al., *HIV-antibody complexes enhance production of type I interferon by plasmacytoid dendritic cells*. J Clin Invest, 2017.
46. Tatsuo, H., et al., *SLAM (CDw150) is a cellular receptor for measles virus*. Nature, 2000. **406**(6798): p. 893-7.
47. Davidson, D., et al., *Genetic evidence linking SAP, the X-linked lymphoproliferative gene product, to Src-related kinase FynT in T(H)2 cytokine regulation*. Immunity, 2004. **21**(5): p. 707-17.
48. Zarama, A., et al., *Cytomegalovirus m154 hinders CD48 cell-surface expression and promotes viral escape from host natural killer cell control*. PLoS Pathog, 2014. **10**(3): p. e1004000.
49. Cartier, F., et al., *The expression of the hepatocyte SLAMF3 (CD229) receptor enhances the hepatitis C virus infection*. PLoS One, 2014. **9**(6): p. e99601.
50. Martinez-Vicente, P., et al., *Subversion of natural killer cell responses by a cytomegalovirus-encoded soluble CD48 decoy receptor*. PLoS Pathog, 2019. **15**(4): p. e1007658.
51. Duev-Cohen, A., et al., *The human 2B4 and NTB-A receptors bind the influenza viral hemagglutinin and co-stimulate NK cell cytotoxicity*. Oncotarget, 2016. **7**(11): p. 13093-105.
52. Blackburn, S.D., et al., *Coregulation of CD8+ T cell exhaustion by multiple inhibitory receptors during chronic viral infection*. Nat Immunol, 2009. **10**(1): p. 29-37.
53. Raziorrouh, B., et al., *The immunoregulatory role of CD244 in chronic hepatitis B infection and its inhibitory potential on virus-specific CD8+ T-cell function*. Hepatology, 2010. **52**(6): p. 1934-47.
54. Schlaphoff, V., et al., *Dual function of the NK cell receptor 2B4 (CD244) in the regulation of HCV-specific CD8+ T cells*. PLoS Pathog, 2011. **7**(5): p. e1002045.
55. Pacheco, Y., et al., *Simultaneous TCR and CD244 signals induce dynamic downmodulation of CD244 on human antiviral T cells*. J Immunol, 2013. **191**(5): p. 2072-81.

56. Yamamoto, T., et al., *Surface expression patterns of negative regulatory molecules identify determinants of virus-specific CD8+ T-cell exhaustion in HIV infection*. Blood, 2011. **117**(18): p. 4805-15.
57. Aldy, K.N., et al., *2B4+ CD8+ T cells play an inhibitory role against constrained HIV epitopes*. Biochem Biophys Res Commun, 2011. **405**(3): p. 503-7.
58. Shah, A.H., et al., *Degranulation of natural killer cells following interaction with HIV-1-infected cells is hindered by downmodulation of NTB-A by Vpu*. Cell Host Microbe, 2010. **8**(5): p. 397-409.
59. Sato, K., et al., *Vpu augments the initial burst phase of HIV-1 propagation and downregulates BST2 and CD4 in humanized mice*. J Virol, 2012. **86**(9): p. 5000-13.
60. Bolduan, S., et al., *HIV-1 Vpu affects the anterograde transport and the glycosylation pattern of NTB-A*. Virology, 2013. **440**(2): p. 190-203.
61. He, B., et al., *HIV-1 envelope triggers polyclonal Ig class switch recombination through a CD40-independent mechanism involving BAFF and C-type lectin receptors*. J Immunol, 2006. **176**(7): p. 3931-41.
62. Shlapatska, L.M., et al., *CD150 association with either the SH2-containing inositol phosphatase or the SH2-containing protein tyrosine phosphatase is regulated by the adaptor protein SH2D1A*. J Immunol, 2001. **166**(9): p. 5480-7.
63. Hashiguchi, T., et al., *Structure of the measles virus hemagglutinin bound to its cellular receptor SLAM*. Nat Struct Mol Biol, 2011. **18**(2): p. 135-41.
64. van der Merwe, P.A., et al., *Human cell-adhesion molecule CD2 binds CD58 (LFA-3) with a very low affinity and an extremely fast dissociation rate but does not bind CD48 or CD59*. Biochemistry, 1994. **33**(33): p. 10149-60.
65. Thorley-Lawson, D.A., et al., *Epstein-Barr virus superinduces a new human B cell differentiation antigen (B-LAST 1) expressed on transformed lymphoblasts*. Cell, 1982. **30**(2): p. 415-25.
66. Ward, J., et al., *HIV modulates the expression of ligands important in triggering natural killer cell cytotoxic responses on infected primary T-cell blasts*. Blood, 2007. **110**(4): p. 1207-14.
67. Chibueze-Nnorom CE, W.Y., Yoshimitsu M and Arima N, *ROLE OF CD48 IN REGULATION OF T-CELL MEDIATED IMMUNITY IN HTLV-1 INFECTION*, in *15th International Congress of Immunology*. 2013: Milan, Italy.
68. Gonzalez-Cabrero, J., et al., *CD48-deficient mice have a pronounced defect in CD4(+) T cell activation*. Proc Natl Acad Sci U S A, 1999. **96**(3): p. 1019-23.

69. Abadia-Molina, A.C., et al., *CD48 controls T-cell and antigen-presenting cell functions in experimental colitis*. *Gastroenterology*, 2006. **130**(2): p. 424-34.
70. Martinez-Martin, N., et al., *The extracellular interactome of the human adenovirus family reveals diverse strategies for immunomodulation*. *Nat Commun*, 2016. **7**: p. 11473.
71. Graham, D.B., et al., *Ly9 (CD229)-deficient mice exhibit T cell defects yet do not share several phenotypic characteristics associated with SLAM- and SAP-deficient mice*. *J Immunol*, 2006. **176**(1): p. 291-300.
72. McNerney, M.E., K.M. Lee, and V. Kumar, *2B4 (CD244) is a non-MHC binding receptor with multiple functions on natural killer cells and CD8+ T cells*. *Mol Immunol*, 2005. **42**(4): p. 489-94.
73. Vaidya, S.V. and P.A. Mathew, *Of mice and men: different functions of the murine and human 2B4 (CD244) receptor on NK cells*. *Immunol Lett*, 2006. **105**(2): p. 180-4.
74. Chlewicki, L.K., et al., *Molecular basis of the dual functions of 2B4 (CD244)*. *J Immunol*, 2008. **180**(12): p. 8159-67.
75. Peritt, D., et al., *C1.7 antigen expression on CD8+ T cells is activation dependent: increased proportion of C1.7+CD8+ T cells in HIV-1-infected patients with progressing disease*. *J Immunol*, 1999. **162**(12): p. 7563-8.
76. Enose-Akahata, Y., et al., *High expression of CD244 and SAP regulated CD8 T cell responses of patients with HTLV-I associated neurologic disease*. *PLoS Pathog*, 2009. **5**(12): p. e1000682.
77. Pombo, C., et al., *Elevated Expression of CD160 and 2B4 Defines a Cytolytic HIV-Specific CD8+ T-Cell Population in Elite Controllers*. *J Infect Dis*, 2015. **212**(9): p. 1376-86.
78. Ostrowski, S.R., et al., *2B4 expression on natural killer cells increases in HIV-1 infected patients followed prospectively during highly active antiretroviral therapy*. *Clin Exp Immunol*, 2005. **141**(3): p. 526-33.
79. Ahmad, F., et al., *Negative Checkpoint Regulatory Molecule 2B4 (CD244) Upregulation Is Associated with Invariant Natural Killer T Cell Alterations and Human Immunodeficiency Virus Disease Progression*. *Front Immunol*, 2017. **8**: p. 338.
80. Schuldt, N.J., et al., *Vaccine platforms combining circumsporozoite protein and potent immune modulators, rEA or EAT-2, paradoxically result in opposing immune responses*. *PLoS One*, 2011. **6**(8): p. e24147.

81. Aldhamen, Y.A., et al., *Improved cytotoxic T-lymphocyte immune responses to a tumor antigen by vaccines co-expressing the SLAM-associated adaptor EAT-2*. *Cancer Gene Ther*, 2013. **20**(10): p. 564-75.
82. Sichien, D., et al., *IRF8 Transcription Factor Controls Survival and Function of Terminally Differentiated Conventional and Plasmacytoid Dendritic Cells, Respectively*. *Immunity*, 2016. **45**(3): p. 626-640.
83. Cannons, J.L., et al., *Optimal germinal center responses require a multistage T cell:B cell adhesion process involving integrins, SLAM-associated protein, and CD84*. *Immunity*, 2010. **32**(2): p. 253-65.
84. Tangye, S.G., et al., *CD84 is up-regulated on a major population of human memory B cells and recruits the SH2 domain containing proteins SAP and EAT-2*. *Eur J Immunol*, 2002. **32**(6): p. 1640-9.
85. Fitzgerald-Bocarsly, P. and E.S. Jacobs, *Plasmacytoid dendritic cells in HIV infection: striking a delicate balance*. *J Leukoc Biol*, 2010. **87**(4): p. 609-20.
86. Lewinsky, H., et al., *CD84 regulates PD-1/PD-L1 expression and function in chronic lymphocytic leukemia*. *J Clin Invest*, 2018. **128**(12): p. 5465-5478.
87. Denton, P.W. and J.V. Garcia, *Novel humanized murine models for HIV research*. *Curr HIV/AIDS Rep*, 2009. **6**(1): p. 13-9.
88. Policicchio, B.B., I. Pandrea, and C. Apetrei, *Animal Models for HIV Cure Research*. *Front Immunol*, 2016. **7**: p. 12.
89. Miller, B.C., et al., *Subsets of exhausted CD8(+) T cells differentially mediate tumor control and respond to checkpoint blockade*. *Nat Immunol*, 2019. **20**(3): p. 326-336.
90. Tassi, I. and M. Colonna, *The cytotoxicity receptor CRACC (CS-1) recruits EAT-2 and activates the PI3K and phospholipase Cgamma signaling pathways in human NK cells*. *J Immunol*, 2005. **175**(12): p. 7996-8002.
91. Cruz-Munoz, M.E., et al., *Influence of CRACC, a SLAM family receptor coupled to the adaptor EAT-2, on natural killer cell function*. *Nat Immunol*, 2009. **10**(3): p. 297-305.
92. Guo, H., et al., *Immune cell inhibition by SLAMF7 is mediated by a mechanism requiring src kinases, CD45, and SHIP-1 that is defective in multiple myeloma cells*. *Mol Cell Biol*, 2015. **35**(1): p. 41-51.
93. Chen, J., et al., *SLAMF7 is critical for phagocytosis of haematopoietic tumour cells via Mac-1 integrin*. *Nature*, 2017. **544**(7651): p. 493-497.

94. Rempel, H., et al., *Interferon-alpha drives monocyte gene expression in chronic unsuppressed HIV-1 infection*. AIDS, 2010. **24**(10): p. 1415-23.
95. Paiardini, M. and M. Muller-Trutwin, *HIV-associated chronic immune activation*. Immunol Rev, 2013. **254**(1): p. 78-101.
96. Li, Y., et al., *CRACC-CRACC interaction between Kupffer and NK cells contributes to poly I:C/D-GalN induced hepatitis*. PLoS One, 2013. **8**(9): p. e76681.
97. Hou, X., et al., *NKG2D-retinoic acid early inducible-1 recognition between natural killer cells and Kupffer cells in a novel murine natural killer cell-dependent fulminant hepatitis*. Hepatology, 2009. **49**(3): p. 940-9.
98. Kingsbury, G.A., et al., *Cloning, expression, and function of BLAME, a novel member of the CD2 family*. J Immunol, 2001. **166**(9): p. 5675-80.
99. Fraser, C.C., et al., *Identification and characterization of SF2000 and SF2001, two new members of the immune receptor SLAM/CD2 family*. Immunogenetics, 2002. **53**(10-11): p. 843-50.
100. Zhang, Y., et al., *An RNA-sequencing transcriptome and splicing database of glia, neurons, and vascular cells of the cerebral cortex*. J Neurosci, 2014. **34**(36): p. 11929-47.
101. Kumar, G.S., et al., *Gene Expression Profiling of Tuberculous Meningitis Co-infected with HIV*. J Proteomics Bioinform, 2012. **5**(9): p. 235-244.
102. Zeng, X., et al., *Combined deficiency of SLAMF8 and SLAMF9 prevents endotoxin-induced liver inflammation by downregulating TLR4 expression on macrophages*. Cell Mol Immunol, 2018.
103. Wang, G., et al., *Migration of myeloid cells during inflammation is differentially regulated by the cell surface receptors Slamf1 and Slamf8*. PLoS One, 2015. **10**(3): p. e0121968.
104. Burdo, T.H., A. Lackner, and K.C. Williams, *Monocyte/macrophages and their role in HIV neuropathogenesis*. Immunol Rev, 2013. **254**(1): p. 102-13.
105. Williams, D.W., et al., *Monocytes mediate HIV neuropathogenesis: mechanisms that contribute to HIV associated neurocognitive disorders*. Curr HIV Res, 2014. **12**(2): p. 85-96.
106. Veenstra, M., et al., *Mechanisms of CNS Viral Seeding by HIV(+) CD14(+) CD16(+) Monocytes: Establishment and Reseeding of Viral Reservoirs Contributing to HIV-Associated Neurocognitive Disorders*. MBio, 2017. **8**(5).

107. Fennelly, J.A., et al., *CD2F-10: a new member of the CD2 subset of the immunoglobulin superfamily*. Immunogenetics, 2001. **53**(7): p. 599-602.
108. Zhang, W., et al., *Genetic approach to insight into the immunobiology of human dendritic cells and identification of CD84-H1, a novel CD84 homologue*. Clin Cancer Res, 2001. **7**(3 Suppl): p. 822s-829s.
109. Wilson, T., J., , et al. *SLAMF9 promotes inflammation and resistance to Salmonella infection*. in *Immunology 2018*. 2018. Austin, TX: The Journal of Immunology.
110. Saitoh, S.I., et al., *TLR7 mediated viral recognition results in focal type I interferon secretion by dendritic cells*. Nat Commun, 2017. **8**(1): p. 1592.
111. Soper, A., et al., *Type I Interferon Responses by HIV-1 Infection: Association with Disease Progression and Control*. Front Immunol, 2017. **8**: p. 1823.
112. Aldhamen, Y.A., et al., *CRACC-targeting Fc-fusion protein induces activation of NK cells and DCs and improves T cell immune responses to antigenic targets*. Vaccine, 2016. **34**(27): p. 3109-18.
113. Aldhamen, Y.A., et al., *Expression of the SLAM family of receptors adapter EAT-2 as a novel strategy for enhancing beneficial immune responses to vaccine antigens*. J Immunol, 2011. **186**(2): p. 722-32.
114. Aldhamen, Y.A., et al., *Manipulation of EAT-2 expression promotes induction of multiple beneficial regulatory and effector functions of the human innate immune system as a novel immunomodulatory strategy*. Int Immunol, 2014. **26**(5): p. 291-303.
115. Wherry, E.J. and M. Kurachi, *Molecular and cellular insights into T cell exhaustion*. Nat Rev Immunol, 2015. **15**(8): p. 486-99.
116. International Multiple Sclerosis Genetics, C., et al., *Analysis of immune-related loci identifies 48 new susceptibility variants for multiple sclerosis*. Nat Genet, 2013. **45**(11): p. 1353-60.
117. Ban, M., et al., *Transcript specific regulation of expression influences susceptibility to multiple sclerosis*. Eur J Hum Genet, 2020. **28**(6): p. 826-834.
118. Beltran, E., et al., *Early adaptive immune activation detected in monozygotic twins with prodromal multiple sclerosis*. J Clin Invest, 2019. **129**(11): p. 4758-4768.
119. Mizrahi, J.S., et al., *Role of SLAMF immunoregulatory molecules in MS disease processes*. The Journal of Immunology, 2017. **198**(1 Supplement): p. 55.24-55.24.

120. York, I.A., et al., *Endoplasmic reticulum aminopeptidase 1 (ERAP1) trims MHC class I-presented peptides in vivo and plays an important role in immunodominance*. Proc Natl Acad Sci U S A, 2006. **103**(24): p. 9202-7.
121. Pepelyayeva, Y. and A. Amalfitano, *The role of ERAP1 in autoinflammation and autoimmunity*. Hum Immunol, 2019. **80**(5): p. 302-309.
122. Wellcome Trust Case Control, C., et al., *Association scan of 14,500 nonsynonymous SNPs in four diseases identifies autoimmunity variants*. Nat Genet, 2007. **39**(11): p. 1329-37.
123. Rastall, D.P., et al., *ERAP1 functions override the intrinsic selection of specific antigens as immunodominant peptides, thereby altering the potency of antigen-specific cytolytic and effector memory T-cell responses*. Int Immunol, 2014. **26**(12): p. 685-95.
124. Rastall, D.P.W., et al., *Mice expressing human ERAP1 variants associated with ankylosing spondylitis have altered T-cell repertoires and NK cell functions, as well as increased in utero and perinatal mortality*. Int Immunol, 2017. **29**(6): p. 277-289.
125. Zervoudi, E., et al., *Rationally designed inhibitor targeting antigen-trimming aminopeptidases enhances antigen presentation and cytotoxic T-cell responses*. Proc Natl Acad Sci U S A, 2013. **110**(49): p. 19890-5.
126. Hearn, A., I.A. York, and K.L. Rock, *The specificity of trimming of MHC class I-presented peptides in the endoplasmic reticulum*. J Immunol, 2009. **183**(9): p. 5526-36.
127. Chang, S.C., et al., *The ER aminopeptidase, ERAP1, trims precursors to lengths of MHC class I peptides by a "molecular ruler" mechanism*. Proc Natl Acad Sci U S A, 2005. **102**(47): p. 17107-12.
128. Evnouchidou, I., et al., *The internal sequence of the peptide-substrate determines its N-terminus trimming by ERAP1*. PLoS One, 2008. **3**(11): p. e3658.
129. Aldhamen, Y.A., et al., *Endoplasmic reticulum aminopeptidase-1 functions regulate key aspects of the innate immune response*. PLoS One, 2013. **8**(7): p. e69539.
130. Aldhamen, Y.A., et al., *Autoimmune disease-associated variants of extracellular endoplasmic reticulum aminopeptidase 1 induce altered innate immune responses by human immune cells*. J Innate Immun, 2015. **7**(3): p. 275-89.
131. Pepelyayeva, Y., et al., *ERAP1 deficient mice have reduced Type 1 regulatory T cells and develop skeletal and intestinal features of Ankylosing Spondylitis*. Sci Rep, 2018. **8**(1): p. 12464.
132. Constantinescu, C.S., et al., *Experimental autoimmune encephalomyelitis (EAE) as a model for multiple sclerosis (MS)*. Br J Pharmacol, 2011. **164**(4): p. 1079-106.

133. Lassmann, H. and M. Bradl, *Multiple sclerosis: experimental models and reality*. Acta Neuropathol, 2017. **133**(2): p. 223-244.
134. Kugler, S., et al., *Pertussis toxin transiently affects barrier integrity, organelle organization and transmigration of monocytes in a human brain microvascular endothelial cell barrier model*. Cell Microbiol, 2007. **9**(3): p. 619-32.
135. Mundt, S., et al., *Conventional DCs sample and present myelin antigens in the healthy CNS and allow parenchymal T cell entry to initiate neuroinflammation*. Sci Immunol, 2019. **4**(31).
136. Salama, S., et al., *MOG antibody-associated encephalomyelitis/encephalitis*. Mult Scler, 2019. **25**(11): p. 1427-1433.
137. Yu, X. and F. Petersen, *A methodological review of induced animal models of autoimmune diseases*. Autoimmun Rev, 2018. **17**(5): p. 473-479.
138. Schmitz, K., G. Geisslinger, and I. Tegeder, *Monoclonal Antibodies in Preclinical EAE Models of Multiple Sclerosis: A Systematic Review*. Int J Mol Sci, 2017. **18**(9).
139. Lyons, J.A., et al., *B cells are critical to induction of experimental allergic encephalomyelitis by protein but not by a short encephalitogenic peptide*. Eur J Immunol, 1999. **29**(11): p. 3432-9.
140. Pierson, E.R., I.M. Stromnes, and J.M. Goverman, *B cells promote induction of experimental autoimmune encephalomyelitis by facilitating reactivation of T cells in the central nervous system*. J Immunol, 2014. **192**(3): p. 929-39.
141. Katlama, C., et al., *Barriers to a cure for HIV: new ways to target and eradicate HIV-1 reservoirs*. Lancet, 2013. **381**(9883): p. 2109-17.
142. Cardoso, S.W., et al., *Aging with HIV: a practical review*. Braz J Infect Dis, 2013. **17**(4): p. 464-79.
143. Sereti, I. and M. Altfeld, *Immune activation and HIV: an enduring relationship*. Curr Opin HIV AIDS, 2016. **11**(2): p. 129-30.
144. Hong, S. and W.A. Banks, *Role of the immune system in HIV-associated neuroinflammation and neurocognitive implications*. Brain Behav Immun, 2015. **45**: p. 1-12.
145. Rho, M.B., et al., *A potential role for interferon-alpha in the pathogenesis of HIV-associated dementia*. Brain Behav Immun, 1995. **9**(4): p. 366-77.
146. Sas, A.R., et al., *Interferon-alpha causes neuronal dysfunction in encephalitis*. J Neurosci, 2009. **29**(12): p. 3948-55.

147. French, M.A., et al., *Plasma levels of cytokines and chemokines and the risk of mortality in HIV-infected individuals: a case-control analysis nested in a large clinical trial*. AIDS, 2015. **29**(7): p. 847-51.
148. Pulliam, L., et al., *A peripheral monocyte interferon phenotype in HIV infection correlates with a decrease in magnetic resonance spectroscopy metabolite concentrations*. AIDS, 2011. **25**(14): p. 1721-6.
149. Rizzo, M.D., et al., *HIV-infected cannabis users have lower circulating CD16+ monocytes and IFN-gamma-inducible protein 10 levels compared with nonusing HIV patients*. AIDS, 2018. **32**(4): p. 419-429.
150. Arico, E., et al., *Concomitant detection of IFNalpha signature and activated monocyte/dendritic cell precursors in the peripheral blood of IFNalpha-treated subjects at early times after repeated local cytokine treatments*. J Transl Med, 2011. **9**: p. 67.
151. McNab, F., et al., *Type I interferons in infectious disease*. Nat Rev Immunol, 2015. **15**(2): p. 87-103.
152. Ploquin, M.J., et al., *Elevated Basal Pre-infection CXCL10 in Plasma and in the Small Intestine after Infection Are Associated with More Rapid HIV/SIV Disease Onset*. PLoS Pathog, 2016. **12**(8): p. e1005774.
153. Ramirez, L.A., et al., *High IP-10 levels decrease T cell function in HIV-1-infected individuals on ART*. J Leukoc Biol, 2014. **96**(6): p. 1055-63.
154. Mehla, R., et al., *Programming of neurotoxic cofactor CXCL-10 in HIV-1-associated dementia: abrogation of CXCL-10-induced neuro-glial toxicity in vitro by PKC activator*. J Neuroinflammation, 2012. **9**: p. 239.
155. van Marle, G., et al., *Human immunodeficiency virus type 1 Nef protein mediates neural cell death: a neurotoxic role for IP-10*. Virology, 2004. **329**(2): p. 302-18.
156. Sui, Y., et al., *CXCL10-induced cell death in neurons: role of calcium dysregulation*. Eur J Neurosci, 2006. **23**(4): p. 957-64.
157. Kamat, A., et al., *A plasma biomarker signature of immune activation in HIV patients on antiretroviral therapy*. PLoS One, 2012. **7**(2): p. e30881.
158. Lee, M., et al., *Neurotoxic factors released by stimulated human monocytes and THP-1 cells*. Brain Res, 2011. **1400**: p. 99-111.
159. Perez-Quintero, L.A., et al., *EAT-2, a SAP-like adaptor, controls NK cell activation through phospholipase Cgamma, Ca⁺⁺, and Erk, leading to granule polarization*. J Exp Med, 2014. **211**(4): p. 727-42.

160. Hsi, E.D., et al., *CS1, a potential new therapeutic antibody target for the treatment of multiple myeloma*. Clin Cancer Res, 2008. **14**(9): p. 2775-84.
161. Wang, C., et al., *In vitro characterization of the anti-PD-1 antibody nivolumab, BMS-936558, and in vivo toxicology in non-human primates*. Cancer Immunol Res, 2014. **2**(9): p. 846-56.
162. Henriquez, J.E., et al., *Delta9-Tetrahydrocannabinol Suppresses Secretion of IFNalpha by Plasmacytoid Dendritic Cells From Healthy and HIV-Infected Individuals*. J Acquir Immune Defic Syndr, 2017. **75**(5): p. 588-596.
163. Simmons, R.P., et al., *HIV-1 infection induces strong production of IP-10 through TLR7/9-dependent pathways*. AIDS, 2013. **27**(16): p. 2505-17.
164. Kim, J.R., et al., *CS1 (SLAMF7) inhibits production of proinflammatory cytokines by activated monocytes*. Inflamm Res, 2013. **62**(8): p. 765-72.
165. Wong, K.L., et al., *The three human monocyte subsets: implications for health and disease*. Immunol Res, 2012. **53**(1-3): p. 41-57.
166. Ziegler-Heitbrock, L., *The CD14+ CD16+ blood monocytes: their role in infection and inflammation*. J Leukoc Biol, 2007. **81**(3): p. 584-92.
167. Ellery, P.J., et al., *The CD16+ monocyte subset is more permissive to infection and preferentially harbors HIV-1 in vivo*. J Immunol, 2007. **178**(10): p. 6581-9.
168. Tuttle, D.L., et al., *Expression of CCR5 increases during monocyte differentiation and directly mediates macrophage susceptibility to infection by human immunodeficiency virus type 1*. J Virol, 1998. **72**(6): p. 4962-9.
169. Stoddart, C.A., M.E. Keir, and J.M. McCune, *IFN-alpha-induced upregulation of CCR5 leads to expanded HIV tropism in vivo*. PLoS Pathog, 2010. **6**(2): p. e1000766.
170. Gonzalez, E., et al., *The influence of CCL3L1 gene-containing segmental duplications on HIV-1/AIDS susceptibility*. Science, 2005. **307**(5714): p. 1434-40.
171. Dolan, M.J., et al., *CCL3L1 and CCR5 influence cell-mediated immunity and affect HIV-AIDS pathogenesis via viral entry-independent mechanisms*. Nat Immunol, 2007. **8**(12): p. 1324-36.
172. Niklas Hagberg, J.T., Gunnar V Alm, Maija-Leena Eloranta, Yenan Bryceson and Lars Rönnblom, *SLE immune complexes upregulate the expression of slamf7 (cd319) on plasmacytoid dendritic cells*. Annals of Rheumatic Disease, 2012. **71**(Supplement 1): p. A3.

173. Walsh, A.M., et al., *Triple DMARD treatment in early rheumatoid arthritis modulates synovial T cell activation and plasmablast/plasma cell differentiation pathways*. PLoS One, 2017. **12**(9): p. e0183928.
174. Jordan S Mizrahi, J.J.P., Raturaj Masvaker and Bibi Bielekova, *Role of SLAMF immunoregulatory molecules in MS disease processes*. The journal of immunology, 2017. **198**(Supplement 1): p. 55.
175. L. de Graaf, K.H.K.-V., Marie; Fischer, Nicolas, *Therapeutic Targeting of Chemokines with Monoclonal Antibodies*. Current Immunology Reviews, 2012. **8**(2): p. 141-148.
176. Yellin, M., et al., *A phase II, randomized, double-blind, placebo-controlled study evaluating the efficacy and safety of MDX-1100, a fully human anti-CXCL10 monoclonal antibody, in combination with methotrexate in patients with rheumatoid arthritis*. Arthritis Rheum, 2012. **64**(6): p. 1730-9.
177. Mayer, L., et al., *Anti-IP-10 antibody (BMS-936557) for ulcerative colitis: a phase II randomised study*. Gut, 2014. **63**(3): p. 442-50.
178. Solari, R., J.E. Pease, and M. Begg, *"Chemokine receptors as therapeutic targets: Why aren't there more drugs?"*. Eur J Pharmacol, 2015. **746**: p. 363-7.
179. Schall, T.J. and A.E. Proudfoot, *Overcoming hurdles in developing successful drugs targeting chemokine receptors*. Nat Rev Immunol, 2011. **11**(5): p. 355-63.
180. Laragione, T., et al., *CXCL10 and its receptor CXCR3 regulate synovial fibroblast invasion in rheumatoid arthritis*. Arthritis Rheum, 2011. **63**(11): p. 3274-83.
181. Shimada, A., et al., *The role of the CXCL10/CXCR3 system in type 1 diabetes*. Rev Diabet Stud, 2009. **6**(2): p. 81-4.
182. Okamoto, H., et al., *Interferon-inducible protein 10/CXCL10 is increased in the cerebrospinal fluid of patients with central nervous system lupus*. Arthritis Rheum, 2004. **50**(11): p. 3731-2.
183. Bonechi, E., et al., *Increased CXCL10 expression in MS MSCs and monocytes is unaffected by AHSCT*. Ann Clin Transl Neurol, 2014. **1**(9): p. 650-8.
184. Zhao, Q., et al., *A novel function of CXCL10 in mediating monocyte production of proinflammatory cytokines*. J Leukoc Biol, 2017. **102**(5): p. 1271-1280.
185. Zhang, W., et al., *The role of CXCR3 in the induction of primary biliary cirrhosis*. Clin Dev Immunol, 2011. **2011**: p. 564062.

186. Feng, A.L., et al., *CD16+ monocytes in breast cancer patients: expanded by monocyte chemoattractant protein-1 and may be useful for early diagnosis*. Clin Exp Immunol, 2011. **164**(1): p. 57-65.
187. Mukherjee, R., et al., *Non-Classical monocytes display inflammatory features: Validation in Sepsis and Systemic Lupus Erythematosus*. Sci Rep, 2015. **5**: p. 13886.
188. Chuluundorj, D., et al., *Expansion and preferential activation of the CD14(+)CD16(+) monocyte subset during multiple sclerosis*. Immunol Cell Biol, 2014. **92**(6): p. 509-17.
189. Giri, M.S., et al., *Circulating monocytes in HIV-1-infected viremic subjects exhibit an antiapoptosis gene signature and virus- and host-mediated apoptosis resistance*. J Immunol, 2009. **182**(7): p. 4459-70.
190. Lopalco, L., *CCR5: From Natural Resistance to a New Anti-HIV Strategy*. Viruses, 2010. **2**(2): p. 574-600.
191. Hensley-McBain, T. and N.R. Klatt, *The Dual Role of Neutrophils in HIV Infection*. Curr HIV/AIDS Rep, 2018. **15**(1): p. 1-10.
192. Makinde, H.M., et al., *Nonclassical Monocytes Mediate Secondary Injury, Neurocognitive Outcome, and Neutrophil Infiltration after Traumatic Brain Injury*. J Immunol, 2017. **199**(10): p. 3583-3591.
193. Mrdjen, D., et al., *High-Dimensional Single-Cell Mapping of Central Nervous System Immune Cells Reveals Distinct Myeloid Subsets in Health, Aging, and Disease*. Immunity, 2018. **48**(2): p. 380-395 e6.
194. Anzinger, J.J., et al., *Monocytes as regulators of inflammation and HIV-related comorbidities during cART*. J Immunol Res, 2014. **2014**: p. 569819.
195. Merino, K.M., et al., *Role of Monocyte/Macrophages during HIV/SIV Infection in Adult and Pediatric Acquired Immune Deficiency Syndrome*. Front Immunol, 2017. **8**: p. 1693.
196. Andrews, L.P., H. Yano, and D.A.A. Vignali, *Inhibitory receptors and ligands beyond PD-1, PD-L1 and CTLA-4: breakthroughs or backups*. Nat Immunol, 2019. **20**(11): p. 1425-1434.
197. Blank, C.U., et al., *Defining 'T cell exhaustion'*. Nat Rev Immunol, 2019. **19**(11): p. 665-674.
198. Philip, M. and A. Schietinger, *Heterogeneity and fate choice: T cell exhaustion in cancer and chronic infections*. Curr Opin Immunol, 2019. **58**: p. 98-103.
199. Hanahan, D. and R.A. Weinberg, *Hallmarks of cancer: the next generation*. Cell, 2011. **144**(5): p. 646-74.

200. Pauken, K.E. and E.J. Wherry, *Overcoming T cell exhaustion in infection and cancer*. Trends Immunol, 2015. **36**(4): p. 265-76.
201. Thommen, D.S. and T.N. Schumacher, *T Cell Dysfunction in Cancer*. Cancer Cell, 2018. **33**(4): p. 547-562.
202. Sen, D.R., et al., *The epigenetic landscape of T cell exhaustion*. Science, 2016. **354**(6316): p. 1165-1169.
203. Philip, M., et al., *Chromatin states define tumour-specific T cell dysfunction and reprogramming*. Nature, 2017. **545**(7655): p. 452-456.
204. Haslam, A. and V. Prasad, *Estimation of the Percentage of US Patients With Cancer Who Are Eligible for and Respond to Checkpoint Inhibitor Immunotherapy Drugs*. JAMA Netw Open, 2019. **2**(5): p. e192535.
205. Soldatos, T.G., et al., *Retrospective Side Effect Profiling of the Metastatic Melanoma Combination Therapy Ipilimumab-Nivolumab Using Adverse Event Data*. Diagnostics (Basel), 2018. **8**(4).
206. Zhou, S., S. Khanal, and H. Zhang, *Risk of immune-related adverse events associated with ipilimumab-plus-nivolumab and nivolumab therapy in cancer patients*. Ther Clin Risk Manag, 2019. **15**: p. 211-221.
207. Cortes, A., et al., *Association study of genes related to bone formation and resorption and the extent of radiographic change in ankylosing spondylitis*. Ann Rheum Dis, 2015. **74**(7): p. 1387-93.
208. Kotecha, R.R., R.J. Motzer, and M.H. Voss, *Towards individualized therapy for metastatic renal cell carcinoma*. Nat Rev Clin Oncol, 2019. **16**(10): p. 621-633.
209. Chevrier, S., et al., *An Immune Atlas of Clear Cell Renal Cell Carcinoma*. Cell, 2017. **169**(4): p. 736-749 e18.
210. Senbabaoglu, Y., et al., *Tumor immune microenvironment characterization in clear cell renal cell carcinoma identifies prognostic and immunotherapeutically relevant messenger RNA signatures*. Genome Biol, 2016. **17**(1): p. 231.
211. Remark, R., et al., *Characteristics and clinical impacts of the immune environments in colorectal and renal cell carcinoma lung metastases: influence of tumor origin*. Clin Cancer Res, 2013. **19**(15): p. 4079-91.
212. Giraldo, N.A., et al., *Orchestration and Prognostic Significance of Immune Checkpoints in the Microenvironment of Primary and Metastatic Renal Cell Cancer*. Clin Cancer Res, 2015. **21**(13): p. 3031-40.

213. Jiang, P., et al., *Signatures of T cell dysfunction and exclusion predict cancer immunotherapy response*. Nat Med, 2018. **24**(10): p. 1550-1558.
214. Motzer, R.J., et al., *Nivolumab plus Ipilimumab versus Sunitinib in Advanced Renal-Cell Carcinoma*. N Engl J Med, 2018. **378**(14): p. 1277-1290.
215. O'Connell, P., A. Amalfitano, and Y.A. Aldhamen, *SLAM Family Receptor Signaling in Viral Infections: HIV and Beyond*. Vaccines (Basel), 2019. **7**(4).
216. O'Connell, P., et al., *SLAMF7 Is a Critical Negative Regulator of IFN-alpha-Mediated CXCL10 Production in Chronic HIV Infection*. J Immunol, 2019. **202**(1): p. 228-238.
217. Yigit, B., et al., *SLAMF6 as a Regulator of Exhausted CD8(+) T Cells in Cancer*. Cancer Immunol Res, 2019. **7**(9): p. 1485-1496.
218. Sade-Feldman, M., et al., *Defining T Cell States Associated with Response to Checkpoint Immunotherapy in Melanoma*. Cell, 2018. **175**(4): p. 998-1013 e20.
219. Kurtulus, S., et al., *Checkpoint Blockade Immunotherapy Induces Dynamic Changes in PD-1(-)CD8(+) Tumor-Infiltrating T Cells*. Immunity, 2019. **50**(1): p. 181-194 e6.
220. O'Connell, P., Zheng, Y.H., Amalfitano, A., Aldhamen, Y. A., *In vitro Infection of Primary Human Monocytes with HIV-1*. bio-protocol, 2019. **9**(13).
221. Liu, J., et al., *An Integrated TCGA Pan-Cancer Clinical Data Resource to Drive High-Quality Survival Outcome Analytics*. Cell, 2018. **173**(2): p. 400-416 e11.
222. Roederer, M., J.L. Nozzi, and M.C. Nason, *SPICE: exploration and analysis of post-cytometric complex multivariate datasets*. Cytometry A, 2011. **79**(2): p. 167-74.
223. Van Gassen, S., et al., *FlowSOM: Using self-organizing maps for visualization and interpretation of cytometry data*. Cytometry A, 2015. **87**(7): p. 636-45.
224. Shin, H., et al., *A role for the transcriptional repressor Blimp-1 in CD8(+) T cell exhaustion during chronic viral infection*. Immunity, 2009. **31**(2): p. 309-20.
225. Shankar, E.M., et al., *Expression of a broad array of negative costimulatory molecules and Blimp-1 in T cells following priming by HIV-1 pulsed dendritic cells*. Mol Med, 2011. **17**(3-4): p. 229-40.
226. He, S., et al., *Ezh2 phosphorylation state determines its capacity to maintain CD8(+) T memory precursors for antitumor immunity*. Nat Commun, 2017. **8**(1): p. 2125.
227. Balkhi, M.Y., et al., *YY1 Upregulates Checkpoint Receptors and Downregulates Type I Cytokines in Exhausted, Chronically Stimulated Human T Cells*. iScience, 2018. **2**: p. 105-122.

228. Sakuishi, K., et al., *TIM3(+)*FOXP3(+) regulatory T cells are tissue-specific promoters of T-cell dysfunction in cancer. *Oncoimmunology*, 2013. **2**(4): p. e23849.
229. Kamada, T., et al., *PD-1(+)* regulatory T cells amplified by PD-1 blockade promote hyperprogression of cancer. *Proc Natl Acad Sci U S A*, 2019. **116**(20): p. 9999-10008.
230. Perez, O.D., et al., *Multiparameter analysis of intracellular phosphoepitopes in immunophenotyped cell populations by flow cytometry*. *Curr Protoc Cytom*, 2005. **Chapter 6**: p. Unit 6 20.
231. Mita, Y., et al., *Crucial role of CD69 in anti-tumor immunity through regulating the exhaustion of tumor-infiltrating T cells*. *Int Immunol*, 2018. **30**(12): p. 559-567.
232. Hofer, T., O. Krichevsky, and G. Altan-Bonnet, *Competition for IL-2 between Regulatory and Effector T Cells to Chisel Immune Responses*. *Front Immunol*, 2012. **3**: p. 268.
233. Beltra, J.C., et al., *IL2Rbeta-dependent signals drive terminal exhaustion and suppress memory development during chronic viral infection*. *Proc Natl Acad Sci U S A*, 2016. **113**(37): p. E5444-53.
234. Zorn, E., et al., *IL-2 regulates FOXP3 expression in human CD4+CD25+ regulatory T cells through a STAT-dependent mechanism and induces the expansion of these cells in vivo*. *Blood*, 2006. **108**(5): p. 1571-9.
235. Banerjee, H. and L.P. Kane, *Immune regulation by Tim-3*. *F1000Res*, 2018. **7**: p. 316.
236. Dannenmann, S.R., et al., *Tumor-associated macrophages subvert T-cell function and correlate with reduced survival in clear cell renal cell carcinoma*. *Oncoimmunology*, 2013. **2**(3): p. e23562.
237. Chapuis, A.G., et al., *Transferred melanoma-specific CD8+ T cells persist, mediate tumor regression, and acquire central memory phenotype*. *Proc Natl Acad Sci U S A*, 2012. **109**(12): p. 4592-7.
238. Alfei, F., et al., *TOX reinforces the phenotype and longevity of exhausted T cells in chronic viral infection*. *Nature*, 2019. **571**(7764): p. 265-269.
239. Khan, O., et al., *TOX transcriptionally and epigenetically programs CD8(+) T cell exhaustion*. *Nature*, 2019. **571**(7764): p. 211-218.
240. Scott, A.C., et al., *TOX is a critical regulator of tumour-specific T cell differentiation*. *Nature*, 2019. **571**(7764): p. 270-274.
241. Beltra, J.C., et al., *Developmental Relationships of Four Exhausted CD8(+) T Cell Subsets Reveals Underlying Transcriptional and Epigenetic Landscape Control Mechanisms*. *Immunity*, 2020. **52**(5): p. 825-841 e8.

242. Johnson, D.E., R.A. O'Keefe, and J.R. Grandis, *Targeting the IL-6/JAK/STAT3 signalling axis in cancer*. Nat Rev Clin Oncol, 2018. **15**(4): p. 234-248.
243. Kim, E., et al., *Phosphorylation of EZH2 activates STAT3 signaling via STAT3 methylation and promotes tumorigenicity of glioblastoma stem-like cells*. Cancer Cell, 2013. **23**(6): p. 839-52.
244. Katsuyama, E., et al., *The CD38/NAD/SIRTUIN1/EZH2 Axis Mitigates Cytotoxic CD8 T Cell Function and Identifies Patients with SLE Prone to Infections*. Cell Rep, 2020. **30**(1): p. 112-123 e4.
245. Bally, A.P., J.W. Austin, and J.M. Boss, *Genetic and Epigenetic Regulation of PD-1 Expression*. J Immunol, 2016. **196**(6): p. 2431-7.
246. Dongre, P., et al., *YY1 and a unique DNA repeat element regulates the transcription of mouse CS1 (CD319, SLAMF7) gene*. Mol Immunol, 2013. **54**(3-4): p. 254-63.
247. Kim, J.R., S.O. Mathew, and P.A. Mathew, *Blimp-1/PRDM1 regulates the transcription of human CS1 (SLAMF7) gene in NK and B cells*. Immunobiology, 2016. **221**(1): p. 31-9.
248. Comte, D., et al., *Signaling Lymphocytic Activation Molecule Family Member 7 Engagement Restores Defective Effector CD8+ T Cell Function in Systemic Lupus Erythematosus*. Arthritis Rheumatol, 2017. **69**(5): p. 1035-1044.
249. Murciano-Goroff, Y.R., A.B. Warner, and J.D. Wolchok, *The future of cancer immunotherapy: microenvironment-targeting combinations*. Cell Res, 2020. **30**(6): p. 507-519.
250. Waldman, A.D., J.M. Fritz, and M.J. Lenardo, *A guide to cancer immunotherapy: from T cell basic science to clinical practice*. Nat Rev Immunol, 2020. **20**(11): p. 651-668.
251. Young, A., Z. Quandt, and J.A. Bluestone, *The Balancing Act between Cancer Immunity and Autoimmunity in Response to Immunotherapy*. Cancer Immunol Res, 2018. **6**(12): p. 1445-1452.
252. Barreto, L., et al., *Resistance to Checkpoint Inhibition in Cancer Immunotherapy*. Transl Oncol, 2020. **13**(3): p. 100738.
253. Morse, M.A., et al., *Novel adenoviral vector induces T-cell responses despite anti-adenoviral neutralizing antibodies in colorectal cancer patients*. Cancer Immunol Immunother, 2013. **62**(8): p. 1293-301.
254. Shaw, A.R. and M. Suzuki, *Immunology of Adenoviral Vectors in Cancer Therapy*. Mol Ther Methods Clin Dev, 2019. **15**: p. 418-429.

255. O'Connell, P., et al., *SLAMF7 Signaling Reprograms T Cells toward Exhaustion in the Tumor Microenvironment*. J Immunol, 2021. **206**(1): p. 193-205.
256. Aldhamen, Y.A., et al., *CRACC-targeting Fc-fusion protein induces activation of NK cells and DCs and improves T cell immune responses to antigenic targets*. Vaccine, 2016. **34**(27): p. 3109-3118.
257. Reilly, R.M., et al., *Problems of delivery of monoclonal antibodies. Pharmaceutical and pharmacokinetic solutions*. Clin Pharmacokinet, 1995. **28**(2): p. 126-42.
258. Samaranyake, H., et al., *Challenges in monoclonal antibody-based therapies*. Ann Med, 2009. **41**(5): p. 322-31.
259. Watanabe, H., et al., *Innate immune response in Th1- and Th2-dominant mouse strains*. Shock, 2004. **22**(5): p. 460-6.
260. Maier, B., et al., *A conserved dendritic-cell regulatory program limits antitumour immunity*. Nature, 2020. **580**(7802): p. 257-262.
261. Culos, A., et al., *Integration of mechanistic immunological knowledge into a machine learning pipeline improves predictions*. Nat Mach Intell, 2020. **2**(10): p. 619-628.
262. Jorgovanovic, D., et al., *Roles of IFN-gamma in tumor progression and regression: a review*. Biomark Res, 2020. **8**: p. 49.
263. Hegde, S., A.M. Leader, and M. Merad, *MDSC: Markers, development, states, and unaddressed complexity*. Immunity, 2021. **54**(5): p. 875-884.
264. Scodeller, P., et al., *Precision Targeting of Tumor Macrophages with a CD206 Binding Peptide*. Sci Rep, 2017. **7**(1): p. 14655.
265. Feng, Q., et al., *Tumor-associated Macrophages as Prognostic and Predictive Biomarkers for Postoperative Adjuvant Chemotherapy in Patients with Stage II Colon Cancer*. Clin Cancer Res, 2019. **25**(13): p. 3896-3907.
266. Tugues, S., et al., *New insights into IL-12-mediated tumor suppression*. Cell Death Differ, 2015. **22**(2): p. 237-46.
267. Fuertes, M.B., et al., *Type I interferon response and innate immune sensing of cancer*. Trends Immunol, 2013. **34**(2): p. 67-73.
268. Musella, M., et al., *Type-I-interferons in infection and cancer: Unanticipated dynamics with therapeutic implications*. Oncoimmunology, 2017. **6**(5): p. e1314424.

269. Way, S.S., et al., *IL-12 and type-I IFN synergize for IFN-gamma production by CD4 T cells, whereas neither are required for IFN-gamma production by CD8 T cells after Listeria monocytogenes infection*. J Immunol, 2007. **178**(7): p. 4498-505.
270. Melero, I., et al., *IL-12 gene therapy for cancer: in synergy with other immunotherapies*. Trends Immunol, 2001. **22**(3): p. 113-5.
271. Fitzgerald-Bocarsly, P., J. Dai, and S. Singh, *Plasmacytoid dendritic cells and type I IFN: 50 years of convergent history*. Cytokine Growth Factor Rev, 2008. **19**(1): p. 3-19.
272. Quatrini, L., et al., *The Immune Checkpoint PD-1 in Natural Killer Cells: Expression, Function and Targeting in Tumour Immunotherapy*. Cancers (Basel), 2020. **12**(11).
273. Jager, L., et al., *A rapid protocol for construction and production of high-capacity adenoviral vectors*. Nat Protoc, 2009. **4**(4): p. 547-64.
274. Herr, W., et al., *Mature dendritic cells pulsed with freeze-thaw cell lysates define an effective in vitro vaccine designed to elicit EBV-specific CD4(+) and CD8(+) T lymphocyte responses*. Blood, 2000. **96**(5): p. 1857-64.
275. Alyaqoub, F.S., et al., *In Vivo Synthesis of Cyclic-di-GMP Using a Recombinant Adenovirus Preferentially Improves Adaptive Immune Responses against Extracellular Antigens*. J Immunol, 2016.
276. Chevrier, S., et al., *Compensation of Signal Spillover in Suspension and Imaging Mass Cytometry*. Cell Syst, 2018. **6**(5): p. 612-620 e5.
277. Tan, Y.S. and Y.L. Lei, *Isolation of Tumor-Infiltrating Lymphocytes by Ficoll-Paque Density Gradient Centrifugation*. Methods Mol Biol, 2019. **1960**: p. 93-99.
278. DeTomaso, D., et al., *Functional interpretation of single cell similarity maps*. Nat Commun, 2019. **10**(1): p. 4376.
279. Appledorn, D.M., et al., *A new adenovirus based vaccine vector expressing an Eimeria tenella derived TLR agonist improves cellular immune responses to an antigenic target*. PLoS One, 2010. **5**(3): p. e9579.
280. Seregin, S.S., et al., *Adenovirus capsid-display of the retro-oriented human complement inhibitor DAF reduces Ad vector-triggered immune responses in vitro and in vivo*. Blood, 2010. **116**(10): p. 1669-77.
281. Seregin, S.S., et al., *beta-Arrestins modulate Adenovirus-vector-induced innate immune responses: differential regulation by beta-arrestin-1 and beta-arrestin-2*. Virus Res, 2010. **147**(1): p. 123-34.

282. Aldhamen, Y.A., S.S. Seregin, and A. Amalfitano, *Immune recognition of gene transfer vectors: focus on adenovirus as a paradigm*. *Front Immunol*, 2011. **2**: p. 40.
283. Appledorn, D.M., et al., *Sublingual administration of an adenovirus serotype 5 (Ad5)-based vaccine confirms Toll-like receptor agonist activity in the oral cavity and elicits improved mucosal and systemic cell-mediated responses against HIV antigens despite preexisting Ad5 immunity*. *Clin Vaccine Immunol*, 2011. **18**(1): p. 150-60.
284. Koestler, B.J., et al., *Stimulation of innate immunity by in vivo cyclic di-GMP synthesis using adenovirus*. *Clin Vaccine Immunol*, 2014. **21**(11): p. 1550-9.
285. Quiroga, D., et al., *Decreased Vector Gene Expression from E2b Gene-Deleted Adenovirus Serotype 5 Vaccines Intensifies Proinflammatory Immune Responses*. *Clin Vaccine Immunol*, 2017. **24**(6).
286. Weber, L., *diffcyt: Differential discovery in high-dimensional cytometry via high-resolution clustering*. 2020: Bioconductor. p. R package.
287. Hirst, C., et al., *Contribution of relapses to disability in multiple sclerosis*. *J Neurol*, 2008. **255**(2): p. 280-7.
288. Murray, T.J., *The history of multiple sclerosis: the changing frame of the disease over the centuries*. *J Neurol Sci*, 2009. **277 Suppl 1**: p. S3-8.
289. Olsson, T., L.F. Barcellos, and L. Alfredsson, *Interactions between genetic, lifestyle and environmental risk factors for multiple sclerosis*. *Nat Rev Neurol*, 2017. **13**(1): p. 25-36.
290. Bergthaler, A. and J. Menche, *The immune system as a social network*. *Nat Immunol*, 2017. **18**(5): p. 481-482.
291. Kveler, K., et al., *Immune-centric network of cytokines and cells in disease context identified by computational mining of PubMed*. *Nat Biotechnol*, 2018. **36**(7): p. 651-659.
292. Filipi, M. and S. Jack, *Interferons in the Treatment of Multiple Sclerosis: A Clinical Efficacy, Safety, and Tolerability Update*. *Int J MS Care*, 2020. **22**(4): p. 165-172.
293. Voge, N.V. and E. Alvarez, *Monoclonal Antibodies in Multiple Sclerosis: Present and Future*. *Biomedicines*, 2019. **7**(1).
294. Syed, Y.Y., *Ocrelizumab: A Review in Multiple Sclerosis*. *CNS Drugs*, 2018. **32**(9): p. 883-890.
295. Hauser, S.L., et al., *Ocrelizumab versus Interferon Beta-1a in Relapsing Multiple Sclerosis*. *N Engl J Med*, 2017. **376**(3): p. 221-234.

296. Niewold, P., et al., *Evaluating spectral cytometry for immune profiling in viral disease*. Cytometry A, 2020. **97**(11): p. 1165-1179.
297. Yadav, S.K., et al., *Advances in the immunopathogenesis of multiple sclerosis*. Curr Opin Neurol, 2015. **28**(3): p. 206-19.
298. Milovanovic, J., et al., *Interleukin-17 in Chronic Inflammatory Neurological Diseases*. Front Immunol, 2020. **11**: p. 947.
299. Hammond, T.R., et al., *Single-Cell RNA Sequencing of Microglia throughout the Mouse Lifespan and in the Injured Brain Reveals Complex Cell-State Changes*. Immunity, 2019. **50**(1): p. 253-271 e6.
300. Deczkowska, A., et al., *Disease-Associated Microglia: A Universal Immune Sensor of Neurodegeneration*. Cell, 2018. **173**(5): p. 1073-1081.
301. Petereit, H.F., et al., *Low interleukin-10 production is associated with higher disability and MRI lesion load in secondary progressive multiple sclerosis*. J Neurol Sci, 2003. **206**(2): p. 209-14.
302. Ersoy, E., et al., *The effects of interferon-beta on interleukin-10 in multiple sclerosis patients*. Eur J Neurol, 2005. **12**(3): p. 208-11.
303. Zhang, X., et al., *IL-10 is involved in the suppression of experimental autoimmune encephalomyelitis by CD25+CD4+ regulatory T cells*. Int Immunol, 2004. **16**(2): p. 249-56.
304. Wei, Y., et al., *Low Serum Interleukin-10 Is an Independent Predictive Factor for the Risk of Second Event in Clinically Isolated Syndromes*. Front Neurol, 2019. **10**: p. 604.
305. Clark, S.E., et al., *NK Cell IL-10 Production Requires IL-15 and IL-10 Driven STAT3 Activation*. Front Immunol, 2019. **10**: p. 2087.
306. Hedrich, C.M., et al., *Stat3 promotes IL-10 expression in lupus T cells through trans-activation and chromatin remodeling*. Proc Natl Acad Sci U S A, 2014. **111**(37): p. 13457-62.
307. Madan, R., et al., *Nonredundant roles for B cell-derived IL-10 in immune counter-regulation*. J Immunol, 2009. **183**(4): p. 2312-20.
308. Boyden, A.W., A.A. Brate, and N.J. Karandikar, *Novel B cell-dependent multiple sclerosis model using extracellular domains of myelin proteolipid protein*. Sci Rep, 2020. **10**(1): p. 5011.
309. Parker Harp, C.R., et al., *B cell antigen presentation is sufficient to drive neuroinflammation in an animal model of multiple sclerosis*. J Immunol, 2015. **194**(11): p. 5077-84.

310. Wu, G.F., et al., *Limited sufficiency of antigen presentation by dendritic cells in models of central nervous system autoimmunity*. J Autoimmun, 2011. **36**(1): p. 56-64.
311. Liu, G., et al., *Unique B cell responses in B cell-dependent and B cell-independent EAE*. Autoimmunity, 2012. **45**(3): p. 199-209.
312. Ray, A., et al., *Mature IgD(low/-) B cells maintain tolerance by promoting regulatory T cell homeostasis*. Nat Commun, 2019. **10**(1): p. 190.
313. Blanc, P., et al., *Mature IgM-expressing plasma cells sense antigen and develop competence for cytokine production upon antigenic challenge*. Nat Commun, 2016. **7**: p. 13600.
314. Reynaud, C.A., et al., *IgM memory B cells: a mouse/human paradox*. Cell Mol Life Sci, 2012. **69**(10): p. 1625-34.
315. Weill, J.C. and C.A. Reynaud, *IgM memory B cells: specific effectors of innate-like and adaptive responses*. Curr Opin Immunol, 2020. **63**: p. 1-6.
316. Cerutti, A., M. Cols, and I. Puga, *Marginal zone B cells: virtues of innate-like antibody-producing lymphocytes*. Nat Rev Immunol, 2013. **13**(2): p. 118-32.
317. Srivastava, B., et al., *Characterization of marginal zone B cell precursors*. J Exp Med, 2005. **202**(9): p. 1225-34.
318. Shaffer, A.L., et al., *Blimp-1 orchestrates plasma cell differentiation by extinguishing the mature B cell gene expression program*. Immunity, 2002. **17**(1): p. 51-62.
319. Hausser-Kinzel, S. and M.S. Weber, *The Role of B Cells and Antibodies in Multiple Sclerosis, Neuromyelitis Optica, and Related Disorders*. Front Immunol, 2019. **10**: p. 201.
320. Wang, Y., et al., *Elotuzumab for the treatment of multiple myeloma*. J Hematol Oncol, 2016. **9**(1): p. 55.
321. Pazina, T., et al., *The anti-SLAMF7 antibody elotuzumab mediates NK cell activation through both CD16-dependent and -independent mechanisms*. Oncoimmunology, 2017. **6**(9): p. e1339853.
322. Ginhoux, F., et al., *Fate mapping analysis reveals that adult microglia derive from primitive macrophages*. Science, 2010. **330**(6005): p. 841-5.
323. Ginhoux, F., et al., *Origin and differentiation of microglia*. Front Cell Neurosci, 2013. **7**: p. 45.

324. Van Hove, H., et al., *A single-cell atlas of mouse brain macrophages reveals unique transcriptional identities shaped by ontogeny and tissue environment*. Nat Neurosci, 2019. **22**(6): p. 1021-1035.
325. Utz, S.G., et al., *Early Fate Defines Microglia and Non-parenchymal Brain Macrophage Development*. Cell, 2020. **181**(3): p. 557-573 e18.
326. Giralt, M., A. Molinero, and J. Hidalgo, *Active Induction of Experimental Autoimmune Encephalomyelitis (EAE) with MOG35-55 in the Mouse*. Methods Mol Biol, 2018. **1791**: p. 227-232.
327. Grabert, K. and B.W. McColl, *Isolation and Phenotyping of Adult Mouse Microglial Cells*. Methods Mol Biol, 2018. **1784**: p. 77-86.
328. Lee, J.K. and M.G. Tansey, *Microglia isolation from adult mouse brain*. Methods Mol Biol, 2013. **1041**: p. 17-23.
329. Leray, E., et al., *Epidemiology of multiple sclerosis*. Rev Neurol (Paris), 2016. **172**(1): p. 3-13.
330. Compston, A. and A. Coles, *Multiple sclerosis*. Lancet, 2008. **372**(9648): p. 1502-17.
331. Ascherio, A. and K.L. Munger, *Epidemiology of Multiple Sclerosis: From Risk Factors to Prevention-An Update*. Semin Neurol, 2016. **36**(2): p. 103-14.
332. McGinley, A.M., et al., *Th17 cells, gammadelta T cells and their interplay in EAE and multiple sclerosis*. J Autoimmun, 2018.
333. Didonna, A. and J.R. Oksenberg, *The Genetics of Multiple Sclerosis*, in *Multiple Sclerosis: Perspectives in Treatment and Pathogenesis*, I.S. Zagon and P.J. McLaughlin, Editors. 2017: Brisbane (AU).
334. Guerini, F.R., et al., *A functional variant in ERAP1 predisposes to multiple sclerosis*. PLoS One, 2012. **7**(1): p. e29931.
335. Serwold, T., et al., *ERAAP customizes peptides for MHC class I molecules in the endoplasmic reticulum*. Nature, 2002. **419**(6906): p. 480-3.
336. Dixon, K.O., et al., *TIM-3 restrains anti-tumour immunity by regulating inflammasome activation*. Nature, 2021. **595**(7865): p. 101-106.
337. Ocana-Guzman, R., L. Torre-Bouscoulet, and I. Sada-Ovalle, *TIM-3 Regulates Distinct Functions in Macrophages*. Front Immunol, 2016. **7**: p. 229.
338. Wolf, Y., A.C. Anderson, and V.K. Kuchroo, *TIM3 comes of age as an inhibitory receptor*. Nat Rev Immunol, 2020. **20**(3): p. 173-185.

339. Battaglia, M., et al., *Tr1 cells: from discovery to their clinical application*. Semin Immunol, 2006. **18**(2): p. 120-7.
340. Gagliani, N., et al., *Coexpression of CD49b and LAG-3 identifies human and mouse T regulatory type 1 cells*. Nat Med, 2013. **19**(6): p. 739-46.
341. Vinay, D.S. and B.S. Kwon, *CD11c+CD8+ T cells: two-faced adaptive immune regulators*. Cell Immunol, 2010. **264**(1): p. 18-22.
342. Kitamura, D., et al., *A B cell-deficient mouse by targeted disruption of the membrane exon of the immunoglobulin mu chain gene*. Nature, 1991. **350**(6317): p. 423-6.
343. Yang, Y., et al., *T-bet is essential for encephalitogenicity of both Th1 and Th17 cells*. J Exp Med, 2009. **206**(7): p. 1549-64.
344. Damsker, J.M., A.M. Hansen, and R.R. Caspi, *Th1 and Th17 cells: adversaries and collaborators*. Ann N Y Acad Sci, 2010. **1183**: p. 211-21.
345. Schafflick, D., et al., *Integrated single cell analysis of blood and cerebrospinal fluid leukocytes in multiple sclerosis*. Nat Commun, 2020. **11**(1): p. 247.
346. Matsushita, T., et al., *Regulatory B cells inhibit EAE initiation in mice while other B cells promote disease progression*. J Clin Invest, 2008. **118**(10): p. 3420-30.
347. Reeves, E. and E. James, *The role of polymorphic ERAP1 in autoinflammatory disease*. Biosci Rep, 2018. **38**(4).
348. Kang, H.M., et al., *Multiplexed droplet single-cell RNA-sequencing using natural genetic variation*. Nat Biotechnol, 2018. **36**(1): p. 89-94.
349. Piccirillo, C.A., et al., *Translational control of immune responses: from transcripts to translates*. Nat Immunol, 2014. **15**(6): p. 503-11.
350. Ganeshan, K. and A. Chawla, *Metabolic regulation of immune responses*. Annu Rev Immunol, 2014. **32**: p. 609-34.
351. La Rocca, C., et al., *Immunometabolic profiling of T cells from patients with relapsing-remitting multiple sclerosis reveals an impairment in glycolysis and mitochondrial respiration*. Metabolism, 2017. **77**: p. 39-46.
352. Levin, L.I., et al., *Primary infection with the Epstein-Barr virus and risk of multiple sclerosis*. Ann Neurol, 2010. **67**(6): p. 824-30.
353. Morris, G., et al., *Emerging role of innate B1 cells in the pathophysiology of autoimmune and neuroimmune diseases: Association with inflammation, oxidative and nitrosative stress and autoimmune responses*. Pharmacol Res, 2019. **148**: p. 104408.

354. Peterson, L.K., I. Tsunoda, and R.S. Fujinami, *Role of CD5+ B-1 cells in EAE pathogenesis*. *Autoimmunity*, 2008. **41**(5): p. 353-62.
355. Rovituso, D., et al., *B1 cells are unaffected by immune modulatory treatment in remitting-relapsing multiple sclerosis patients*. *J Neuroimmunol*, 2014. **272**(1-2): p. 86-90.
356. Takeda, A., et al., *CD45-associated protein inhibits CD45 dimerization and up-regulates its protein tyrosine phosphatase activity*. *Blood*, 2004. **103**(9): p. 3440-7.
357. Johnson, P., et al., *CD45 (PTPRC)*, in *Encyclopedia of Signaling Molecules*, S. Choi, Editor. 2012, Springer New York: New York, NY. p. 328-334.
358. Gobel, K., T. Ruck, and S.G. Meuth, *Cytokine signaling in multiple sclerosis: Lost in translation*. *Mult Scler*, 2018. **24**(4): p. 432-439.
359. Wang, X., et al., *ER stress modulates cellular metabolism*. *Biochem J*, 2011. **435**(1): p. 285-96.
360. Oakes, S.A. and F.R. Papa, *The role of endoplasmic reticulum stress in human pathology*. *Annu Rev Pathol*, 2015. **10**: p. 173-94.
361. Gaudette, B.T., et al., *mTORC1 coordinates an immediate unfolded protein response-related transcriptome in activated B cells preceding antibody secretion*. *Nat Commun*, 2020. **11**(1): p. 723.
362. So, J.S., *Roles of Endoplasmic Reticulum Stress in Immune Responses*. *Mol Cells*, 2018. **41**(8): p. 705-716.
363. Li, A., et al., *The Emerging Roles of Endoplasmic Reticulum Stress in Balancing Immunity and Tolerance in Health and Diseases: Mechanisms and Opportunities*. *Front Immunol*, 2019. **10**: p. 3154.
364. Sauzay, C., et al., *CD90/Thy-1, a Cancer-Associated Cell Surface Signaling Molecule*. *Front Cell Dev Biol*, 2019. **7**: p. 66.
365. Haeryfar, S.M. and D.W. Hoskin, *Thy-1: more than a mouse pan-T cell marker*. *J Immunol*, 2004. **173**(6): p. 3581-8.
366. Willis, S.N., et al., *Investigating the Antigen Specificity of Multiple Sclerosis Central Nervous System-Derived Immunoglobulins*. *Front Immunol*, 2015. **6**: p. 600.
367. Wang, J., et al., *HLA-DR15 Molecules Jointly Shape an Autoreactive T Cell Repertoire in Multiple Sclerosis*. *Cell*, 2020. **183**(5): p. 1264-1281 e20.

368. Huda, S., et al., *Neuromyelitis optica spectrum disorders*. Clin Med (Lond), 2019. **19**(2): p. 169-176.
369. Lopez de Castro, J.A., *How ERAP1 and ERAP2 Shape the Peptidomes of Disease-Associated MHC-I Proteins*. Front Immunol, 2018. **9**: p. 2463.
370. Hammer, G.E., et al., *The aminopeptidase ERAAP shapes the peptide repertoire displayed by major histocompatibility complex class I molecules*. Nat Immunol, 2006. **7**(1): p. 103-12.
371. Shemer, A., et al., *Interleukin-10 Prevents Pathological Microglia Hyperactivation following Peripheral Endotoxin Challenge*. Immunity, 2020. **53**(5): p. 1033-1049 e7.
372. Lobo-Silva, D., et al., *Balancing the immune response in the brain: IL-10 and its regulation*. J Neuroinflammation, 2016. **13**(1): p. 297.
373. Iyer, S.S. and G. Cheng, *Role of interleukin 10 transcriptional regulation in inflammation and autoimmune disease*. Crit Rev Immunol, 2012. **32**(1): p. 23-63.
374. Brown, C.Y., et al., *Differential regulation of the stability of cytokine mRNAs in lipopolysaccharide-activated blood monocytes in response to interleukin-10*. J Biol Chem, 1996. **271**(33): p. 20108-12.
375. Zhang, X., et al., *Coactivation of Syk kinase and MyD88 adaptor protein pathways by bacteria promotes regulatory properties of neutrophils*. Immunity, 2009. **31**(5): p. 761-71.
376. Ozkan, M., Y.C. Eskiocak, and G. Wingender, *The IL-10GFP (VeRT-X) mouse strain is not suitable for the detection of IL-10 production by granulocytes during lung inflammation*. PLoS One, 2021. **16**(5): p. e0247895.
377. Bonmassar, L., et al., *Detection of circulating tumor cells is improved by drug-induced antigen up-regulation: preclinical and clinical studies*. Anticancer Res, 2010. **30**(11): p. 4721-30.
378. Cillo, A.R., et al., *Immune Landscape of Viral- and Carcinogen-Driven Head and Neck Cancer*. Immunity, 2020. **52**(1): p. 183-199 e9.
379. Wen, W., et al., *Immune cell profiling of COVID-19 patients in the recovery stage by single-cell sequencing*. Cell Discov, 2020. **6**(1): p. 31.
380. Zhang, J.Y., et al., *Single-cell landscape of immunological responses in patients with COVID-19*. Nat Immunol, 2020. **21**(9): p. 1107-1118.
381. Zheng, G.X., et al., *Massively parallel digital transcriptional profiling of single cells*. Nat Commun, 2017. **8**: p. 14049.

382. Wilk, A.J., et al., *A single-cell atlas of the peripheral immune response in patients with severe COVID-19*. Nat Med, 2020. **26**(7): p. 1070-1076.
383. Hao, Y., et al., *Integrated analysis of multimodal single-cell data*. Cell, 2021. **184**(13): p. 3573-3587 e29.
384. Korsunsky, I., et al., *Fast, sensitive and accurate integration of single-cell data with Harmony*. Nat Methods, 2019. **16**(12): p. 1289-1296.
385. Aran, D., et al., *Reference-based analysis of lung single-cell sequencing reveals a transitional profibrotic macrophage*. Nat Immunol, 2019. **20**(2): p. 163-172.
386. Finak, G., et al., *MAST: a flexible statistical framework for assessing transcriptional changes and characterizing heterogeneity in single-cell RNA sequencing data*. Genome Biol, 2015. **16**: p. 278.
387. Crow, M.K., M. Olferviev, and K.A. Kirou, *Type I Interferons in Autoimmune Disease*. Annu Rev Pathol, 2019. **14**: p. 369-393.
388. Lee, A.J. and A.A. Ashkar, *The Dual Nature of Type I and Type II Interferons*. Front Immunol, 2018. **9**: p. 2061.
389. Boukhaled, G.M., S. Harding, and D.G. Brooks, *Opposing Roles of Type I Interferons in Cancer Immunity*. Annu Rev Pathol, 2021. **16**: p. 167-198.
390. Lin, F. and K. Shen, *Type I interferon: From innate response to treatment for COVID-19*. Pediatr Investig, 2020. **4**(4): p. 275-280.
391. O'Connell, P. and Y.A. Aldhamen, *Systemic innate and adaptive immune responses to SARS-CoV-2 as it relates to other coronaviruses*. Hum Vaccin Immunother, 2020. **16**(12): p. 2980-2991.
392. Wu, Y., et al. *SLAMF7 Regulates Inflammatory Response In Macrophage During Polymicrobial Sepsis*. 2021.
393. Meckiff, B.J., et al., *Imbalance of Regulatory and Cytotoxic SARS-CoV-2-Reactive CD4(+) T Cells in COVID-19*. Cell, 2020. **183**(5): p. 1340-1353 e16.
394. Policard, M., et al., *Immune characterization and profiles of SARS-CoV-2 infected patients reveals potential host therapeutic targets and SARS-CoV-2 oncogenesis mechanism*. Virus Res, 2021. **301**: p. 198464.
395. Yi, J.S., M.A. Cox, and A.J. Zajac, *T-cell exhaustion: characteristics, causes and conversion*. Immunology, 2010. **129**(4): p. 474-81.

396. Labrijn, A.F., et al., *Bispecific antibodies: a mechanistic review of the pipeline*. Nat Rev Drug Discov, 2019. **18**(8): p. 585-608.
397. Cugurra, A., et al., *Skull and vertebral bone marrow are myeloid cell reservoirs for the meninges and CNS parenchyma*. Science, 2021.
398. Brioschi, S., et al., *Heterogeneity of meningeal B cells reveals a lymphopoietic niche at the CNS borders*. Science, 2021.
399. Swanson, E., et al., *Simultaneous trimodal single-cell measurement of transcripts, epitopes, and chromatin accessibility using TEA-seq*. Elife, 2021. **10**.
400. Yates, K.B., et al., *Epigenetic scars of CD8(+) T cell exhaustion persist after cure of chronic infection in humans*. Nat Immunol, 2021. **22**(8): p. 1020-1029.
401. Abdel-Hakeem, M.S., et al., *Epigenetic scarring of exhausted T cells hinders memory differentiation upon eliminating chronic antigenic stimulation*. Nat Immunol, 2021. **22**(8): p. 1008-1019.
402. Hutchins, A.P., D. Diez, and D. Miranda-Saavedra, *The IL-10/STAT3-mediated anti-inflammatory response: recent developments and future challenges*. Brief Funct Genomics, 2013. **12**(6): p. 489-98.